Quantifying impacts from natural hazards on World Heritage - A case study from Frontiers of the Roman Empire: Hadrian's Wall

By

Lesley Davidson MA

A thesis submitted for the degree of Doctor of Philosophy

School of Engineering

Newcastle University

October 2022

Abstract

World Heritage (WH) sites are vulnerable to natural hazards, which have the potential to depreciate Outstanding Universal Value, including through erosion of its archaeological record. Safeguarding WH for future generations proves challenging as the effects of climate change are considered to be a risk multiplier to pre-existing conditions. Heritage professionals raised concerns about the resilience of WH to climate change to the WH Committee in 2005, leading to the 2007 Policy Document on the Impacts of Climate Change on World Heritage. Despite over 15 years of progress, the effects of natural hazards on WH sites is still poorly understood due to inadequate methods for assessing impact. Currently, there is no protocol for quantifying impact in a rigorous scientific manner.

The aim of this research was to combine advanced geospatial methods to quantify the impact of natural hazards on WH. This workflow was demonstrated on an at-risk archaeological site from Hadrian's Wall WH site where coastal dune erosion has been observed. By combining change detection and predictive modelling, historic coastal change of the study area was tracked c. 150 years into the past and forecasted 20 years into the future. The results showed that the dunes have receded in the area where the archaeology is most vulnerable by up to 50 m at a rate of 0.33 m/year +/- 0.02 m. The total area of detectable change from the continuous stretch of erosion along the same location was c. 7800 m^2 with an estimated volume of sediment loss of c. 31000 m^3. Future modelling predicted a further retreat of these dunes by c. 31 m, albeit with a large uncertainty (c. +/- 12 m), in 20 years' time. In the event of the worst case scenario, if the dunes were left unmanaged and no archaeological mitigation were to be undertaken, this would result in a loss of over half of the current known extents of the archaeological remains buried within the sand dunes.

Acknowledgments

I would like to thank my team of supervisors, Professor Jon Mills (Newcastle University), Professor Ian Haynes (Newcastle University), Professor Charles Augarde (Durham University), Paul Bryan (Historic England) and Mark Douglas (English Heritage) for all their guidance, encouragement and support throughout my PhD research.

Thank you to the IAPETUS Doctoral Training Partnership and Historic England for providing me with the opportunity to undertake this research by funding my studentship. Thank you for the training opportunities that were provided. I really enjoyed my experience at Historic England working with the Geospatial Imaging and Aerial Imaging teams.

Thanks to Dr Maria-Valasia Peppa for all of her guidance and advice. You helped me take my geospatial skills to the next level. Hopefully, we will be able to collaborate in the future.

A big thank you to Martin Robertson, James Goodyear and Nathan Harrap for help with and access to the RPAS equipment, in addition to the fieldwork assistance you all provided. Thanks to everyone else who also took time to help me undertake fieldwork, which was always sunny and hopefully enjoyable! I wouldn't have been able to complete the aerial surveys without your help Nicky Garland, Johannes Senn, Marine Roger, Aleksandra Zaforemska, Niels Dabaut, Soetkin Vervust, and Eric Tourigny. Thank you to David Dick and his colleagues for building the bespoke lidar targets.

Thank you to Melissa Ware and the rest of the team in Cassie reception for pointing me in the right direction for all things administrative!

Thanks to my parents and the rest of the family – both the Davidsons and the Garlands for being so caring and understanding. You were all super supportive, particularly at the end when I needed some extra motivation to make it past the finish line.

Best for last, and most importantly I would like to thank my biggest supporter - my better half Dr Nicky Garland. Thank you so much for your support from the very beginning to the end and then some. Leaving our jobs to move to the other end of the country was a risk, but one that paid off. If it wasn't for all your help and encouragement, I'd still be writing my thesis! Looking forward to whatever comes next. Love you the mostest.

Table of Contents

List of Figures

List of Tables

Abbreviations

2D: 2-Dimensional

3D: 3-Dimensional

AONB: Area of Outstanding Natural Beauty

BFEP: Beckfoot Fort and Environs Project

CHT2:   Cultural Heritage through Time

CPs: Control Points

CUCAP: Cambridge University Committee for Air Photography

DEFRA: Department of Food and Rural Affairs

DEM: Digital Elevation Model

DSAS: Digital Shoreline Analysis System

DoD: DEMs of Difference

dpi: dots per inch

EA: Environment Agency

EH: English Heritage

FRE: Frontier of the Roman Empire

GCD: Geomorphic Change Detection

GCPs: Ground Control Points

GIS: Geographical Information System

HAR: Heritage at risk

HE: Historic England

ICP: Iterative Closest Point

Lidar: light detection and ranging

M3C2:   Multiscale Model to Model Cloud Comparison

NGR: National Grid Reference

NLS: National Library Scotland

OPALS: Orientation and Processing of Airborne Laser Scanning Data

OS: Ordnance Survey

OSGB36:   Ordnance Survey Great Britain 1936 (coordinate system)

RMSE: Root Mean Square Error

RAF: Royal Air Force

RCHME: Royal Commission on the Historical Monuments of England

SSSI: Site of Special Scientific Interest

SfM: Structure from Motion

SM/SM's: Scheduled Monument/Schedule Monument's

SMP: Shoreline Management Plan

TLS: Terrestrial Laser Scanner

The Wall: Hadrian's Wall

WallCAP: Hadrian's Wall Community Archaeology Project

UK: United Kingdom

USGS: United States Geological Survey

WH: World Heritage

XBeach: eXtreme Beach Behaviour

Chapter 1: Introduction

1.1 Background

Climate change has very likely affected weather and climate extremes in all regions of the Earth (IPCC, 2021, p. 85). Global surface temperatures are expected to continue to increase until at least the mid-21st-century (IPCC, 2021, p. 17). The target of limiting global warming to 1.5° C above pre-industrial levels, as agreed upon in Article 2 (a) of the Paris Agreement at Conference of the Parties (COP) 21 in 2015 (United Nations, 2015, p. 22), was reaffirmed at the Glasgow Climate Pact, by 200 countries at COP 26 in 2021 (United Nations Climate Change and UK Government, 2021, p. 3). According to the Climate Action Tracker (CAT), an independent scientific analysis of government adherence to the Paris Agreement, the 2030 emissions targets to fulfil this target temperature limit are inadequate, and as such, it is expected that the 1.5°C temperature cap will be exceeded by at least 0.3°C (Fig. 1.1) (Climate Analytics and New Climate Institute, 2021a, p. 1). Even if more stringent targets were to be achieved, and global surface temperatures were stabilised, many of the effects of climate change will likely continue for hundreds to thousands of years into the future (Collins *et al.*, 2013, p. 1033).

Increasing global surface temperatures has led to regional variations in weather and climatic conditions. Based on historical and modelled data, the latest UK climate change projections 2018 (UKCP18) indicated a future of warmer wetter winters and hotter, drier summers (Lowe *et al.*, 2019, p. 3) with an increase in the frequency of hot spells (Met Office, 2021, p. 8), increase in frequency and intensity of extremes (Met Office, 2021, p. 7) and non-uniform sea level rise (Palmer *et al.*, 2018, p. 8). Along with these variates in weather and climatic conditions, comes an increase in frequency and intensity of natural hazards, the effects of which are already being experienced today.

Understanding the impact of natural hazards on World Heritage (WH) properties has become a pressing issue in light of modern climate change posing significant threats to the Outstanding Universal Value (OUV) of these heritage properties (UNESCO and WHC, 2021a, p. 1). Natural hazards threaten the survival of WH properties, along with their associated archaeological remains in several ways, including impacts on geomorphology that have led to the destruction of the archaeological record. Climate change is considered both a direct threat and a 'risk multiplier' to cultural heritage, placing further strains on the already

fragmented and vulnerable archaeological resource (Croft, 2013, p. 8; Markham *et al.*, 2016, p. 12; Historic England, 2017a, p. 30). Repercussions associated with climate change will likely occur because of the development of new hazards, but also due to the acceleration of pre-existing hazards. Pre-existing hazards include those caused by specific types of land use (i.e. arable ploughing and tourism) or natural processes such as coastal erosion.
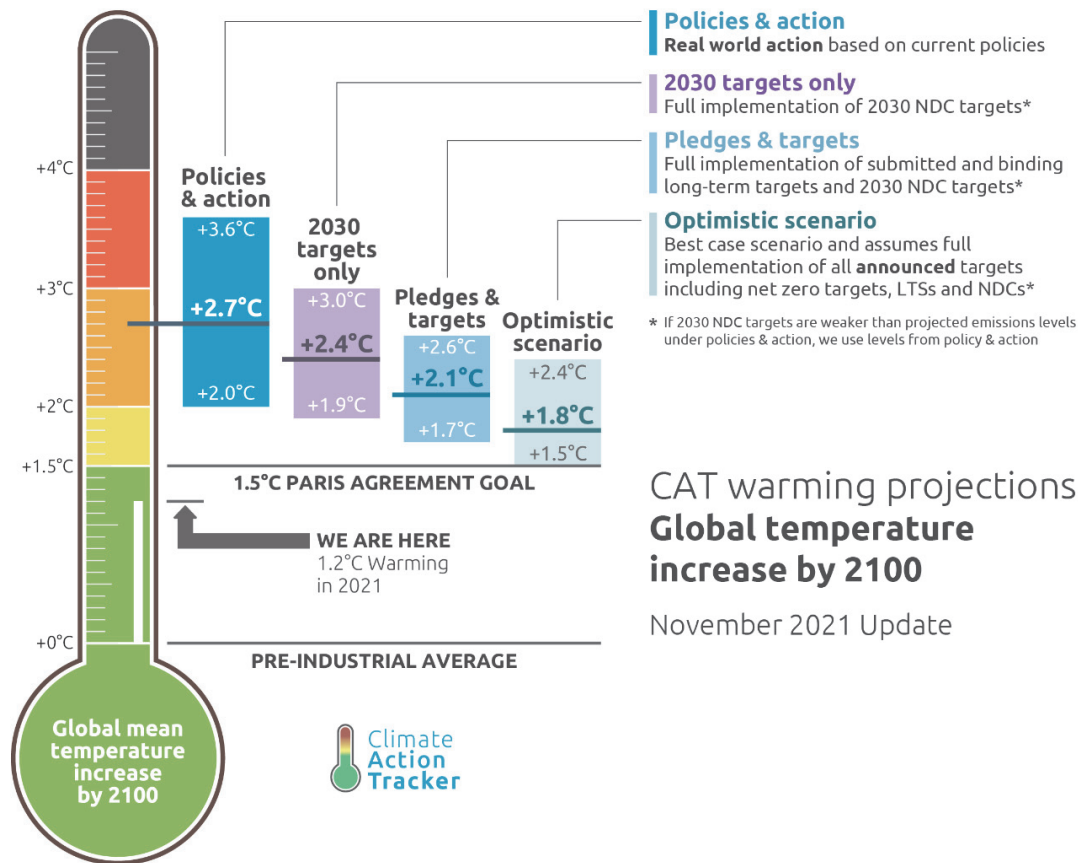
Figure 1.1: Climate Action Tracker warming projections of global temperature increase by 2100 (Climate Analytics and New Climate Institute, 2021b, © Climate Analytics and New Climate Institute).

The archaeological record is impacted upon by climate change in multiple ways. Archaeological remains survive in the ground when in balance with the hydrological, chemical and biological processes of the soil (UNESCO, 2007, p. 25). If this balance is compromised, through fluctuations to waterlogged, anaerobic and anoxic conditions, the preservation of archaeological material is expected to further deteriorate (UNESCO, 2007, p. 25). Moreover, the raising or lowering of the water table, drying or inundation of soils, and changes to the freeze-thaw cycles can damage stratigraphic integrity as soils become unstable and begin to heave, crack, or subside (UNESCO, 2007, p. 25). More frequent and severe rainfall, sea level rise and an increase in storminess is expected to cause flooding and erosion to heritage sites located in low-lying coastal and riparian environments (UNESCO,

2007, p. 25). In addition these physical processes, exacerbated by climate change, can also lead to erosion of exposed and unstable ground and landslides of sloped topography, each of which can also result in destruction of the archaeological resource buried in these at risk locations (UNESCO, 2007, p. 25).

1.2 Scope of research

1.2.1 Problem statement

Current management practices for understanding the impact of natural hazards on cultural WH are unsatisfactory. UNESCO has produced guidance on Disaster Risk Reduction for managing natural hazards at WH properties (UNESCO *et al.*, 2010), however, as the nomenclature suggests, the main focus is preparing for disastrous events, rather than slow onset naturally occurring hazards (UNESCO *et al.*, 2010, p. 6). Generally, risk assessments, such as the Heritage Impact Assessment (HIA) for cultural WH, are initiated by proposals for development (ICOMOS, 2011) and therefore risk from natural hazards are often overlooked while human driven changes are given priority. While the Climate Vulnerability Index (CVI) has been developed for assessing impact from climate change on WH sites (Day *et al.*, 2019), it is still in its infancy. In addition, CVI appears to be based largely on scientific expertise and subjective observation rather than scientific measurements. It provides a starting point for conceptualizing hazards in descriptive terms and assigning levels (low, medium or high) of risk based on vulnerability and exposure while also considering socio-economic factors (Day *et al.*, 2019). The CVI provides no attempt to make a quantitative analysis of the damage already incurred, nor to provide a time frame for potential future impacts. If risk, assessed through the CVI framework or by other similar means, is deemed to be medium or high, then further in-depth studies should ensue.

Studies should include quantitative approaches of both past and future geomorphological changes when interactions of natural processes with the archaeological and cultural heritage landscape of WH properties results in erosion of the ground surface. Recently, a number of large international projects, such as CHERISH (CHERISH, 2021), PROTHEGO (PROTHEGO, 2017), CHT2 (CHT2, 2019), CLIMA (CLIMA, 2021), EAMENA (Rayne et al, 2020) and Dynamic Coasts (Dynamic Coast, 2021a) have or continue to address this problem through advanced geospatial methods for monitoring and/or predicting impact from natural hazards. However, as of yet, no formalised framework for quantifying impact from natural hazards has been put forward.

3

Harkin *et al.* (2020, p. 616) state that loss of heritage assets due to the impacts of climate change is inevitable but quantifying the combined impacts of environmental threats to cultural heritage is a key challenge (Harkin *et al.*, 2020, p. 638). If loss of heritage assets to natural hazards is unavoidable, then efforts need to be made to preserve through mitigation measures or through record. Quantify past change can aid in the prediction of future impact giving an indication of urgency for action. Advanced geospatial technologies have played a key role in measurement, documentation, modelling and monitoring cultural WH (Xiao *et al.*, 2018, p. 392) and offer methods for studying evolution over time (Xiao *et al.*, 2018, p. 393). While progress has been made to employ geospatial data and technologies beyond feature detection and digital documentation of heritage assets, there remains a need for in-depth multi-temporal geospatial analysis of impact from natural hazards as attested to by sustainable Development Goal Target 11.4: 'strengthen efforts to protect and safeguard the world's cultural and natural heritage' (United Nations, 2018, p. 63).

1.2.2 Motivation

This doctoral research developed out of Cultural Heritage Through Time project (CHT2) (2015 – 2018) (CHT2, 2019). In this project, researchers from across Europe merged heterogeneous spatial data into four-dimensional digital products of cultural heritage, by incorporating the temporal dimension. Using Structure-from-Motion, Multi-View-Stereo (SfM-MVS), researchers, from Newcastle University's School of Engineering, created 2D and 3D orthomosaics and models from archived aerial imagery for three sites associated with Hadrian's Wall WH site (Fieber *et al.*, 2017, p. 297). The SfM-MVS outputs were combined with airborne Light Detecting and Ranging (lidar), modern 3D orthomosaics, Aerial Investigation and Mapping (formerly the National Mapping Programme) data, legacy data (old excavation plans), and geophysical survey results to enhance our understanding of temporal landscape changes to the three selected sites (Fieber *et al.*, 2017, p. 299). CHT2's research has been further developed, within this doctoral research, to quantify past and future impacts from natural hazards on an at risk site from the Roman Frontier.

1.2.3 Aims

The aim of this doctoral research is to develop a geospatial framework for quantitative impact assessment of natural hazards on cultural heritage landscapes. The approach will provide a scientifically rigorous understanding of loss and destruction of the archaeological record by comparing areal, volume and rates of change calculations of erosional processes

to the known archaeology. This framework will be demonstrated on a world-renowned archaeological site using multi-spatiotemporal data and multi-modal geospatial methods.

1.2.4 Objectives

To achieve the above aim, the following objectives have been identified:

Objective 1: Critically evaluate impact assessment practices regarding natural hazards on WH properties and provide a comprehensive review of threats to at risk heritage from Hadrian's Wall WH site.

Objective 2: Review current spatiotemporal data and methods for quantifying impact from natural hazards.

Objective 3: Develop an innovative geospatial framework for assessing impact from natural hazards on WH sites, using a fully integrated spatiotemporal time series.

Objective 4: Provide a conceptual understanding of the impacts from natural hazards on the archaeological record for an at risk site from the Hadrian's Wall WH site.

Objective 5: Quantify impacts from natural hazards for an at risk site from the Hadrian's Wall WH site and interpret results in the context of the archaeological record.

1.2.5 Research questions

The following research questions will be addressed in fulfilment of the five objectives listed above.

1. What are the current methods for assessing impact on cultural WH properties and are these appropriate for quantifying impact from natural hazards?
2. How can historical analogue data be optimally combined with modern digital remote sensing data to effectively quantify past and future impact from natural hazards on cultural WH?
3. What geospatial methods exist for quantifying deformation of the Earth's surface diachronically and can these methods be applied in the context of cultural WH?
4. How can the archaeological record aid in the interpretation of results?

1.3 Conceptual framework

The conceptual framework of this thesis (Fig. 1.2) is appropriate for cultural WH properties where natural hazards present themselves as deformations to the Earth's surface. The framework provides a method for quantifying impacts of natural hazards on cultural heritage

landscapes that can be divided into two main approaches. The first approach measures past geomorphic change from a spatiotemporal time series representing topography compiled from legacy analogue and digital remote sensing data using geomorphic change detection techniques. Where possible, the results are refined by evidence from the archaeological record. The second approach uses predictive models to demonstrate their use in quantifying future impact from natural hazard. The results of both approaches are compared to the known archaeology in order to assess potential future impact. This allows for conclusions to be drawn regarding the impact on the archaeological remains of the cultural WH property in question.
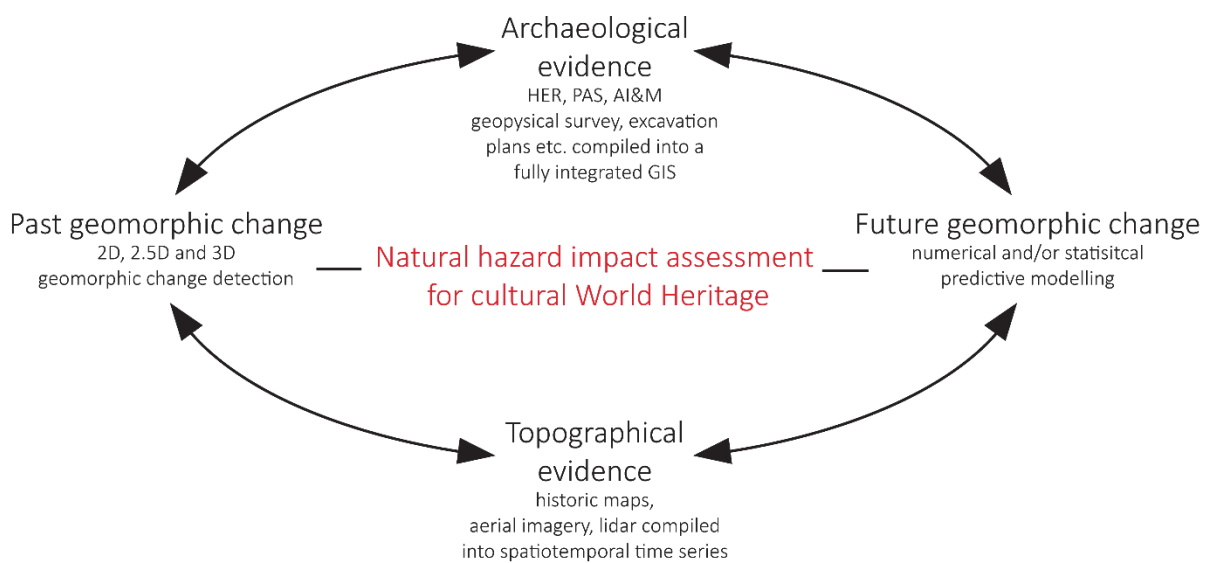
Figure. 1.2: Conceptual framework for natural hazard impact assessment for cultural WH properties.

1.4 Chapter structure

This thesis is presented across seven chapters. The following provides a brief summary for each of the chapters.

Chapter 2: World Heritage and Hadrian's Wall: the need for natural hazard impact assessment reviews the literature surrounding guidance and management practices for WH properties. This chapter defines key terminology, outlines the responsibilities of the State Parties, and details the consequence of failure in safeguarding WH. In addition, a critique of the methods for assessing impact on WH is presented. The chapter then turns the focus to Hadrian's Wall WH site detailing the hazards threatening its survival. The chapter reviews the research previously conducted into impact of natural hazards at locations from across the Hadrian's Wall WH site.

Chapter 3: Spatiotemporal analysis: measuring past and future changes to the Earth's surface reviews methods for measuring surface change based on multi-temporal topographic data. The chapter presents a discussion of the data types appropriate for inclusion in a time series representing topography. It assesses 2D, 2.5D and 3D change detection methods for measuring past change and reviews modelling techniques for predicting future change. Furthermore, the chapter discusses change detection and modelling methods used in the context of archaeology.

Chapter 4: Implementing the framework for natural hazard impact assessment for cultural World Heritage sites describes the methodology for undertaking the proposed natural hazard impact assessment framework, which quantifies past and future changes of the Earth's surface resulting from natural hazards in order to understand the sustainability of a cultural WH site. The chapter details the topographic time series, along with data specific pre-processing methods and co-registration required for change detection. The 2D, 2.5D and 3D change detection methodology is described, followed by strategies for modelling future change.

In ***Chapter 5: The Beckfoot study area and coastal erosion: a conceptual model*** the archaeological record is situated within its built and natural environmental setting. This information is set alongside the hydro- and morpho-dynamics of the coastal zone, which poses potentially the greatest threat to the archaeological remains of Hadrian's Wall WH site. The information is drawn together into a conceptual understanding of the natural processes interacting with and impacting upon the study area.

Chapter 6: Natural Hazard Impact assessment for the Beckfoot study area details the erosion of the coastal dunes over a 153 year period based on the results from the 2D, 2.5D and 3D change detection analyses. The results are interpreted in conjunction with the archaeological evidence to assess impact and provide refinement where possible. Potential impact in 10 and 20 years into the future is also presented through forecasting the 2029 and 2039 coastline positions. This is followed by results of a complex numerical model used to simulate coastal processes under storm conditions. The purpose of which was to demonstrate the potential of this kind of modelling applied to the historic environment.

Finally, ***Chapter 7: Discussion and conclusion***, revisits the aims and the objectives and addresses the research questions. The significant findings of the research along with its

contribution to the wider field and the limitations encountered are described. The chapter closes with suggestions for future research directions which builds upon the research presented in this thesis.

Chapter 2: World Heritage and Hadrian's Wall: the need for natural hazard impact assessment

2.1 Introduction

Cultural World Heritage (WH) properties are considered the most significant heritage sites with global value, as attested to through the possession of Outstanding Universal Value assigned by United Nations Educational, Scientific and Cultural Organization (UNESCO) World Heritage Committee (OUV) (UNESCO, 2021b, p. 24). A key responsibility of State Parties is to safeguard WH properties within their jurisdiction for future generations, however, WH properties are under threat of deterioration and destruction from human actions and natural processes. As the climate changes and disaster risk increases, threats to WH properties are anticipated to worsen. WH properties, thus require enhanced protection from ongoing and emerging natural hazards (UNESCO, 2015, p. 5).

Depending on the magnitude of loss arising from a hazard (natural or human induced), a WH property may be stripped of its prestigious title (UNESCO, 2021b, p. 62). This can result in a much greater loss than that of status, but also a loss in knowledge of the human past, loss of identity through connection to these historic places and a loss to the economy due to a decrease in tourism, to name a few. While policy and guidance documents layout regulations and provide advice regarding the management of WH (UNESCO, 2007b; UNESCO, 2015; UNESCO World Heritage Centre, 2019; UNESCO, 2021b; UNESCO World Heritage Centre, 2021a), these documents are insufficient due to generalities necessary for inclusivity of all the State Parties regardless of technological capabilities. This gives State Parties a wide scope for the implementation of strategies to assess and safeguard WH properties for future generations.

Until recently, heritage impact assessment guidance, such as those published by the International Council on Monuments and Sites (ICOMOS) (ICOMOS, 2011) were triggered in response to proposed development projects rather than threats posed by natural hazards. The Climate Vulnerability Index (CVI) was created as an alternative tool for rapid assessment of climate change risk to OUV and to the community (Day *et al.*, 2019, p. 1). While employing CVI on WH properties is an important step in conceptualising threats and assigning levels of severity, such an undertaking should be followed on with in-depth research which seeks to

quantify loss and destruction when the severity of the threats have been assigned to moderate or high categories.

This chapter is divided into two main sections. Section 2.1 discusses WH, including definitions, policy, types of hazards and current challenges faced by those who manage WH properties. Section 2.2 narrows the focus to the Frontiers of the Roman Empire: Hadrian's Wall WH site from which the study area was selected. The chapter concludes with a summary before introducing the next chapter where geospatial methods and their applicability to assessing hazards on cultural WH sites is discussed.

2.2 World Heritage

2.2.1 The need for the World Heritage Convention

The original ethos eventually leading to the WH Convention was to protect exceptional cultural heritage sites from threats posed during times of political upheaval, or conflict, such as during war when cultural sites were deliberately destroyed (Alberts and Hazen, 2010, pp. 56 - 57). While the need to protect cultural heritage became evident during WWII (Alberts and Hazen, 2010, p. 56), it was approximately two decades later before the Convention was fully realised. The final catalyst for the creation of the Convention was the threat of flooding to the Abu Simbel temples, resulting from the proposed construction of the Aswan High Dam (Alberts and Hazen, 2010, p. 57). This led to an international campaign, which dismantled, relocated and reassembled the temples (Hassan, 2007). Shortly after these rescue works, which were funded by an international community, UNESCO along with the ICOMOS began preparing a draft convention for the protection of cultural heritage (Alberts and Hazen, 2010, p. 57). This evolved to incorporate natural heritage as it was believed that the two types of heritage were intrinsically linked (Slatyer, 1983, p. 138). The Convention was adopted in 1972 by UNESCO's general conference and became operational in 1975 with 20 nations having ratified it (Slatyer, 1983, p. 138).The Convention, as of the 23rd of October, 2020 has been ratified by 194 State Parties (UNESCO, 2020).

2.2.2 Defining World Heritage

The UNESCO distinction of WH is the highest ranking that can be awarded to both natural and cultural heritage sites, of which there are three categories: cultural, natural and mixed WH. The third type are sites that are acknowledged as having OUV for both cultural and natural reasons. Cultural WH consists of monuments, groups of buildings and sites that are

the works of people (or the combined works of people and nature), which are deemed to be of OUV from the perspective of history, art, science, aesthetics, ethnology and anthropology (UNESCO, 1972, p. 2). In contrast, Natural WH are natural features, geological and physiographical formations that are of OUV from the perspective of aesthetics, science, conservation and natural beauty (UNESCO, 1972, p. 2).

To be given the prestigious title of WH, properties must meet at least one of ten selection criteria for OUV, which are outlined in the Operational Guidelines for the Implementation of the WH Convention (UNESCO World Heritage Centre, 2019, pp. 25 - 26). As such, sites that are inscribed on the WH list are considered to be exceptionally significant, transcend national boundaries and are of common importance to all people (UNESCO World Heritage Centre, 2019, p. 20). By ratifying the WH Convention, State Parties, under the guidance of WH Committee, accept the responsibility of *identification, conservation, preservation and transmission to future generations of cultural and natural heritage* (UNESCO, 1972, p. 3). Therefore, it is the responsibility of each State Party to enact legislative and regulatory measures which uphold WH authenticity, integrity and OUV (Alberts and Hazen, 2010, p. 56).

Integrity and authenticity are values used to measure whether a heritage property possesses OUV for inclusion on the WH list (UNESCO World Heritage Centre, 2019, p. 26). Integrity refers to properties completeness (UNESCO World Heritage Centre, 2019, p. 27). The condition of a property needs to be sufficiently whole or intact in order to express its OUV (UNESCO World Heritage Centre, 2019, p. 27). For cultural heritage properties, this means that their fabric and/or significant features need to be in good condition and that intervening measures should be taken to control deterioration (UNESCO World Heritage Centre, 2019, p. 27). Authenticity refers to a property's credibleness and truthfulness in relation to the property's original and subsequent characteristics (UNESCO World Heritage Centre, 2019, p. 26). Due to the cultural differences that exist around the world, authenticity is not judged by a set of fixed criteria, but rather within the property's cultural context (UNESCO World Heritage Centre, 2019, p. 26). Authenticity may be judged based on the following attributes: design; materials and substance; use and function; traditions and techniques; location and setting; and spirit and feeling; and may include other factors, both internal and external (UNESCO World Heritage Centre, 2019, p. 27). Upholding the integrity and authenticity of a WH property and therefore its OUV is the number one priority of State Parties not only to maintain WH status but also to safeguarding WH from both human and

natural hazards for future generations. Therefore, State Parties must uphold OUV through the implementation of adequate protection measures and management practices to meet the expectations set out by the Convention (UNESCO World Heritage Centre, 2019, p. 26).

2.2.3 Hazards and World Heritage

A particular concern to those who manage WH properties are hazards that threaten the OUV of the property. UNESCO *et al.* (2010, p. 58) subscribes to the following definition of hazard as defined by Abarquex and Murshed (2004, p. 6) - a hazard is *any phenomenon, substance or situation, which has the potential to cause disruption or damage to infrastructure and services, people, their property and their environment*. Hazards can fall into several categories that are either naturally occurring or anthropogenic in origin. These categories of hazards include meteorological, hydrological, geological/geomorphological, biological, astrophysical, human-induced and climate change (UNESCO *et al.*, 2010, pp. 59 - 60).

2.2.4 Natural Hazards

A natural hazard has been defined as *an unexpected and/or uncontrollable natural event of unusual magnitude that might threaten people* (Bokwa, 2013, p. 711). It is associated with geophysical processes that have the potential to cause damage or loss to human life (Stillwell, 1992, p. 133). When a geophysical process interacts with a cultural heritage property in a way that threatens that properties value to society, it thereby affects human life and can be deemed a natural hazard. A natural hazard can happen quickly over the course of an event such an earthquake, landslide or flash flood (Bokwa, 2013, p. 724), causing irreversible loss of a heritage asset in short period of time. Alternatively a natural hazard may have a slow onset resulting in gradual loss such as the erosion of soil (Bokwa, 2013, p. 724) resulting in loss of heritage assets over the long-term.

According to Nicu (2020, p. 7642), in excess of 1500 cultural and natural WH properties across 144 countries have been exposed to one or more types of natural hazards. An example of a WH property where WH is at risk from natural hazards can be found at Skara Brae, part of the Heart of Neolithic Orkney WH property, located on the Bay of Skaill, Mainland, Orkney, Scotland. The site was initially discovered through destructive weather related forces, when in 1850 a storm removed dune material revealing the remains of a Neolithic settlement (Day *et al.*, 2019a, p. 23). Today, further destructive forces, particularly rising sea levels and increased storminess, has led to coastal erosion, which poses the greatest threat to the site (Day *et al.*, 2019a, p. 23). This threat has resulted in partial loss of

the coastal dunes, likely along with valuable archaeological material buried within the dunes, particularly in the area adjacent to the seawall, originally constructed in the 1920's (Day et al., 2019a p. 20). This type of erosion associated with seawalls is referred to as terminal or flanking erosion. Since the early 1900's, actions have been taken to safeguard Skara Brae for future generation, including the construction of the sea wall mentioned above. Furthermore, laser scanning has been undertaken every two years to monitor the condition of the property (Day et al., 2019a, p. 22). While terminal erosion has been observed, the WH property's integrity and authenticity and therefore its OUV appear to still be intact. This is in part owing to the active management of this cultural heritage resource in reaction to the ongoing hazards.

2.2.5 Consequence of loss to OUV

In the event that the aims of the Convention are not met, thereby compromising the integrity, authenticity and OUV of a WH property, whether due to the impact of a human hazard or a natural hazard, the site may be transferred onto the WH in danger list. The WH in danger list recognises that some sites are more vulnerable (Alberts and Hazen, 2010, p. 58) to threats resulting in disappearance caused by human actions, such as development projects, and natural hazards, such as earthquakes, landslides and volcanic eruptions (UNESCO, 1972, p. 6). If State Parties fail to fulfil their obligations resulting in the irreversible loss of integrity, authenticity and OUV, that property may be deleted from the WH list (UNESCO, 2019, p. 32). A recent example of this rare occurrence is the Liverpool – Maritime Mercantile City formerly on the cultural WH list, which was first inscribed in 2004 meeting three of the ten criterion for OUV (UNESCO, 2021a). In 2012, due to the redevelopment of the historic docklands, the property was placed on the WH in danger list (UNESCO, 2012, p. 184). Despite warnings from the WH Committee that development posed a threat to the property's OUV, resulting in *…serious deterioration and irreversible loss of attributes conveying the OUV of the property…*, further development in this area went ahead and led to the ultimate consequence of delisting in 2021 (UNESCO, 2021d, p. 58). The Liverpool – Maritime Mercantile City was the third WH property to be removed from the WH list (UNESCO World Heritage Centre, 2021b) following the Arabian Oryx Sanctuary, delisted in 2007 (UNESCO, 2007a, p. 51), and the Dresden Elbe Valley, delisted in 2009 (UNESCO, 2009b, p. 44). This most recent delisting reinforces the commitment of the WH Committee to upholding the values outlined in the Convention and Operational Guidelines.

The delisting of the Liverpool – Maritime Mercantile City WH site is an example of human-induced hazards leading to the removal of a WH property from the list. However, inaction to protect a WH property from the impacts of natural hazards, which adversely effects the integrity, authenticity and OUV of the WH property, can also result in the consequence of delisting. UNESCO anticipates that climate change will have negative impacts on WH properties in the coming decades and recognises that this impact may be beyond the control of the State Parties (UNESCO World Heritage Centre, 2021a, p. 8), therefore UNESCO concludes that an *"evolving" assessment of OUV* may be required (UNESCO World Heritage Centre, 2021a, p. 8). While this phraseology was not explicitly defined, presumably, the term OUV will adapt over time to make some level of exception for the impacts from natural hazards as they become greater risks due to climate change. To date no WH sites have been removed from the list for this reason, however, natural hazards, and the changing climate regime, present a real cause for concern for those managing WH properties.

2.2.6 World Heritage guidance on impact assessment

ICOMOS provides guidance for conducting Heritage Impact Assessments (HIA) for Cultural WH. The guidance has been created for the purpose of carrying out HIAs in relation to potential threats to OUV arising from planning proposals for development of new infrastructure, green energy solutions, tall or box buildings, etc. (ICOMOS, 2011, p. 1), not in relation to threats posed by natural hazards. The assessment is simple and involves defining the heritage at risk, identifying why it is important in terms of the WH properties OUV, assessing the impact of the development on the OUV and considering methods of avoidance, reduction, rehabilitation or compensation for said impact (ICOMOS, 2011, pp. 4 - 5).

Recently, an alternative guidance document to HIA was created, although it was not developed specifically for cultural WH properties, but for heritage properties in general. The Institute of Environmental Management and Assessment (IEMA) published what is considered to be the first UK guidance for Cultural Heritage Impact Assessment (CHIA). Like HIA, the guidance produced by ICOMOS, CHIA would be undertaken in response to a proposal for change driven by human motivations and actions, such as a plan, policy or project that could result in change to the cultural heritage asset (IEMA, 2021, p. 5). The two main tasks of CHIA are to present an understanding of the cultural heritage asset and to evaluate the consequences of the proposed change (IEMA, 2021, p. 6). The first task, understanding the cultural heritage asset, refers to providing a comprehension of the asset

in question in descriptive terms, including in regards to its significance and importance (IEMA, 2021, p. 7). While the second task, evaluation of the consequence of change, requires understanding the change, assessing the impact and weighting the effect (IEMA, 2021, p. 10).

IEMA (2021, p. 10) define impact as *a change in a cultural heritage asset or the experience of an asset in its setting that affects its cultural significance*. According IEMA, the outcome of an impact can be negative or positive. Impact is measured in relation to a heritage assets significance and not the cultural heritage itself (IEMA, 2021, p. 10). Impact can be loss or destruction, change in setting, change in character, change in appearance, or alterations in soil chemistry (IEMA, 2021, p. 11).

The drawback of HIA and CHIA is that both provide a framework to evaluate potential impact to proposed human-driven changes. Both guidance documents are therefore reactive to planned changes to the environment through human actions. As such, HIA, CHIA and other types of impact assessments are activated by the proposal for change. In addition, these do not account for change which result from natural processes even in instances where the natural processes have already been realised as hazards eroding cultural WH.

The Climate Vulnerability Index (CVI) was developed by researchers from James Cook University, Australia, as an alternative impact assessment tool, which specifically addresses impacts to WH from climate related hazards (Day *et al.*, 2019, pp. 1 - 2). This tool is used to determine the top three climate related drivers for change, and assess OUV and community vulnerability (Day *et al.*, 2019, pp. 1 - 2). It accounts for exposure and sensitivity, identifies potential impacts and considers adaptive capacity in relation to the three drivers (Day *et al.*, 2019, pp. 1 - 2). The CVI has been successfully put to practice at a number of WH properties, including at the Old and New Towns of Edinburgh WH site (Jones *et al.*, 2022) and at the Heart of Neolithic Orkney WH site (Day *et al.*, 2019a).

Guidance specific to WH in relation to disaster risk management has been published by UNESCO. The purpose of which was to aid WH managers in reducing risk from disasters caused by humans as well as those that are naturally occurring (UNESCO *et al.*, 2010, p. 6). The focus of this document was on catastrophic events which have the potential to be disastrous causing a large amount of damage over a short period of time rather than gradual, cumulative processes (UNESCO *et al.*, 2010, p. 6). UNESCO outlines three stages to

a disaster risk management plan each associated with timing of the hazards. These are pre-, during, and post- disaster stages. The pre-disaster stage involves conducting a risk assessment, creating mitigation strategies and taking preventative measures, and preparations for emergencies (UNESCO *et al.*, 2010, p. 13). Emergency response procedures are initiated during the disaster, while damage assessment, treatment, such as repairs, restoration and retrofitting, and recovery/rehabilitation occur post-disaster event (UNESCO *et al.*, 2010, p. 13). It is an iterative process which needs updating as and when required (UNESCO *et al.*, 2010, p. 14). The construction of a GIS to produce thematic maps, such as those identifying hot spots of risk, has been advised as part of disaster risk reduction (UNESCO *et al.*, 2010, p. 23). The process should also involve creating various disaster scenarios to predict the potential outcomes if a catastrophic event(s) should occur (UNESCO *et al.*, 2010, p. 27). The evaluation should indicate the probability of the disaster scenario occurring as either high, medium or low and assess the severity of the consequences (UNESCO *et al.*, 2010, p. 29). Mitigation strategies should not have a negative impact on the property's authenticity and integrity (UNESCO *et al.*, 2010, p. 38).

2.2.7 Climate change policy guidance

Possibly the biggest challenge currently faced by humanity is anticipating, preparing for and mitigating against the effects of climate change. Starting with the Industrial Revolution releasing greenhouse gasses into the atmosphere at an unprecedented rate leading to global warming, the world is now experiencing what is being aptly referred to as a climate emergency and the climate crises. Even with actions taken to reduce global emissions, the effects of climate change such as rising sea levels, increased storminess and extreme temperatures, will continue for years to come. In November 2021, World leaders came together at the Conference of the Parties 26 (COP26), the UN annual climate change conference, in Glasgow to reach a consensus on what further measures can be taken to achieve the goal of limiting global warming to 1.5°C, as originally agreed upon in the Paris Agreement in 2015 (UN Climate Change Conference UK 2021, 2021, p. 47). With this goal in mind, the future consequences are thought to be serious rather than severe when compared to a 2°C rise in temperature (UN Climate Change Conference UK 2021, 2021, p. 47). Although, as discussed in chapter 1, this goal is not likely to be met.

World Heritage is not immune to the impacts of the effects of climate change. In fact, climate change has been attributed as one of the most significant threats to WH (UNESCO,

2021c, p. 2), placing further stress on an already fragmented and vulnerable cultural heritage resource (Croft, 2013, p. 8; Markham *et al.*, 2016, p. 12; Historic England, 2017a, p. 30). As climate change is considered a 'risk-multiplier', exacerbating hazards, exposures and vulnerabilities, understanding the impacts of climate change are particularly urgent where physical effects from natural hazards, such as coastal erosion or weathering of stone, are pre-existing conditions (UNESCO World Heritage Centre, 2021a, p. 10) as WH properties.

2.2.8 Word Heritage climate change policy

According to UNESCO World Heritage Centre (2021a, p. 1) concerns regarding the impact of climate change on WH properties was first raised to the WH Committee in 2005. Since then, UNESCO has produced several documents and case studies on the topic including those relevant to cultural WH (UNESCO, 2006; Colette, 2007; UNESCO, 2007b; UNESCO *et al.*, 2010; Markham *et al.*, 2016; UNESCO World Heritage Centre, 2021a). Most recently UNESCO has released the *Draft policy document on climate actions for World Heritage (2021)*. The purpose of 2021 policy document was to provide a *high-level guidance on enhancing the protection and conservation of heritage of Outstanding Universal Value…* and *an outcome-oriented policy framework for development of goals and targets at national and heritage site levels…*, with climate change being the motivating factor (UNESCO World Heritage Centre, 2021a, p. 4).

The draft Policy Document (2021) also set out four WH Climate Action goals relating to: 1. Risk assessment; 2. Adaptation; 3. Mitigation; and 4. Knowledge sharing, capacity building and awareness (UNESCO World Heritage Centre, 2021a, p. 6). In regard to climate actions goals 1 and 2, the policy declares that State Parties should develop tools to assess potential damage, both reversible and irreversible, to the OUV of WH and to establish and implement adaptation frameworks that demonstrates measurable progress on monitoring, assessing and reducing risk and vulnerabilities (UNESCO World Heritage Centre, 2021a, p. 6). The policy also maintains that State Parties should work toward achieving these goals by 2030 (UNESCO World Heritage Centre, 2021a, p. 6) in line with measures taken as a result of COP26, the Paris Agreement and the Sustainable Development Goals.

The *Draft policy document on Climate Actions for World Heritage* (UNESCO World Heritage Centre, 2021a), states that it is imperative that WH managers implement strategies to understand the impacts of natural hazards and the implications these have regarding the OUV of the WH sites in their care. As Howard (2013) suggested, strategies for assessing

impact should rely on understanding the interaction of natural processes with the physiographic context and surrounding natural landforms to comprehend past and contemporary process driven geomorphological change (Howard, 2013, p. 642). Furthermore, understanding these processes will allow us to monitor current processes and, model and predict future change (Howard, 2013, p. 652).

2.3 Frontiers of the Roman Empire: Hadrian's Wall World Heritage Site

2.3.1 Introduction

Hadrian's Wall is considered to be the most complex and best preserved frontier of the Roman Empire. It was first inscribed on the WH List in 1987, meeting three of the six criterion of OUV (UNESCO, 1988) demonstrating its national and global importance to all of humanity from both present and future generations. The UNESCO Committee agreed Hadrian's Wall possessed the following criteria of OUV:

> *(ii) exhibit an important interchange of human values, over a span of time or within a cultural area of the world, on developments in architecture or technology, monumental arts or town-planning and landscape design (UNESCO World Heritage Centre, 2021c, p. 29)*

> *(iii) bear a unique or at least exceptional testimony to a cultural tradition or to a civilisation which is living or which has disappeared (UNESCO World Heritage Centre, 2021c, p. 29)*

> *(iv) be an outstanding example of a type of building or architectural or technological ensemble or landscape which illustrates (a) significant stage (s) in human history (UNESCO World Heritage Centre, 2021c, p. 29)*

Hadrian's Wall, together with the inscription of the Upper German-Raetian Limes in 2005 (UNESCO, 2005), was united into a single WH site known as *Frontiers of the Roman Empire*, which in 2008 also incorporated the Antonine Wall (UNESCO, 2009a). In 2021, further remains of the Roman Frontier were inscribed on the WH list (UNESCO World Heritage Centre, 2021e). These included the lower German Limes located in the Netherlands and Germany (UNESCO World Heritage Centre, 2021e). There are intentions to add further remains of the frontier, which would encompass the Middle East and North Africa (Hadrian's Wall Country, 2018a). The Hadrian's Wall portion of the inscribed WH Site is known as *Frontiers of the Roman Empire: Hadrian's Wall* WH Site, but will also be referred to as Hadrian's Wall in this thesis.

The Hadrian's Wall WH site and buffer zone covers an area of c. 17 square kilometres and 450 square kilometres respectively. The WH site stretches from Wallsend, in the east to Bowness-on-Solway, in the west where it then runs southwards along the Cumbrian coast for approximately thirty-six kilometres. The WH site consists of various monument types including the remains of the turf wall, the stone wall, Roman forts, milefortlets, turrets, roads, the vallum, bridges, cemeteries, extramural settlements and other archaeological remains. These features comprising the WH site are situated on and within varying topographical and geological settings which are subjected to different natural and human-driven stressors.

2.3.2 Management

Management of Hadrian's Wall presents challenges due to its vast scale, its diversity of monument types, a varied landscape setting and its interactions with the climate and people. The Lack of a central management body presents difficulties due to competing agendas. This is further complicated by the large number of key stakeholders including nine local authorities, two government bodies (Historic England and Natural England), six trusts and museums, as well as the researchers, local business and communities and land owners (Collins and Symonds, 2019, pp. 5 - 6). Large portions of the WH site are held in private ownership, with approximately 1000 different landowners (Collins and Symonds, 2019, p. 5). Currently the WH site Management Plan and Committee Partnership Board provide expertise and oversight (Collins and Symonds, 2019, p. 6).

There are 190 Scheduled Monuments associated with the Hadrian's Wall WH Site on the National Heritage List for England (NHLE) – the official record of nationally important historic buildings and sites in England (Fluck and Wiggins, 2017, p. 160). Extensive stretches of the frontier are located within urban areas. There are also a number of isolated associated elements that have yet to be designated and therefore are not officially apart of the Hadrian's Wall WH site (Hadrian's Wall Country, 2018d). The official WH site also excludes large extents of known archaeological remains discovered through aerial photography or geophysical survey which fall outside of the area designated as Scheduled Monuments. This is likely due to their presence being unknown at the time of scheduling. The unscheduled remains of Hadrian's Wall WH site, therefore, are not officially covered by legislation that affords protection to designated Scheduled Monuments. However, due to their association

with Hadrian's Wall WH site, should be given the same consideration regarding protection (Hadrian's Wall Country, 2018d).

The Scheduled remains of Hadrian's Wall WH site are protected by various legislation, including the Ancient Monuments and Archaeological Areas Act 1979, the Town and Country Planning Act 1990, and the Planning (Listed Buildings and Conservations Areas) Act 1990 (Hadrian's Wall Country, 2018c). Areas of the WH site, which have significant geological importance are also protected through the Site of Special Scientific Interest (SSSI) designation (Fluck and Wiggins 2017 p 161, Hadrian's Wall Country, 2018c), such as the Roman Wall Escarpment (Hadrian's Wall Country, 2018c). Those areas that coincide with National Parks and Areas of Outstanding Natural Beauty also receive the same protection given to such designations (Hadrian's Wall Country, 2018c). Local planning authorities include policies to protect the WH site (Hadrian's Wall Country, 2018c). The unscheduled remains are given consideration through the National Planning Policy Framework (NPPF) which mitigates impact from development projects (Fluck and Wiggins, 2017, p. 162).

While the Hadrian's Wall complex has been a part of the landscape for the past c.1900 years, it does not survive in its entirety. Over time, parts of the cultural WH site and associated unlisted remains have been subjected to change by human actions, including deliberate destruction of the Wall. Agricultural practices, pillaging of stones for building material, roads, pipelines, canal and railway works, quarrying, and the creation of a reservoir have led to partial loss and in some instances complete destruction (Hadrian's Wall Country, 2018b). In addition, natural processes such as erosion of river banks, coastal erosion and landslips have caused damage to the Hadrian's Wall complex (Hadrian's Wall Country, 2008, p. 54).

2.3.3 Heritage at Risk

Currently, of the 190 scheduled monuments from the Hadrian's Wall WH site, 23 were included on the Heritage at Risk (HAR) 2021 registers for North West and North East and Yorkshire (Historic England, 2021b; Historic England, 2021a). These sites were considered susceptible to a number of threats including animal burrowing, arable ploughing, coastal/stock/visitor erosion, development requiring planning permission, plant growth/bracken/scrub/tree growth, loose stone work/unconsolidated sections of the Wall and unlicensed metal detection (Historic England, 2021b; Historic England, 2021a). The HAR included *Beckfoot Roman Fort* (SM 1007170) for being under threat from arable ploughing (Historic England, 2021b, p. 11) and *Roman fortlet 40 metres SSW of Castle Fields*, otherwise

referred to as Milefortlet 15 in this thesis, (1007171) due to extensive significant problems caused by coastal erosion (Historic England, 2021b, p. 11).

2.3.4 Natural hazards

Destruction from natural hazard may be exemplified at Willowford, Cumbria where the Wall crossed the River Irthing on a bridge. Due to river migration and a consequence of flooding the remains of the bridge no longer stand (Bidwell and Holbrook, 1989). This was paralleled at Chesters and Corbridge. At Corbridge mitigation work in response to river dynamics was undertaken to relocate what was remaining of the Roman Bridge to above the known flood level of the River Tyne (Hadrian's Wall Country, 2008, p. 48).

While the Tyne River at Corbridge has flooded the surrounding landscape on a number of occasions throughout history, inundation is not the main threat. As Corbridge Roman town, was located on elevated land, its archaeological remains are believed to be safe from flooding and inundation. Rather, the threat from arable ploughing on the land surrounding the English Heritage property boundary poses greater threat to the archaeological remains at this location. As such soil creep and other types of soil erosion, due to the sloped topography in combination with the farming practices and unfavourable weather conditions put the buried archaeological remains of the Roman town at risk.

Fluvial erosion of the River Irthing and the River Tyne, which may be exacerbated by increased and/or intense rainfall still threaten the archaeology of Hadrian's Wall today. Archaeological remains along the River Irthing of particular concern are those associated with Birdoswald Roman fort including the remains of a Roman cremation cemetery and Harrowscar Milecastle (Hadrian's Wall Country, 2008, p. 47). Birdoswald Roman fort was located on a spur of land with a steep slope down to the River Irthing. Continual undercutting of the river bank along with water seepage into the boulder clay has resulted in slope instability inducing landslide at a number of locations along the cliff crest (Wilmott, 1997, p. 2). At Chesters Roman fort, located on the River North Tyne, the remains of walls associated with buildings from the extramural settlement were visible in the eroding river bank (Symonds and Mason, 2009a). Evidence from geophysical survey undertaken at Chesters also suggested that the area to the east of the fort is at threat from fluvial erosion (Symonds and Mason, 2009b, pp. 29 - 30). In addition, fluvial erosion of the Cam Beck has resulted in the loss of the northwest front of Castlesteads Roman fort (Symonds and Mason, 2009a, p. 91).

Coastal erosion threaten a number of sites along the Cumbrian coast. These include Bowness-on-Solway (Symonds and Mason, 2009a, p. 99), Ravenglass (Hadrian's Wall Country, 2008, p. 48; Symonds and Mason, 2009b, p. 106), Burrow Walls (Symonds and Mason, 2009b, pp. 63, 104 - 105), and Beckfoot Roman cremation cemetery (Hadrian's Wall Country, 2008, p. 48; Symonds and Mason, 2009b, pp. 136 - 140) which is also the conjectured location of Milefortlet 15. There has been very limited evidence for Milefortlet 15. It is therefore believed to have been lost to the sea (Bellhouse, 1957, p. 22). Coastal erosion at Beckfoot continues to present a threat to the sand dune system and the remains of the Roman cremation cemetery buried within them.

The anaerobic soil conditions found at Magna Roman fort are believed to be at risk from rising temperatures causing a change in the wetting and drying cycles (Guiney *et al.*, 2021, p. 2). This poses a threat to the preservation of the archaeological remains buried within these soils (Guiney *et al.*, 2021, p. 2). The threat the archaeological preservation within these soils is further escalated by water-driven soil erosion during wet periods (Guiney *et al.*, 2021, p. 3).

2.3.5 Anticipated climate change impacts

Climate change, in particular, is thought to be a major long-term risk to Hadrian's Wall WH site (Hadrian's Wall Country, 2008, p. 47). Concerns over fire risk to the WH site and its wider landscape, due to an expected decrease in summer precipitation and increase in temperature have also been raised (Hadrian's Wall Country, 2008, p. 48). In addition, climate change mitigation strategies, which may be the result of legally binding directives, could also have negative impact upon this cultural heritage landscape and its OUV. Additional environmental threats including physical changes associated with severe precipitation, wind, relative temperature or humidity, compression, dewatering, chemical change due to pollutants, acidification and corrosion, and biological change from microbial, invasive plants, insects and invertebrates, larger burrowing and roosting animals (Croft, 2013, p. 3) could also pose conservation issues for Hadrian's Wall WH site.

2.3.6 Relevant geospatial studies

Geospatial data, technologies and methods have provided invaluable tools in understanding the archaeology of Hadrian's Wall. Many geospatial studies associated with the Wall have generally been applied in the context of site prospection. Few studies have focused on land

surface dynamics and the impacts of natural hazards on the preservation of the archaeological record. Those that have, are discussed below.

A team of researchers from Newcastle University built multi-temporal 3D models and orthomosaics from archived aerial images. This was completed for three locations (Beckfoot, Birdoswald and Corbridge) within the Hadrian's Wall WH site with the aim of providing enhanced 4D digital products to assess coastal, fluvial and soil erosion (Fieber *et al.*, 2017). Peppa *et al.* (2018, p. 869) presented an image enhancement workflow coupled with Structure-from-Motion-Multi-View-Stereo (SfM-MVS) for 3D/2D feature location detection from both visible and near infrared archived aerial photographs. This was undertaken for three epochs dating to 1984, 2006 and 2016 for Corbridge Roman town (Peppa *et al.*, 2018, p. 870). As part of this study DEM differencing was undertaken to quantify elevation change between epoch pairs in order to identify change associated with fluvial erosion (Peppa *et al.*, 2018, p. 871). However, change identified in the results was interpreted as being indicative of crop change due to time of year that the varying datasets were acquired or was the product of registration error (Peppa *et al.*, 2018, p. 871).

At Magna Roman fort, Guiney *et al.* (2021) assessed the Roman hydraulic system through comparison of archaeological evidence with a parallel found at Vindolanda. In addition, the Revised Universal Soil Loss Equation (RUSLE) was applied to predict spatial pattern of soil erosion (Guiney et al., 2021, p. 3). The aim of the project was to characterise physical landscape change through time to facilitate improved management (Guiney et al., 2021, p. 2).

A focus of the Hadrian's Wall Community Archaeology Project (WallCAP), led by Rob Collins, was to research and conserve heritage at risk along the Wall (Collins and Symonds, 2019, p. 12). An aim of the project was the removal of at risk sites from the HAR registers where possible (Collins *et al.*, 2018, p. 37). In addition, WallCAP aimed to build a bespoke Hadrian's Wall geographic information system (WallGIS) for the purpose of providing an overarching management system (Collins *et al.*, 2018, p. 39).

Hadrian's Wall WH site was subjected to the Aerial Investigation and Mapping (formerly the National Mapping Programme) which undertook digital mapping mainly from evidence identified on aerial photographs to enhance the archaeological record (Oakey, 2009, p. 1 –

3). According to Oakey (2009, p. 15) understanding coastal erosion through the examination of historic photography at Beckfoot formed part of this work.

A vulnerability index for coastal heritage assets from the NHLE database which includes WH sites, registered battlefields, registered parks and gardens, scheduled monuments, listed buildings protected wrecks and heritage at risks was created by Land Use Consultants (LUC) in 2019 (Land Use Consultants, 2019). A scoring system was devised to assess the likely level of effect experienced by the heritage asset in relation to erosion, flooding and sea level rise (Land Use Consultants, 2019, p. 15). This was based on a heritage assets importance, sensitivity to change and magnitude of predicted change (Land Use Consultants, 2019, p. 15). If the heritage asset was also on the HAR register, a weighting was applied to reflect this fact (Land Use Consultants, 2019, p. 15). The results for Hadrian's Wall WH site showed that it was at risk from coastal flooding and erosion but the level of risk was considered low (Land Use Consultants, 2019, p. 57). This was due to the fact that the assessment was conducted on the Hadrian's Wall WH property in its entirety (Land Use Consultants, 2019, p. 57). Therefore the extent of the affected area was small in relation to the whole complex (Land Use Consultants, 2019, p. 57). However, if these coastal sites which form part of the Hadrian's Wall WH site were scored in isolation, they likely would have received a higher value for level of risk.

2.4 Conclusion

Cultural WH properties from around the globe, including Hadrian's Wall WH site, are being adversely impacted upon by natural hazards which are being exacerbated by climate change. These hazards have the ability to cause irreversible loss and destruction to cultural WH through erosive process of the soils in which archaeological remains are buried. This can lead to a degradation of integrity, authenticity and OUV. Depending on the level of impact, the ultimate consequence a natural hazard can have on a cultural WH property is delisting. This also has other negative societal impact as cultural heritage are a highly valued heritage assets amongst both academic communities and the general public. Current impact assessment methods are insufficient in that these methods do not attempt to quantify or predict impact through scientific measurement of quantities and rates of change. Rather these methods offer a starting point to conceptualise the problem through subjective observation. There is a clear need for approaches based on scientific observation and

prediction, not as a replacement, but to follow on where risk is perceived to be medium or high.

Due to the wealth of spatial legacy data now available, advances in remote sensing technologies and computer applications, geospatial sciences offers solutions for addressing impact from natural hazards. The following chapter reviews current methods available for assessing geomorphic change. It also provides an assessment of the various data types available for constructing a spatiotemporal time series. The chapter then focuses on modelling practices as these provide a means for predicting and simulating future change.

Chapter 3: Spatiotemporal analysis: measuring past and future changes to the Earth's surface

3.1 Introduction

Accurate representations of topography have been recorded by a variety of means for the past c. 200 years. This has been achieved through scientific mapping, captured by imagery sensors and recorded by lidar. These topographic datasets can be complied into a spatiotemporal time series for the purpose of applying change detection techniques in order to reveal alterations to the terrain. This allows for a diachronic comparison of the Earth's surface by measuring: the difference in the horizontal position of a feature; the difference in height between two epochs containing elevation values; or the distance between two point clouds along the surface normals. The purpose of such an analysis is to identify and quantify patterns of past geomorphic change resulting from a physical processes interacting with the Earth's surface. Depending on context, the change may be attributed to natural hazards. For example, cliff recession caused by a landslide may present itself as a change in the horizontal position of the cliff edge, or as areas of surface lowering and rising associated with erosion or deposition, respectively. The results from change detection analyses can be used to infer impact from natural hazards to cultural WH through comparison to the known archaeological record. The results may also be used to inform predictive models to understand future impact from ongoing threats. Through the application of appropriate predictive models, an understanding of potential future rates and directions of change can be derived.

This chapter is presented across four main sections. Section 3.2 presents a review of the data sources that contribute to a spatiotemporal time series for analysis of geomorphic change. Section 3.3 details methods for quantifying past geomorphic change, while Section 3.4 introduces the reader to concepts of modelling future geomorphic change. The final section of the chapter, section 3.5, examines the use of change detection and modelling of natural hazards specifically within archaeological research.

3.2 Quantifying past geomorphic change

3.2.1 Definition

Change detection provides methods for analysing the alterations to the Earth's surface that occurred in the past. Many reviews on change detection (Lu *et al.*, 2004, p. 2366; Hussain *et*

al., 2013, p. 91; Qin *et al.*, 2016, p. 41; Okyay *et al.*, 2019, p. 2) follow Singh's (1989, p. 989) definition who describes change detection as *…the process of identifying differences in the state of an object or phenomenon by observing it at different times*. As such, change detection of the surface of the Earth relies on a spatiotemporal time series that is composed of a minimum of two spatially aligned epochs of varying dates, each representing the same location on Earth (Lu *et al.*, 2004, p. 2366). By applying change detection algorithms to a spatiotemporal time series of topography consecutively on a pairwise basis, differences in terrain surface can be tracked through time. Where those differences exceed a certain threshold level, they are considered to have been real change as opposed to noise that occurred due to error and/or uncertainty in the datasets.

3.2.2 Pre-requisites to geomorphic change detection

Co-registration is a fundamental prerequisite for accurate change detection (Singh, 1989, p. 990; Lu *et al.*, 2004, p. 2366) that involves spatially aligning all epochs in a time series to one another. For scanned images of 2D topographic data, such as OS historic maps, this can be achieved through georeferencing to a common coordinate system (See Chapter 4 Section 4.4.1). For data collected for the purpose of 3D reconstruction of the Earth's Surface, such as airborne lidar or Remotely Piloted Aircraft Systems (RPAS) photographs, initial approximate alignment is provided either through direct or indirect georeferencing means. Subsequent co-registration is required in order to reduce alignment error which may exists between epochs. Fine co-registration methods such as least squares surface matching (Miller *et al.,* 2008), morphology-based co-registration (Peppa *et al.,* 2019) and Iterative Closest Point (ICP) (Chen and Medioni, 1991; Besl and McKay, 1992) have been developed for this purpose. For 3D models (Rusinkiewicz and Levoy, 2001, p. 1) and point clouds (Li *et al.,* 2020 p. 68030), Iterative Closest Point (ICP) is the most commonly used co-registration method. The purpose of the ICP algorithm is to optimally align two or more overlapping point clouds (Glira *et al.*, 2015, p. 276), based on inherent geometric properties (Rusinkiewicz and Levoy, 2001, p. 1).

The ICP algorithm was introduced in the early nineties by Chen and Medioni (1991) and Besl and McKay (1992) (Glira *et al.*, 2015, p. 277). Chen and Medioni (1991, p. 2724) proposed a method to build a 3D model of an object based on combining multiple view range data. Their method assumed an initial approximate transformation (Chen and Medioni, 1991, p. 2723) followed by an iterative process that minimized the least square error based on point to

plane distances (Chen and Medioni, 1991, p. 2724). ICP has since gone through several improvements, demonstrated by numerous variations of the algorithm (Pomerleau *et al.*, 2015, p. 7), and is now considered a comprehensive registration method (Cheng *et al.*, 2018, p. 2).

Prior to applying the ICP algorithm, point cloud epochs need to be coarsely registered to one another (Nguyen *et al.*, 2020, p. 2). This means that the initial relative orientation of the point clouds need to be adequately estimated (Glira *et al.*, 2015, p. 277). As mentioned in the above paragraph, this can the can be achieved through direct or indirect georeferencing means. Direct georeferencing is provided by an on board Position and Orientation System (POS) (see section 3.2.1), while indirect georeferencing requires the applications of Ground Control Points (GCP) to provide spatial location and scale.

Once two or more point clouds are coarsely registered to one another, fine registration can be completed through the application of an algorithm, such as ICP. According to Glira *et al.* (2015), there are 5 steps, 6, if the convergence criterion test is included, in the application of the ICP algorithm offered by Orientation and Processing of Airborne Laser Scanning data (OPALS) software, used to co-register a 'loose' point cloud to a 'fixed' point cloud. These are:

1. Selection: point selection for determining correspondence between the point clouds. This can be done through random selection, through a uniform selection based on the closest point to centre of a voxel structure, or through a maximum leverage sampling strategy that selects points based on the distribution of the point's normal in angular space.

2. Matching: this step establishes the correspondence of points from step 1 to matching points in the 'fixed' point cloud.

3. Rejection: outliers are filtered out of the calculation, based on the distances between corresponding points.

4. Minimisation: transformation parameters are estimated by minimizing distances between corresponding points.

5. Transformation: There are five types of transformation. These include zShift (only computes the shift along the vertical direction), shifts (computes a 3D shift), rigid (this is a 6 parameter transformation which includes 3 rotations and 3 shifts), helmert (this is a 7 parameter transformation, same as the previous but also includes scale) and full (this is a 3D 12 parameter affine transformation). In the case of airborne lidar

rigid should suffice, however, if errors are present in the data a full transformation may be required (Glira *et al.*, 2015).

6. Convergence criterion test: the steps are repeated until the convergence criteria has been met.

3.2.3 Methods

An overwhelming number of change detection methods are 2D image based techniques that have been developed for use in satellite remote sensing applications (Chughtai *et al.*, 2021, p. 1). This is due to the repetitive acquisition (Singh, 1989, p. 989; Lu *et al.*, 2004, p. 2366), taken in short equally spaced intervals, consistent image quality (Singh, 1989, p. 989), synoptic viewing and the digital format offered by satellite imagery (Lu *et al.*, 2004, p. 2366). Two-dimensional image based techniques include both traditional pixel-based methods and more recent object-based methods, which detect differences in radiance (Singh, 1989) or spectra (Okyay *et al.*, 2019, p. 2). These methods require that the imagery was collected from the same sensor with the same radiometric and spatial resolution (Lu *et al.*, 2004, p. 2369). In addition, Lu *et al.* (2004, p. 2369) state that epochs should have anniversary acquisition dates so as not to introduce error from changes in the angle of the sun, seasons, or phenology. The restriction of sensor type also restricts the temporal range of the time series to that of the satellites mission length. In addition, according to Qin *et al.* (2016, p. 41) change detection studies that used very high resolution satellite images (0.3 – 1 m) were found to suffer from the higher spectral variability in addition to perspective distortions (Qin *et al.*, 2016, p. 42). Finally, these image-based methods are unable to calculate volumetric measurements of change due to the lack of elevation data (Qin *et al.*, 2016, p. 42) therefore, applications requiring the third dimension, such as 3D deformation analysis, cannot be undertaken.

While advancements continue to be made in satellite remote sensing change detection (Lu *et al.*, 2004, p. 2367), alternative 2D, 2.5D and 3D methods have also been developed to study geomorphological changes. Multi-temporal geospatial input data for these methods can be derived from various sources (see section 3.2). Two-dimensional geomorphic change detection measures the difference in the planar position of a series of vectorised boundary features (Williams, 2012, p. 2), for example, between a time series of the mean high water mark positions. Both 2.5D and 3D change detection are achieved with the addition of elevation (Z) values mapped to XY positions (Qin *et al.*, 2016, p. 41). The addition of the third

dimensions allows for height differencing, areal and volumetric calculations and measurements of 3D Euclidean distances (Qin *et al.*, 2016, p. 46). The results of these various geomorphic change detection methods can be interpreted as retreat/surface lowering/erosion or advancement/surface raising/deposition/accretion. Through comparison with historic data such as weather events, and sea level records, the cause of change can be also sometimes be inferred (Williams, 2012, p. 1).

3.2.3.1 2D geomorphic change detection

Measuring the changes in the planar position of a series of vectorised shoreline features is a form of Historic Trend Analysis (HTA) (Oyedotun, 2014, p. 2). This can be extended to any boundary data that can be represented as a vector polyline. HTA is a data driven method (HR Wallingford *et al.*, 2006, p. 27) used in geomorphology to identify directional morphological trends, including rates of change statistics, from a time series representing either a physical process (i.e. mean high water mark) or morphological features (i.e. edge of a coastal cliff) (HR Wallingford *et al.*, 2006, p. 65). HTA calculations are based on the planar positions of the physical process/morphological feature over time in relation to a baseline, allowing for the detection of changes in the horizontal position. HTA calculations are independent of the drivers for change (Blott *et al.*, 2006, p. 186), however, the driving forces causing the measured change should be considered in the interpretation (HR Wallingford *et al.*, 2006, p. 65). HTA is commonly used for shoreline change detection, however, it can be applied to any morphological change that can take the form of a vectorised boundary line. The analysis is generally computed on times scales of decades to centuries (HR Wallingford *et al.*, 2006, p. 65). In the UK the technique is often used to assess changes in estuarine environments (HR Wallingford *et al.*, 2006, p. 66) and is considered a useful tool for assessing historical change rates to help anticipate future changes (HR Wallingford *et al.*, 2006, p. 66; Oyedotun, 2014, p. 2). The drawback of this method is that it does not provide a means for areal and volumetric quantification, which is offered by Digital Elevation Model (DEM) differencing. However, benefits of such an analysis is that information from historic maps can also be included in the analysis, extending the temporal range further into the past (James *et al.*, 2012, p. 198; Sutherland, 2012, p. 189).

3.2.3.2 2.5D geomorphic change detection

Since the early 1990's repeat topographic surveys have been used to produce DEMs for the purpose of differencing to measure changes in elevation (Wheaton *et al.*, 2010, p. 136). This

calculation is referred to as DEM differencing. DEM differencing is a 2.5D geomorphic change detection method, which requires multi-epoch topographic data to contain elevation information. Elevation can be inherent in the spatial data, as is the case for laser scanned point clouds, or can be reconstructed from overlapping images of the same scene and captured on the same date, using a Structure-from-Motion-Multi-View-Stereo (SfM-MVS) workflow. The topographic data representing the ground (i.e. the above ground points classified as buildings, vegetation etc. have been removed from the point cloud) from each time step is transformed into a raster DEM through interpolation where each pixel in the raster DEM contains a value representing elevation. Once transformed, the old DEM is subtracted from the new DEM (Equation 1) (Wheaton *et al.*, 2010, p. 138; Williams, 2012, p. 2). The calculation is carried out on a pixel-by-pixel basis (Wheaton *et al.,* 2010 p. 138; Lague *et al.*, 2013, p. 4) resulting in a DEM of Difference (DoD) - a raster map depicting a change in elevation indicating surface lowering, surface raising or no change. As mentioned in section 3.2.3, a negative value may be associated with surface lowering, retreat or erosion, while a positive value may represent surface raising, advancement, deposition or accretion. Aggregating the elevation changes through budget segregation polygons produces areal and volumetric measurements.

$\delta E = Z\_nDEM - Z\_oDEM$ (Equation 1)

Where δE is the output DEM containing the change values, Z_nDEM is the new DEM and Z_oDEM is the old DEM (Williams, 2012, p. 2).

According to *Essential best practices guidelines to support change detection* (Riverscapes Consortium, 2020), for accurate results, the multi-temporal DEMs must be orthogonal, concurrent and share the same resolution. This means that the raster DEMs that are being differenced need to be vertically/horizontally aligned and the pixels from each need to share the same spatial resolution and grid centres (Riverscapes Consortium, 2020). In addition, DEM error or uncertainty should be evaluated and included in the change detection calculation in order to distinguish real geomorphic change from noise (Wheaton *et al.* 2010, p. 136).

Error exists in DEMs for multiple reasons, including those associated with sampling strategies, topographic complexity, geodetic control, survey point precision, processing methods, interpolation and resolution of the dataset (Wheaton *et al.*, 2010, p. 137).

Applying a minimum level of detection threshold, a user defined value for a spatially uniform error surface, is the most common way of dealing with uncertainties in DEMs (Wheaton *et al.*, 2010, p. 137). If change is detected below this threshold, it is discarded as being noise and does not represent real change (Wheaton *et al.*, 2010, p. 137). This approach to error can lead to either an over or under estimation of real change due to an inappropriate minimum level of detection threshold.

A disadvantage of DEM differencing is that it is not truly a 3D method. It therefore requires additional processing to convert the 3D vector data to a 2.5D raster. Interpolation, is therefore, a required step, increasing processing time. Interpolation can be a time-consuming task, especially when working with a long time series comprised of high resolution datasets which cover a large geographic region. In addition, conversion from a vector point cloud to a raster surface over simplifies steep slopes due to interpolation methods decreasing the density of topographic information proportionally to surface steepness (Lague *et al.*, 2013, p. 4). This means that topographic variation decreases as slope steepness increases. In addition, overhanging topographic details will be lost in the interpolated DEM as 2.5D raster surfaces are unable to cope with this kind of geometry. Therefore, DEM differencing results, present on the DoD, are less accurate for vertical surfaces and more accurate for horizontal surface.

3.2.3.3 3D geomorphic change detection

Alternative methods to DEM differencing include cloud-to-cloud comparison (C2C), cloud-to-mesh comparison (C2M) and multiscale model-to-model cloud comparison (M3C2). These alternative methods are considered 3D change detection techniques as interpolation of the point cloud to raster DEM is not required. Calculations are performed using the point clouds themselves. Although, the C2M method relies on one of the two epochs to be meshed. Like interpolation to raster DEM, meshing can be a time consuming and computationally intensive task requiring advanced skills, particularly when converting large, complex point clouds (Girardeau-Montaut *et al.,* 2005, p. 31). Meshing is made more difficult if the point cloud roughness is large at all scales and if the point cloud contains occlusions (Lague *et al.*, 2013, p. 5). As this approach works best on horizontal surfaces, Barnhart and Crosby (2013, p. 2815) recommended segmenting surfaces based on orientation prior to C2M when the surface contains significant variations in orientation.

The C2C method calculates distances between two point clouds minimizing processing time as neither point cloud epoch requires interpolation or meshing. In the C2C method distances are measured based on the principal of nearest neighbour. Lague *et al.* (2013, p. 12) demonstrated that this method is sensitive to cloud roughness, outliers and point spacing and advised that it should only be applied for its original intended use - for rapid change detection on very dense point clouds.

The M3C2 method also calculates distance between two point clouds, however, in contrast to C2C, the M3C2 distance measurements are based on the surface normals of the reference point cloud.
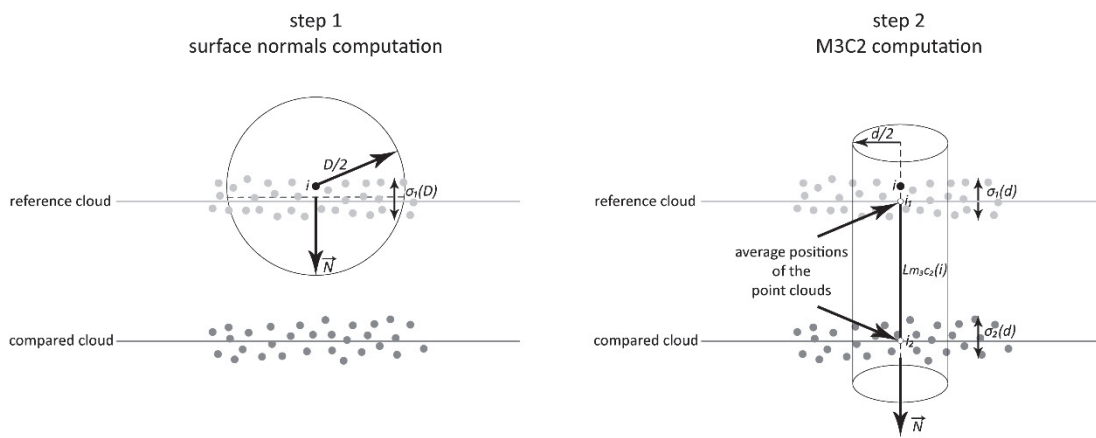
Figure 3.1: Conceptual diagram of M3C2 algorithm (Adapted from an original figure that was published in Lague *et al.,* 2013, p. 14, Copyright Elsevier (2013)).

The M3C2 algorithm can be broken down into two steps (Fig. 3.1). First the normals are calculated for each of the core points in the reference cloud. Secondly, the distance, based on the normal vector, calculated in the first step, and the associated average position of each cloud, are measured between the reference cloud and the compared cloud.

In step one, the normal vector $(\vec{N})$ of each core point, i, in the reference cloud, Ref$_{cloud}$, is calculated (Lague *et al.,* 2013, p. 14). Core points are a subset of points from the reference cloud based on minimum point spacing specified by the user (Lague *et al.,* 2013, p. 13). The user may instead choose to use the reference cloud in its entirety in which case processing time is increased as every point in the reference cloud is considered a core point (Lague *et al.,* 2013, p. 13). For each core point a $\vec{N}$ is defined based on a neighbourhood of points (NN) that fall within a user specified radius ($D/2$) around the core point (i) (Lague *et al.,* 2013, p. 14). Local cloud roughness $\sigma_i(D)$ is measured by recording the standard deviation of the distance of the neighbours NN_i to the best fit plane (Lague et al., 2013, p. 14). According to

Lague *et al.* (2013 p. 15) *D* should be twenty to twenty-five times the roughness of the reference cloud as the uncertainty becomes insignificant around these stated values. Alternatively, the optimal value for *D* can be determined by M3C2 by using a range of scales selected by the user (Lague *et al.,* 2013, p. 15). The scale at which a plane best fits the 3D surface, based on the results of Principal Component Analysis (PCA), will be selected for determining the $\vec{N}$ (Lague *et al.,* 2013, p. 15).

In step two, cylinders with a user defined radius *d*/2, each with their axis intercepting the reference cloud at a core point and aligning with the associated $\vec{N}$ is extended through the reference cloud and the compared cloud (Lague *et al.,* 2013 p. 14). The distributions of the subset of points from each cloud selected from inside the cylinder are then used to calculate their average positions (i_1 and i_2) along the $\vec{N}$ (Lague *et al.,* 2013, p. 14). These averaged positions are used to calculate a distance measurement $L_{M3C2}(i)$ (Lague *et al.,* 2013, p. 14). The standard deviation $\sigma_1(d)$ and $\sigma_2(d)$ of the subset clouds are also recorded giving an indication of point cloud roughness along the $\vec{N}$ (Lague *et al.,* 2013, p. 14). The roughness measurements along with point density and registration error are used to calculate a spatially variable confidence interval for each measurement (Lague *et al.,* 2013, p. 15). According to the authors (Lague *et al.*, 2013, p. 24) *d* should be large enough to average at least twenty points, but not too large that it leads to degradation of the measurement resolution by spatial averaging.

3.2.4 Spatiotemporal time series

A spatiotemporal time series is a collection of data representing the same geographic location captured at different points in time. Compiling an extended spatiotemporal time series is made possible through the use of heterogeneous datasets, as each has a different, although sometimes overlapping, temporal range. Therefore, by incorporating multi source spatial data, the temporal range can be extended beyond that of a single data source. Historic maps, aerial photographs, satellite imagery, and lidar have captured detailed snapshots in time of past representations of the Earth's surface and therefore are ideal. Each dataset also has a specific temporal scale due to technological advancements leading to new ways of capturing topographic data. Historic maps stretch a spatiotemporal time series furthest into the past, followed by aerial photograph, satellite imagery and finally lidar. Together, these datasets form a spatiotemporal time series that enable four-dimensional (the 4th dimension being time) analyses of historic landscape change. In the UK this allows us

to extend into the past by up to 175 years, depending upon regional location and data availability.

The following section discusses the spatiotemporal data that provides good sources of topographic information for geomorphic change detection. In order to efficiently and effectively utilise this data for geomorphic change detection, the properties, including extent and accuracy of each of these datasets needs to be understood. The data presented here offer complete or near complete coverage of the UK and include Ordnance Survey (OS) historic maps, archived aerial photography and airborne lidar. A spatiotemporal time series composed of these data sources can be supplemented with targeted topographic surveys from ground based methods and low altitude aerial based methods such as terrestrial laser scanning and RPAS lidar/photography. The temporal ranges of each of the data sources are specific to England, however other details may be common amongst data type regardless of geographic location. Satellite imagery has not been discussed in further detail as it was not used in this research due to the low resolution of the freely available imagery. The following section explores each of the three datasets in turn with a view to incorporate each within a wider spatiotemporal time series (see Chapter 4).

3.2.4.1 Historic Maps

OS historic maps extend a spatiotemporal time series the furthest into the past, which allows for the establishment of trends over a longer duration. Due to developments in survey methodology and technology, OS historic maps provide the earliest accurate depiction of topography that pre-date other types of cartographic representations. Maps which predate the OS, are not suitable for quantitative analysis but may have potential for assessing general geomorphological trends (Sutherland, 2012, p. 189).

Little is known about the mapping methods of early (prior to 1750) cartographic outputs (Carr, 1962 p. 135). Many of these early maps emphasised aesthetics over spatial accuracy (Carr, 1962 p. 135). John Speed's (1610) Map of Cumberland, for example contains several decorative elements such as a picture frame border, coat of arms, vignettes, ships and isometric drawing of stone altars. The detail of the map shows physical features such as hills, mountains, rivers, parks, and forests, as well as place-names and symbols marking the location of significant places, such as cathedrals, churches and settlements. The map also depicts the line of Hadrian's Wall, labelled as '*THE PICTS WALL*', and an inset detail map of Carlisle. While there is a clear definition between the land and the sea, there is no way of

establishing what proxy was used to represent the shoreline. While Speed's map does contains a scale bar, the map provides an approximate depiction rather than an accurate measurements. For these reasons, it is advised that these early maps be used with caution and for qualitative purposes (Carr, 1962 p. 142).

To properly utilise historic maps within a topographic time series it is important to understand the development of OS mapping over time and consider the relative accuracy of the different map series.

The origins of accurate mapping methods within the UK began with the triangulation that connected the observatory of Greenwich geodetically with the observatory of Paris (Close, 1969, p. 12), which was undertaken to clarify their relative geographic positions (Oliver, 1993, p. 15; Higley, 2011, p. 1). This work was completed on the 17th of October 1787 (Close, 1969, p. 21). The British side employed a Ramsden theodolite, known as the 3-ft Theodolite R.S (Close, 1969) and referred to as the *father of accurate theodolites* (Close, 1969, p. 15). The survey was conducted under the direction of Major-General William Roy of the Royal Engineers (Oliver, 1993, p. 15). This triangulation connecting the two observatories became was gradually extended and covered most Britain by 1823 (Oilver, 1993, p. 16). According to Higley, 2011, p. 2) this extension in part due to need for highly accurate maps in response to the threat of invasion of the southern coast of England during war with France in 1793. As triangulation continued across the British Isles, surveyors followed behind creating maps from the network of fixed points (Higley, 2011, p. 2). These early OS maps, which cover all of England and Wales, with the exceptions of the Scilly Isles, were later referred to as the Old Series maps (Oliver, 2013, p. 51).

The Old Series maps were produced by OS at a scale of 1:63,630 (Oliver, 2013, p. 51), (1 inch to 1 mile) (Harley, 1975, p. 17). Work on the Old Series first began in 1795 with the topographic survey of Kent (Harley, 1964, p. 7). The Map of Kent, was the first OS map published privately by William Faden in 1801 (Oliver, 2013, p. 51; Harley, 1964, p. 7). The one inch scale became the standard scale for mapping with the intention of providing national coverage, starting with the southern counties before moving to the north (Harley, 1964, p. 9).

By the time the survey reached the northern counties, work on the County Series had begun. As such, the Old Series maps of counties north of the Preston-Hull line were reduced from

the County Series maps that consisted of 6 inch and 25 inch to 1 mile maps (Harley, 1964, p.9). The 6 inch to a mile scale was first adopted in 1840 after successful implementation in the mapping of Ireland (Harley, 1964, p. 9). While this 6 inch to 1 mile scale was recognised as being superior to its predecessor as it provided greater detail, it was inadequate for all mapping needs (Harley, 1975, p.3). After roughly a 20 year debate knowns as the *Battle of the Scales*, it was decided, in 1858, that the 6 inch scale would be retained for uncultivated areas, that the 25 inch scale would be used for rural districts, and a scale of 1:500 would be used for towns exceeding a population of 4000 or more (Halrey , 1964, p. 9; Harley, 1975, p.3). In 1863, survey work began on counties south of the Preston-Hall line to map at a scale of 25 inch to the mile for reduction to 1 inch to the mile (Higley, 2011, p. 30). These reduced maps then formed the New Series (Higley, 2011, p. 30).

The Old Series and early County Series maps of England and Wales were mapped to a number of independent Cassini projections using multiple central meridians (Harley, 1975, p. 16). This projection was used by the OS until 1945 when it was succeeded with a modified version of the Transverse Mercator (Harley, 1975, p. 17; Higley, 2011, p. 15). The purpose of employing multiple central meridians was to mitigate against distortion associated with the Cassini and other transverse cylindrical projections (Higley, 2011, p. 15). The Cassini projection's scale along the central meridian and at right angles to it remained true, however, the scale was increasingly distorted north to south with the square of the distance from the meridian, making it unsuitable for land masses with a great longitudinal extent (Harley, 1975, p. 17) and large areas at scales greater than or equal to 1:10560 (Oliver, 1993, p. 27). For example, if Great Britain were to adopt a Cassini projection, which used only one central meridian, the eastern and western extents of the country would be lengthened by approximately 0.1 per cent in the north and south directions (Harley, 1975, p. 19).

While there were a variety of theories regarding the number of meridians used for the Old Series maps, including one meridian for the whole of England and Wales, or six separate meridians for the maps sheets between Greenwich and Devon, these theories were unlikely (Harley, 1975, p. 17). Rather, there were likely two central meridians for maps sheets of southern England (Butterton Hill and Greenwich), and one for those covering the area north of the Preston-Hull line, (Delamere) (Harley, 1975, p. 17; Higley, 2011, p. 27).

As mentioned above, prior to the adoption of the National Grid, the early County Series maps also used the Cassini projection and several central meridians (Harley, 1975; Oliver,

1993; Higley, 2011, p. 100). Many of these meridians were county specific, although in some cases multiple counties shared the same meridian (Harley, 1975, p. 17; Higley, 2011, p. 100; Oliver, 2013, p. 27). Again, this was to minimize distortion associated with the Cassini projection (Oliver, 2013, p. 27). While, multiple meridians may have decreased distortions associated with the Cassini projection, problems soon arose. This method led to discontinuities at county boundaries (Harley, 1975, p. 18). In addition, it hindered an integrated referencing system for the whole of the UK (Harley, 1975, p. 18).

The Davidson Committee (1935 – 38) was selected to address the issue of OS-mapping being outdated (Oliver, 2013, p. 25). In 1938, the Committee made a number of recommendations. These included: 1. All OS maps be re-casted on a metric grid using the Transverse Mercator projection (Oliver, 2013, p. 19), thuse creating a National Grid; 2. Continuous revision of large scale maps; and 3. Experimental mapping over photo-enlargement at 1:1250 and 1:25 000 (Oliver, 2013, p. 19).

The Transverse Mercator projection was selected for the national referencing system of the United Kingdom as it was particularly suited for countries that had their greatest extents in the north-south direction (Harley, 1975, p. 19). This projection made it possible to map the entirety of Britain on a single central meridian (Oliver, 2013, p. 27), resolving issues associated with the several independent Cassini projections along with associated meridians. In contrast to the Cassini projection, Transverse Mercator, preserves shapes and angles within a map sheet as the scale is constant in all directions (Higley, 2011, p. 15, Harley, 1975, p. 19). Still, as with all projections, representing the surface of the Earth on a plane surface, distance and/or angle distortions are introduced (Higley, 2011, p. 15). For maps of Great Britain using the Transverse Mercator projection, distortion increased with an increase in distance from the origin (49° N, 2° W) in which the central meridian passes through (Higley, 2011, p. 15). To reduce this error a scale factor of 0.9996 was applied across the mapping area (Higley, 2011, p. 16).

The National Grid large-scale mapping program started in 1944 – 45 with an emphasis placed on mapping urban areas at 1:1250 and limited mapping at 1:2500 taking place (Oliver, 2013, p. 19). From 1962 to 1982, the focus was on mapping rural areas at 1:2500 and on continuous revision (Oliver, 2013, p. 19). In 1969, the OS replaced the 1:10560 maps with 1:10000, and the one inch maps with 1:50000 in order to adopt a metric unit of

measurement (Oliver, 2013, p. 19). This unit was also applied to contours and altitudes at this time (Oliver, 2013, p. 19).

Between 1991 and 1997, conventional paper publication of OS large-scale mapping was phased out in favour of digital mapping (Oliver, 2013, p. 26). OS maps thus no longer offered snapshots in time of landscapes on individual sheets (Oliver, 2013, p. 26). While the OS experimented with digital mapping practices as early as the late 1960's, 1973 marked the first digital production of an OS map at 1:2500 (Oliver, 2013, p. 20). The increase in the need for digital content, led to a digitising programme of OS maps which was completed in 1995 (Oliver, 2013, p. 26). Six years later, in 2001, OS launched OS MasterMap – a digital map providing a replacement for the former paper maps produced at 1:1250, 1:2500 and 1:1000 (Oliver, 2013, p. 26). With digital being the preferred over analogue, creating maps from aerial imagery, supplemented with ground survey became the dominate practice (Oliver, 2013, p. 26).

3.2.4.2 Aerial photography

Archived vertical and oblique aerial photographs exists in the millions. The National Collection of Aerial Photography (NCAP), the Historic England Archive and the Cambridge University Collection of Aerial Photography (CUCAP) together hold a combined total that exceeds 30 million aerial photographs, ranging in date from the early 19th century to present day. Aerial images held within these archives include those captured by the Royal Air Force, United States Army Air Force, German Luftwaffe, Royal Canadian Air Force, South African Air Force and Directorate of Overseas Surveys (National Collection of Aerial Photography, 2019), the Royal Commission of the Historical Monuments of England's (RCHME) Air Photo Unit (APU), the vertical aerial photograph collection from the Department of Environment, Meridan Airmaps Ltd, Ordnance Survey, the Aerofilm photographic collections (Grady, 2019) and the collection of JK St Joseph. A large portion of the aerial imagery within these archives were collected as stereoscopic pairs for photo interpretation using 3D views (Cowley *et al.*, 2013, p. 14).

Aerial photography began in the 1800's, with the first successfully captured aerial photographs taken by means of a balloon in 1858 by Parisian photographer Gaspard-Félix Tournachon of Val de Bievre near Paris (Barber, 2011 p. 66; Leisz, 2013, p. 7). The first known aerial photograph of an archaeological monument within the UK was that of

Stonehenge captured from a hot air military balloon in 1906 (Capper, 1907 p. 571; Barber, 2011, p. 3).

Rapid developments in aerial photography can be attributed to the invention of the aeroplane along with wartime efforts. While the first photograph captured from an aeroplane dated to 1908, advancements in camera technology, photographic methods and stereo imagery can be attributed to WWI (Aber *et al.*, 2010, p. 6). Throughout this time of war, cameras were mounted in aircrafts for purposes of gaining photographic intelligence on enemy lines (Aber *et al.*, 2010, p. 6). During the interwar period, aerial photography was exploited for civilian and commercial use, however, little progress was made until the next World War (Aber *et al.*, 2010, p. 6). WWII brought about further rapid advancements in technology and reconnaissance methods to improve aerial photography capabilities (Aber *et al.*, 2010, p. 6). Approximately 50 million aerial photographs were captured during WWII (Cassetari, 2004, p. 95). A great number of these photographs were taken as verticals for mapping purposes (Cassettari, 2004, p. 95).

After WWII, the RAF was commissioned to undertake an aerial survey of the whole UK on behalf of the OS (Cassetari, 2004, p. 96). This aerial mapping programme, starting in 1946, was named Revue (Cassetari, 2004, pp. 95 - 6). Aerial mapping by the OS continued until 1954, when it was stopped due the risk of sensitive locations, such as military and industrial sites, becoming common knowledge (Cassetari, 2004, p. 96). The OS began an aerial photo mapping programme of Great Britain again in 2002 (Cassetari, 2004, p. 96). These aerial photographs were published alongside OS MasterMap as continuous ortho-rectified images (Cassetari, 2004, p. 96).

The near vertical photographs taken during the mid-1940s by the RAF were captured along flight stripes in overlapping pairs. This method of capture, along with advancements in digital photogrammetry and computer vision, means that archived aerial photographs have the potential for 3D, 2.5D and 2D topographic reconstruction for inclusion in geomorphic change detection studies.

The International Society for Photogrammetry and Remote Sensing *Statutes 2019* (Statute II – Definitions) define photogrammetry as *the science and technology of extracting reliable three-dimensional geometric and thematic information, often over time, of objects and scenes from image and range data*. The application of photogrammetry, allows for accurate

and reliable measurements to be taken from imagery. Traditional photogrammetric methods require a series of overlapping images taken from the ground (terrestrial photogrammetry) or from the air (aerial photogrammetry) along with camera calibration parameters and control data, (to provide scale and/or spatial alignment to a coordinate system), in order to reconstruct a scene's or object's geometry using triangulation to map points in 3D space.

According to Polidori (2020, p. 894), while a number of prior innovations played a role in the emergence of photogrammetry, Colonel Aimé Laussedat, of the French Army Corps of Engineers, has often been cited as the *father of photogrammetry*. This recognition was owing to Laussedat's research on taking measurements in perspective view to improve accuracy and efficiency of topographic mapping methods (Polidori, 2020, p. 893). Lausesedat's novel approach was initially completed by hand using a camera lucida but later employed photographic images, thus making Laussedat the first person to use photographic images for topographic mapping purposes (Polidori, 2020, p. 893).

Structure-from-motion, multi-view-stereo (SfM-MVS) developed out of photogrammetry combined with 3D computer vision algorithms (Smith *et al.,* 2015, p. 251). SfM-MVS can reconstruct 3D geometry of a scene from a series of overlapping photographs acquired from multiple viewpoints (Smith *et al.*, 2015, p. 253) without imaging parameters and network geometry (Luo *et al.*, 2019, p. 20). This method contrasts traditional photogrammetric methods that require camera calibration parameters to be known (Sevara *et al.*, 2017, p. 613; Feurer and Vinatier, 2018, p. 496; Luo *et al.*, 2019, p. 20), whereas, with the SfM-MVS method the internal camera geometry as well as camera position and orientation are automatically determined through auto-calibration (Feurer and Vinatier, 2018, p. 496). As external information regarding imaging parameters and network geometry are often unknown for archived aerial photographs due to missing camera calibration certificates (Feurer and Vinatier, 2018, p. 496), SfM-MVS is a potential method for 3D topographic reconstruction of this historic scenes using this legacy data source. However, for accurate reconstruction from archived aerial photographs, ground control points are necessary to provide both scale and registration to a geographic coordinate system.

Typical steps carried out in SfM-MVS software are described by Smith *et al.* (2015, pp. 251-254) and summarised below:

1. Feature detection, most commonly done using the Scale Invariant Feature Transform (SIFT) object recognition system.

2. Determination of correspondences between keypoints using the SIFT descriptor, k-dimensional trees and Approximate Nearest Neighbour solution.

3. Correspondences filtered to remove erroneous keypoint matches by applying the fundamental matrix to assess collinearity of keyponts in image pairs which are evaluated using random sample consensus (RANSAC) method.

4. SfM bundle adjustment implemented to estimate 3D geometry, camera poses (intrinsic calibration) and camera intrinsic parameters resulting in a sparse point cloud.

5. Scale and orientation determined using Ground Control Points containing XYZ coordinates.

6. Optimization of image alignment by re-running bundle adjustment; and

7. Application of MVS image matching algorithm increasing the density of the point cloud by at least two orders of magnitude resulting in a dense point cloud (Smith *et al.,* 2015 p 251-254 Structure from motion photogrammetry in physical geography).

Sevara *et al.* (2017) and Feurer and Vinatier (2018) have both proposed methodologies for the construction of digital terrain models (DTMs) from archived aerial photographs for use in detecting variations in elevation between epochs. Both approaches used a SfM-MVS stereo workflow. Sevara *et al.* (2017, pp. 614 - 615) method requires that analogue copies of the photographs are scanned at a high resolution on a photogrammetric scanner. This is not always possible as photogrammetric scanning facilities and expertise is not ubiquitous across all archives. In addition, original material may not be permitted to leave the archive for scanning at a secondary location, as is the case for the Historic England Archive. If scanned properly, digital image pre-processing steps proposed by Sevara *et al.* (2017, p. 620) include co-registration of all the photographs in the time series based on the fiducial markers, de-noising/image enhancement, cropping, contrast enhancement, downsampling and mask creation. After these steps, archived aerial photographs are ready to use in a normal SfM-MVS workflow such as that offered by Agisoft Metashape. Sevara *et al.* (2017, p. 624) further processed the outputs from the SfM-MVS workflow into raster DEMs for use in geomorphic change detection of western Sicily, an area that is rich in archaeological remains.
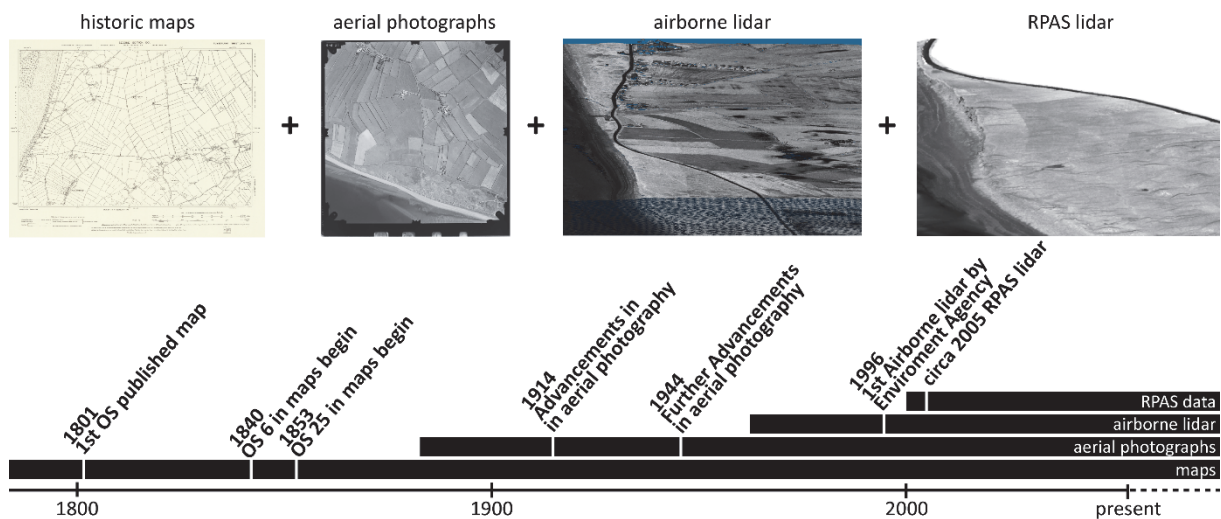
Figure 3.2: Spatiotemporal time series data sources for geomorphic change detection (Sources: Historic map: National Library Scotland,https://maps.nls.uk/index.html, aerial photograph: © Historic England. English Heritage Trust, airborne lidar: © Environment Agency copyright and/or database right 2015. All rights reserved).

Feurer and Vinatier (2018) proposed an alternative method that initially processes multi-epoch images in a single block. This method assumed that a number of keypoints remain invariant to image rotation and scale throughout time (Feurer and Vinatier, 2018, p. 498). Once an estimation of interior and exterior orientation was completed through this initial step, the epochs were then separated by epoch for subsequent processing steps (Feurer and Vinatier, 2018, p. 498). The authors tested their method under multiple conditions, which included using the various combinations of scanned images as is, scanned image cropped to remove the image border, or scanned images resampled based on their fiducial marks with nine additional Ground Control Points (GCP), the manual addition of 200 more tie points or 200 additional GCPs (Feurer and Vinatier, 2018, p. 497). While further testing is needed for different geomorphological settings (Feurer and Vinatier, 2018, p. 504), the best results were achieved by processing multi-epoch resampled images based on fiducial marks in a single block before separating by date for further processing, including manually adding nine ground control points (Feurer and Vinatier, 2018, p. 500).

3.2.4.3 Airborne Lidar

Airborne Light Detection and Ranging (lidar), also referred to as airborne laser scanning (ALS) uses laser technology to accurately measure the Earth's topographic and bathymetric surfaces from an aircraft, including aeroplanes, helicopters and most recently RPAS. Lidar is an active remote sensing technology meaning, unlike aerial photography and other imagery that rely on radiation from the sun, lidar emits its own energy. Therefore, lidar can operate

in various lighting conditions, including at night (Dong and Chen, 2017, pp. 2-3). Based on time of flight (i.e. the amount of time between when the signal is emitted and when it is received) in combination with a position and orientation system and GNSS, x, y and z positions of each return are calculated resulting in a 3D point cloud (Dong and Chen, 2017, pp. 10-11). Another advantage of lidar over aerial photography, is its ability to record ground points in wooded locations through gaps in tree canopy. This ability is improved with multiple return lidar, which allows the laser signal to intercept with multiple objects increasing the chances of a ground return (Shan and Toth, 2018, p. 391). Being able to filter ground points from above ground points, such as trees, is important in geomorphic change detection, which is concerned with calculating changes of the ground surface.

In England, the Environment Agency (EA) has been collecting airborne lidar on a piecemeal basis since 1998, concentrating on flood plains, urban areas and coastal zones (Environment Agency, 2019f). Through consultation of the Department for Environment Food & Rural Affairs (Defra) Survey Data Download platform (DEFRA, 2020), these priority areas are likely to have been subjected to repeat survey, while other areas have yet to receive any survey. EA's lidar missions take place from late fall to early spring during leaf-off conditions, which also increases the likelihood of the laser reaching the ground in areas with tree cover (Environment Agency, 2019f). The EA are currently undertaking a Full Coverage National LIDAR programme, aimed to provide complete coverage of England at 1 m spatial resolution, in addition to site-specific high-resolution (25 cm and 50 cm spatial resolution) surveys by mid-2020 (Winter, 2018).

In 2015, the EA's airborne lidar became freely available for use under the Open Government Licence (OGL) (Winter, 2017b; Winter, 2017a; DEFRA, 2020). Currently airborne lidar ranging from 25 cm to 2 m spatial resolution is downloadable through the DEFRA Data Service Platform and covers 80 percent of England and 95 percent of the coastline and flood zones (Environment Agency, 2019e). The data was recorded using ETRS89 coordinate system which was transformed to Ordnance Survey Great Britain 36 (OSGB36) coordinate system (Environment Agency, 2019a). Elevations are reported above Ordnance Datum Newlyn (ODN) (Environment Agency, 2019e). After the 26th August 2016 lidar coordinates transformation used OSTN15 and OSGM15 models (Environment Agency, 2019a). Earlier lidar was transformed using the up-to-date models at the time (Environment Agency, 2019a). EA work to specifications that state that the absolute vertical accuracy of their lidar

datasets should not exceed +/- 0.15 m (Environment Agency, 2019a). The absolute horizontal accuracy of the EA airborne lidar is +/- 0.40 m (Environment Agency, 2019a).

The EA airborne lidar data is offered in a variety of formats. These include raster Digital Terrain Models (DTM), raster Digital Surface Models (DSM) (Environment Agency, 2019b) and point cloud data provided as x, y, z text or LAZ file format (zipped LAS file format) (Environment Agency, 2019c). The DTMs were created from last returns only and exclude surface objects (Environment Agency, 2019b). The DSMs were also created from last returns only but include surface objects (Environment Agency, 2019b). The DTM and DSM raster files are provided both as LIDAR Composite and LIDAR Raster Tiles. The LIDAR Composite, which is updated annually, merges data of the same spatial resolution but from different epochs into composite DTMs/DSMs across England (Environment Agency, 2019d). Where more than one dataset exists in the same area, the most recent epoch was used in the composite (Environment Agency, 2019d). The LIDAR Raster Tiles only contain data that was gathered from one survey date (Environment Agency, 2019g). This data is available at 500 x 500 m tiles, 1 x 1 km tiles or 2 x 2 km dependent upon spatial resolution (i.e. 25 cm vs 50 cm vs 1 and 2 m spatial resolution respectively) (Environment Agency, 2019g).

The lidar point clouds collected prior to 2010, where available, were converted to LAS file format from simple x,y,z txt files (Environment Agency, 2019c). Datasets dating from 2010 onwards contain additional information, including intensity, laser return (the current system receives up to 8 returns per laser pulse), classification, GPS time (recorded either as GPS seconds of the week or GPS absolute time) and a point source ID (Environment Agency, 2019c). The EA use a fully automatic classification routine for assigning the points to one of the following ASPRS defined lidar point classes; 1. Default, 2. Ground. 3. Low surface object, 4. Medium surface object, 5 high surface object or 8. Model keypoints (Environment Agency, 2019b). Automatic classification results in a portion of the point cloud being misclassified (Environment Agency, 2019b). As the EA edit the DSM and DTM directly, point cloud data downloaded from the EA will likely contain misclassified points (Environment Agency, 2019b).

3.3 Quantifying future geomorphic change

3.3.1 Introduction

The prediction of future geomorphic change is possible through the application of sophisticated models that draw on existing data. The results of past change detection can be utilised to better understand the future changes from natural hazards. This section details the concepts of models, both conceptual and mathematical, and how they have been applied to understand complex natural and anthropogenic systems.

3.3.2 Definition

The term 'model' has been used widely having been assigned various meanings. Model has been used to describe concepts, hypotheses, laws, paradigms, descriptions, analogies, idealisations, equations, calculations, algorithms, datasets and maps (Baas, 2013, p. 1). More specifically the term model has been used by scientists and engineers to describe scaled physical replicas, drawings, governing equations and computer simulations (Parry *et al.*, 2014, p. 690). The International Association for Engineering Geology and the Environment (IAEG) define a model as *…an approximation of reality created for the purpose of solving a problem* (Parry *et al.*, 2014, p. 690). A model can provide a means of simplifying reality to aid in understanding of that reality. The purpose of a model is not always prediction. A model can be useful for generating hypothesis, rejecting concepts, and directing observation to new phenomena (Wilcock and Iverson, 2003a, p. 4). Models therefore can exist without prediction (Wilcock and Iverson, 2003a, p. 4). However, according to Wilcock and Iverson (2003a, p. 14) prediction, which is a foretelling of an event or condition, without modelling is speculation.

3.3.3 Types of models

Common types of models, each defined by their methodology, include conceptual models, physical/scaled/analogue models, analytical models and quantitative/ mathematical/ numerical models (Baas, 2017, p. 1).

Conceptual models are based on knowledge and experience (Parry *et al.*, 2014, p. 690). They represent an exercise in critical thinking that involve breaking down problems into descriptive and schematic diagrams to hypothesis possible outcomes under various scenarios (Hooke, 2003, p. 53). Conceptual models should be the first step in modelling (Parry *et al.*, 2014, p. 692) as these types of models provide foundations for subsequent

quantitative models (Hooke, 2003, p. 51). In addition a good conceptual model should be able to anticipate most issues that may be encountered within the system (Parry *et al.*, 2014, p. 697).

Physical/scaled/analogue models are simplified physical replicas of a system used to model the interaction between form and process (Green, 2014, p. 1). Physical models are important for visualising, interpreting, observing and measuring physical processes that would otherwise prove problematic with a full scale or real world counterpart (Green, 2014, p. 1). Physical models, particularly unscaled models, are used to aid with the development of a conceptual model and may also be employed for predictive purposes when using scaled models (Hooke, 2003, p. 54).

Analytical models define a problem using equations. These equations are then solved for to find a solution (Hooke, 2003, p. 54). Models which fall under this category are appropriate for straightforward systems with simple boundary conditions (Hooke, 2003, p. 54). While analytical models are useful for providing preliminary estimates, as most natural systems are complex, numerical models may be a better solution (Hooke, 2003, p. 55).

Quantitative/mathematical/numerical models use mathematical expressions, numerical variables, parameters and coefficients to quantify features, objects and the relationships between them (Baas, 2013, p. 1). In geomorphology, numerical models provide a way to study landscape change through the application of equations, which aim to describe the relationship between landscape form and process (Hutton, 2012, p. 1). In order to successfully apply a numerical model to geomorphological problems the form-process interactions as well as scale of enquiry need to be identified (Hutton, 2012, p. 2). These interactions then need to be correctly represented by mathematical equations (Hutton, 2012, p. 2). In addition, boundary conditions which constrain model parameters and model validation both need to be considered (Hutton, 2012, p. 2). Numerical models often develop from conceptual models and in many instances are tested against physical models (Baas, 2017, p. 1).

3.3.4 Modelling complex natural and anthropogenic systems

Models in geomorphology represent the interactions between Earth surface processes and landforms (Baas, 2017, p. 1). Such models can be used as tools to benefit natural hazard impact studies for investigating landscape change (Fookes, 2006, p. 236) The complexity of

geomorphic systems, which can include both natural and anthropogenic properties, lead to difficulties in precisely defining the relationship between process and form (Pelletier, 2008, p. ix). Prediction in geomorphology is further complicated by the need to represent the full complexity of processes, feedbacks and multi-scale diversity of the Earth's surface (Pelletier, 2008, p. ix). However, geomorphologists have made significant progress in quantifying transport and erosion laws for geomorphic systems (Pelletier, 2008, p. ix).

Conceptual models, in geomorphology, are often verbal or visual representations of a natural system or site within its natural system and can be communicated through relationship statements, flow diagrams and schematics in graphical form (Baas, 2017, p. 1). Physical, scaled or analogue models are physically or temporally scaled representations of the systems, used for observation in a reproducible manner (Baas, 2013, p. 1; Baas, 2017, p. 1) within a controlled laboratory setting (Green, 2014, p. 1).

Mathematical models are a powerful tool for addressing geomorphological enquiries (Pelletier, 2008, p. ix). These types of models represent complex geomorphological systems as equations to simulate the interaction between the Earth's surface and natural processes (Hutton, 2012, p. 1). Mathematical models can extend cognitive ability beyond observation of past and present events by simulating and predicting the influence of a behaviour on a system under different hypothesized scenarios (Hutton, 2012, p. 1).

Mathematical modelling has progressed rapidly due to an increase in the availability of computational power and the ability to acquire large amounts of data (Wilcock and Iverson, 2003a, p. 4). Numerous mathematical models are used in Earth Sciences, attested to by the number of models available on the Community Surface Dynamics Modelling System (CSDMS) online repository, which holds 407 open source models and tools (CSDMS, 2021). These models have a wide scope of spatial and temporal scales, ranging from particle to plate tectonics and milliseconds to millennial respectively (Hutton, 2012, p. 1). Mathematical models can be calculated in 1, 2 or 3-dimensions, with time providing the fourth dimension. A 1D model has one independent spatial variable (Pelletier, 2008, p. xi). An example of a 1D model in geomorphology would be one that quantifies changes in a topographic profile, $h(x, t)$, even though the profile itself is two-dimensional (Pelletier 2008 xi). While a topographic surface is a 3D landform, in modelling it is classed as 2D when the surface is represented by $h(x, y, t)$ (Pelletier, 2008, p. xi). Coastal area models can be divided into 2D horizontal (2DH) models and 3D models (Roelvink and Reniers, 2012, p. 145). The former uses the depth-

averaged equations while the latter resolves the vertical variations in flow and transport (Roelvink and Reniers, 2012, p. 145).

Geomorphology is influenced by fluid dynamics, which has a determining factor on topography, while in turn topography influences the way in which fluids flow (Pelletier, 2008, p. ix). Geomorphic models often incorporate hydrologic models through predictions of the location and flux of water, which are based on physical theory and measurement (Wilcock and Iverson, 2003b, p. vii). For example, the modelling of surface gravity waves is an essential component of modelling coastal hydro- and morpho-dynamic systems (Roelvink and Reniers, 2012, p. 3). These types of models are commonly used by coastal engineers to study the impact of waves, tides and currents on nearshore sediment flow under various coastal management scenarios, such as the addition of breakwaters or groynes (Bird, 2001, p. 24).

Models range in complexity from simple equations, such as those used by the Digital Shoreline Analysis Systems (DSAS), to complex models that simulate multiple physical parameters within a system, such as the eXtreme Beach behaviour (XBeach) model. It is important that the appropriate model is selected for a given scenario. Regarding coastal environments, which are highly dynamic, monitoring should be undertaken to validate predictions and obtain further data for refinement of models (Bird, 2001, p. 129).

3.4 Applications to cultural heritage studies

3.4.1 Introduction

Applications of change detection within archaeology often focus on monitoring past changes driven by human actions such as urban sprawl (Lasaponara *et al.*, 2016, p. 620), agricultural practices (Lasaponara *et al.*, 2016, p. 620; Chyla, 2017, p. 2) and looting using satellite imagery (Tapete *et al.*, 2016, p. 43; Lasaponara and Masini, 2018, p. 1330; Agapiou, 2020, p. 235). Satellite remote sensing change detection methods have also proved advantageous in damage assessment of inaccessible areas, potentially due to remoteness of the location or human conflict. The Palmyra cultural WH site located in Syria, for example, was the target of deliberate destruction by the Islamic State (Cerra *et al.*, 2016, p. 1). The presence of the Islamic State, hindered on the ground assessment of the damage. However, by applying a change detection methods, difference of Gabor features and Robust Difference, to pre- and post-damage WorldView-2 images, Cerra *et al.* (2016, pp. 5-6) were able to remotely

document the locations and define areas of destruction without introducing risk to the researchers. Cerra *et al.* (2016, p. 10) also applied a similar methodology at Nimrud, an archaeological site on UNESCO's tentative list.

Morphological changes that have occurred at cultural heritage sites as a result of natural processes have also been detected using satellite remote sensing change detection methods. Cigna *et al.* (2013, p. 123) were able to identify surface variations of both natural and artificial objects with ENVISAT ASAR in the Nasca region in Peru, including the Nasca Lines WH site. In addition, Kincey *et al.* (2014, p. 50) used normalised difference vegetation index (NDVI) image differencing derived from a time series of multispectral satellite data from archived Landsat imagery. The technique was used to assess erosion from natural processes, particularly surface run-off and slope instability, of an industrial archaeological site at Alston Moore, UK.

3.4.2 2D change detection methods applied to cultural heritage

Regarding the historic environment, 2D change detection methods that quantify the changes in planimetric position of a boundary feature over time, have most often been used in coastal erosion studies (Radosavljevic *et al.*, 2016; Westley, 2019; Hil, 2020; Nicu *et al.*, 2020). They have also been applied in the context of gully erosion (Nicu, 2021) and riverine environments (Asăndulesei *et al.*, 2020). Westley (2019) has argued that coastal archaeological vulnerability assessments could be improved through the application of shoreline change assessment. This was demonstrated on a case study from the eastern shoreline of Lough Foyle using the DSAS ArcMap plugin (Westley, 2019, p. 229). Six shoreline positions were extracted from one historic map, four orthophotos and one modern map ranging in date from 1923 to 2017 (Westley, 2019, p. 231). While no predictive modelling was undertaken, Westley (2019) suggested that for a specific location where coastal erosion was identified, that if the landward trend continued the archaeological remains would be destroyed within 20 – 25 years (Westley, 2019). Hil (2020) followed a similar approach to Westley (2019) for shoreline positions digitised from aerial imagery for Blueskin Bay, New Zealand dating in range from 1982 to 2013. In addition to calculating rates of change in shoreline position, Hil (2020, p. 106) also modelled prospective impact from Sea Level Rise (SLR). This impact was based on virtually flooding a digital elevation model derived from lidar (Hil, 2020). Values for inundating the DEM were taken from the IPCC 2014 best- and worst-case scenarios of SLR and added to the mean high water spring value (Hil, 2020, p. 116).

DSAS has also been applied to a riverine setting for Ripiceni-*Holm*, a Chalcolithic site located on the Prut River, Romania (Asăndulesei *et al.*, 2020). Rates of change statistics of the riverbank were calculated using data digitised from topographic maps, orthophotos, GNSS survey data and lidar ranging in date from 1939 to 2015 (Asăndulesei *et al.*, 2020). Reconstruction of the extent of the archaeological site was attempted, based on evidence from historic maps and geophysical survey data (Asăndulesei *et al.*, 2020). Shoreline positions were compared to the known and reconstructed archaeological horizon to estimate loss of the archaeological record (Asăndulesei *et al.*, 2020). In addition, Asăndulesei *et al.* (2020, p. 13) used the DSAS beta forecasting tool to estimate the destruction of an area of approximately 1 ha that was in danger of being destroyed within 20 years.

3.4.3 2.5D change detection methods applied to cultural heritage

2.5D elevation change detection methods, such as those discussed in section 3.3.4, have been applied at a limited number of archaeological sites as a means of detecting surface deformation (Collins *et al.*, 2009; Collins *et al.*, 2012; Risbøl *et al.*, 2015; Kincey *et al.*, 2017; Sevara *et al.*, 2017; Peppa *et al.*, 2019). Kincey *et al.* (2017), Collins *et al.* (2012) and Collins *et al.* (2009) used repeat terrestrial laser scanning (TLS) to produce DEMs for the compilations of spatiotemporal time series for subsequent change detection. These were completed on a landscape containing post-medieval mines in Garrigill, Cumbria (Kincey *et al.*, 2017, p. 406) and on select archaeological sites from within the Grand Canyon National Park, Arizona (Collins *et al.*, 2009; Collins *et al.*, 2012). While these studies benefitted from short time intervals between epochs, the temporal range was reduced to that of the duration of the TLS field campaigns.

Peppa *et al.* (2019) derived multi-epoch DEMs from analogue and digital aerial photographs, using a SfM-MVS workflow and applied change detection to Corbridge Roman town, an archaeological site from Hadrian's Wall WH site. While the temporal range covered 32 years, only 3 epochs were included in the spatiotemporal time series due to a large amount of time elapsing between aerial reconnaissance missions. The limited number of epochs meant that only two pairwise DoD's could be calculated, the first with a 22 year gap and the second with a 10 year gap between epochs. Change in the intervening years, therefore, went undetected due to these large temporal gaps. In addition, the change detected was attributed to a change in vegetation rather than change inflicted through erosional processes. The spatiotemporal time series complied by Sevara *et al.* (2017), also included DEMs derived

from archived analogue and digital aerial images as well as aerial laser scanning. Using this multi-source spatiotemporal time series, geomorphic change detection was calculated on a pairwise basis for the Mazaro River corridor, Sicily, Italy, an area rich in archaeological remains. The study spanned a 75 year time period from 1941 to 2016. By including digital aerial photographs and airborne lidar, the temporal range of the analysis was extended by 24 years. Similar to the research undertaken by Peppa *et al.* (2019), the time between epochs is large, ranging between 14 and 25 years. While change in the intervening years went undetected, Sevara *et al.* (2017) successfully identified surface change associated with quarrying and agricultural practices. Risbøl *et al.* (2015) extended an earlier TLS derived DEM change detection study for Mølen, an Iron Age site in Vestfold County, Norway, with DEMs created from archived aerial photographs. The purpose of this study was to extend the temporal range of the elevation change detection analysis by approximately 50 years into the past. Comparison to historical records, provided a plausible interpretation for change. Risbøl *et al.* (2015) detected surface lowering that was attributed to actions taken during the Second World War, in which pits were dug into the Mølen Iron Age cairns for the placement of machine gun emplacements

Past research conducted to assess change on cultural heritage sites has generally used single sensor (Collins *et al.*, 2009; Collins *et al.*, 2012; Kincey *et al.*, 2017) or combine similar sensors (Peppa *et al.*, 2019). In rarer instances sites have been assessed using the combination of multi sensor data for change detection (Risbøl *et al.*, 2015; Sevara *et al.*, 2017). In each instance only one type of change detection method was applied, which calculated elevation change between raster DEM epochs apart from that of Peppa *et al.* (2019) who employed the M3C2 algorithm using point cloud data. This was to demonstrate the effectiveness of ICP fine registration in minimising point-to-point difference between epochs and to remove a systematic tilt error in the 1984 dense point cloud (Peppa *et al.*, 2019, p. 871), rather than to identify surface change attributed to natural or anthropogenic hazards.

3.4.4 3D change detection methods applied to cultural heritage
3D change detection has been conducted within cultural heritage studies to quantify surface changes diachronically. These change detection studies rely on multi-temporal 3D representations of an object or a scene made possible through developments in non-contact 3D object acquisition techniques, such as the use of laser scanners or optical range sensors

resulting in either point clouds or several overlapping image outputs. The latter output of the two techniques would then subsequently be used for reconstruction of geometry using a digital photogrammetry workflow. 3D change detection methods have been employed on a variety of scales, ranging from cultural objects (including sculptures and other works of art) to historic buildings and archaeological landscapes

Guidi *et al.* (2004) created a 3D model, from multiple overlapping photographs, of the entire surface of Leonardo Da Vinci's unfinished panel painting titled *Adorazione dei Magi*. Diagnostic tests of overall structure of the painting were then undertaken for the purpose of informing conservation strategies (Guidi *et al.*, 2004, p. 1). To quantify surface deformation of the painting, the 3D model was compared to a plane surface (Guidi *et al.,* 2004, p. 5). The theory behind the methodology was that the painting, constructed from a number of planks of wood, while 2D, could be examined as a flat surface (Guidi *et al.,* 2004 p. 1). However, panel paintings which constructed of wood, such as the *Adorazione dei Magi*, suffer from curving, warping and cracking caused by aging, humidity and temperature fluctuations, internal stresses and vibration, these in turn result in negative implications for the actual painted surface (Guidi *et al.,* 2004 p. 1). By measuring the standard deviation of the displacement between the 3D modelled surface and the theoretical original surface represented by a plane, along the x, y and z axis, patterns of surface deformation could be identified and quantified (Guidi *et al.,* 2004 p. 3). The importance of this research is that it was the first to demonstrate the use of geometric primitives used in the application of change detection to identify surface deformation of cultural heritage objects.

Recently, Palma *et al.,* (2019) published further research regarding the *Adorazione dei Magi*. This work analysed the surface of the painting as a whole, the type of geometrical deformation of each individual plank and studied the deformations temporally (Palma *et al.,* 2019, p. 175). Three-dimensional models of the front and the back of the painting were captured using two methods, photogrammetry and structured light scanners in 2002 and 2015 (Palma *et al.,* 2019, p. 176). After aligning each model to the same reference system, the models were compared to an ideal flat plane (Palma *et al.,* 2019, p. 179) as per Guidi *et al.,* (2004). In addition, the individual panels were each fitted with a quadric surface in order to describe the type of warping that had occurred over time, such as concave up/down cupping, concave up/down bowing, and twisting (Palma *et al.,* 2019, p. 180). Finally, a novel method using a non-rigid registration algorithm, based on research by Li *et al.* (2008) and

Palma *et al.* (2018) was employed for the temporal comparison (Palma *et al.,* 2019, pp. 180 - 181). The output after the application of non-rigid registration algorithm was a 2002 model, a 2015 model and a deformed 2002 model (Palma *et al.,* 2019, p. 181). The deformed 2002 model was then compared to the 2002 the 2015 models using the point-to-mesh method. Through the comparison of the models before and after the deformation computed by the non-rigid algorithm, the authors were able to robustly separate low-frequency deformation of the panel to structural changes introduced by the restorations (Palma *et al.,* 2019, p. 184).

Research undertaken by Guidi *et al.* (2007) applied methods, from mechanical engineering, to model the same wooden test object in two different geometric states and to measure the change from the original state to the altered state. Overlapping images were captured using high resolution range cameras of a wooden sculpture of a foot sculpted wood (Guidi *et al.,* 2007, p. 2). The images were taken prior to and after the expansion of wood fibres induced by the application of extreme temperature and humidity (Guidi *et al.,* 2007, p. 2). The 3D reference model and a 3D altered model were constructed from the relevant images using triangulation with fringe projection (Guidi *et al.,* 2007, p. 2). Deviation maps were then generated to highlight the difference between the two models (Guide *et al.,* 2007, p. 2). 3D model creation and the deviation maps were completed in a commercial software package called IMInspect^TM (Guide *et al.,* 2007, p. 3). The results of the analysis detected small dimensional deviations caused by the sudden change in environmental parameters and demonstrated the application of the methodology to deformation studies of cultural heritage objects constructed from wood (Guide *et al.,* 2007, p. 5).

Using six TLS scans, surveyed annually between 2012 to 2017 (Lercari, 2019, p. 156), Lercari (2019, p. 153) applied the M3C2 algorithm to identify surface deformation of earthen architecture from Çatalhöyük WH site, a 9000 year old Neolithic city in central Anatolia. The purpose of this research was to demonstrate the viability of the workflow (Lercari, 2019, p. 161) for detecting material loss in walls and buildings with millimetre accuracy (Lercari, 2019, p. 153). Campiani *et al.* (2019) undertook environmental spatial analysis of both temperature and humidity for the same WH site to produce environmental risk maps. The study also included M3C2 change detection of the earthen architecture to evaluate the efficacy of conservation efforts (Campiani *et al.,* 2019, p. 173). Feature averages were calculated from the M3C2 results using a bespoke MATLAB routine and exported to a

Geographic Information System (GIS) for comparison to deterioration risk factors (Campiani *et al.*, 2019, p. 174).

Multi-temporal spatial analysis using the M3C2 algorithm has been conducted at the Engare Sero footprint site in northern Tanzania (Zimmer *et al.*, 2018). Dense point clouds dating to 2010, 2012 and 2017, each derived from SfM-MVS workflow, were compared to identify rates and spatial distribution of erosion on a number of the fossilised footprints (Zimmer *et al.*, 2018, pp. 229-230). Zimmer et al (2018) not only identified areas of erosion, but also provided three modes of that erosion; flaking, abrasion or boring of holes (Zimmer *et al.*, 2018, p. 239). They concluded that the erosion was likely due to episodic events such as major flooding, followed by periods of stabilisation (Zimmer *et al.*, 2018, p. 239).

M3C2 was used to monitor the impact of multi-annual archaeological excavations of a Palaeolithic site in Burgos, Northern Spain (Martínez-Fernández *et al.*, 2020). The site was surveyed by TLS over the course of seven years between 2012 and 2018 (Martínez-Fernández *et al.*, 2020, p. 6). The M3C2 analysis allowed the assessment of the stratigraphic stability and integrity of excavation walls, along with the preservation of Palaeolithic surfaces to be assessed from year to year (Martínez-Fernández *et al.*, 2020, p. 14).

3.4.5 Modelling applied to cultural heritage

A variety of numeric models have been employed across WH properties, including those associated with built heritage. Many models, for example, have been employed for the purpose of structural analysis (Bartoli *et al.*, 2015; Saloustros *et al.*, 2015; Badillo-Almaraz *et al.*, 2018; Quezada *et al.*, 2018; Clemente *et al.*, 2019; Kościuk and Kogut, 2019). Modelling has also been undertaken to assess natural processes such as cliff stability (Alcaíno-Olivares *et al.*, 2021), impact of weather-related events causing natural hazards such as debris-flow (Musumeci *et al.*, 2021), seismic hazard assessment (Pagliaroli *et al.*, 2014), ground water modelling (de Beer *et al.*, 2012), and flood risk assessment (Vojinovic *et al.*, 2021a; Vojinovic *et al.*, 2021b). Numerical modelling of micro climates of urban areas of Cairo, Egypt was undertaken by Elnabawi *et al.* (2015) to identify excessive solar exposure linked to outdoor thermal comfort. Cutajar *et al.* (2019) used an integrated multidisciplinary approach to simulated air flow of the Ħal Saflieni Hypogeum using a computational fluid dynamic model. At Derwent Valley Mills WH site, a numerical model was utilised to inform land management decisions (Howard *et al.*, 2017). The numerical model simulated the river behaviour associated with the removal of weirs (Howard *et al.*, 2017) and suggested that although the

removal of the weirs would not significantly change the valley morphology, localised erosion would occur due to the river readjusting its base level (Howard *et al.*, 2017). Recently the revised universal soil loss equation (RUSLE) has been applied to various archaeological sites to predict the effects of erosion on the archaeological record. including at Magna Roman fort (part of the Frontiers of the Roman Empire: Hadrian's Wall WH site) (Guiney *et al.*, 2021), at number of open-air archaeological sites along the Doring River, South Africa (Ames *et al.*, 2020), and at Khirbat Nuqayb al-Asaymir, a Middle Islamic site in Southern Jordan (Howland *et al.*, 2018 p. 64).

3.5 Conclusion

Where natural hazards are known to intersect with the archaeological record of WH landscapes, advanced geospatial data and methods can provide solutions for assessing landscape change driven by natural hazards. Spatiotemporal data can be complied into a time series to quantify past change and to validate models of future change. Change detection provides methods to quantify past impact through the analysis of a spatiotemporal time series which represents topographic conditions at different points in time. Impact can be determined by the change in planimetric position of a boundary feature or a change in surface elevation. Mathematical models can then be used to predict future outcomes under varying scenarios. Studies applied to the archaeological record generally focus either on past change or future change, rather than using the full potential of advanced geospatial methods by combining the two. In addition, these studies tend to focus on a single data source, thereby limiting the temporal range to establish trends through time.

The following chapter details the methodology used in this research for natural hazard impact assessment of WH properties. A multi-temporal and multi-modal geospatial approach is implemented for quantify past and future changes to the Earth's surface. The methodology seeks to understand amounts and rates of past change using the change detection techniques that were described in this current chapter. It also employs numerical models to predict future and simulate potential change under various scenarios.

Chapter 4: Implementing the framework for natural hazard impact assessment for cultural World Heritage properties

4.1 Introduction

To undertake a quantitative natural hazard impact assessment an advanced geospatial methodology has been proposed which incorporates interpretation of the results in conjunction with evidence derived from the archaeological record. Incorporation of the archaeological evidence is demonstrated in Chapter 6.

This chapter presents the methodology undertaken for assessing past and future geomorphic change as a result of the destructive forces from natural hazards. The chapter begins by briefly introducing the study area followed by detailing the three change detection methods used to assess past change. Specifics of the spatiotemporal time series representing topography are described including data specific pre-processing steps, co-registration procedures, feature extraction and interpolation to a raster surface representing elevation. Details of how error was considered is within each of the change detection methods is also provided. The chapter then focuses on the two methods for assessing future change. These models were selected as they were developed for the purpose of forecasting coastal change. Finally the chapter concludes with a summary prior to introducing Chapter 5.

4.2 Study area

Beckfoot Roman fort and hinterland was selected as the study area, here after referred to as 'the Beckfoot study area'. The Beckfoot study area has been identified through consultation with Mike Collins (Collins, 2017) - Historic England's Inspector of Ancient Monuments for Hadrian's Wall, as requiring scientific analysis to understand the natural processes that influence site survival.

The Beckfoot study area is situated on the west coast of Cumbria along the outer Solway Firth in a dynamic hydrological and morphological system. The Beckfoot study area contains multiple sites from the Hadrian's Wall WH site. These include Beckfoot Roman fort and extramural settlement, Roman cremation cemetery, conjectured location of Mileforlet 15, and Roman tower 15a. These sites are all located within 200 m of the coastline, which is the area considered to be at risk from flooding and erosion (CH2M, 2018, p. 57). Beckfoot Roman fort and Milefortlet 15 were both listed in the most recent Heritage at Risk (HAR) register for threats posed by arable ploughing (Historic England, 2021, p. 11) and coastal

erosion (Historic England, 2021, p. 11) respectively. The conjectured location of Milefortlet 15 and Roman cemetery site are located within the Mawbray Bank sand dunes, which are vulnerable to coastal erosion. According to the HAR (2021, p. 11), Milefortlet 15 is suffering from extensive significant problems due to coastal erosion which and is in a state of decline. At present no definitive evidence exists for Milefortlet 15 and it has been suggested that it may have already been destroyed by coastal erosion (Bellhouse, 1957, p. 22). The remains of the Roman cremation cemetery which is also buried within the dunes at conjectured location of Milefortlet 15 has been eroding out of the sand dunes since at least the early 1900's (Caruana, 2004, p. 136). As Roman cemeteries, associated with the Roman frontier are poorly understood (Petts, 2009, p. 160; Symonds and Mason, 2009a, p. 65), this location within the Beckfoot study area is of particular importance.

4.3 Detecting past geomorphic change

To gain insights into past impacts of natural hazards on the archaeological remains of the Beckfoot study area, three types of spatiotemporal change detection analyses were undertaken. These included 2-dimensional (2D), 2.5-dimensional (2.5D) and 3-dimensional (3D) methods. The 2D change detection method allowed for the change in the horizontal position of a phenomena to be measured. The 2.5D change detection analysis calculated elevation change between successive epochs represented by digital elevation models (DEM). The 3D change detection method measured distances between two epochs based on their point clouds, rather than derivatives created from them, such as DEMs.

Combining the three techniques allowed for the following:

- Using the 2D change detection analyses meant that OS historic maps could be included, thereby extending the time series further into the past and providing a longer narrative for geomorphic change.
- The 2.5D change detection provided areal and volumetric change values giving an indication of sediment loss and gain.
- The 3D techniques provided nuanced change, which measures change based on a point's surface normal rather than from a strictly vertical plane.

4.3.1 Geomorphic change detection

4.3.1.1 2D change detection

The 2D change detection analysis was undertaken in ArcMap 10.6 using the Digital Shoreline Analysis System (DSAS) AddIn (Fig. 4.1 and 4.2). DSAS was developed by United States Geological Survey (USGS) to measure past shoreline rates-of-change statistics from a time series of shorelines represented by vector polylines (Himmelstoss *et al.*, 2021, p. 1). The software is offered as an open source AddIn for ArcMap versions 10.4 – 10.7 (Himmelstoss *et al.*, 2021, p. 1). While developed specifically for analysing coastal change, the application may also be used to measure past rates-of-change statistics for any kind of boundary data that can take the form of a vector polyline (Himmelstoss *et al.*, 2021, p. 1). The most recent version (v. 5.0) of the application includes a method for forecasting shoreline location in 10 and 20 years' time (Himmelstoss *et al.*, 2021, p. 1). The DSAS required that the input data be held within a geodatabase that used a projected coordinate system with the unit metres (Himmelstoss *et al.*, 2021, p. 9). For this research, concerned with site located within the UK, the projected coordinate system was set to OSGB36, which met the metre requirement. The input data included two user defined and one DSAS generated feature classes.
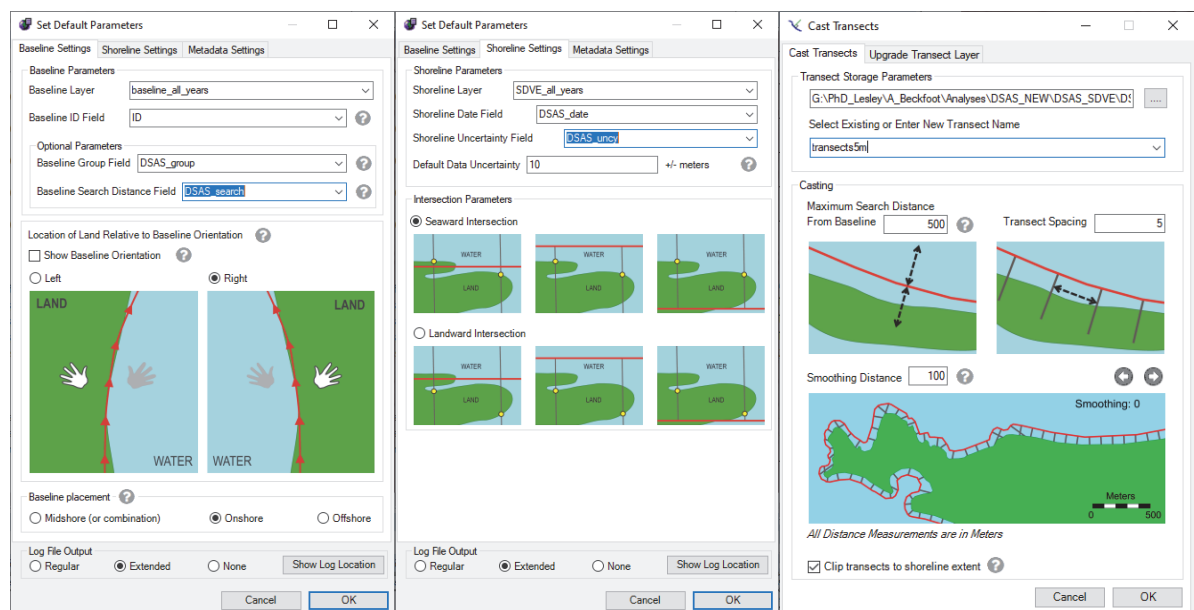
Figure 4.1: Digital Shoreline Analysis System (DSAS) ArcMap AddIn graphical user interface; (left) Set Default Parameters – Baseline settings; (middle) Set Default Parameters - Shoreline Settings; and (right) Cast Transects.
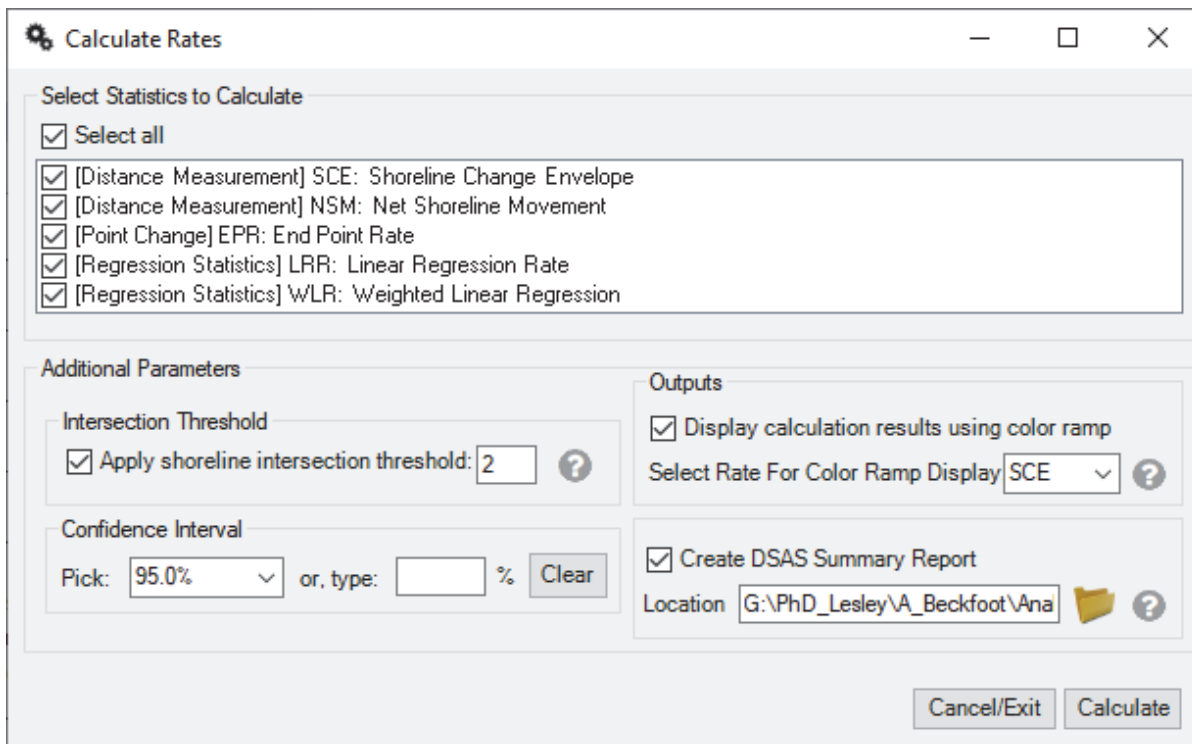
Figure 4.2: DSAS ArcMap AddIn graphical user interface for calculating rates of change statistics.

The first user defined feature class held all the boundary polylines representing the phenomena in which change was measured. For the Beckfoot study area, this was the coastline as defined by the boundary between the coastal dune system and the beach. Some required attributes of the boundary feature class were auto-generated by ArcMap while the date and uncertainty fields (DSAS_date and DSAS_uncy) were created by the user, the specifics for which are found in the DSAS user manual. The date of each epoch was input into the attribute table in the form of YYYYMMDD. The uncertainty values are provided section 4.3.7.1. In the event that the day and or month was unknown 01 or 0101 (the 1st day of the month or 1st of January) was nominally selected for the DD or MMDD values.

The second user defined feature class contained the baseline polyline(s). The baseline vector polyline for the study area was created by buffering one of the boundary feature polylines and tracing one length of the resulting polygon. This ensured that the baselines were roughly parallel to the boundary features. The baseline feature class was used to cast transects perpendicular to the baseline across the boundary feature polylines. The transects were generated by the DSAS software using the baseline and boundary feature class, as well a user selected spacing. A spacing of 5 m was chosen for this research in order to provide sufficient resolution for detecting detailed changes along the coastline. Transects were

visually inspected for quality. Any transect which crossed each other were manually rotated until they no longer intersected.

Measurements were then taken from the baseline to the points where each transect intersected each of the polylines. Measurements were stored in the geodatabase as a point intersect feature class. Based on the intersect measurements DSAS calculated a number of statistical outputs, which were stored as a transect rates feature class also found within the geodatabase. The calculations were completed with a confidence interval of 95 per cent.

Statistic	Abbreviation	Description	Calculation
Net shoreline movement	NSM	The distance between the oldest boundary feature and the youngest boundary feature crossing each transect	NSM = $d_{oldest} - d_{youngest}$ d = distance in m
Shoreline change envelope	SCE	The greatest distance between all shorelines for a transect	SCE = $d_{furthest} - d_{closest}$ d = distance in m
End point rate	EPR	NSM divided by the number of years between the oldest and the youngest boundary feature crossing each transect	EPR = NSM/($Y_{latest} - Y_{earliest}$) Y = year
Linear regression rate	LRR	The rate of change statistic determined by fitting a least-squares regression line to all boundary feature intersection points for a transect. The LRR is the slope of the line. This calculation is sensitive to outliers and can underestimate the rate of change statistic.	LLR is the slope of the equation describing the regression line: y = a +bX a = intercept b = slope
Weighted linear regression rate	WLR	Similar to LRR, however in WLR emphasis is placed on boundary feature intersection points	Weighting applied to data points uncertainty value before fitting linear regression line: $w = 1/e^2$ w = weight e = shoreline uncertainty

Table 4.1. Statistics calculated by the DSAS (Source: Himmelstoss *et al.*, 2021, pp. 50 - 53).

The statistics calculated by DSAS included net shoreline movement, shoreline change envelope, end point rate, linear regression rate and weighted linear regression rate. The last

three statistics listed provided rates of change, while the first two were distance measurements. Descriptions of the statistical calculations can be found in Table 4.1.

DSAS also calculated uncertainty values associated with the end point rate results. This was the EPRunc value field within the transect rates feature class. For linear regression rate and weighted linear regression rate the standard error (LSE and WSE), confidence interval (LCI and WCI) and r-squared values (LR2 and WR2) were reported within the transects rates feature class.

4.3.1.2 2.5D change detection

Geomorphic Change Detection (GCD) software was used to calculate the raster based change in elevation between two surfaces of the same location but varying in time (Fig. 4.3). The software was freely available as an ArcMap AddIn as well as a standalone version (Riverscape Consortium, 2021). It was developed by Riverscape Consortium with the intention of detecting change in river morphology over time (Riverscape Consortium, 2021) based on methodological developments by Wheaton *et al.* (2009). Regardless of its original purpose, its applications are far reaching and can be applied to any surface elevation change detection derived from repeat topographic surveys (Riverscape Consortium, 2021). As such, it was concluded to be suitable for assessing geomorphic change, focusing on coastal sand dunes and beach morpho-dynamics for the Beckfoot study area. The analyses excluded epochs that did not contain elevation data. These epochs were those derived from OS historic maps, early archived aerial photographs whose structure-from-motion-multi-view-stereo (SfM-MVS) results were unsatisfactory, and orthophotographs (see section 4.3.2, table 4.2).

All DEMs and associated reference surfaces, i.e. slope, point density and cloud point density ratio, were added to new a GCD project. DEM survey properties were updated to include the date of acquisition. The properties of the associated surfaces were also updated to reflect surface type.

GCD software built spatially variable error surfaces for each epoch, with the exception of one epoch. Uniform error surfaces based on the SfM-MVS RMSE results were created for epoch 6. The spatially variable error surfaces were derived from point density and cloud point density ratio surfaces and the custom Fuzzy Inference System, discussed section 4.3.7.2, which was added to the FIS library.

Multiple epoch change detection was then carried out by the GCD software. DEM differencing was calculated for all DEMs minus the previous DEM. The error surfaces associated with each DEM were incorporated within the calculation using probabilistic thresholding and a confidence level of 95 per cent.

The outputs included tables containing both the raw and thresholded areal and volumetric totals for surface lowering (erosion) and surface rising (deposition) across the study area. The associated error values were also recorded in these tables. DEMs of Difference (DoD) – raster surfaces representing surface lowering and surface rising – were also generated per each pairwise change detection.
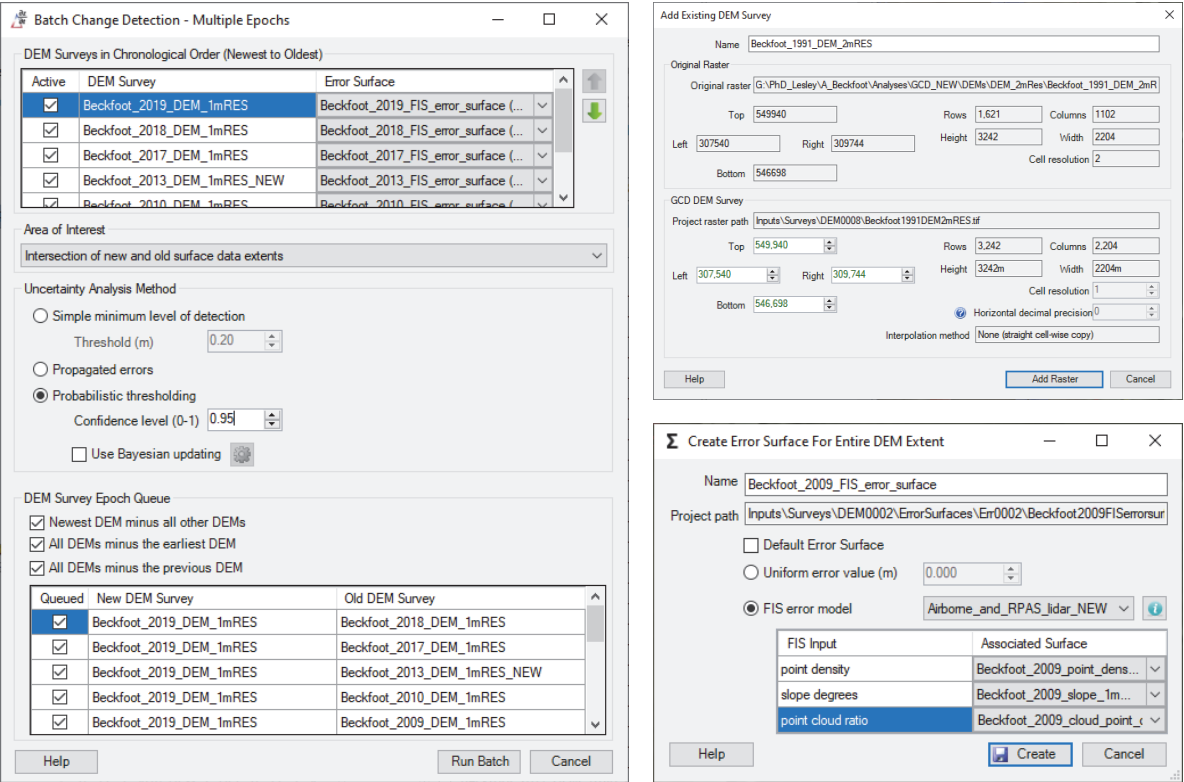
Figure 4.3: Geomorphic Change Detection interface; (left) batch change detection; (right top) Add existing DEM survey; and (right bottom) Create error surface for entire DEM extent. (source: © RiverscapeConsortium, doi: https://doi.org/10.5281/zenodo.7248344).

Polygons masks were drawn around various geomorphological features to be used as budget segregation polygons, which enabled the quantification of change within the given area to be totalled. For the Beckfoot study area, these included polygons which encompassed the beach, sand dune cliff edge, sand dunes and the coastal hinterland.

4.3.1.3 3D change detection

In total six pairwise 3D change detections were undertaken using the dense point cloud dating to 1991, the airborne lidar point clouds dating to 2009, 2010, 2013, 2017, and

September 2018, and the April 2019 RPAS lidar point cloud. The lidar files containing only the ground points within the area of interest for each epoch were opened in CloudCompare. Two epochs were selected at a time for 3D change detection, which was completed using the M3C2 plugin developed by Lague et al (2013). In each pairwise calculation the earliest epoch served as the reference (Cloud #1) for which the surface normal of each point was calculated using a multi-scale approach. Parameters for calculating surface normals are presented in Figure 4.4. By employing a multi-scale approach, the normal of each point was selected based on when the calculations were most planar. Once normal were computed M3C2 measured the distance along the normal of each point in Cloud #1 to each corresponding point in Cloud #2. This resulted in a point cloud containing the M3C2 distance values, significant change values (1 or 0, 1 being significant change) and distance uncertainty values for each point in the output point cloud.
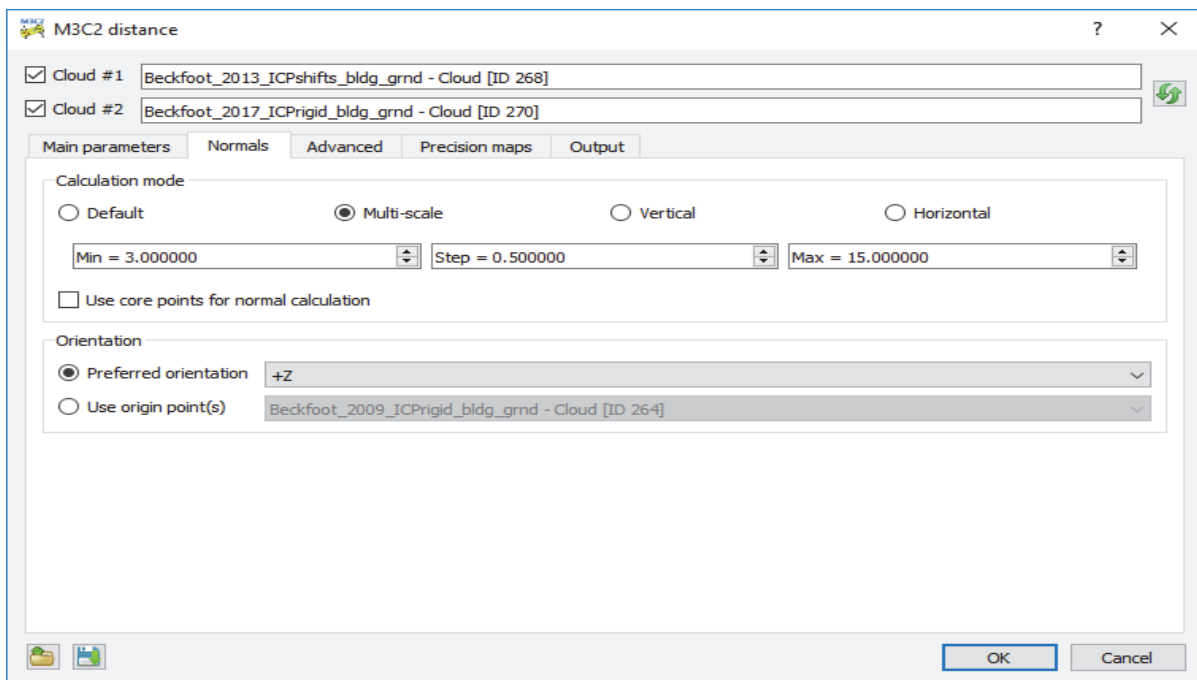
Figure 4.4: M3C2 interface in CloudCompare, showing M3C2 parameters for calculating surface normal (source: © EDF R7D/TELECOM ParisTech (ENST – TSI).

4.3.2 Spatiotemporal time series

The above methods rely on a spatiotemporal time series consisting of a minimum of two epochs, representing ground conditions at specific points in time, in order to derive input data for calculating change. For the Beckfoot study area, the spatiotemporal time series was compiled of 16 epochs comprising of topographic data derived from Ordnance Survey (OS) historic maps, archived aerial photographs, orthophotographs, airborne lidar, and Remotely Piloted Airborne System (RPAS) lidar. Table 4.2 provides details regarding the date, data type

and method of change detection analysis per epoch. All epochs were aligned to the Ordnance Survey Great Britain 1936 (OSGB36) coordinate system. Details of alignment are provided in subsequent sections.

The temporal range of the time series was reflective of the available data for the three separate analyses (2D, 2.5D and 3D - see section 4.3.1). The 2D change detection spans the greatest period, from 1866 to 2019, covering 153 years, while both the 2.5D and 3D analysis date between 1991 and 2019, shortening the relevant change detection analyses (2.5D and 3D) to a period of 28 years.

Beckfoot study area spatiotemporal time series			
Epoch	**Date of capture**	**Data type**	**Analysis**
Epoch 1	1866	OS historic map	2D CD
Epoch 2	1899	OS historic map	2D CD
Epoch 3	1923-4	OS historic map	2D CD
Epoch 4	7th Jul. 1948	Archived aerial photographs	2D CD
Epoch 5	1957	OS historic map	2D CD
Epoch 6	5th Sep. 1991	Archived aerial photographs	2D, 2.5D & 3D CD
Epoch 7	3rd to 20th Apr. 2009	Airborne lidar	2D, 2.5D & 3D CD
Epoch 8	1st Apr. 2010	Airborne lidar	2D, 2.5D & 3D CD
Epoch 9	17th to 26th Feb. 2013	Airborne lidar	2D, 2.5D & 3D CD
Epoch 10	10th Sep. 2014	Orthophotograph	2D CD
Epoch 11	10th Jun. 2015	Orthophotograph	2D CD
Epoch 12	29th April and 5th to 8th May 2017	Airborne lidar	2D, 2.5D & 3D CD
Epoch 13	24th Jun. and 2nd July 2018	Orthophotograph	2D CD
Epoch 14	23rd to 28th Sep. 2018	Airborne lidar	2D, 2.5D & 3D CD
Epoch 15	29th and 30th of Apr. 2019	RPAS lidar	2D CD
Epoch 16	27th Jun. 2019	Orthophotograph	2D, 2.5D & 3D CD

Table 4.2: Spatiotemporal time series for the Beckfoot study area.

4.3.2.1 Historic maps

Four epochs were derived from OS historic maps, details for which are provided in Table 4.3. High resolution scanned images of these maps, epochs 2 and 3 were obtained from the National Library of Scotland (NLS). Each map was provided digitally as jpeg imagery with a resolution of 400 pixels per inch (ppi). Epochs 1 and 5 were added to the spatiotemporal

time series at a later date and were downloaded from Digimap as georectified raster mosaics.

OS historic map details			
Epoch no	Date	OS map series	No of sheets
Epoch 1	1866	OS County Series 6" (1:10560)	Raster mosaic downloaded from Digimap
Epoch 2	1899	OS County Series 6" (1:10560)	3
Epoch 3	1923-4	OS County Series 6" (1:10560)	3
Epoch 5	1957	National Grid (1:10560)	Raster mosaic downloaded from Digimap

Table 4.3: OS historic map epoch details.

4.3.2.2 Archived aerial photographs

Two epochs, epochs 4 and 6, in the spatiotemporal time series were derived from archived aerial photographs, sourced from the Historic England Archive in Swindon. The earliest photographs in the time series were taken 1948 (epoch 4) by the Royal Air Force (RAF). The photos captured in 1991 (epoch 6) were collected by the Ordnance Survey. Details of the archived aerial photograph epochs are provided in Table 4.4.

Unfortunately the photographs taken by the RAF (epoch 4) were not accompanied with a camera calibration certificate. As such there was no information regarding the camera's interior orientation parameters, however, some details were found on the. Photographs comprising epoch 4 were taken on the 27th of July 1945 by RAF squadron 541 on sortie 541/A/434 with a 20" lens. According to Nesbit (1997) and Stanley II (1981) RAF squadron 541 (A Flight) piloted a Spitfire PR XIX. Based on the photographic image size, which was 7 X 8.25 inches, and overlap, these aeroplanes were likely equipped with two Williamson F.52 cameras (See Figure 4.5 - left). The cameras were mounted in the fuselage between the tail and the wings in a slightly offset vertical split formation which would have been operated together to provide greater ground coverage (Air Ministry A.C.A.S., 1945) as indicated in Figure 4.5 (centre).

According to details found on the image border, the 1991 photographs (epoch 6) were captured on the 6th of September 1991 with a Zeiss 630 camera. The focal length was recorded as 304.79 and flying altitude as 7600 feet. Further details regarding camera

calibration were provided by Ordnance Survey (Holland pers. comm), including the fiducial mark coordinates, details of which are provided in Table 4.5.

Archived aerial photograph details		
	Epoch 4	**Epoch 6**
Vertical/oblique	vertical	vertical
Date captured	27/7/1948	06/09/1991
Captured by	Royal Air Force (541/A/434)	Ordnance Survey 91301
No. of photos	6	4
Flying height	not available	6120 – 6130 ft
Camera type	Williamson F.52	Zeiss 630
Scale	1:10000	1:7600
Focal length	20 in	12 in
Film format	8.25 by 7.5 in	9 by 9 in
Fiducial marks	no	4 corner, 4 side
Scanned from	Paper copy	Slide
Scan resolution	600 dpi	600 dpi
Example thumbnail	©Historic England. English Heritage Trust.	©Historic England. English Heritage Trust.

Table 4.4: Epochs derived from archived aerial photographs for the Beckfoot study area.
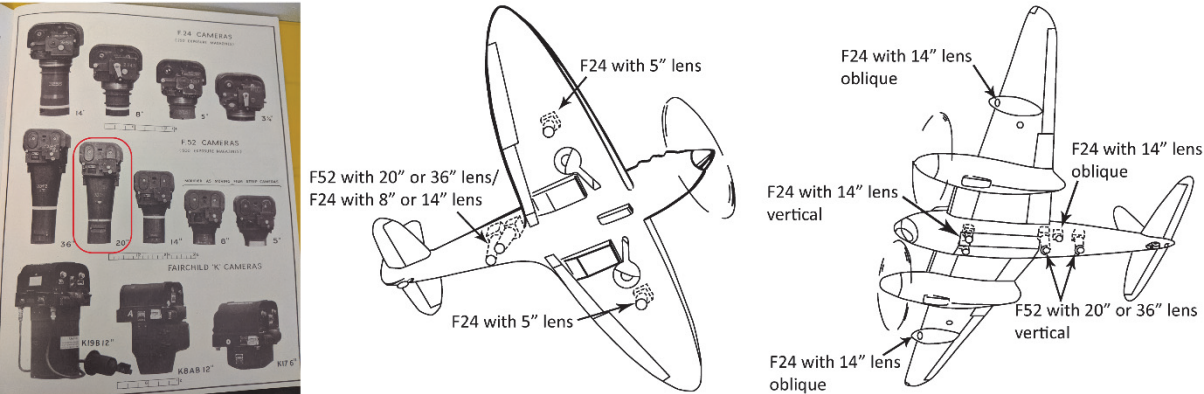
Figure 4.5: (left) cameras and lenses used by the RAF – Williamson F.52 with 20" lens circled in red; (middle) camera installation in the PR Spitfire; and (right) camera installation in the PR Mosquito. (Adapted from original figures from Air Ministry A.C.A.S, 1945, pp. 11, 12 and 14, republished in 2003 by GeoInformation Group, © Crown Copyright 945/MOD. Reproduced with the permission of the Controller of Her Majesty's Stationery Office, © 2003 The GeoInformation Group).

Fiducial ID	X coordinate (mm)	Y coordinate (mm)
Fiducial 1	112.992	-0.015
Fiducial 2	-112.989	0.03
Fiducial 3	0.029	112.985
Fiducial 4	-0.03	-112.99
Fiducial 5	103.96	103.925
Fiducial 6	-103.971	-103.926
Fiducial 7	-103.916	103.945
Fiducial 8	103.922	-103.956

Table 4.5: Fiducial coordinates (mm) for 1991 aerial photographs.

4.3.2.3 Orthophotographs

In total four epochs were composed from orthophotographs; epochs 11, 12, 14 and 17 (See Table 4.1). The vertical aerial photographs were taken by Getmapping Plc and downloaded from Digimap.

Getmapping Plc, formerly Millennium Mapping Co., have been conducting national aerial photographic surveys of the UK since 1999 (Getmapping Plc, 2021). The photographs taken between 1999 and 2018 were available for academic research through Aerial Digimap (Edina Digimap, 2021a). The aerial images that make up part of the spatiotemporal time series were downloaded as jpeg images. Each image covered an area of 1 km square at 25 cm resolution (Edina Digimap, 2021a). The RMSE of the aerial imagery as reported to Digimap by Getmapping Plc is +/- 0.75m (Edina Digimap, 2021b).

4.3.2.4 Airborne lidar

Airborne lidar details			
Epoch no	Capture Date	Avg. point spacing (m)	Source
Epoch 7	3rd to 20th Apr. 2009	1.00	Environment Agency
Epoch 8	1st Apr. 2010	0.89	Environment Agency
Epoch 9	17th to 26th Feb. 2013	1.03	Environment Agency
Epoch 12	29th April and 5th to 8th of May 2017	0.67	Environment Agency
Epoch 14	23rd to 28th Sep. 2018	0.83	Environment Agency

Table 4.6: Airborne lidar epoch details.

All airborne lidar point clouds were collected by the Environment Agency's Geomatics Group and were downloaded from the Department for Environmental Food & Rural Affairs' (DEFRA) Data Services Platform. This is with the exception of epoch 14, which was supplied through email directly from the Environment Agency as it had not yet been made available

through the platform. The average point density of the airborne lidar epochs was approximately 1 point per square metre.

Epochs 7, 8, 9, 12 and 14 for the Beckfoot study area were derived from airborne lidar (summarised in Table 4.6).

4.3.2.5 RPAS lidar

Epoch 15 was derived from a RPAS lidar survey. The RPAS lidar survey was undertaken at a select location within the Beckfoot study area. The purpose of the RPAS lidar survey was to extend the time series to the present (i.e. date of the survey) by providing an up-to-date and accurate ultra-high resolution point cloud representing the current ground conditions.

The survey took place on the 29th and 30th of April 2019. In total four data collection flights were undertaken that covered approximately 62.5 hectares of the Mawbray Banks sand dunes. This location was selected for the RPAS lidar survey as it is the position of what appeared to be ongoing erosion along the sand dune cliff face. Erosion here coincides with the location of the Roman cremation cemetery causing loss of the archaeological remains. The resulting average point space and average point density calculated using the first returns of the classified point cloud were 0.12 m and 66.09 points per m^2, respectively.

The lidar data was collected with a ROBIN MINI UAV LiDAR system mounted on a DJI Matrice 600 Pro RPAS. This aerial campaign was accompanied by a Global Navigation Satellite System (GNSS) ground control survey to assess the horizontal and vertical accuracy of the point cloud and for vertical datum registration purposes. Ground targets designed specifically for RPAS lidar (Davidson *et al.*, 2019) were placed in the study area and their locations were recorded using survey grade GNSS equipment.

4.3.3 Pre-processing workflow

Prior to undertaking change detection and modelling, each epoch needed to undergo data type specific pre-processing steps. Figure 4.6 illustrates these steps for each of the four main data types that comprise the spatiotemporal time series. Data pre-processing included alignment to the desired coordinate system, classification of point cloud data, co-registration between epochs and generation of secondary products (i.e. Digital Elevation Model (DEM), and vectorisation of feature of interest (i.e. the coastline). Uncertainty associated with each of the data types was also measured and incorporated into the change detection analyses in order to account for error and help identify real change versus noise.
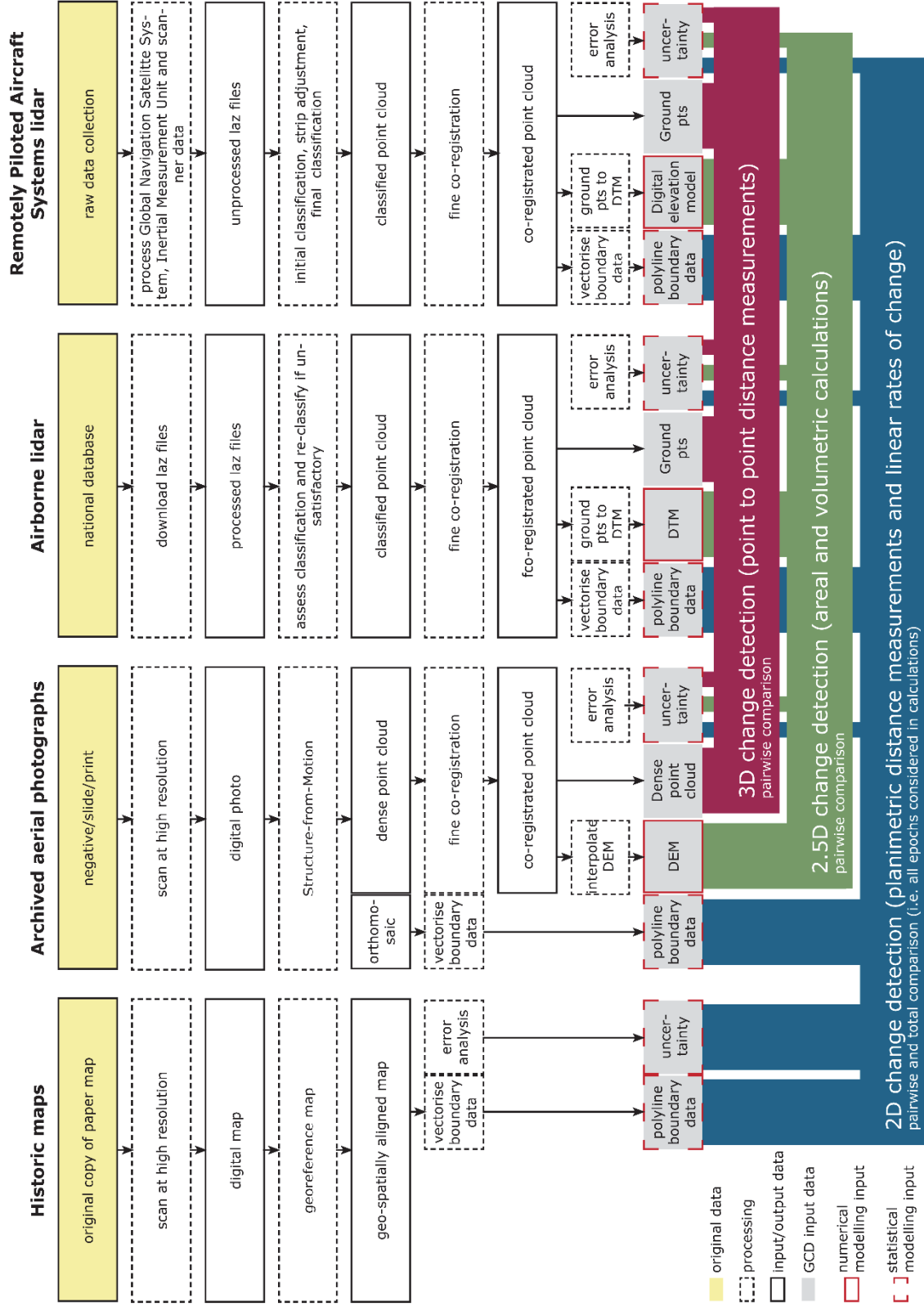
Figure 4.6: Data pre-processing steps per data type prior to undertaking geomorphic change detection and predictive modelling.

4.3.3.1 Historic maps

The historic maps were aligned to the OSGB36 coordinate system through georeferencing. This process was completed in Esri's ArcMap 10.6, which utilised the 2017 OS MasterMap as the spatially referenced map to which the remaining OS historic maps were aligned. Control points common to both the OS historic map and 2017 OS MasterMap were used to align the historic map to the projected coordinate system using a first order polynomial (affine) transformation.

The OS MasterMap, downloaded from Edina Digimap, was a spatially referenced dataset supplied in the desired coordinate system (OSGB36). OS MasterMap has a high geometric and positional accuracy that varies according to the scale of the original survey (see Table 4.5). The scale of the map is dependent upon whether the area depicted is urban, rural or uninhabited. The study area, is located outside of any urban area, and therefore the accuracy coincided with the values stated in table 4.7 for the 1:2500 scale, the basic scale at which rural locations are mapped.

Original survey scale	99% confidence level (m)	95% confidence level (m)	RMSE (m)
1:1250			
Absolute accuracy	0.9	0.8	0.5
Relative accuracy	+/- 1.1 (up to 60)	+/- 0.9 (up to 60)	+/-0.5 (up to 60)
1:2500			
Absolute accuracy	2.4	1.9	1.1
Relative accuracy	+/- 2.5 (up to 100)	+/- 1.9 (up to 100)	+/- 1.0 (up to 100)
1:10000			
Absolute accuracy	8.8	7.1	4.1
Relative accuracy	+/- 10.1 (up to 500)	+/- 7.7 (up to 500)	+/-4.0 (up to 500)

Table 4.7: OS map accuracy (source: Ordnance Survey, 2021).

The control points were chosen as those that are common to both the historic map and the spatially referenced map, such as a road intersection. The precise coordinates are taken from the modern map. Control points may also be provided through field observations, such as those derived from GNSS survey or extracted from Airborne/RPAS lidar data and are also be referred to as Ground Control Points (GCPs). As mentioned above, in regards to historic map registration, the control points were extracted from a modern spatially referenced map for georeferencing.

Beckfoot study area			
Epoch no	**Map sheet**	**Number of CPs**	**RMSE (m)**
Epoch 1	County Series 1st Edition 1:2500 Downloaded mosaic covering extent of study area from Digimap	11	**3.02**
Epoch 2	6" (Second edition 1901) Cumberland XXVII N.E. Revised in 1899	26	3.20
	6" (Second edition 1901) Cumberland XXVII N.W. Revised in 1899	8	3.12
	6" (Second edition 1901) Cumberland XXVII S.W. Revised in 1898-99	16	2.78
Mean RMSE			**3.03**
Epoch 3	6" (Edition of 1926) Cumberland XXVII N.E. Revised in 1923	27	3.62
	6" (Edition of 1926) Cumberland XXVII N.W. Revised in 1923-4	8	2.44
	6" (Edition of 1926) Cumberland XXVII S.W. Revised in 1923-4	16	2.35
Mean RMSE			**2.80**
Epoch 5	National Grid 1:10560 (1st Imperial Edition) Downloaded mosaic covering extent of study area from Digimap	11	**3.67**

Table 4.8: Georeferencing results for Beckfoot study area. The bold numbers were those used to provide uncertainty values in the subsequent 2D change detection analyses.

First order polynomial (affine) transformations were used to align each OS historic map sheet to OSGB36. This is a projective transformation that preserves collinearity, meaning that points, which formed a line in the original data, will form a line in the transformed data (Weisstein, 2022). In addition, ratios of distances are preserved, therefore, the original midpoint of a line remains the same after transformation (Weisstein, 2022). Angles and lengths, however, may change (Weisstein, 2022). While a minimum of three control points are required to solve the six unknowns of this transformation, more are recommended to identify and remove inaccurate control points from the calculation resulting in improved overall accuracy of the transformation (ESRI, 2021). The number of control points varied according to map sheet coverage and was limited by the occurrence of common points.

Control points were evenly distributed, as much as the data would allow, with one located roughly in each corner, if available.

Table 4.8 provide the details of the number of control points used per map sheet and their associated RMSE. Epochs 1 and 5 maps were downloaded from Digimap as a georectified raster mosaic. To assess the quality of the spatial alignment of these maps that had already been registered to the desired coordinate system, links (polylines) were created between points found on the georectified OS historic map to their associated point on the 2017 OS MasterMap. The RMSE of the links was then calculated using the *Calculate Transformation Error* tool offered by ArcMap. For this calculation the method was set to affine.

4.3.3.2 Archived aerial photographs

The archived aerial photographs were scanned at the Historic England archive premises on a non-photogrammetric scanner with a resolution of 600 dpi. Where possible, the negatives or slides were scanned directly. When slides and negatives are unavailable the paper copies are scanned instead. The Historic England archive did not have the means of photogrammetric scanning for the aerial photographs (Rogers, 2019). Moreover, it was not permitted to remove the archived material from the premises, thereby prohibiting photogrammetric scanning at a secondary location (Bryan, 2019).

Orthomosaics and 3D dense point clouds of the study area were created in Agisoft Metashape Professional Edition, version 1.5.2 from archived aerial photographs using a SfM-MVS workflow. Photographs were cropped to the film size before being loaded into a new Metashape project. Within the Metashape project, masks were drawn around any remaining image borders and bodies of water to exclude this information from image alignment and subsequent processing steps. For epoch 6, as the camera calibration report was retrieved by David Holland of Ordnance Survey, therefore, the fiducial parameters were updated accordingly (see section 4.3.2.2, Table 4.5). Fiducial markers were placed in the precise location on each of the photographs as indicated by the fiducial marks on the scanned images. Once these initial steps were completed, the scanned images were then aligned using the highest accuracy setting with generic preselection resulting in the tie point cloud. Key point and tie point limits for the creation of the sparse point cloud were each set to zero. By setting the key limit to zero there is no limit to the number of key points and therefore MetaShape can find as many as possible, however this may lead to some

unreliable results (Agisoft, 2021, p.31). When using a value of zero for the tie point limit, no filtering of tie points is applied (Agisoft, 2021, p. 31).

This alignment process estimated the exterior orientation parameters (positions and orientations) of the cameras based on 3 translation components and 3 Eurler rotation angles, and the interior orientation parameters (camera focal length, principle point image coordinates and distortion coefficients) of the images. In Metashape these two parameters were calculated using aerotrianguation with a bundle block adjustment based on the collinearity equations (Agisoft, 2021, p. 28).

To provide scale and spatial referencing to real world coordinates, GCPs were selected from locations found on the Environments Agency's latest airborne lidar dataset (Epoch 14 - 2018) that corresponded to locations on the archived aerial photographs. OSGB36 coordinates in the form of easting, northing and orthometric height values were extracted from the lidar point cloud to an Excel table and given a unique ID. Numbered markers, labelled with the relevant unique ID were placed on each of the scanned images in the corresponding locations within the Metashape project. The numbered markers were then assigned OSGB36 grid coordinates by importing the Excel table. . The coordinate and marker reference settings, marker and image accuracy settings and capture distance were updated in the reference system settings. The coordinate and marker references were set to OSGB1936/British National Grid + ODN height (EPSG::7405). The marker accuracy was set to 0.18/0.05 m. Camera accuracy in metres and degrees as well as capture distance varied in each of the Metashape projects according to the camera properties. Using these reference settings along with the GCPs, the camera alignment was optimised for f (focal length in pixels), K1, K2, and K3 (radial distortion coefficients), P1 and P2 (tangential distortion coefficients) and B1 and B2 (affinity and non-orthogonality (skew) in pixels coefficients. This was completed by Metashape using a bundle adjustment which refined the exterior camera and interior image orientation parameters along with the triangulated tie point coordinates.

Once the bundle adjustment was completed a dense point cloud was then constructed within the Metashape project using the optimised exterior and interior orientation parameters, the depth maps and dense stereo matching. From the dense point cloud a mesh was created. Texture derived from the scanned photographs was added to the mesh. This textured mesh was saved and used for display purposed only. The following, table 4.9, provides details regarding the ground control points RMSE for each epoch.

Epoch no.	Year	Number of GCPs	X error (m)	Y error (m)	Z error (m)	XY error (m)	Total error (m)	No. of photos
4	1948	19	0.467241	0.66759	0.74476	0.814856	1.10393	6
6	1991	30	0.58782	0.674404	0.0167037	0.894624	0.89478	4

Table 4.9: Spatial error in metres as reported by Metashape.
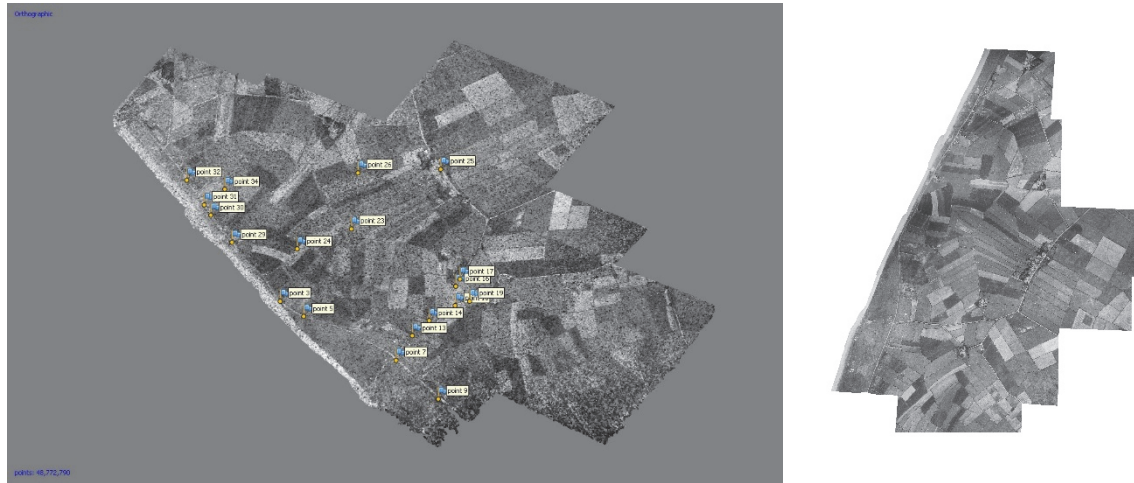
Figure 4.7: Epoch 4; 1948 (left) dense point cloud with GCPs; and (right) orthomosaic.
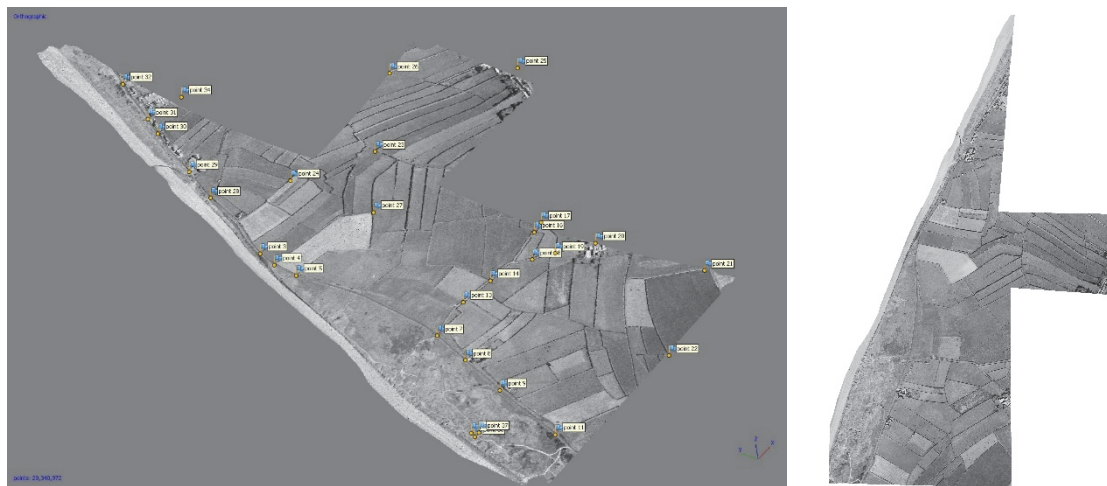
Figure 4.8: Epoch 6; 1991 (left) dense point cloud with GCPs; and (right) orthomosaic.

DEMs were created from the dense point cloud (Figure 4.7 and Figure 4.8) in order to provide surface input to build the orthomosaic. The DEMs along with the scanned photographs, were used to generate an orthomosaics. The Orthomosaics and the dense point clouds were the output products that were used in the subsequent change detection analyses. For the 2D change detection analysis the orthomosaic provided the proxy data for change detection. For the 2.5D change detection a DEM was constructed in ArcMap from the 1991 dense point cloud (section 4.3.6). The 1991 dense point cloud itself was used in the 3D change detection analysis. Co-registration was completed prior to DEM generation and 3D change detection.

4.3.3.3 Orthophotographs

The orthophotographs did not require any pre-processing. These images were supplied as georectified imagery aligned to the appropriate spatial referencing system used in this research.

4.3.3.4 Airborne lidar

The point clouds were provided as pre-classified laz files (las zipped files). As the Environment Agency used a fully automatic classification routine, not all points were classified correctly. To improve the classification of ground points, lidar point clouds were reclassified using TerraSolid's TerraScan in Bentley MicroStation. All points were first assigned to 1-unclassified. Classification routines were then used to filter out 7-low points and noise and 73-thinned points, in the point clouds. This was followed by a ground classification routine that was parametrised to suit the terrain type to classify 2-ground points. Vegetation classification routines were used to assign points to 3-Low, 4-medium and 5-high vegetation points. Finally, 6-buildings points were also classified.

Even with the use of a ground classification routine optimised for terrain type, several points that should have been assigned to 2-ground were not included. These points were located mainly in areas with sharp break of slopes, such as those found along the crest of a cliff, and in areas of dense vegetation. Therefore, manual editing was undertaken focusing on these two areas. This editing was assisted by an editable surface model created from the ground points. The editable surface model would dynamically update as points were added to/removed from 2-ground class. Once satisfaction was achieved 2-ground and 6-building points were then saved in las 1.2 file format.

4.3.3.5 RPAS lidar

There were several steps required to process the RPAS lidar data (epoch 15) for the Beckfoot study area. These steps have been summarised below:

1. Process GNSS base station observations against OS Net base station using Leica Infinity.
2. Create data folder structure with MMProcess and save raw IMU .bin files and raw lidar .rpx files to relevant folders.
3. Convert IMU data with SBG System to a format that can be read by Inertial Explorer.

4. Process converted IMU data using the processed base station coordinates (results from step 1) in Inertial Explorer.

5. Export results from step 4 as .pos file (file containing processed position coordinates of RPAS).

6. Import .pos and .rpx file into MMProcess, update processing parameters and run. This step outputs trajectory .trj files and a lidar point cloud .las file.

7. Create TerraScan Project in MicroStation.

8. Create processing block boundaries, to encompass up to 30 million points – this is the recommended maximum number of points to work within a block.

9. Add trajectories (.trj files) and edit to remove unwanted data (i.e., take-off and landing trajectories, IMU initialisation trajectories and turning trajectories).

10. Load .las file into TerraScan project which has coordinate system defined as OSGB36.

11. Run initial classification routine to clean the point cloud (as per method described in 4.3.3.4).

12. Perform strip adjustment with TerraMatch to remove systematic errors and co-register points per flight line to one another (Figure 4.9).

13. Run classification routine on adjusted point cloud (as per method described in 4.3.3.4).

14. Check classification and manually edit classes using dynamically updated surface model (as per method described in 4.3.3.4).

15. Apply vertical corrections using GCPs.

16. Assess vertical and horizontal accuracy using GCPs.

17. Output point cloud (Figure 4.10).
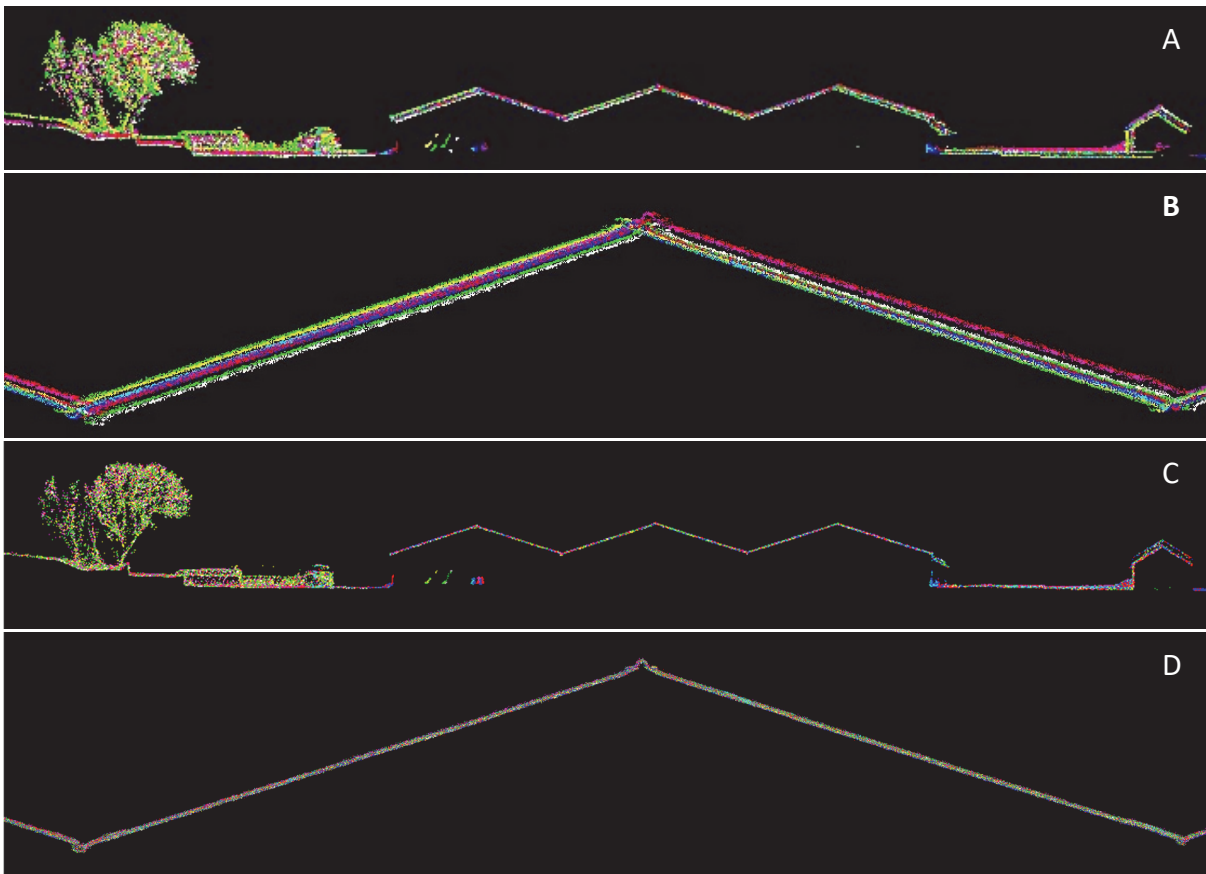
Figure 4.9: Strip adjustment from calibration flight: (A and B) pre strip-adjustment; and (C and D) post strip-adjustment.
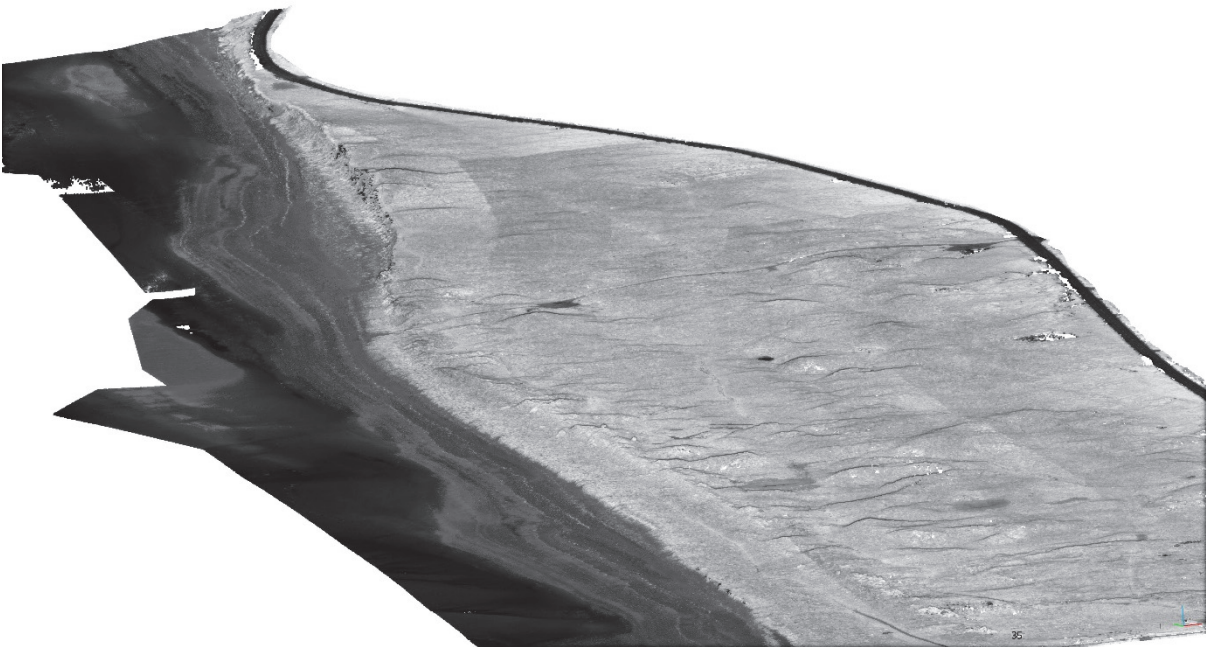
Figure 4.10: RPAS lidar point cloud of the Mawbray Sand Dune SSSI, collected in April 2019.

4.3.4 Co-registration of 3D data

Epochs 6, 7, 8, 9, 12, 14 and 15 – those derived from airborne lidar (Epochs 7, 8, 9, 12 and14), RPAS (Epoch 15) lidar, and archived aerial photographs (Epoch 6) (with an

acceptable quality achieved through the SfM-MVS processing steps) were co-registered to one another using the Iterative Closest Point (ICP) algorithm. See Figure 4.11 for a visual example of two misaligned point clouds that were finely registered using the ICP algorithm. This process of finely co-registering the relevant epochs was undertaken in the Orientation and Processing of Airborne Laser Scanning Data (OPALS) software. OPALS is a modular airborne lidar processing software developed by The Vienna University of Technology, Department of Geodesy and Geoinfromation (GEO). The purpose of the software is to provide a complete workflow for airborne lidar data processing with applications in forestry, hydrography, city modelling and power lines etc. (The Vienna University of Technology - Department of Geodesy and Geoinformation, 2019). The ICP algorithm, within OPALS, is a group of surface matching algorithms that establish correspondences between point clouds iteratively, using the closest point, more generally referred to as the corresponding point (The Vienna University of Technology - Department of Geodesy and Geoinformation, 2019).
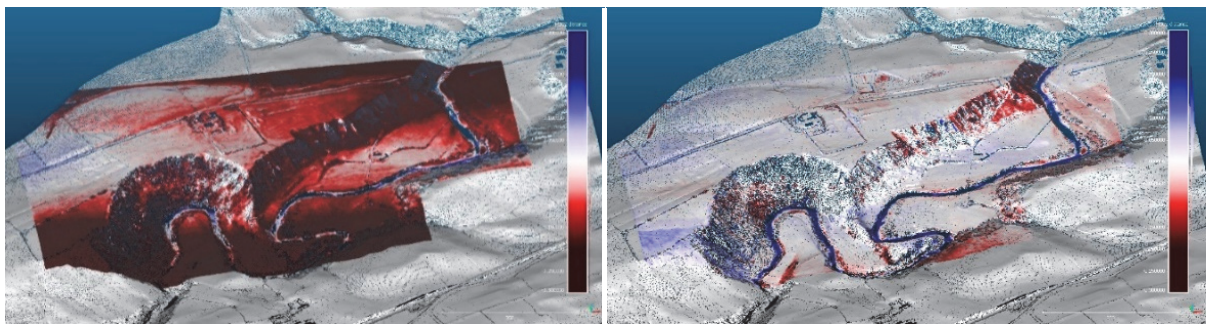
Figure 4.11: M3C2 distances; (left) pre; and (right) post co-registration demonstrating misalignment between original epochs minimized through the application of the ICP algorithm.

The most recent epoch with the most complete coverage of the study area was selected as the 'fixed' cloud, i.e. the point cloud to which all other epochs, referred to as 'loose' clouds, were aligned to. For the Beckfoot study area, Epoch 14 served as the 'fixed' cloud, while epochs 6, 7, 8, 9, 12, and 15 were 'loose' clouds.

OPALS Module ICP was run three times using the following three transformation types; Rigid, Full and Helmert. To confirm co-registration had been achieved correctly the ICP results were assessed using the M3C2 algorithm to compare pre and post co-registration results (Table 4.10). This was done in accordance with research completed by the CHT2 project for sites from Hadrian's Wall (Peppa *et al.,* 2018, p. 10). Alternatively, assessment of the ICP algorithm may be completed through comparison to a mesh (i.e. cloud-to-mesh described in Chapter 3 section 3.2.3.3) as per Guidi et al (2020). The M3C2 point clouds with

the lowest RMSE determined the co-registered point cloud per epoch to use in the subsequent change detection analysis. These are highlighted in bold in the table below.

Epoch pair	M3C2 statistics pre ICP co-registration			M3C2 statistics post ICP co-registration			Transf. type
	Mean (m)	SD (m)	RMSE (m)	Mean (m)	SD (m)	RMSE (m)	
2018 - 1991	0.152	0.644	0.662	0.902	1.118	1.437	Helmert
				0.905	1.118	1.438	Rigid
				0.244	0.557	0.608	**Full**
2018 - 2009	0.177	0.296	0.345	0.039	0.295	0.297	**Helmert**
				0.039	0.295	0.297	Rigid
				0.041	0.296	0.299	Shifts
2018 - 2010	0.147	0.277	0.313	0.036	0.277	0.279	Helmert
				0.036	0.277	0.279	Rigid
				0.036	0.277	0.279	**Shifts**
2018 – 2013	0.154695	0.306437	0.34327	0.059	0.308	0.313	Helmert
				0.059	0.307	0.313	Rigid
				0.054	0.306	0.311	**Shifts**
2018 - 2017	0.019	0.259	0.260	0.004	0.259	0.259	**Helmert**
				0.004	0.259	0.259	Rigid
				0.006	0.259	0.259	Shifts
2018 - 2019	0.104	0.341	0.357	0.018	0.369	0.370	Helmert
				0.057	0.337	0.342	**Rigid**
				0.008	0.373	0.373	Shifts

Table 4.10: Results of M3C2 analyses to assess ICP transformation. The transformation type in bold indicates the transformed point cloud data used in subsequent change detection analysis.

4.3.5 Boundary feature definition and vectorisation

Defining a boundary feature that is common across all epochs is an essential step to 2D change detection, which enables multi-temporal comparison of geomorphic change. The boundary delineates a features position at discrete points in time in which change can be measured, such as a spatiotemporal time series of shorelines, cliff edges, glacier limits, land

use/cover limits or river banks (Himmelstoss *et al.*, 2021, p. 1). The chosen boundary feature needs to be represented by vector polyline(s) for each epoch in the spatiotemporal time series. In this research, this was achieved either by digitising from clearly marked features on georeferenced historic maps, orthomosaics and orthophotographs, or by extracting these features from airborne and RPAS lidar datasets.

For the Beckfoot study area, the coastline as defined by the boundary between the beach and the sand dunes served as the boundary feature. The coastline was chosen as there were documented accounts of dune erosion within the study area dating back to at least the early 1900s. In addition, as stated above (section 4.2) the remains of a Roman cremation cemetery are buried within the sand dunes, which are being destroyed through natural processes causing coastal erosion. Consequently the evolution of the seaward extent of the dunes as indicated by the coastline (defined above) was the focus of the 2D change detection analyses.

Digitising the relevant boundary features from each epoch derived from OS historic maps and aerial photographs was completed with ArcMap 10.6 Editor tools. First a polygon feature class was created with a text field to input the date of each epoch into the adjoining attribute table. Then, within an editing session, the line demarcating the edge of the dunes found on OS historic maps, and the boundary between the dunes and the beach as indicated by the change from vegetation to beach deposits as seen on the aerial photographs were manually traced as polylines within a feature class. After which the date field was updated in the attribute table. .

Extracting the relevant boundary features from the epochs derived from lidar was a two-fold process. First, CloudCompare was used to extract the desired points and second ArcMap was used to create the boundary feature polyline based on the extracted points. Figure 4.12 shows the workflow in CloudCompare. Verticality was calculated across the point cloud ground points. The data was then filtered by value based on the verticality results to exclude flat terrain, such as the beach in the Beckfoot study area. Manual editing was necessary to clip unwanted points that remained in the filtered cloud. The remaining points were then saved as .las files for import into ArcMap as multipoints. Polygons were automatically drawn around the multipoints and clipped so that only the polyline representing the boundary feature remained.
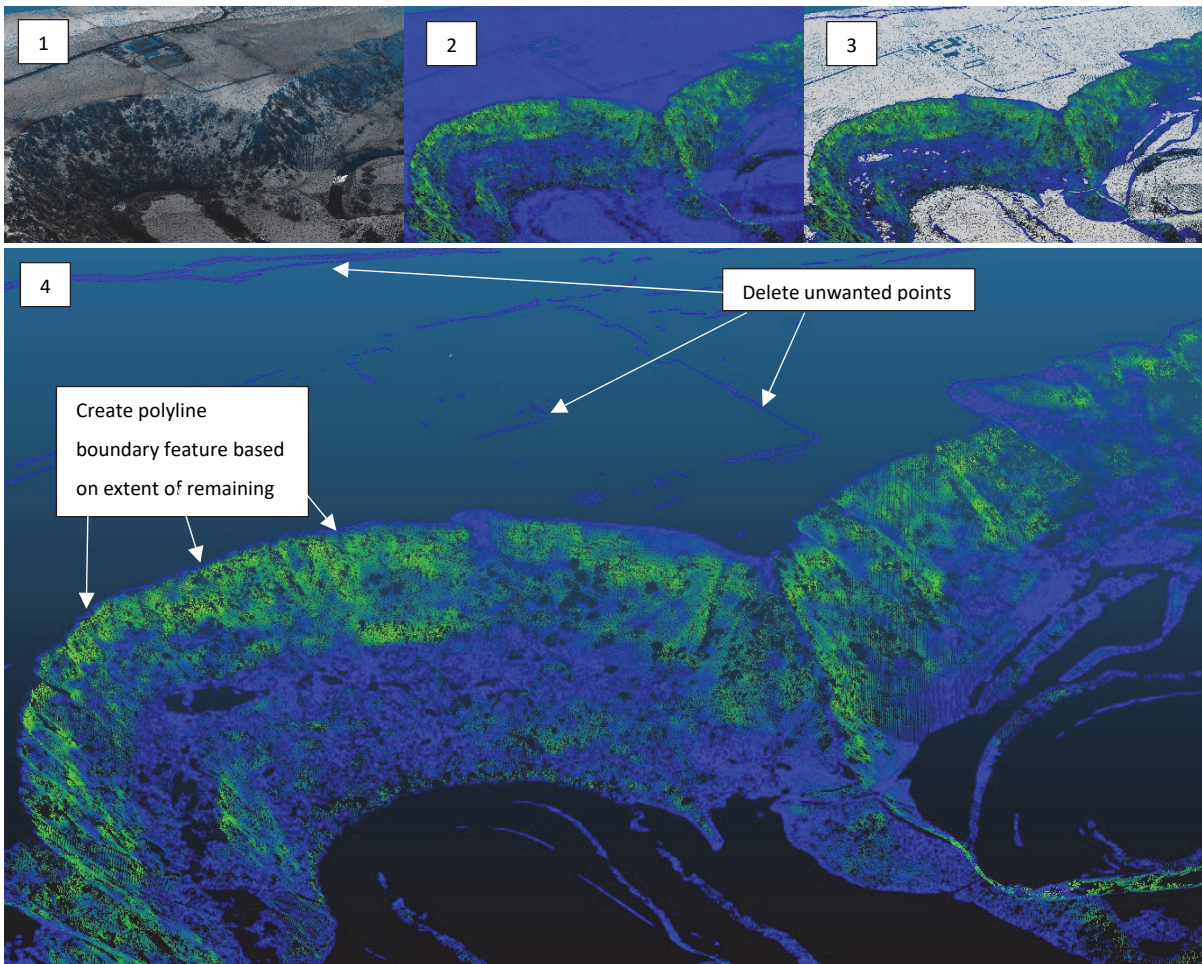
Figure 4.12: Extracting boundary feature points from lidar epochs; 1: ground points displayed by intensity; 2: ground points displayed by verticality (calculated with a search radius of 3); 3: point removal selection; and 4: remaining points.

4.3.6 DEM generation

Digital elevation models (DEMs) were created for epochs that contained 3D information. These included epochs derived from archived aerial photographs that had acceptable results from the pre-processing methodology, as well as airborne and RPAS lidar. For epochs derived from archived aerial photographs, the dense point cloud was used as the input data for DEM generation. For airborne and RPAS lidar, the input data were the classified ground points.

All DEMs were created using ESRI's ArcMap 10.6.1. As ArcMap does not directly read las data, these files were converted to MultiPoint features, using the las to multipoint tool found in the 3D analyst toolbox. The average point spacing was used as part of the las to multipoint conversion. Each multipoint dataset was saved as a point feature class within a feature dataset all of which were located within a file geodatabase.

A polygon feature class, named 'boundary', was created to define the limits of the processing area for conversion from a point cloud to a DEM raster. A polygon was drawn around the desired extent of the study area using this feature class. The boundary feature class, the multipoint feature class and the average point spacing were then used to create a triangulated irregular network (TIN) terrain. For this, the boundary feature class was set to hard clip, while the multipoint feature class provided the height data and was set to mass points. The resulting terrain was then converted to a raster DEM using the terrain to raster tool, also found in the 3D analyst toolbox. The output datatype for the raster DEM was set to float, the method was natural neighbours and the cell size was set to 1 m for a 1 m resolution DEM. In the environments menu the predetermined extents were inputted, using values generated by the *Raster Orthogonality & Concurrency Calculator* developed by North Arrow research. These values ensured the output DEM raster's were concurrent, orthogonal and dimensionally divisible. The DEM derived from the 'fixed' cloud for fine registration was created first. This was then used as a snap raster for all subsequent DEMs, so that the cell alignment matched throughout the time series. Finally all DEM raster's were exported as tiffs for use in the 2.5D geomorphic change detection analysis.

4.3.7 Quantifying uncertainty

4.3.7.1 For 2D change detection

Each epoch had an associated uncertainty value based on data type which was included in the 2D change detection analyses. The uncertainty values per data type were determined as follows:

- For OS historic map epochs the average RMSE across each of the map sheets per epoch served as the uncertainty value (see Table 4.8 in section 4.3.3.1 for details).
- The XY error reported by Agisoft Metashape represented the uncertainty values for the boundary features digitised from orthomosaics generated from overlapping aerial photographs (see Table 4.9 in section 4.3.3.2 for details).
- According to Edina Digimap (2021b), Getmapping Plc reported the accuracy of the orthophotographs to be +/- 0.75 m.
- The environment agency stated that their point cloud data had a horizontal accuracy of +/-0.40m. This horizontal accuracy served as the uncertainty value.
- Target locations in the RPAS lidar point cloud (observed) were compared to those recorded by GNSS survey (predicted). The distance between the observed and

predicted ranged between 0.03m and 0.14m. Therefore an uncertainty value of +/-
0.15 m was selected for 2D geomorphic change detection.

4.3.7.2 For 2.5D change detection

Uncertainty associated with each of the input DEMs was considered within the 2.5D change detection analyses, which measured the change in elevation between successive epochs derived from archived aerial photographs and lidar.

A uniform error surface was created for the DEM derived from the archived 1991 aerial photographs (Epoch 6) which was based on the RMSE of the SfM-MVS results.

For epoch derived from airborne and RPAS lidar (Epochs 7, 8, 9, 12, 14 and 15), spatially variable error surfaces were created using fuzzy logic. Using fuzzy logic, a fuzzy inference systems (FIS) was created which that outputted a raster surface representing elevation uncertainty, where ever pixel was assigned an uncertainty value based on three DEM surface characteristics and a set of FIS membership categories and rules – these are explained below.

There were three input categories used in the FIS calculations; slope, point density and cloud point density ratio. Table 4.11 defines the FIS membership functions per input category. Slope and point density are common outputs from DEM analyses. However, cloud point density ratio, which is less common, is a metric that accounts for the influence on DEM uncertainty from the presence of vegetation (Schaffrath *et al.*, 2015). This metric calculates the ratio between the density of what Schaffrath *et al.* (2015) refer to as the total point cloud and the above ground point cloud. The total point cloud contains all classified points excluding those deemed noise and overlap, while ground points have also been removed from the above ground point cloud (Schaffrath *et al.*, 2015). A cloud point density ratio close to 1 indicates a high density of above ground points, while a value close to zero indicates a low density of above ground points (Schaffrath *et al.*, 2015), the greater the value the greater the error.

A series of fuzzy logic rules, i.e. 'if… then' statements were then composed which were used to determine the uncertainty value of every cell within the raster error surface. For example, rule number 1 in the Table 4.12, which describes the FIS rules for elevation uncertainty, states that if the slope is low, the point density is low and the cloud point density ratio is low then the output uncertainty value will be average. While rule number 40 states that if the

slope is high, the point density is low and the cloud point density ratio is high then the elevation uncertainty value will be high.

	Low	Medium	High	Extreme
Slope degrees	0-5 (0 0 2 5) No slope to gentle slope	2-17 (2 5 14 17) Moderate	14-32 (14 17 29 32) Steep	29-90 (29 32 90 90) Extremely steep to excessive
Point density	0-1.25 (0 0 1 1.25)	1-2.5 (1 1.25 2 2.5)	2-5 (2 2.25 4 5)	4-132 (4 5 132 132)
Cloud point density ratio	0-0.15 (0 0 0.1 0.15)	0.1-0.45 (0.1 0.15 0.4 0.45)	0.40-0.85 (0.4 0.45 0.75 0.85)	0.75-1.0 (0.75 0.85 1 1)
Output	0-0.3 (0 0 0.2 0.3)	0.2-0.6 (0.2 0.3 0.5 0.6)	0.4-0.85 (0.4 0.45 0.75 0.85)	0.8-1 (0.8 0.9 1 1)

Table 4.11: Lidar FIS membership functions defined per input category.

Table 4.12 (below): FIS rules governing the elevation uncertainty at each pixel within a DEM.

Rule number	Slope category	Point Density	Cloud point ratio	Elevation uncertainty
1	Low	Low	Low	Average
2	Low	Medium	Low	Low
3	Low	High	Low	Low
4	Low	Extreme	Low	Low
5	Low	Low	Medium	Average
6	Low	Medium	Medium	Average
7	Low	High	Medium	Low
8	Low	Extreme	Medium	Low
9	Low	Low	High	Average
10	Low	Medium	High	Average
11	Low	High	High	Average
12	Low	Extreme	High	Low
13	Low	Low	Extreme	High
14	Low	Medium	Extreme	Average
15	Low	High	Extreme	Average
16	Low	Extreme	Extreme	Average
17	Medium	Low	Low	Average
18	Medium	Medium	Low	Average
19	Medium	High	Low	Low
20	Medium	Extreme	Low	Low
21	Medium	Low	Medium	Average
22	Medium	Medium	Medium	Average
23	Medium	High	Medium	Average
24	Medium	Extreme	Medium	Low
25	Medium	Low	High	High
26	Medium	Medium	High	Average
27	Medium	High	High	Average
28	Medium	Extreme	High	Average

Rule number	Slope category	Point Density	Cloud point ratio	Elevation uncertainty
29	Medium	Low	Extreme	High
30	Medium	Medium	Extreme	High
31	Medium	High	Extreme	Average
32	High	Low	Low	Average
33	High	Medium	Low	Average
34	High	High	Low	Average
35	High	Extreme	Low	Low
36	High	Low	Medium	High
37	High	Medium	Medium	Average
38	High	High	Medium	Average
39	High	Extreme	Medium	Average
40	High	Low	High	High
41	High	Medium	High	High
42	High	High	High	Average
43	High	Extreme	High	Average
44	High	Low	Extreme	Extreme
45	High	Medium	Extreme	High
46	High	High	Extreme	High
47	High	Extreme	Extreme	Average

Table 4.12 (continued): FIS rules governing the elevation uncertainty at each pixel within a DEM.

4.3.7.3 For 3D change detection

For 3D change detection surface roughness of the point clouds was used as a measurement of uncertainty. This was calculated as part of the M3C2 algorithm, which provides a spatially variable confidence interval for each M3C2 distance measurement (See Chapter 3, section 3.2.4.3 for M3C2 details).

4.4 Modelling future geomorphic change

4.4.1 DSAS Beta Shoreline Forecasting

The DSAS Beta Shoreline Forecasting tool was used to forecast the position of the coastline from within the Beckfoot study area in 10 and 20 years' time. This forecast was based on the historical positions of the coastlines defined for the 2D change detection analysis described in section 4.3.1.1. The Beta Shoreline Forecasting tools uses the linear regression rate, therefore, 2D change detection using the DSAS must be completed prior to applying the forecasting tool (Himmelstoss *et al.*, 2021, p. 56).

Using the earliest coastline position in the time series (1866) the Beta Shoreline Forecasting tool estimated the coastline position for each successive time step until the next coastline

position was detected (Himmelstoss *et al.*, 2021, p. 57). A Kalman filter that was further developed by Long and Plant, was then applied to analyse and minimise error between the forecasted and observed coastline positions, to improve the forecast and update the associated rate of change and uncertainties (Himmelstoss *et al.*, 2021, p. 57). The process was then repeated with the updated rate until the next coastline position was detected (Himmelstoss *et al.*, 2021, p. 57). Again, the Kalman Filter was applied for the same reasons as previously described (Himmelstoss *et al.*, 2021, p. 57). This process was repeated with the new rate and so on until the forecast date was reached (Himmelstoss *et al.*, 2021, p. 57).

The Beta Shoreline Forecasting tool was first run on the historical coastline positions dating to 2009 and earlier. In doing so, the 2019 position was forecasted. This forecasted 2019 position was then compared to the 2019 coastline position known from orthophotographs (Epoch 17). This allowed for the assessment of the tools forecasting capabilities.

In order to forecast the 2029 and 2039 coastline positions, the tool was run a second time. In each instance all coastline positions in the spatiotemporal time series were included in the calculation.

4.4.2 XBeach

Predicting coastal dune erosion was explored using the XBeach model, in order to demonstrate the potential of numerical modelling within a cultural heritage context. The reaction the coastline within the Beckfoot study area was modelled under two different coastal management strategies XBeach. These were based on strategies outlined in the coastal management plan (ref). The first model was under the current management strategy which employs a rock armour wall to protect the coast road B5300, while the second model was under the management strategy of no active intervention. In this scenario, nature is left to take its course.

XBeach, which stands for eXtreme Beach behaviour, was originally developed to model the impact of hurricanes on sandy coasts (Roelvink *et al.*, 2009, p. 1133). It has been further developed to simulate storm impacts on other types of coasts. The model has undergone rigorous testing and has been applied to several coastal types including gravel, coral, vegetated, dune and urban coasts (Deltares, 2018, p. 1).

XBeach is a 2DH process-based numerical model, which is capable of modelling complex systems with significant alongshore variability that can include the presence of hard

structures such as a sea walls (Roelvink *et al.*, 2009, p. 1133). The model can also be nested into a Simulating Waves Nearshore (SWAN) model (Deltares, 2018, p. 33). This model includes physics regarding both hydrodynamic and morpho-dynamic processes. The former accounts for short wave transformation (refraction, shoaling and breaking), long wave transformation (generation, propagation and dissipation), wave-induced setup and unsteady currents, as well as overwash and inundation, while the latter accounts for bead load and suspended sediment transport, dune face avalanching, bed update and breaching (Deltares, 2018, p. 1).

An irregular computational grid was created with a minimum grid size of 5 by 5 m in the nearshore and coastal dune area. The grid increased to a maximum of 20 by 20 m in the offshore area. By creating an irregular grid, the computational time was decreased. Both models used the 2013 lidar point cloud to provide the combined topographic and bathymetric (topobathy) surface of the study area. The grid and topobathy was extended seaward with an increasing depth of up to 15 m in order to create deep water in which to initiate wave conditions. Both models also simulated hydro- and morpho- dynamics under storm conditions. Wave and tide data was altered to be more representative of the Solway Firth. The first model included a non-erodible layer containing information regarding the location of the rock armour wall. This layer stopped erosion from occurring in the specified location. The second model was run without this layer.

4.5 Conclusion

This chapter briefly introduced the Beckfoot study area, which was selected for a detailed natural hazard impact assessment. It highlighted the main reasons for selection being proximity to the coast, vulnerability of the sand dunes to coastal erosion and poorly understood Roman burial practices associated with the Frontier.

This chapter presented the various data types and change detection methods employed to quantify past geomorphic change. Due to characteristics of each of the datasets, not all change detection methods were appropriate for all data types. Therefore, a multi-modal approach was taken in order to assess change over a longer temporal range but also to provide additional details which are not offered by one method alone. In addition, by combining the three techniques, distances and rates of change could be calculated through 2D change detection, areal and volume measurements were derived through 2.5D change

detection, and finer details of geomorphic change were visualised by means of 3D change detection.

Details of the spatiotemporal time series, which was comprised of OS historic maps, archived aerial photographs, orthophotographs, airborne lidar and RPAS lidar, were provided. Each data type required specific pre-processing steps to prepare the spatiotemporal time series for change detection analyses. These included alignment to one another either through georeferencing to a common coordinate system or co-registering through the application of the IPC algorithm to reduce alignment error. This was an important step to reduce the detection of change attributed to noise. Reclassification of lidar points so as to ensure accurate representation of the ground surface, particularly along breaks of slopes was also completed prior to co-registration. Once co-registration was achieved the 3D point clouds were ready for 3D change detection, however further steps were required for both the 2D and 2.5D change detection methods. These steps included vectorization of the boundary feature, necessary for comparison of its position through time and interpolation to DEMs, a requirement for elevation differencing.

The way in which uncertainty associated with each of the datasets was then discussed. This varied according to change detection method and data type. For example the stated error for airborne lidar was used in the 2D change detection analysis, however a spatially variable error surface was generated for the 2.5D change detection method. Accounting for uncertainty improves by increasing the detection of real change versus change associated with error.

The two methods for forecasting geomorphic change were also detailed. Unlike the past change detection methods which have wide applicability, no one predictive model provides a single solution for understanding future trends and patterns FIS rules governing the elevation uncertainty at each pixel within a DEM.. Rather, it is important to choose appropriate models based on the physical processes one wishes to simulate. Within this research the selected models were developed specifically to study coastal change as coastal erosion is threatening and impacting upon the archaeological remains of the Study area.

The following chapter provides a detailed background of the Beckfoot study area. The chapter focuses on both the archaeological evidence and information regarding the hydro- and morpho-dynamics occurring within the study area. A conceptual model is presented to

provide a detailed understanding of the interactions within the natural system and influences of mitigation strategies with the archaeological landscape associated with Hadrian's Wall WH site. In doing so, inferences regarding impact on the archaeological record can be made. Having a detailed knowledge of the dynamic system can help with interpreting the change detection and future modelling results.

Chapter 5: The Beckfoot study area and coastal erosion: a conceptual model

5.1 Introduction

This chapter presents a conceptual model for the foci of this research; the Beckfoot study area. This chapter reviews the archaeological evidence within the study area in conjunction with its wider topographical, geological and hydrodynamic settings to understand the way natural hazards are impacting upon this cultural heritage landscape. The chapter concludes by drawing together the extensive array of evidence within a single conceptual model to guide the resulting analysis presented in Chapter 6.

The chapter begins by outlining the key points that justify the use of this landscape as the study area for this research (section 5.2). This section is followed by an examination of the national and regional statutory designations within the study area (Section 5.3), representing both archaeological and conservation concerns, followed by a detailed description of the topographic and geographic setting of the study area (Section 5.3). Next, the chapter introduces the archaeological sites of the Frontiers of the Roman Empire World Heritage (WH) site and highlights the key historical and archaeological sites that are found within the Beckfoot study area (section 5.5). A summary of the known information about these keys sites from cartographic data, aerial imagery, lidar data and more than 100 years of archaeological investigation are discussed to provide a detailed assessment of the current extent and knowledge of each of these sites (section 5.6.1-5.6.4). The final section discusses the hydro-dynamic setting of the study area considering the context of the Solway Firth estuary, as well as sediments, tides and the wave and wind climate (section 5.7). Finally, the chapter concludes by discussing the evidence for coastal dune erosion destroying the aforementioned archaeological sites to provide a baseline for the following analysis (section 5.7.5).

5.2 Justification

The Beckfoot study area was selected for detailed analysis for a variety of reasons:

- The study area is located in a highly dynamic coastal zone where natural hazards have justified a coastal management strategy to mitigate against coastal dune erosion threatening the coast road B5300.
- Erosion of the dune system has resulted in the partial destruction of the remains of the Roman cremation cemetery.

- Archaeologists acknowledge that coastal dune erosion has occurred at the Roman cremation cemetery site and recognise that the impact of the erosion is not fully understood on a quantitative level.

- It is believed that Milefortlet 15 has already succumbed to coastal erosion.

- Beckfoot Roman fort and extramural settlement fall within 200 m of the coastline; an area which is considered to be at risk from flooding and erosion (CH2M, 2018, p. 57).

- Roman burials and cemeteries associated with the Roman frontier in Britain, are poorly understood (Petts, 2009, p. 160), due in part to the lack of large scale research excavations (Symonds and Mason, 2009a, p. 65). It is imperative that those managing this internationally important cultural heritage site understand the magnitude and rates of past and future natural hazards events that impact negatively upon this rare, unique and irreplaceable resource.

5.3 Location, topography and geology

5.3.1 Location

The study area is located in North-West England, along the Cumbrian coast on the outer Solway Firth. It is centred on national grid reference (NGR) NY 08642 48318 (Fig. 5.1). The study area measured approximately 291 hectares, and extended for 3000 m, from just beyond Beckfoot Farm in the north to Mawbray in the south.

5.3.2. Topography

The area can be divided into 3 broad topographic regions; the beach, the sand dune system and the coastal hinterland (Fig. 5.2). The beach has a wide shallow intertidal zone (Natural England, 2015, p. 82). It is comprised of a sandy foreshore (Jacobs, 2020b, p. 2) with a sand and pebble upper beach (Natural England, 2015, p. 57) and is backed by low dune cliffs and sand dunes (Natura England, 2015, p. 82). These form part of the Silloth and Mawbray Bank sand dune system. The dunes are narrowest at the point where the B5300 is furthest west. At this location a rock armour wall was constructed in 2013 to protect the B5300 coast road from damage due to the threat of erosion (Coastal Engineering UK Ltd, 2014b, p. 202; Coastal Engineering UK Ltd, 2015a, p. 40). The coastal hinterland, while elevated above the beach, is low lying, with flat or gently undulating fields used as farmland (Natural England, 2015, p. 103). Beckfoot Village is the only settlement located within the Beckfoot study area.
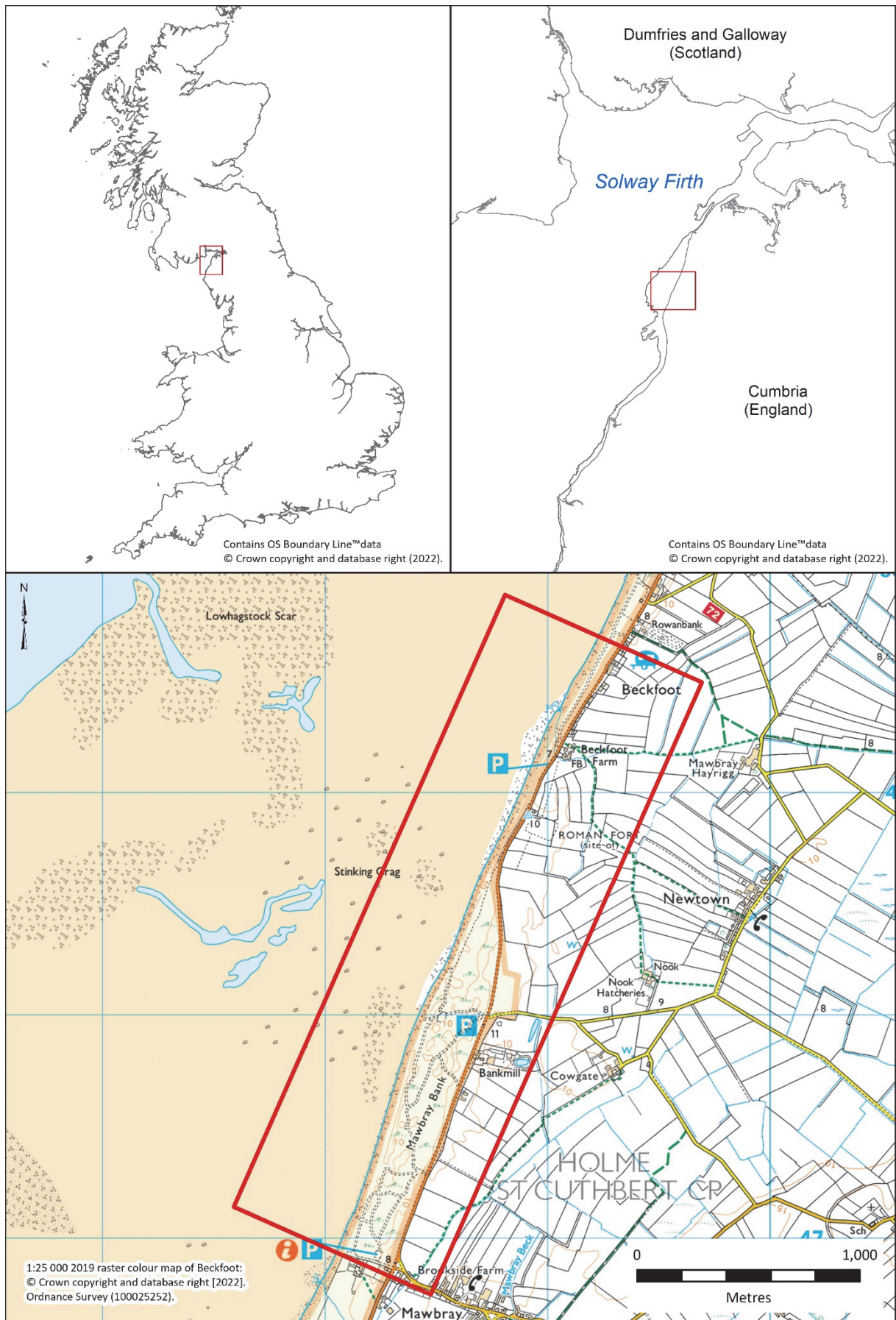
Figure 5.1: Beckfoot study area location map.
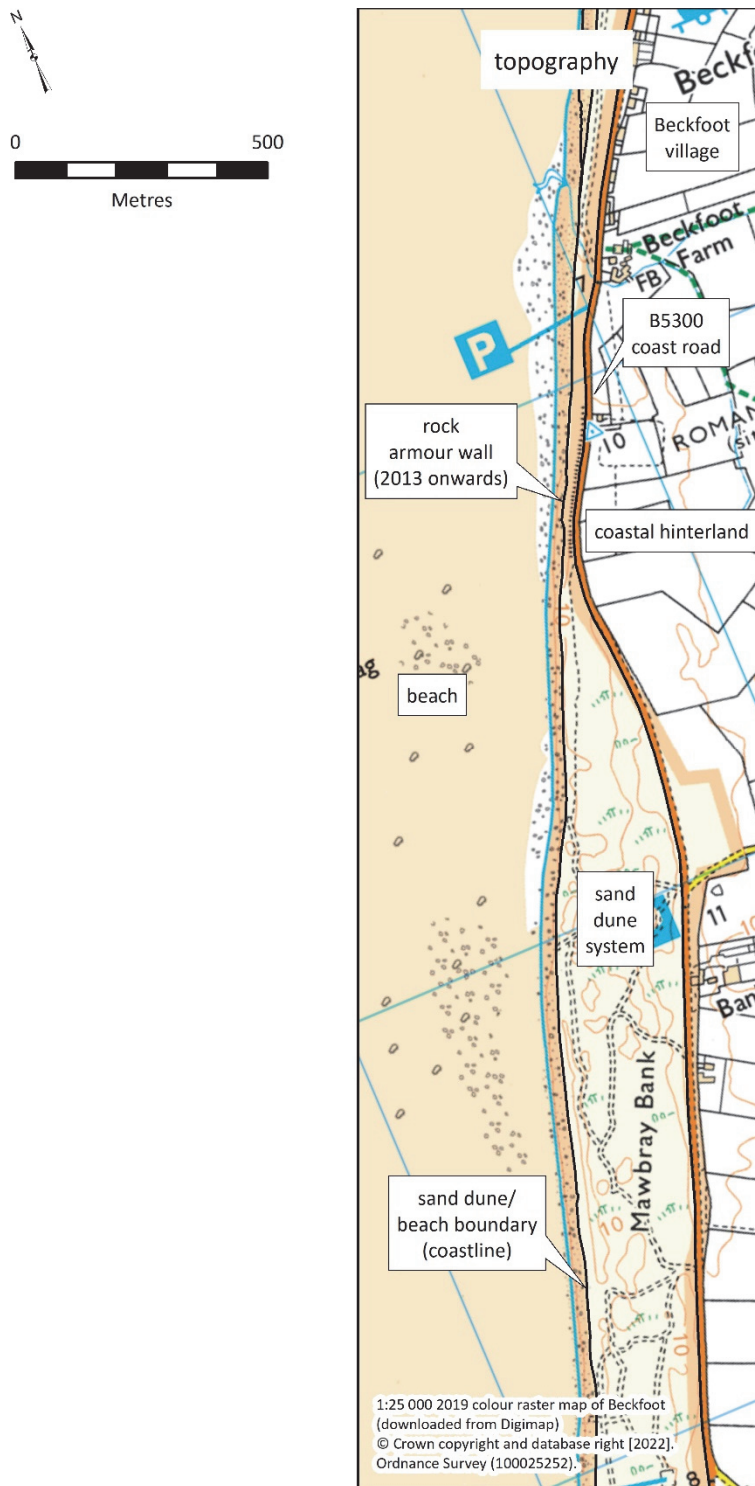
Figure 5.2: Beckfoot study area topography.

5.3.3 Geology

The bedrock geology (Figure 5.3 (left)) is consistent across the study area and belongs to the Mercia Mudstone Group (British Geological Survey, 2021). This group is composed of mudstone with gypsum-stone and/or anhydrite-stone and formed approximately 200 to 251 million years ago during the Triassic period, when the local environment was previously dominated by hot deserts (British Geological Survey, 2021).

The superficial geology (Figure 5.3 (right)) across the study area is spatially variable. Two kinds of superficial geology are present on the beach; intertidal sandflat deposits and marine beach deposits (British Geological Survey, 2021). The intertidal sandflat deposits are located further seaward and are composed of sand, while the marine beach deposits are located closer to the sand dune foot and are composed of sand and gravel (British Geological Survey, 2021). Blown sand composes the superficial geology across the sand dunes. Within the sand dunes there are three areas of raised marine beach deposits. Two of these areas are found in the northern half of Mawbray Bank sand dunes SSSI and the third is located in south-western corner of the SSSI (British Geological Survey, 2021).

Towards the coastal hinterland there is a change in superficial geology from blown sand to raised marine beach deposits, which are composed of sand and gravel (British Geological Survey, 2021). Further inland raised marine deposits can be seen intermixed with a few areas of raised marine beach deposits, which are composed of clay and silt (British Geological Survey, 2021). All of the superficial geological deposits were formed up to 2 and up to 3 million years ago during the Quaternary Period, when the local environment was dominated by shorelines, windblown deposits and shallow seas (British Geological Survey, 2021).

5.4 Designations

There are several statutory designations of natural and heritage value within the Beckfoot study area (Figure 5.4). Statutory designations are given to locations that are considered of national and/or international importance and signify the value and significance of places that meet pre-defined designation specific criteria. These designated places are afforded a level of protection that seeks to maintain or enhance the characteristics that justified designation in the first place. The following designations were sourced from the Multi-Agency Geographic Information for the Countryside (MAGIC) website (DEFRA, 2021).

- The study area is situated within the Solway Coast Area of Outstanding Natural Beauty (AONB), which recognises the natural beauty of the landscape and seeks to conserve and enhance it.
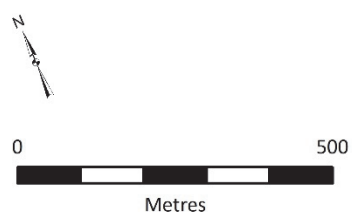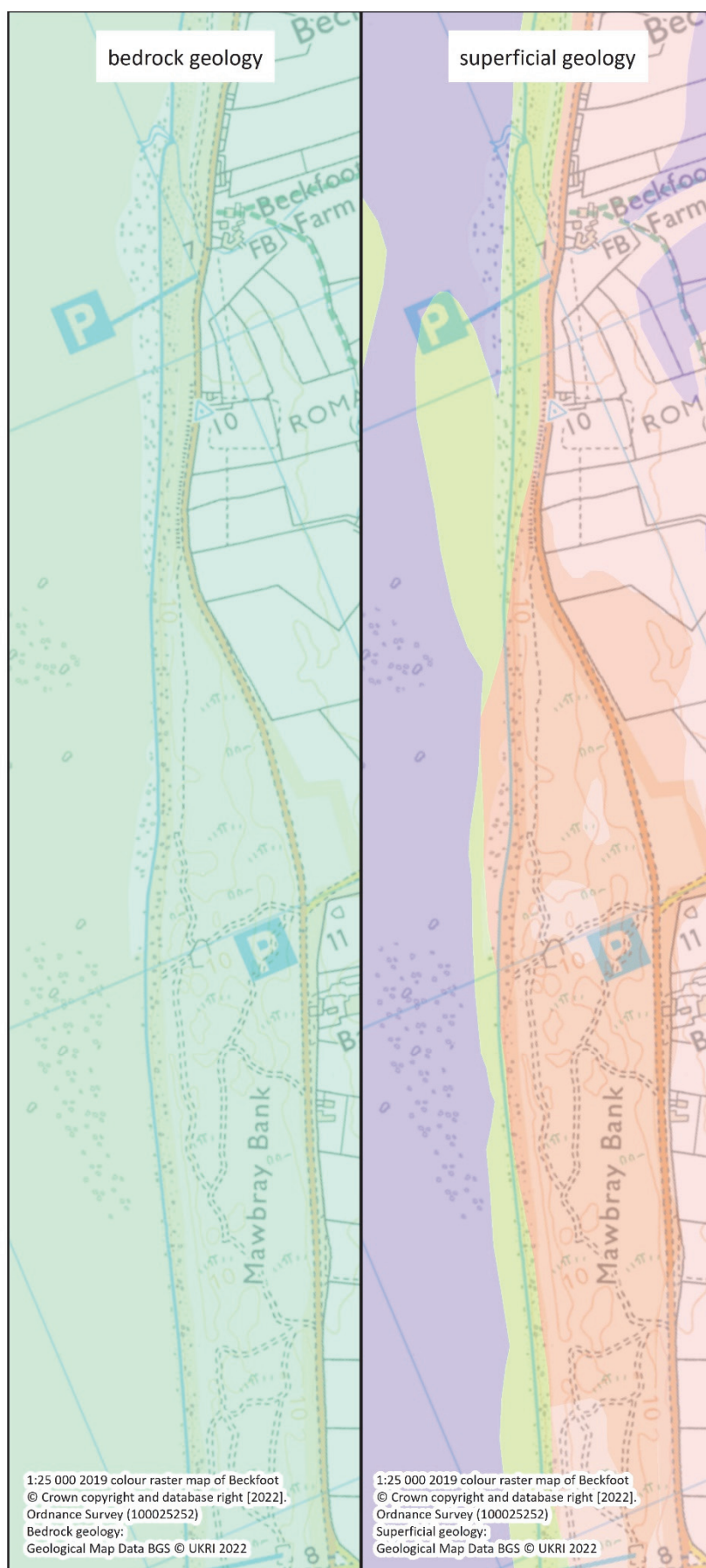
Figure 5.3: (left) Bedrock geology and (right) superficial geology of the Beckfoot study area.

- The study area is located within the Frontiers of the Roman Empire: Hadrian's Wall WH site (WHS 1000098) and buffer zone.

- There are three scheduled monuments (SM) located within the study area. They include Beckfoot Roman Fort (SM 1007170), Roman fortlet (Milefortlet 15) 40m SSW of Castle fields (SM 1007171), and Bank Mill tower 15a, 250m north-west of Belmont house, part of the Roman frontier defences along the Cumbrian coast (SM 1014808). The Roman cremation cemetery located within Mawbray Bank sand dunes is not listed as a scheduled monument, however, the cemetery site coincides with and extends beyond scheduled area for Milforlet 15

- The study area is located partly within the Silloth Dunes and Mawbray Bank Site of Special Scientific Interest (SSSI). The conjectured location of Milefortlet 15, Bank Mill tower 15a and the Roman cremation cemetery site are also located within the SSSI. The SSSI encompasses the coastal dunes stretching from Silloth in the North to Dubmill point in the South, excluding a narrow length of land behind a rock armour wall opposite Beckfoot Roman fort and extramural settlement to the north of the fort. Table 5.1 provides specific details as to present status of the SSSI.

Site status	Percentage of overall SSSI area	Definition
Unfavourable – declining	11.95%	"becoming progressively worse" "will not reach favourable condition without human intervention"
Unfavourable – no change	4.97%	"results not moving towards the desired state" "will not reach favourable condition unless there are changes to the site management"
Unfavourable – recovering	52.34%	"not yet fully conserved but all the necessary management mechanisms are in place" "Provided that the recovery work is sustained, the unit/feature will reach favourable condition in time."
Favourable	30.75%	"designated feature(s) …. are being adequately conserved" "A unit can only be considered favourable when all the component designated features are favourable."

Table 5.1: Silloth Dunes and Mawbray Bank SSSI site classification (Source: Natural England 2021a; Natural England 2021b).

- The beach within the study area is part of the Upper Solway Flats and Marshes SSSI. The area of the SSSI is split into *favourable* (25.25%), *unfavourable – recovering* condition (74.49 %), and *unfavourable - no change* (0.26%) (Natural England, 2021c).

This SSSI is also a designated Ramsar site, a wetland of national importance, and a Special Protection Area, both of which share the same title as the SSSI.

Natural designations

- Solway Coast AONB
- Silloth Dunes and Mawbray Bank SSSI
- Upper Solway Flats & Marshes SSSI

Heritage designatons

- WHS buffer zone
- Scheduled monument

Beckfoot Roman fort SM 1007170

Roman fortlet (milefortlet 150 SM 1007171

Bank Mill tower 15a SM 1014808

natural designations

heritage designations

1:25 000 2019 colour raster map of Beckfoot:
© Crown copyright and database right [2022].
Ordnance Survey (100025252).
AONB and SSSI designations:
© Natural England copyright. Contains Ordnance Survey © crown copyright and database [2022].

1:25 000 2019 colour raster map of Beckfoot:
© Crown copyright and database right [2022].
Ordnance Survey (100025252).
SM and World Heritage designations:
© Historic England [2022]. Contains Ordnance Survey © crown copyright and database [2022].

Figure 5.4: (left) Natural designations and (right) heritage designations associated with the Beckfoot study area.

5.5 Frontiers of the Roman Empire within the Beckfoot study area

5.5.1 Introduction

The study area forms part of the Frontiers of the Roman Empire (FRE) WH site. The FRE represented the physical border of the Roman Empire and stretched for over 5000 km across Europe and North Africa (UNESCO World Heritage Centre, 2021d). This border defined the greatest extent of Roman Empire as it stood in the 2nd century AD (UNESCO World Heritage Centre, 2021d). In Britain, the FRE is represented by two lines of Frontier; the later Antonine Wall in Scotland, which stretched for 60 km from the Firth of Forth to Old Kirkpatrick on the River Clyde (UNESCO WHC, 2021d), and Hadrian's Wall. Hadrian's Wall was constructed in the mid-2nd century AD on orders from the Emperor Hadrian in AD 122 (UNESCO World Heritage Centre, 2021d). It stretched across the landscape for approximately 130 km from the mouth of the River Tyne to the Solway Firth on the Cumbrian coast (UNESCO World Heritage Centre, 2021d). I then continued southwards along the coast for approximately 36 km as a series of military installations (UNESCO World Heritage Centre, 2021d) rather than as a physical wall.

Specifically, the study area focused on part of the Cumbrian Roman coastal defence system (a continuation of Hadrian's Wall in the form of a series of forts, milefortlets, and towers), which stretched from Bowness-on-Solway along the coastline to as far south as Flimby, a village south of Maryport and possibly further, although this has yet to be proven (Bruce and Breeze, 2006, pp. 93-94). In comparison to the extensive knowledge about the main line of Hadrian's Wall and its component parts, the coastal system is much less understood. We do know that the coastal system in the Roman period was represented by a series of milefortlets and towers that protected the western coastline of Britannia from incursion. A series of military forts are also known along the coastline, at Maryport, Beckfoot, Burrow Walls and Moresby (Breeze, 2004, 78), however, the relationship between these and the milefortlets and towers is currently not understood very well (Bruce and Breeze, 2006, p. 96).

The following sections introduce the key archaeological sites within the study area and discusses the significance of these archaeological remains. This is followed by the examination of detailed evidence for each of these sites drawing from cartographic, aerial imagery, and laser scanning data, as well as the archaeological discoveries and investigations from the past 100 years.

5.5.2 Key archaeological sites

Within the Beckfoot study area there are three sites of specific archaeological importance, which are considered within this research. These sites are each introduced below.

Site 1: Beckfoot Roman fort and extramural settlement;

Site 2: Roman cremation cemetery and conjectured location of Milefortlet 15;

Site 3: Roman tower 15A.

5.5.2.1 Site 1: Beckfoot Roman Fort

The remains of Beckfoot Roman fort, also referred to as *Bibra,* are buried within a series of slightly elevated fields adjacent to the B5300 coast road. Specifically the fort is located in an arable field referred to as 'Castlefields', immediately south of the house known as 'Romanway'. The fort stood on land that was approximately 10.5 m Above Ordnance Datum Newlyn (AODN), providing strategic views across the narrow dune system and the Solway Firth, to the land now comprising Dumfries and Galloway, Scotland and further out into the Irish Sea. Our understanding of the fort is incomplete, in part due to limited modern archaeological investigation (see section 5.4.3), however, based on our current knowledge we can outline an understanding of the extent, density and significance of the archaeological remains of this military installation. The fort conforms to the size, shape and internal layout typical of most Roman military forts. Diagnostic pottery and a coin recovered from the fort suggests that it was in use from the Hadrianic period through to the 4th century AD (Bruce and Daniels, 1978, pp. 268 - 69). Based on a stone inscription discovered from the fort (RIB 880), we know that the second cohort of Pannonians were stationed at Beckfoot Roman fort (Robinson, 1881, 143). Recent geophysical survey of the fields outside the fort (see section 5.6.4) indicated that it was surrounded by an extensive extramural settlement, which grew around the fort to the north, south and west (Haynes, 2019, p. 202), after its construction and would have played important economic and social role within the wider landscape. Evidence from geophysical survey suggested that the extramural settlement extended on both sides of the Roman road as far north as the beck, just south of Beckfoot Farm, and continued south of the fort (Haynes, 2019, p. 203) for at least 260 metres. These recent surveys demonstrated the scope of the archaeological evidence beyond the remains of the fort and highlight the greater significance of the site as a source of information about Roman military life beyond that uncovered in earlier investigations.

5.5.2.2 Site 2: Beckfoot Roman cremation cemetery and Milefortlet 15

Approximately 200 m south-west of the fort, found within the Mawbray Bank sand dunes, was the location of both the conjectured location of Mileforlet 15 and known location of a Roman cremation. Milefortlets within the Cumbrian coastal system were timber structures with clay or turf ramparts, similar to the milecastles within the western turf section of Hadrian's Wall (Bruce and Breeze, 2006, p. 94). These structures measured approximately 15 m by 18 m with a rampart measuring 6 m in width (Bruce and Breeze 2006, p. 94). The evidence for Milefortlet 15 is relatively limited and is based predominantly on observations and test pits excavated by Bellhouse in the 1950s (Bellhouse, 1957, pp. 21-22). It is thought, based in part on an investigation of the proposed 1980s location of Milefortlet 15 (Breeze, 2004, p. 76), that the structure may have already been destroyed by coastal erosion (Bellhouse, 1957, p. 22; Caruana, 2004, p. 168).

The position of the Roman cremation cemetery is known from the recognition of archaeological evidence eroding from the sand dunes, as well as recent archaeological evaluations of the site (section 5.6.4). Based on this evidence it would appear that the main burial rite represented in the cemetery was cremation (Collins, 2009, p. 164). These burials took various forms such as pit burials, burials within ditches, burials within ring ditches, pyre dumps, and cist burials (Collins, 2009, p. 164). Pottery and other dating material recovered from the Roman cremation cemetery site provided evidence that suggested the cemetery was in use from the 2nd century AD (Howard-Davis *et al.*, 2017, p. 49) into the 3rd and possibly 4th century AD (Howard-Davis *et al.*, 2017, p. 79). As such it has been argued that the Roman cremation cemetery may have been used by people stationed at Milefortlet 15 before it fell out of use (Collins, 2009, p. 164). The cemetery was then subsequently used by those stationed at the fort and living within the extramural settlement (Collins, 2009, p. 164).

The true extent of the Roman cremation cemetery site is currently unknown, and due to erosion of the western boundary, can never fully be known. Attempts, however, have been made to characterise the site, including its extents (Martin, 2006; Healey, 2007; Collison, 2019). Figure 5.5 depicts our current understanding of the Roman cremation cemetery boundaries. The most recent evaluation, was undertaken by Northern Archaeological Associates (NAA) in 2019. Funerary features found in NAA Trench 1, located between the rock armour wall and the B5300 coast road, indicated that the cremation cemetery extended
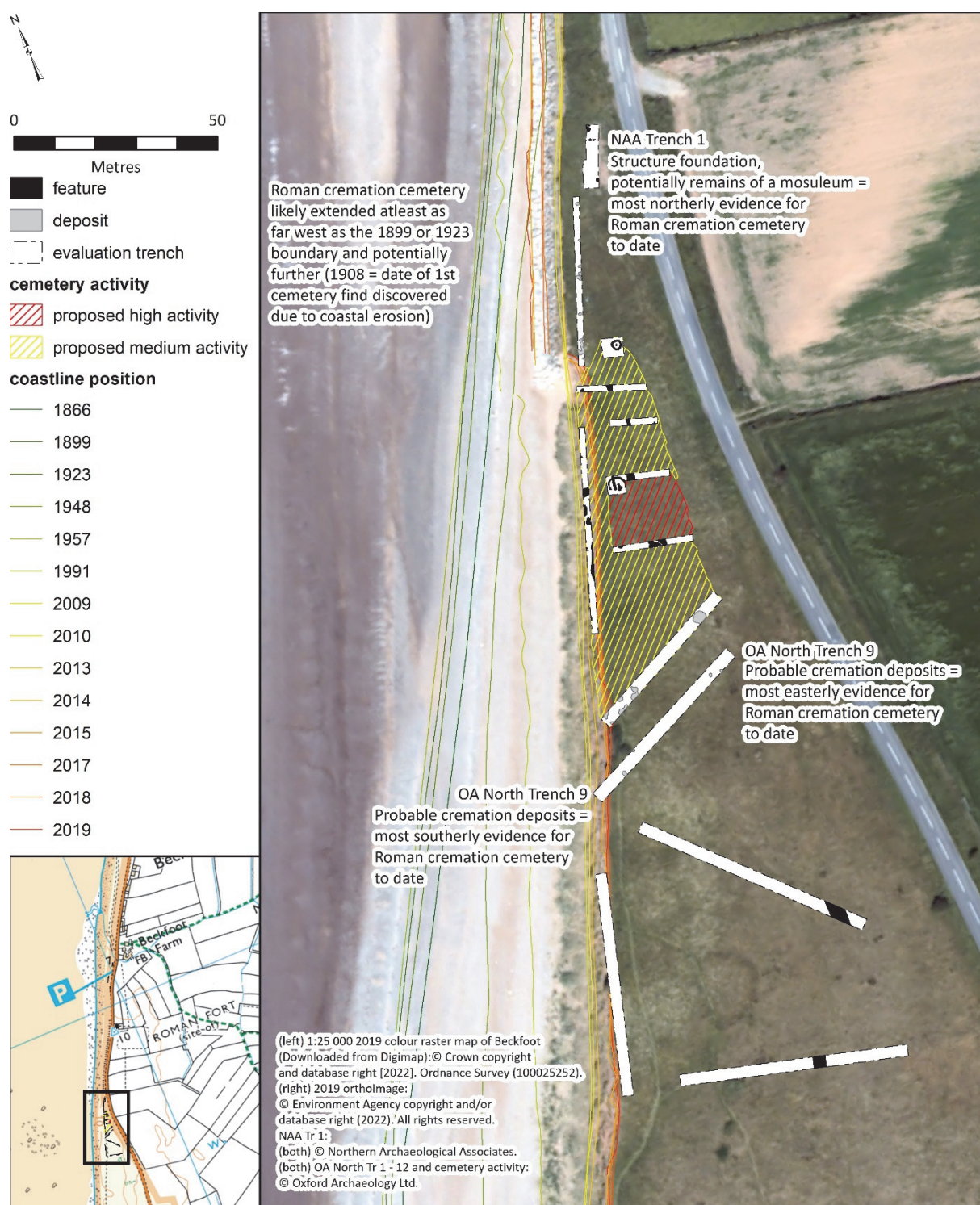
Figure 5.5: Current understanding of the known extents of Roman cremation cemetery site. NAA Trench 1 provided by Northern Archaeological Associates. All other trenches adapted from: Howard-Davis *et.al* (2017, p. 46).

further north than previously thought (Collison, 2019, p. 8). Based on this evidence, Collision (2019, p. 9) suggested that the cemetery likely extended further north of these features. At present, the most southerly evidence for the Roman cremation cemetery, comes from the evaluation conducted by Oxford Archaeology (OA) North (2007). Located approximately 100 m south of the southern terminal end of the rock armour wall, were multiple probable

cremation related deposits (Healey, 2007, p. 92 and 100 - Figure 2). OA North, proposed areas of medium and high cemetery activity based on the quantity of archaeological features discovered in each evaluation trench. Given the funerary features found in trench 1 of the NAA evaluation, these areas may need to be updated.

The investigation of Roman cemeteries has been an identified as a key research priority providing information about funerary tradition, diet and military and civilian life (Symonds and Mason, 2009b, p. 51). Moreover, this is the area that is most at risk of the three defined sites listed above, as coastal dune erosion is not just a threat but an active process, which has resulted in partial loss of the cemetery site and perhaps complete destruction of Milefortlet 15 (Bellhouse, 1962a, pp. 62 - 3).

5.5.2.3 Site 3: Roman Tower 15a

The third area of importance is the location of the buried remains of Roman Tower 15a at Bank Hill. Tower 15a was located approximately 950 m south-west of Beckfoot Roman fort and stood within the Mawbray Bank sand dune system. The position and layout of this Tower has been established through excavations undertaken by Bellhouse during the 1950s (Bellhouse, 1954). The investigations uncovered remains of all four exterior walls and their foundations, as well as an internal hearth, an entranceway in the north-eastern corner and possible evidence for demolition (Bellhouse, 1945, pp. 36 – 40). No further investigations of Roman Tower 15ahave been undertaken, as such the condition of the site is currently unknown.

5.6 Evidence for the key archaeological sites

5.6.1 Historic Maps

Some of the early county maps of Cumberland depict the line of Hadrian's Wall, often labelled as the Picts Wall (Robert Morden map of Cumberland; Speed 1610, Donald 1770-71, Blaeu Atlas Maior 1662-5 Cvmbria, Vulgo Cumberland,) or Scite of the Picts Wall (Greenwood, 1823). None of these maps, including the Cassini Old Series One-Inch map of Carlisle and Solway Firth surveyed between 1791 and 1874 and published in 1897, feature the Roman coastal defence system.

Beckfoot Roman fort does not appear as a feature on any maps until the creation of the Ordnance Survey (OS) 6 inch and 25 inch map series. A cross marking the 'Supposed site of CAMP' at Castle Fields was present on the OS 6 inch map that was surveyed in 1866 and

published in 1868. The 1899 revision of the 6 inch OS map, published in 1901, details a dotted line delineating the outline of the fort, giving an indication of the fort's size. The Roman road extending both north and south of the fort was also indicated on the map as dotted lines. These features were labelled as 'ROMAN CAMP (Site of)' and 'ROMAN ROAD (Site of)', respectively. These Roman roads were also depicted on the 1923 revision, published in 1926, and the 1946 revision, published in 1952, except for the labelling. 'ROMAN ROAD (Site of)' was labelled 'ROMAN ROAD (Course of)' on the later revision. There was no indication of Milefortlet 15 or the Roman cremation cemetery on any of these early OS maps.

The OS 25 inch maps followed the same pattern as the 6 inch versions discussed above. The earliest 25 inch map of the area, surveyed in 1864 and published in 1865, marked the location of Beckfoot Roman fort with a cross labelled '(Supposed site of) CAMP'. The 1899 revision, published in 1900, used a dotted line to delineate the 'Site of ROMAN CAMP' and the 'Site of ROMAN ROAD', while the 1923 revision, published in 1925, changed the labelling of the roman road to 'ROMAN ROAD (Course of)'.

The first edition OS 1:25,000 map, surveyed between 1923 and 1951 and published in 1953, used both a cross and a dotted line to mark the location of the Beckfoot Roman Fort labelling it as 'ROMAN FORT (site of)'. The Roman road north and south of the fort was indicated by a dotted line, however, these features were not labelled. Milefortlet 15 was not present on this map, however, the 'ROMAN BURIAL GROUND' was marked by a cross close to the seaward boundary of the sand dune system. This was the first mention of the Roman cremation cemetery on cartographic sources. The labelled cemetery site may have been included presumably due to cremated remains having been reported to be eroding from the sand dune cliff face during this period (see section 5.6.4.2). A solid line was also included on this map and was labelled 'High Water Mark of Ordinary Tides'. On the OS 1:10,000 map revision, surveyed sometime between pre 1930-1956 and published in 1957, Beckfoot Roman Fort is marked by a dotted line indicating its location, shape and size. The fort is labelled on this map as 'BIBRA ROMAN FORT (site of)'. The 'ROMAN ROAD (course of)' was only present as a dotted line south of the fort. Neither Milefortlet 15 nor the roman cremation cemetery appeared as features on this map.

Dashed lines representing the location, size and shape of 'BIBRA ROMAN FORT (site of)' and the course of 'ROMAN ROAD (course of)' north and south of the fort were present on the OS

1:10000 Map, which was surveyed 1969-71 and published in 1972. This map also marked the location of Roman tower 15a with a cross, which was labelled 'ROMAN TOWER 15A (site of)'.

On all the OS maps discussed above, except for the 1969-71/1972 map, the extent of the sand dune system was depicted by a dashed line and hachuring marking the seaward boundary and by 'rough pasture' symbology representing the coverage of the dunes. On the 1969-71/1972 OS map, the limits of the sand dunes can be inferred from the landward edge of the shingle beach symbology. On all the maps a solid line represented the mean high-water mark, however, these were labelled differently depending on year. The earlier maps used the nomenclature M.W.M (mean water mark) (1864/65), High Water Mark of Ordinary Spring Tides (1866/1868), High Water Mark of Ordinary Tides (1899/1900, 1899/1901, 1923/26 and 1946/52) or HWMOT (high watermark of ordinary tides) (1923/25), while the later maps used 'High Water Mark of Ordinary Tides' (1923-1951/1953), 'High Water Mark of Medium Tides' (pre 1930-1956/1957) and Mean High Water (1969-71/1972).

5.6.2 Aerial Photography

Aerial photographs taken during dry summers when archaeological remains were visible as parch marks due to drought-like conditions, have played an early role in understanding Beckfoot Roman fort (Frere and St Jospeh, 1983, pp. 72-3). They provided additional details, particularly of the fort's internal features, that were not seen on the historic maps or in the early work undertaken by Robinson (see Section 5.6.4).

The archaeological remains of Beckfoot Roman fort were particularly receptive to aerial photographs taken in July 1949, 1975 and July 1977 (Fig. 5.6). The parch mark patterns captured on the aerial photographs have enabled the identification of the Roman road, both north and south of the fort, as well as internal fort features including buildings, roads, the headquarters, the commanding officers house, granaries and barrack blocks (St Joseph, 1951, p. 56). In the oblique aerial photographs taken during July 1949, the Roman road can be seen leading to the fort's south west gate and continuing through the fort as the *via principalis*, the main transverse street, passing in front of the headquarters building (Frere and St Joseph, 1983, p. 72). The *praetentura* (the front division of a fort or camp) was visible west of the *via principalis* (Frere and St Joseph, 1983, p. 72). A buttressed *horreum* (granary) occupied the south-east quadrant of the *praetentura* just inside the southwest gate (Frere and St Joseph, 1983, p. 72). A second *horreum* flanked the opposite side of the *via principalis* in this location (Frere and St Joseph, 1983, p. 72). The headquarters was located centrally

and the commander's house furthest north within the fort's north wall, both situated along the east side of the *via principalis* (Frere and St Joseph, 1983, p. 72). Next to the east *horreum* was potentially a military hospital (Frere and St Joseph, 1983, p. 73). Four to six centurial barracks, possibly supplemented by workshops, were identified in the area between the potential military hospital, headquarters and commander's house and the eastern wall of the fort (Frere and St Joseph, 1983, p. 73). Based on the parch mark evidence, Frere and St Joseph (1983, p. 73) suggested that two barracks were built in the *praetentura* at some point during the fort's use. Some further details, although far less prominent, were located just outside the fort's north-east corner and alluded to a field system suggesting possible evidence for the *vicus* (the extramural settlement) (Frere and St Joseph, 1983, p. 73). Many of the same details have also been revealed as parch marks captured on oblique aerial photographs dating to 1975 and July 1977, although arguably not as well defined as those present on those photographs dating to 1949. In addition to the fort's internal layout, more details for the Roman road could be discerned from the 1975 photographs, including a length of road and part of the extramural settlement extending to the north of the fort.

Figure 5.6: Aerial photographs showing parch mark evidence of Beckfoot Roman fort, extramural settlement and the Roman road. The aerial photographs date to: (left to right) July 1949; 1975; and July 1977 (Source: © Historic England. English Heritage Trust).

Faint parch marks can also be identified on subsequent oblique aerial photographs taken in 1952, 1979, 1983, 1986 and 2006 (Fig. 5.7). These features mostly related to the Roman road leading to and from the fort. A partial foot-print of Beckfoot Roman fort was also visible on photos taken during 1979, 1983 and 1988 (Fig. 5.7), however, there was no evidence for internal fort features. Indication of the extramural settlement north of Beckfoot Roman fort was also present on aerial photographs taken in 2006.

Figure 5.7: Aerial photographs with faint parch marks relating to the Roman road and/or the footprint of Beckfoot Roman fort. The aerial photographs date to: (top, left to right) 1952, 1979, and 1983; and (bottom, left to right) 1988 and 2006 (Source: © Historic England. English Heritage Trust).

Archaeological features were not detected on vertical photographs dating to 1948 and 1991, likely due to weather conditions being unfavourable for parch marks at the time of capture. However, these vertical aerial photographs hold valuable information regarding the changing coastline. As these photos were also collected in a series of overlapping flight strips, they were included in the change detection analyses (See chapter 4)

The North West Rapid Coastal Zone Assessment by Archaeological Research Services Ltd (2009, p. 189) referred to some evidence of Milefortlet 15 being visible from aerial photographs, however, no details of these photographs were provided. No evidence for Milefortlet 15 was visible on the aerial photographs assessed as part of this research.

5.6.3 Airborne Lidar

The *Frontiers of the Roman Empire Digital Humanities Initiative* (FREDHI) assessed the available airborne lidar data from the Environment Agency for the Hadrian's Wall corridor and Cumbrian coastline to identify new archaeological features associated with the Roman landscape (Collins, 2015). At Beckfoot Roman fort, the project identified a linear feature that was interpreted as a possible interior rampart, a modification commonly associated with the later Roman Empire, but not identified before in the northern frontier zone (Collins, 2015, p. 9). The validity of this features has yet to be confirmed via further archaeological investigation.

5.6.4 Archaeological Investigations

5.6.4.1 Beckfoot Roman Fort and extramural settlement

The account of a *Roman camp* or *fort* at *New Mawbray* reported by Hutchinson (1794, pp. 346) in *The history of the County of Cumberland* appears to be the first mention of a Roman military site at Beckfoot (Collingwood, 1936, p. 76), which was later referred to as *a small camp at Mowbray* in 1876, (Ferguson, 1878, p. 72), a *Roman camp near Beckfoot* in 1880 (Robinson, 1881) and today, Beckfoot Roman fort. According to Hutchinson (1794, p. 346), the older inhabitants of New Mawbray recall remains of a standing wall that formed part of the Roman fort, however, at the time of his writings the Roman site had been levelled and turned into arable land. The levelling of this area left no trace of the archaeological remains visible on the ground and, according to Collingwood (1936, pp. 76 - 7), this meant that approximately eighty years passed before anyone became interested in the possibility of a Roman fort or camp at Beckfoot. It was not until the 1870's when Ferguson visited the area multiple times and identified the location of the fort based on parch marks within the field (Collingwood, 1936, pp. 76 - 77). Later in 1879, independent of Ferguson, Joseph Robinson visited the area and upon enquiring about the possibility of a Roman camp, the locals pointed him in the direction of Castlefields (Robinson, 1881, pp. 136 - 38). Prior to February 1767, Castlefields was 43 lots across 30 acres of unenclosed "rig and reann" called Newtown Castle, which was later merged and divided into 8 fields and renamed Castlefields (Robinson, 1881, p. 138). Based on a raised elevation in the south-west corner of one of the eight fields, Robinson identified what he thought was a plausible location of the Roman camp, which was first mentioned by Hutchinson (Robinson, 1881, pp. 137 - 38).

As discussed above (Section 5.6.1), Beckfoot Roman fort was labelled on both the 1st edition OS 25 inch and 6 inch map, (Fig. 5.8). Robinson (1881, p. 138) became aware of the presence of a 'CAMP' marked on the OS 6 inch map shortly after his identification of its location in person. At this time, there was no mention of the Roman cremation cemetery or of Milefortlet 15 within the historic texts or historic maps.

Figure 5.8: (left) Portion of OS 25 inch map, surveyed in 1864, published in 1865/ and (right) portion of OS 6 inch map, surveyed in 1866, published in 1868, both showing 'Supposed site of CAMP'. (Source: National Library Scotland, https://maps.nls.uk/index.html).

Much of our early knowledge of the structure of Beckfoot Roman fort is due to Robinson's targeted excavation in 1879, which successfully confirmed the fort's location (Bellhouse 1992, pp. 31-61). The first trench yielded no definitive results, however, the second trench uncovered the remains of the outer western wall of the fort (Robinson, 1881, p. 139). Robinson excavated over 30 trenches along the length of this western wall (Robinson, 1881, p. 139; Collingwood, 1936, p. 77), from which he discovered undisturbed dressed stone forming the second course above the foundation of the fort wall (Robinson, 1881, p. 139). During the remainder of his fieldwork at Beckfoot, which took place between October and December of 1879, and at some point in time over the next year, Robinson discovered the north, east and west outer walls of the fort and uncovered the fort's four rounded corners (Robinson, 1881, p. 141). The fort's northern, eastern and southern gates were also discovered, however, he failed to locate the western gate (Robinson 1881, p. 141; Collingwood, 1936, p. 78). The western gate was later found by Mr Harold Duff who uncovered masonry in the probable location that was interpreted as the gates *spina* (Collingwood, 1936, p. 78). Robinson (1881, p. 141) also traced a portion of the Roman road leading to/from the fort's north and south gates. His findings can be seen on a plan surveyed by Harvey and examined by Robinson in 1879-80 (Fig. 5.9) (Robinson, 1881).
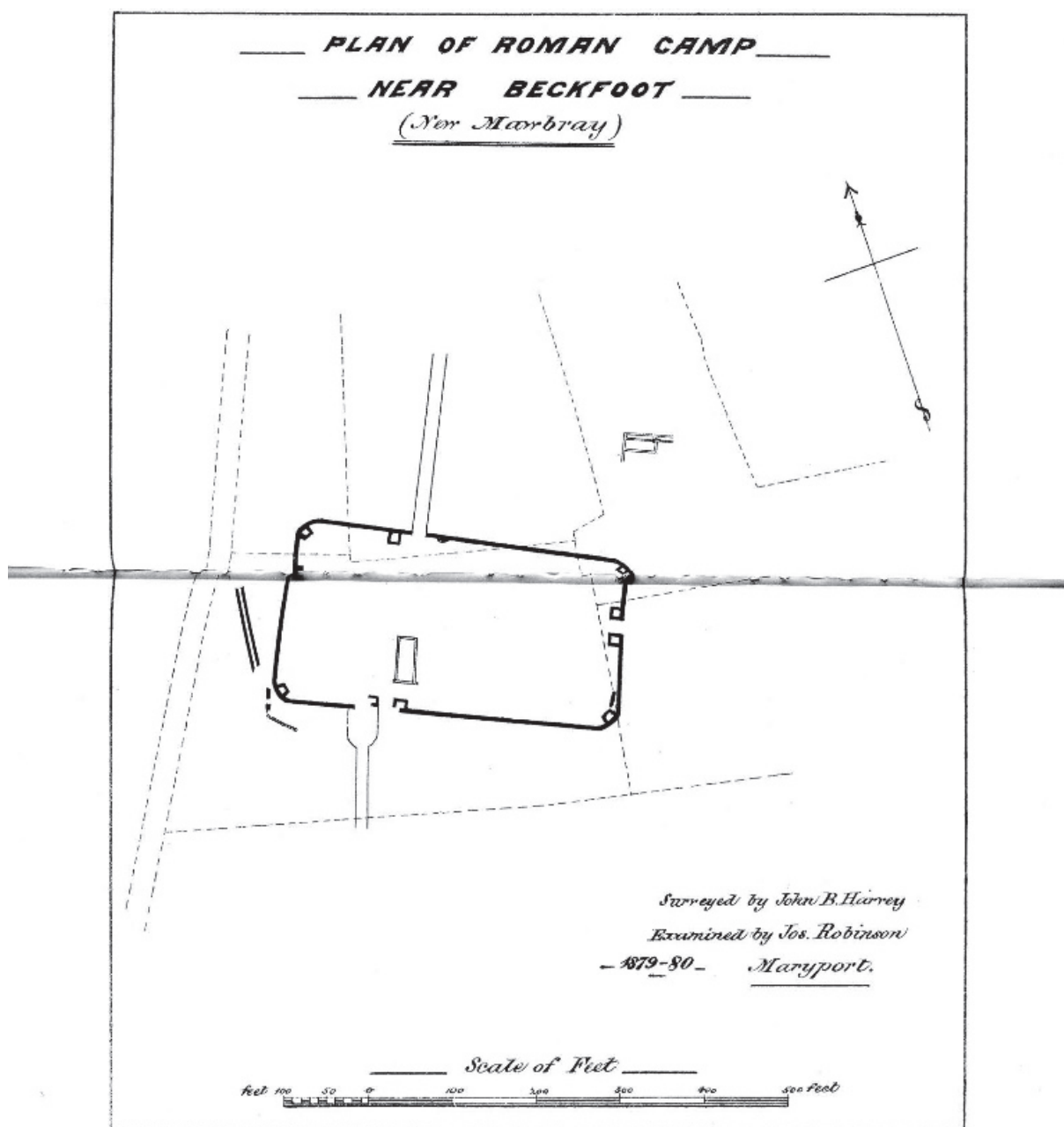
Figure 5.9: Plan of Beckfoot Roman fort surveyed by Harvey in 1879 - 80 and examined by Robinson (Source: Robinson, 1881, found between pages 138 and 139).

Beckfoot Roman fort was next subjected to archaeological investigation in 1935 by Harold Duff. No records of Duff's work exist, with the exception of Collingwood's (1936) article referring to the investigation of the western gate. The fort itself has not been subjected to archaeological excavation since, however, limited excavation has taken place outside the fort walls.

Between August 2007 and September 2009, Archaeological Research Service Ltd undertook the North West Rapid Coastal Zone Assessment (NWRCZA) on behalf of English Heritage

(now Historic England) (Johnson, 2009). This report was a desk-based assessment using Historic Environment Record (HER) data, National Mapping Programme (NMP) data (now referred to as the Aerial Investigation and Mapping data), unpublished sources, historic maps and aerial photographs to evaluate the threat of sea level rise and coastal erosion on heritage assets in North West England (Johnson, 2009, p. 1). The NWRCZA concluded that the remains of Beckfoot Roman fort was not at risk of erosion in the near future (Johnson, 2009, 181).
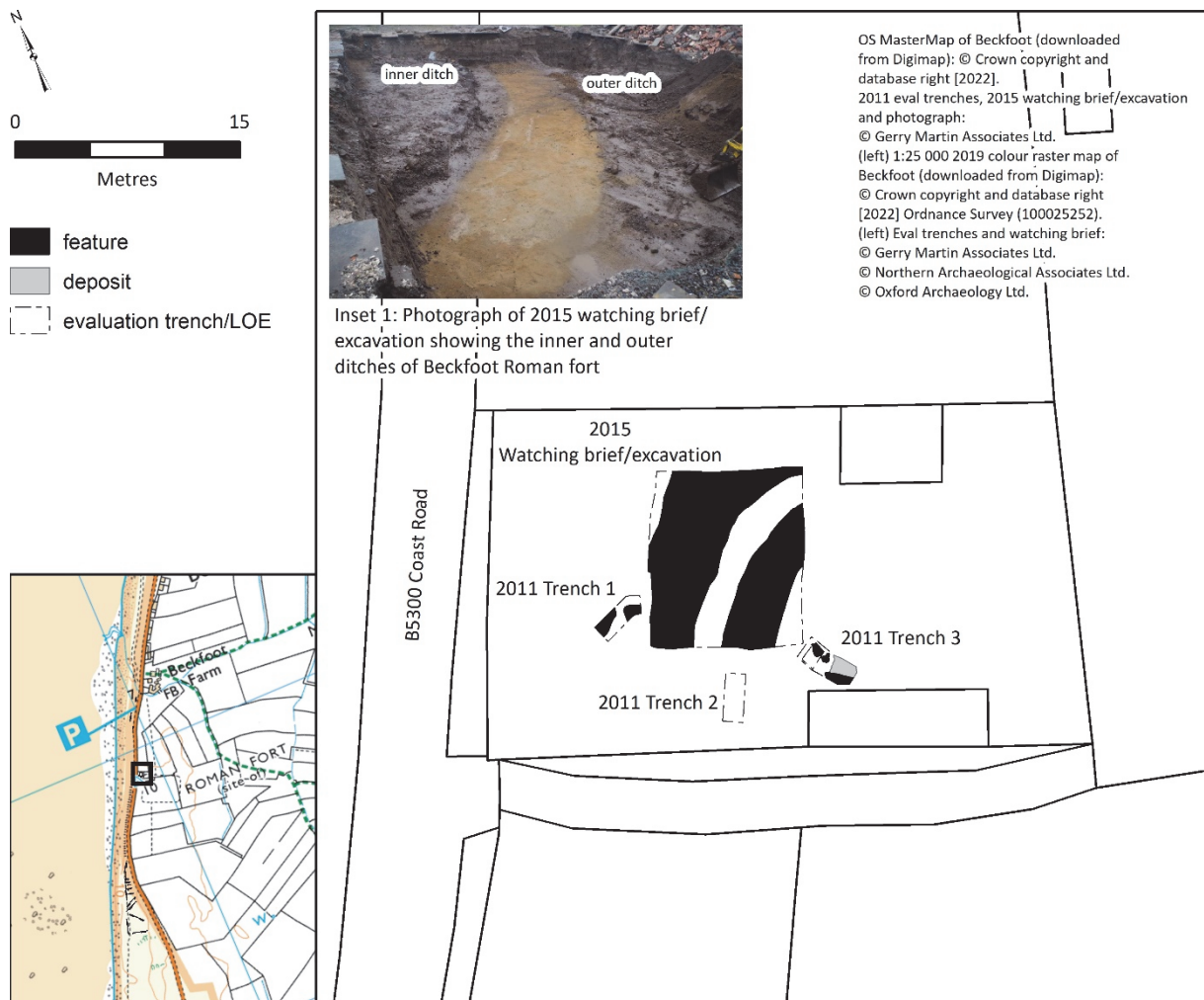
Figure 5.10: Archaeological investigations (2011 and 2015) by Gerry Martin Associates Ltd. (Adapted from: Martin, 2011 and Martin, 2015).

In July 2011, Gerry Martin Associates Ltd undertook an evaluation outside of the fort's outer wall (Martin, 2011). This evaluation was conducted as part of planning permission in advance of the rebuilding of the bungalow, named Roman Way, which is situated on the north western corner of the fort (Martin, 2011, p. 7). Three evaluation trenches were placed outside of the proposed footprint of the rebuild as the bungalow was still standing at the time of the investigation (Fig. 5.10) (Martin, 2011, p. 6). While dating evidence from the

evaluation was limited, all of the features encountered were attributed to the Roman period, except for an unexcavated horse burial dating to the late 19th/early 20th century (Martin, 2011, pp. 12 - 13). Only one of the five sherds of Roman pottery discovered was from a stratigraphically secure deposit (Martin, 2011, p. 12).From March to May 2015, Gerry Martin Associates Ltd conducted a watching brief and excavation (Martin 2015, p. 5). This work uncovered the remains of the inner and outer ditch fortifications of Beckfoot Roman fort (Martin, 2015, p. 5).

In 2016 Newcastle University excavated a small trench in the area southeast of where Beckfoot beck runs under the B5300 Coast Road (Haynes, 2019, p. 203). This work was conducted in response to archaeological material uncovered by the landowner (Haynes, 2019, p. 203). The excavators found remains associated with a demolished carding mill that stood adjacent to the site (Haynes, 2019, p. 203). No evidence for Roman activity was uncovered during this investigation, which led to the interpretation of the beck as marking the northern boundary of the forts extramural settlement (Haynes, 2019, p. 203).

Figure 5.11: Results from 2011 resistivity survey, part of an undergratuate dissertation (Adapted from: Williams, 2011, p. 16).

While archaeological excavation in this area has been relatively sparse, Beckfoot Roman fort and the surrounding landscape has been the subject of extensive geophysical survey. The

results of the magnetometer and resistivity surveys have greatly improved our knowledge of the fort itself revealing the layout of internal features, while also characterising the nature and extent of the surrounding extramural settlement. These surveys have revealed evidence for a densely occupied landscape during the Roman period. These investigations include a geophysical survey that was undertaken in 1995 south of Beckfoot Roman fort (Burnham *et al.*, 1996, pp. 406 - 407). The investigation, undertaken by Owen and Zangara (from Universities of Manchester and Catania respectively) revealed a 700 m stretch of the Roman road, as well as evidence for the presence of an extramural settlement (Burnham *et al.*, 1996, p. 407).

The area located behind the house knowns as 'Romanway' was the focus of a dissertation project, which used geophysical survey to investigate the archaeological remains associated with a section of Beckfoot Roman fort (Williams, 2011). In 2011, an undergraduate student from University of Central Lancashire undertook a resistivity survey of an area of 0.6 ha immediately north of the fort (Williams, 2011, p. 12). Anomalies in the results have been interpreted as a small portion of the northern wall of the fort, the line of the Roman road and evidence of the extramural settlement (Fig. 5.11) (Williams, 2011, p. 25).

In 2013 Wardell Armstrong Archaeology were commissioned by the Maryport and District Archaeological Society to carry out a 6.0 ha magnetometer survey across 7 fields (Mounsey, 2014). This survey demonstrated the presence of Roman settlement activity north of the fort as far as the beck (stream). Interpretation plots (Fig. 5.12) of the results show extramural settlement on either side of a roughly north-south aligned Roman road (Mounsey, 2014 - Figures 3 to 7). A second Roman road can be seen extending north-east from the fort leading to an anomaly that has been interpreted as a robbed out bathhouse (Mounsey, 2014, p. 18). The settlement activity may have extended further west beyond the coast road B5300 and may have been subjected to coastal erosion (Mounsey, 2014, p. 19). This interpretation was likely reached as magnetic anomalies appear to extend beyond the western limits of the survey.

In 2015, Newcastle University began carrying out a series of geophysical surveys (Fig. 5.13), which was later formalised as the Beckfoot Fort Environs Project (BFEP). The earliest was a resistivity survey in the field bordered by the beck, south of Beckfoot farm (Haynes and Arbuthnot, 2016). The aims of this survey were to extend knowledge of the fort's relationship with the extramural settlement, to gain an understanding of the structures

within the fort, the settlement and the cemetery, and to produce a unique, accurate and integrated analysis (Haynes and Arbuthnot, 2016, p. 16). Newcastle University undertook gradiometer and earth resistance surveys in 2015 and 2016 in a fields north and south of the Beckfoot Roman fort outside of the scheduled area (Haynes and Arbuthnot, 2016, p. 13). BFEP is ongoing and since 2016 the survey has expanded to incorporate fields between the earlier survey areas (Haynes, 2019, pp. 201-03). This research has revealed evidence for trackways, settlement activity, field systems and a ditched enclosure possibly representing an area of funerary activity (Haynes, 2019, pp. 201 – 03). The position of these surveys has filled in gaps from earlier surveys, revealing both additional evidence for extramural settlement north of the fort and, for the first time, evidence for extramural settlement to the south (Haynes, 2019, p. 203).
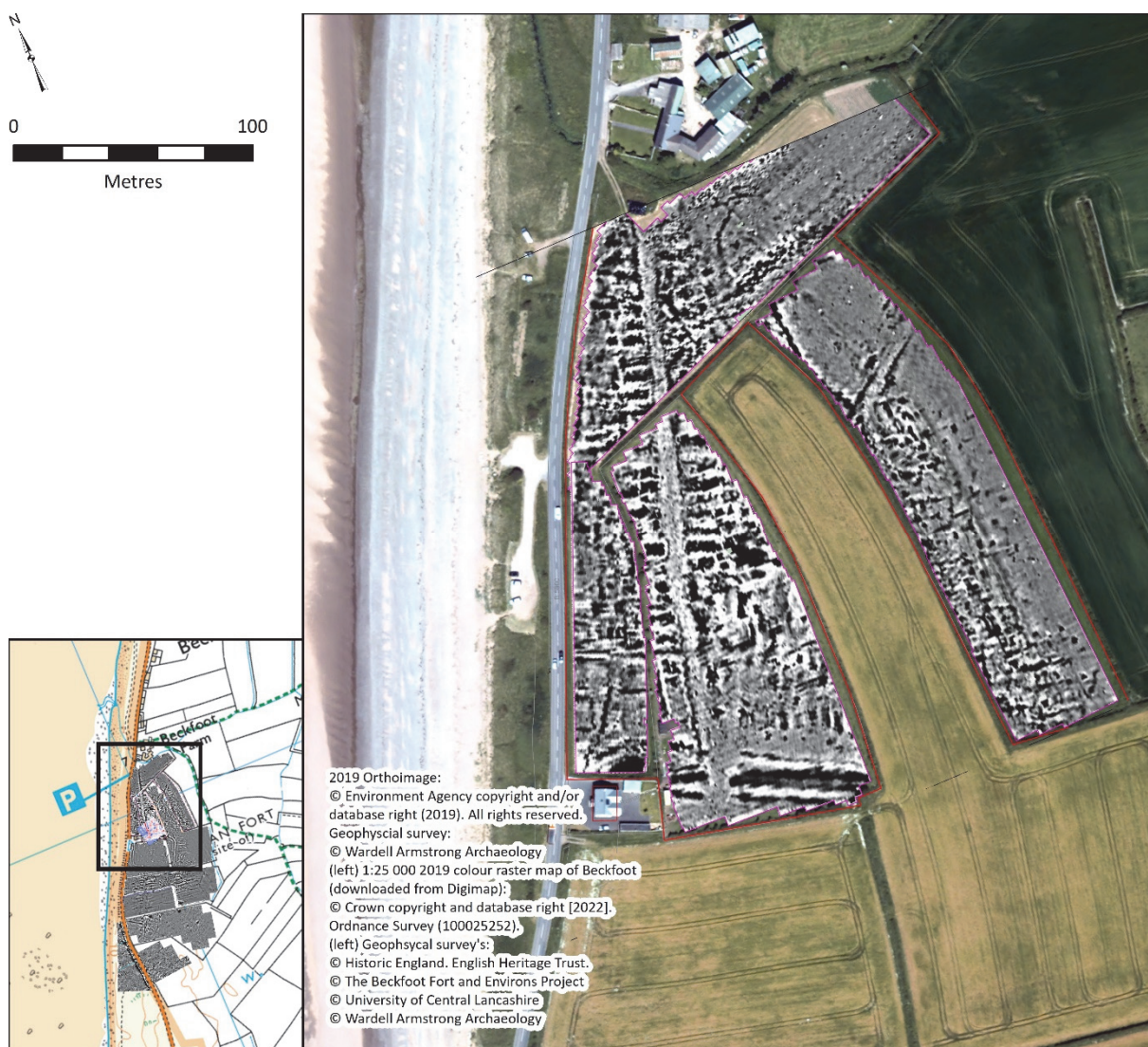
Figure 5.12: Wardell Armstrong magnetometer survey results. Geophysical survey plots provided by Wardell Armstrong Archaeology.

Fig. 5.13: Beckfoot Fort and Environs Survey geophysical survey results. (Geophysical survey plots provided by Beckfoot Fort Environs Survey, directed by Ian Haynes and Alex Turner).

Beckfoot Roman fort and the surrounding farmland also formed one of the three focus areas within Case 2 - Hadrian's Wall and its landscape (UK) case study of the 'Cultural Heritage Through Time (CHT2)' project (CHT2, 2019). A team of researchers from Newcastle University used archived aerial photographs to build time-varying 3D models and orthomosaic images of archaeological landscapes, with the aim of delivering enhanced four-dimensional (the 4th dimension referring to time) digital products of heritage sites (Fieber *et al.*, 2017, 297). These images were supplemented with RPAS RGB and Near Infrared (NIR) imagery collected in 2016 (Fieber *et al.*, 2017, 300). These datasets were compared to

airborne lidar, modern aerial photographs and archaeological sources to study the temporal changes of Beckfoot Roman fort and the surrounding farmland (Fieber *et al.*, 2017, 299).

5.6.4.2 Roman cremation cemetery and Milefortlet 15

The presence of a Roman cremation cemetery within the Mawbray Bank sand dunes, as well as its susceptibility to coastal erosion, has been known since as early as the 1900's. Many of these earlier discoveries have been catalogued by Caruana (2004), who presented these within his *Schedule of finds from Beckfoot cemetery*, including *Stray finds and other features*. Table 5.2 summarises these key findings from Caruna (2004, pp. 136 - 42), along with some recent additions including finds reported to the Portable Antiquities Scheme. The earliest known discovery at the site (Table 5.2 - ID 1) was a cinerary urn that contained cremated bone, which was found on the 12th of December 1908 by W. Armstrong and given to Carlisle Museum (Hope and May 1917, p. 173; Caruana, 2004, p. 136).

The first excavation of the cemetery occurred in 1948, when Hogg (1949) investigated the remains of a Roman funerary pyre (Table 5.2 - ID 6). According to Hogg (1949, p. 32) it was not uncommon for debris of human remains to be found along the shoreline south of the fort. Hogg (1949, p. 32) stated that extensive coastal erosion had probably led to the destruction of part of the Roman cemetery. While Hogg's investigation is the first published account of the Roman cemetery site at Beckfoot (Caruana, 2004, p. 134), Hogg attributes the awareness of the cemetery site at Beckfoot to Harold Duff (Hogg, 1949, p. 32).

Prior to 1948 excavation, Duff collected a series of Romano-British finds from this area in the 1920s (Table 5.2 - ID 2) (Caruana, 2004, p. 136). However, in Hope's reporting of the finds in 1921 there was no mention of a cemetery and it has been suggested that the finds collected were those that would typically be associated with the extramural settlement, rather than cemetery remains (Collingwood, 1936, p. 84). These finds were reported by Hope to have been found in the sand-dunes north of the Roman fort at Mawbray, where encroachment of the Solway is now exposing remains long buried' (Anon, 1921). The location of Duff's discoveries appears to have been incorrectly stated in the *Proceedings of the Pilgrimage of the Roman Wall 1920* (Anon 1921, pp. 270 - 71), an error that was repeated by Collingwood (1936, p. 84). Although it was originally stated that these Romano-British finds were located in the dunes north of the fort; this error was later corrected when Bellhouse (1989, pp. 47 - 48) confirmed with Duff personally that they were in fact from the dunes located south of the fort (Caruana, 2004, pp. 136 - 37). If the first account of the location of the artefacts was

correct, and they were indeed found in the dunes north of the fort, this would suggest that the extramural settlement could have extended into the seaward limits of dunes in the 1920s. This would also indicate that part of the extramural settlement may have been partially lost to dune erosion.

In 1956, Ian Moffat was encouraged by R. L. Bellhouse to …*keep his eye on the cliff-section just to the north of the measured position of mile-fortlet 15, for there was a risk that anything might turn up there – and be missed – as the cliff tumbled away…*.(Bellhouse and Moffat, 1958)*.* Bellhouse (1962a, pp. 62 - 63) was certain of the existence of Milefortlet 15 but believed it was lost, along with part of the Roman cemetery, due to substantial erosion caused by wind and tides. Bellhouse stated that during his investigation of the Roman signal-tower 15a (Roman Tower 15a) he came across the traces of nine cremated remains from separate burials in the Roman level of the eroding sand dunes (Bellhouse and Moffat, 1958, p. 57). During the Easter holiday of 1957, while examining the dune face by trowel, Moffat also discovered the remains of an urn-burial (Bellhouse and Moffat, 1958, p. 57 - 59). Other finds discovered in the dunes include a mortise and tenon joint in oak found in 1956, and a stone-lined grave found in the levels of the cliff face in 1957 (Bellhouse and Moffat, 1958, pp. 61 - 62).

In June 1960, cemetery remains were also retrieved from the dune cliff face when a stone cist burial was found by Arthur Hall (Table 5.2 – ID 13) (Hogg, 1962, p. 323). Three sides of the stone cist were recovered by Hogg and Hall, but the fourth side of the cist had been lost to erosion (Hogg, 1962, p. 323). In September 1985, N.M. Marshall discovered a disc-type brooch by means of a metal detector on the beach near Beckfoot (Richardson, 1990, p. 23). The brooch appeared to have been subjected to heat damage that may indicate it was burnt possibly as part of the cremation process (Richardson, 1990, p. 23). It is possible that the brooch eroded from a burial from within the dune face and carried to the beach through water action. Two years later, in 1987, fragments of an urn was also found by S.T. Collins within a 'layer of black earth' from the cemetery site (Richardson, 1990, p. 39).

Since 1987, a series of further finds were found due to erosion of the sand dune cliff face at Beckfoot. Several of these finds have been reported to the Portable Antiquities Scheme and include both cremated human remains and pottery that likely originated from several different funerary urns (Table 5.2 – ID 29-31 and 35).

In 2005, 1.4 ha of Mawbray Bank sand dune system was subjected to geophysical survey by Historic England, then English Heritage (Martin, 2006) (Fig. 5.14). Magnetometer and resistivity surveys were conducted in the location of the Roman cemetery site and conjectured location of Milefortlet 15 (Martin, 2006, pp. 1 - 2). The aim of the survey was to locate features associated with both Milefortlet 15 and the cremation cemetery to inform the location of subsequent evaluation trenches (see below) (Martin, 2006, p. 2). The geophysical surveys did not reveal any evidence that could definitively be linked to Mileforlet 15, however, there were discrete positive anomalies on the magnetometer survey results that potentially indicate burning. These anomalies were interpreted as possibly representing evidence for the Roman cremation cemetery, or plausibly evidence for hearths (Martin, 2006, pp. 4 - 5).

Figure 5.14: English Heritage 2006 magnetometer survey results (Adapted from: Martin, 2006, Figure 2).

Table 5.2: Finds from Beckfoot Roman cremation, not including those found during excavation (Adapted from: Caruana, 2004 and the Portable Antiquities Scheme).

ID	Date recovered	Recovered by	Repository	Description of find	Original Source/Accession no./PAS ID
1	12th December 1908	W. Armstrong	Carlisle Museum	Cinerary urn containing cremated bone	Hope and May 1917, p. 61; No. 191; TH Acc 24-1909
2	c. 1921	Harold Duff	Carlisle Museum	A cooking pot; a number of colour-coated sherds from at least two vessels; fragments of Castor ware, two fruit stones. Potentially these finds have been mixed up with those from Billericay, Essex, as their description does not match the original in Hope (1921)	Hope, 1921, pp. 270-71; The cooking pot is TH Acc. 7-1921.1; The colour-coated sherds are 7-1921.2
3	1920s	Harold Duff		Miscellaneous finds form 'erosion...of the sand dunes opposite the site of the fort...'; likely the remains of a burial; include half a burnt silver ring; carved bone (knife handle?); charcoal; iron; roof tiles and pottery including a mortaria	Hope, 1923, p. 295; Collingwood, 1936, p. 84; Bellhouse, 1989, p. 38
4	c. 1940	Mr W. Armstrong	Carlisle Museum	Cremation urn containing bones	Th Acc 20-1942
5	c. 1945/1946	Found in a private enterprise by three boys from Abbeytown		Pot found one mile south of the fort on the west side of the road, in blown sand at a depth of 0.61m	TH Acc 9 - 1947
6	April 1948	Excavated by R. Hogg and A. Hall		Funeral bed and pyre. Included the bed, the pyre, nails, iron fittings, fragmentary bronze human cranial bone fragments, iron weapons (spear head, bent sword, four-barbed arrow head)	Hogg, 1949; TH Acc. 28-1948
7	March 1949			Fragment of a tombstone, 4th-century style	Birley, 1958, pp. 182 - 83;

121

ID	Date recovered	Recovered by	Repository	Description of find	Original Source/Accession no./PAS ID
					JRS 49(1959), 135; Wright and Philips, 1975, p. 160
8	c.1954	Excavated by R. L. Bellhouse		Cremation pyre, contained pine charcoal, calcined bone, sherds from miniature grey ware cooking pot, nails, traces of an oak bed-frame with *in situ* nails, charred feathers and probably wool	Bellhouse, 1954, pp. 51 - 3; TH Acc. 22-1956.2
9	1956	R.L. Bellhouse		Charred oak mortice-and-tenon joint, possibly from a funerary couch	Bellhouse and Moffat, 1958, p. 61
10	1957	R.L. Bellhouse		Cist – stone walls, no human remains, no grave goods	Bellhosue and Moffat, 1958, p. 61-2
11	April 1957	Ian Moffat		Tomb group, calcined bone was placed in a samian-ware vessel of the shape Dragendorff 30, made by the potter Cinnamus and dated to AD150/190. It was covered with 2nd-C BB 1 dish, other finds included iron nails and charcoal	Bellhouse and Moffat 1958, p. 60; TH Acc. 44-1960
12	Prior to 1958	R.L. Bellhouse		Nine separate traces of cremation, charred timber (non-oak), collection of bone fragments	Bellhouse and Moffat, 1958, p. 57
13	1960	R. Hogg		Cist, no artefacts were recovered	Hogg, 1962, pp. 323 - 24
14	1961	R.L. Bellhouse		Disc brooch, mid-third/fourth century, distorted by burning and presumably came from a cremation	Hogg, 1962, p. 324; TH Acc 126-1961
15	27th March 1972	Ian Clark		Cremation burial (unpublished), described in the Museum Accession Register as 'Romano-British olla-type cinerary urn with calcined bones and associated iron nails and fitting…The olla is complete (Gillam Type 118, AD125/160)…contained calcined bones of an adult human. Dug out of the shore section…6 feet beneath the modern surface…corroded nails and	TH Acc 16-1972

ID	Date recovered	Recovered by	Repository	Description of find	Original Source/Accession no./PAS ID
				fittings and pieces of burnt wood....animal origin of some of the fragments	
16	1973	Ian Clark		Burial group, included cooking pot with calcined bone fragments of animal bone, unidentified brushwood, charcoal, and two beakers of cooking-pot form	Th Acc 27-1974
17	23rd August 1985			Small circular pit c. 40cm in diameter and 20cm deep, contained charcoal and burnt sand, located opposite the eight groyne of the sea defences in a stretch of slumped dune, calcined bones visible in the cultural horizon and iron was also recognisable, potentially evidence for test pits dug by Richard Bellhosue when searching for Milefortlet 15, bone, included fragments of animal bone, charcoal, heat distorted globules, which have the appearance of small beads, small pieces of fired clay, 15 or so pieces of iron, including two probably hob nails, four nails and two possible rivets, a segment of iron band with an oval cross-section	?
18	13th August 1985			Area of burning and calcined bone in slumped dune opposite fourth groyne, small portion found in situ, the rest had been eroded, 4 tiny pieces of calcined bone, some charcoal, a fragment of charcoal found in roots above the feature, and more charcoal and two pieces of iron, one a square-sectioned nail in the loose sand below it	?
19	1985	Neil Marshall,		Roman bronze brooch found on the beach	Richardson, 1990, p. 23 No 35; TH Acc 21-1986.1

123

ID	Date recovered	Recovered by	Repository	Description of find	Original Source/Accession no./PAS ID
20	23rd August 1985	metal detector		Unstratisfied charcoal, one piece of calcined bone (non-human?), two fragments of grey pot	?
21	1987	Mr S T Collins/Alan James		A small pit found after pottery was reported by Mr S T Collins. The majority of fill of the pit had collapsed down the face of the sand cliff. A small portion of the pit remained in situ and was excavated by Alan James, sherds of an urn, bone, pottery, charcoal	Richardson, 1990, p. 39, No. 78; TH Acc. 1-1988
22	1952	Mr and Mrs K Watson of Stanwix		A grey cooking-pot of early-fourth-century data, used as a cremation urn. The pot bore the graffito VROCATE (RIB II, 2503.160)	?
23	1956-57	R.L. Bellhouse		Stray pottery finds dating to the second-fourth century, including a Hadrianic-Antonine cooking pot, and Gillam Types 147 and 148 (AD290-370)	Bellhouse and Moffat, 1958, p. 61; Bellhouse, 1962, p. 71; TH Acc. 48-1965.2
24	1971	W.M. Wilson		Divided bow-brooch of third-century date, the brooch was attached to roots in the sand cliff, no signs of burning	Hogg, 1972; TH Acc 18-1971
25	10th November1 984			Charred deposit observed below the buried soil horizon, the feature comprised a jumble of charcoal, charred leather and textile, no obvious sign of bone – likely a modern feature	?
26	May 1985	Neil Marshall, metal detector		Dupondius of Trajan found on the beach below the cemetery, its poor condition was due to erosion rather than burning. There is no evidence to associate this with the cemetery rather than Milefortlet 15	Shotter, 1986, p. 257, no 20; Probably RIC 411, dated AD99-100,
27	23rd August 1985			Flat feature composed of small shattered stones over a length of 1.1m. The stones, angular sandstone were	?

ID	Date recovered	Recovered by	Repository	Description of find	Original Source/Accession no./PAS ID
				mixed with black sand and some charcoal. No calcined bone in the feature and no artefacts were associated wither directly or indirectly. It lay considerably to the south of than of the recorded cremation burials but was definitely within the ancient undisturbed levels of the dune	
28	1985 – 1987	Caruana, Alan James, Derke Wellsby		Various unstratified fines, mainly pottery, but also charcoal, a hobnail, calcined bone	?
29	January 2005	Portable Antiquities Scheme		Several cremated bones along with four nails and four sherds of pottery.	Unique ID: LANCUM-DD0B54.
30	January 2005	Portable Antiquities Scheme		Pottery sherds likely from a cremation burial. Found in the same location as LANCUM-DD0B54 (No 29)	Unique ID: LANCUM-DD4565
31	May 2009	Portable Antiquities Scheme		Two vessels, one used as an urn that contained cremated human remains, while the other was used as the urns lid (Pitts 2009, Noon 2010). This assemblage was discovered by locals Jon Murray and Graham Ryan after heavy rains washed it out of the sand dunes (Pitts 2009).	Unique ID: LANCUM-413CA5
32	June 2009	NWRCZA phase 1 states that finds were reported in British		A complete pottery vessel containing cremated human bone was found on the foreshore/ a complete urn containing the cremated remains of more than one individual was reported to the Portable Antiquities Scheme	

ID	Date recovered	Recovered by	Repository	Description of find	Original Source/Accession no./PAS ID
		Archaeology Magazine September – October 2009/NWRCZA phse 2 cites Noon 2009, 7			
33	2010-2011	NWRCZA phase 2 cites Mark Brennand pers com		Two further vessels were reported	
34	August/ September 2011	NWRCZA phase 2		Two possible cut features recorded eroding from the dune system. The first had the appearance of a post hole. The second had the appearance of a possible pit or post hole	
35	May 2012	Portable Antiquities Scheme		A fragment of oxidised coarse ware beaker and multiple fragments of a Bronze Age collard urn, respectively (Noon 2012). The urn could indicate an earlier phase of the cemetery site (Noon 2012).	Unique ID: LANCUM-546D25 and LANCUM-545A51

Table 5.2: Finds from Beckfoot Roman cremation, not including those found during excavation (Adapted from: Caruana, 2004 and the Portable Antiquities Scheme).

In 2006, a targeted archaeological evaluation took place within the location of the Beckfoot Roman cremation cemetery and conjectured location of Milefortlet 15 (Healey, 2007). Oxford Archaeology (OA) North excavated twelve trenches across the supposed area of the Roman cemetery, encompassing the scheduled boundary of location of Milefortlet 15 (Fig. 5.15, OA Nort Tr 1 - 12) (Healey, 2007, p. 14). The purpose of the evaluation was to assess the extent and survival of the cemetery, the quality and preservation of the archaeological remains and investigate the location of Milefortlet 15 (Healey, 2007, p. 15). As with the geophysical survey, the evaluation results did not yield any evidence for Milefortlet 15 and therefore it was concluded that the theory that the structure had already succumbed to coastal erosion was likely (Healey, 2007, p. 23). OA North were unable to establish the extent of the cremation cemetery from the evaluation results but did propose areas of dense activity versus areas of medium activity (Healey, 2007, p. 16).

As discussed above (section 5.6.4.1), a rapid coastal zone assessment (NWRCZA) was undertaken for the North West of England in between August 2007 and September 2009 (Johnson, 2009, p. vii). The NWRCZA assessment highlighted the importance of the cemetery site, stating that it was in need of urgent archaeological intervention as erosion of the sand dune was occurring at a rate of 0.3 m/year with a loss up to 30 m in total (Johnson, 2009, p. 191). Phase 2 of the assessment ranked coastal sites according to threat level (Eadie, 2012, p. 1). The Roman cremation cemetery ranked 2nd scoring 56 out of 60, while Roman Milefortlet 15 ranked 6th with a score of 53 (Eadie, 2012, p. 422). Sites that scored 50+ were considered to be under imminent risk from immediate or on-going threat and in need of further work (Eadie, 2012, p. 420). Roman tower 15A ranked 69th receiving a score of 37 and was considered to be at intermediate risk (Eadie, 2012, p. 427).
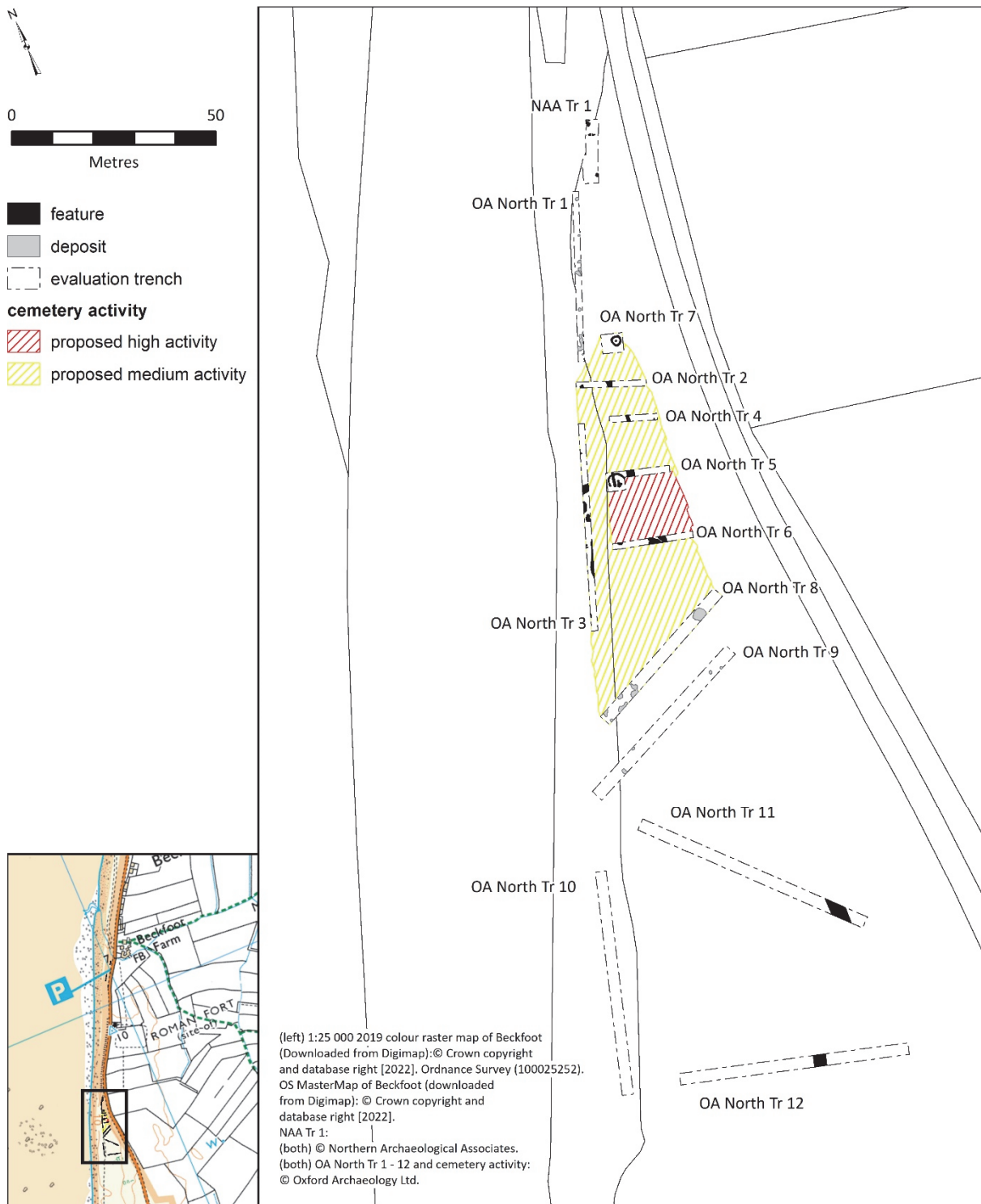
Figure 5.15: Plan of evaluations undertaken in 2007 (by Oxford Archaeology North) and 2019 (by Northern Archaeological Associates). NAA Tr 1 supplied by Northern Archaeological Associates, all other trenches adapted from: Howard-Davis *et a*l. (2017, p. 46).

Short term monitoring of the Roman cremation cemetery site and the conjectured location of Milefortlet 15 formed part of Phase 2 of the NWRCZA (Eadie, 2012, pp. 161-378). The lines representing the cliff toe and the cliff crest were recorded on two occasions, first in August 2011 and then again in April 2012 (Eadie, 2012, p. 317). The largest change in the position of the dune face between these two dates was 2.45 m landward, however, engineering

preparation work for the rock amour wall had begun at this time (Eadie, 2012, p. 317). Scouring back of the cliff face as preparations for the wall was likely the catalyst for much of this movement landward and as such the more representative value measured by phase 2 was a retreat of 0.7 m (Eadie, 2012, p. 317). Eadie (2012, p. 317) notes that slumping of dune material and moderate levels of vegetation growth indicated that the dune erosion was active at the time of the August/September 2011 site visits. Two cut features, a probable post hole and a possible post hole were observed during the first visit, however, in March 2012 these features could not be relocated in the cliff face suggesting that they had too been lost to erosion (Eadie, 2012, pp. 317 - 18). Phase 2 of the NWRCZA survey also mapped earthwork remains within the dune system, which they have interpreted as potentially representing evidence for the buried remains of Milefortlet 15 (Eadie, 2012, p. 321). The interpretation of this discovery contradicted the generally accepted notion that was originally proposed by Bellhouse (1962a, pp. 62 - 63) that the structure had succumbed to erosion.

An evaluation was conducted by Northern Archaeology Associates in 2019 in advance of a new cycleway between Allonby and Silloth (Collison, 2019, p. 1). The aim of the evaluation was to assess the nature of the archaeological remains and the potential impacts caused by the construction of the cycle path (Collison, 2019, 2). Four trenches were excavated, three of which were located in the dunes north of the rock armour wall (Collison, 2019 - Figure 2). These trenches (2 to 4) did not uncover any significant archaeological remains (Collison, 2019). Trench 1 (Fig. 5.14, NAA Tr 1) was located in the dunes behind the southern portion of the rock armour wall and revealed evidence for the Roman cremation cemetery (Collison, 2019, pp. 3 - 5). Four sherds of Roman pottery were recovered out of a secure context during the initial cleaning of the trench (Collison, 2019, p. 4). An in-situ urn cremation burial (Fig. 5.16 (left) was located in the southern end of the trench and a discrete deposit of pyre debris along with the foundation of a structure (potentially a mausoleam or memorial) (Fig. 5.16 (right) were located at the northern end of the trench (Collison, 2019, pp. 2 - 5). The burial related finds discovered in the northern part of the trench demonstrated that the cemetery extended further north than previously defined by the OA North 2006 evaluation (Collison, 2019, p. 8).

Figure 5.16: Cemetery remains discovered in NAA evaluation trench 1: (left) in situ cremation urn; and (right) pyre debris and foundation of a structure (Source: Collison, 2019 – Figures 6 and 7, © Northern Archaeological Associates).

5.7 Hydrodynamic setting

5.7.1 The Solway Firth Estuary

The Solway Firth is a large shallow estuary located on the west coast of the United Kingdom. (Coastal Engineering UK Ltd 2013, p. 60). It is an embayment estuary with a wide mouth that formed during the Holocene due to physical processes that include the retreat of the ice sheets after the last glaciation, post glacial sea level rise and fluvial erosion (Coastal Engineering UK Ltd 2013, p. 60). Water depths in the estuary are generally less than 20 m (Coastal Engineering UK Ltd 2013, p. 61). The seaward limit of the estuary, where it mixes with the Irish Sea, is generally accepted to be marked by a line between St Bee's Head, Cumbria and Burrow Head, Dumfries and Galloway. The inner Solway Firth is delimited by a line between Dubmill Point on the English coast and Southerness Point on the Scottish coast.

The coast north of Allonby to the River Sark is heavily influenced by the Solway Firth. Littoral drift occurs close to the shoreline and is mainly driven by wave action but can change dependent upon the prevailing wind conditions (Halcrow Group Limited, 2010, p. 117). St Bees Head acts a barrier to littoral drift from the south and therefore also has an influencing factor on coastal evolution. Sand with concentrations of gravel dominate along the high energy portion of the shoreline (Halcrow Group Limited, 2010, p. 117).

5.7.2 Sediments and sediment transport

Between 2014 and 2015, Sefton Council commissioned the *North West Strategic Monitoring Regional Sediment Analysi*s to determine particle size from intertidal locations between Great Orme's Head, Llandudno and the River Eden (Coastal Engineering UK Ltd, 2015c, p. 4).

Samples were taken along profiles at three specific points that included top of beach (above Mean High Water level), mid beach (between Mean High Water and mid tide level), and lower foreshore (between mid-tide and Mean Low Water level) and were collected from the uppermost 10 – 15 sediment (Coastal Engineering UK Ltd 2015c, p. 4). Results from the 2014-2015 sediment analysis were compared to those from the 2009-2010 sediment analysis. Sediments collected in 2009-2010 in the locale of the Roman cremation cemetery and opposite Beckfoot Roman fort consisted of mainly of sand, sandy gravel and to a lesser extent gravel. Those collected in 2014-2015 consisted of mainly sand, slightly gravelly sand and gravelly sand (Coastal Engineering UK Ltd 2015c, p. 94-6).

5.7.3 Tides

The Solway Firth is a macrotidal estuary (Coastal Engineering UK Ltd, 2013, p. 68). The tidal regime is semi-diurnal meaning that the area experiences two high tides per day every 12 to 13 hours (Coastal Engineering UK Ltd, 2013, p. 68). According to Marine Scotland Maps NMPI the mean spring tidal range of the Solway Firth is between 7.1 to 8.0 m (Marine Scotland, 2021). Historic records for the tide gauge at Workington date back to 1992 and are available through the BODC website (British Oceanographic Data Centre, 2021). These records show that the monthly highs ranged between 5.76 mAODN (1997) and 4.808 mAODN (2013) and the monthly lows ranged between -3.815 mAODN (1994) and -4.24 mAODN (2016). The largest tidal range between the monthly high was 9.96 m (1997) and the lowest was 8.749 m (2004).

5.7.4 Wave and wind climate

Wind fields crossing the Irish Sea are the predominant contributor to wave conditions in the outer Solway Firth (Coastal Engineering UK Ltd, 2013, p. 70). These wind fields typically approach the coast from directions between 190° and 250° whole circle bearing (WCB) (Coastal Engineering UK Ltd, 2013, p. 70). Swell waves are also capable of penetrating into this section of the coastal zone (Coastal Engineering UK Ltd, 2013, p. 70). Waves travel between the Isle of Man and the southern shore of Scotland from a sector of the 240° – 265° WCB of the Irish Sea into the Solway Firth and strike the shoreline obliquely (Coastal Engineering UK Ltd, 2013, p. 26).

To date, there has been no targeted long-term monitoring of the wave climate within the Solway Firth. There has, however, been a short-term monitoring campaign that took place between the 3rd of February 2014 and the 10th of March 2014; the data for which has been

made freely available through the National Network of Regional Coastal Monitoring Programmes of England website (NNRCMP, 2021). An Acoustic Wave and Current profiler (AWAC) was deployed approximately 10 km east of Maryport (NGR: 293149, 538499) at a depth of 25 m + tide with a sample interval of 60 minutes. According to the data collected over this two month period (Fig. 5.17), approximately 60 % of waves approached the coast from a south westerly direction with the majority of waves reaching a significant wave height (Hm0) of between 0.22 m and 6.41 m.
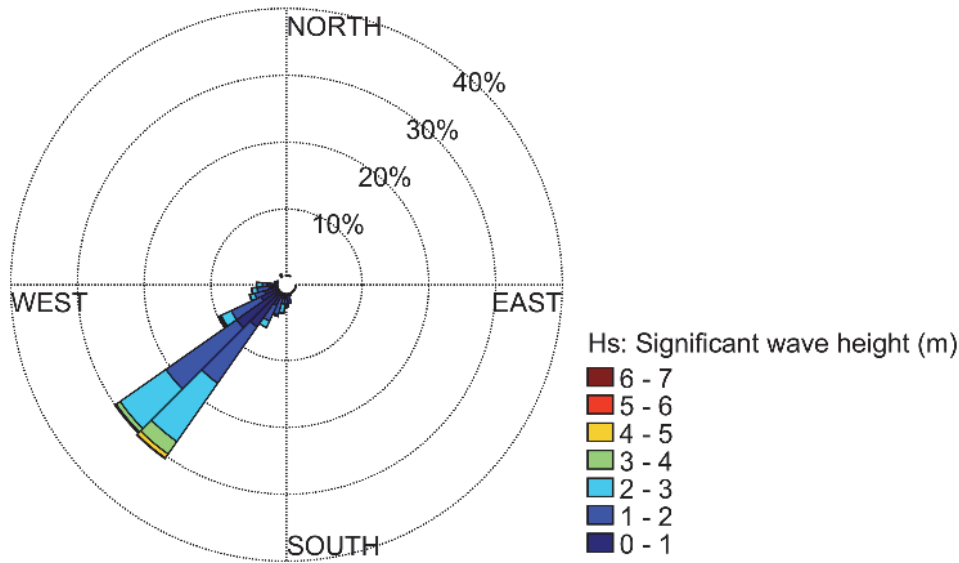
Figure 5.17: Waverose showing the significant wave height and direction from a short-term monitoring campaign of a point 10 km east of Maryport (Source: Coastal Monitoring, 2021).

SEASTATES Wave Hindcast Model (SWHM), provided by ABPmer, was also consulted due to the short nature of the wave monitoring campaign described in the above paragraph. SWHM provides long-term, high-resolution wave hindcast data, respective bathymetries and wind field data for the North Western European Continental Shelf and Baltic Sea (ABPMer, 2021). The model covers the period between 1979 and 2012. The wave hindcast data is based on state-of-the-art third generation spectral wave modelling undertaken in MIKE by DHI (ABPmer, 2018).
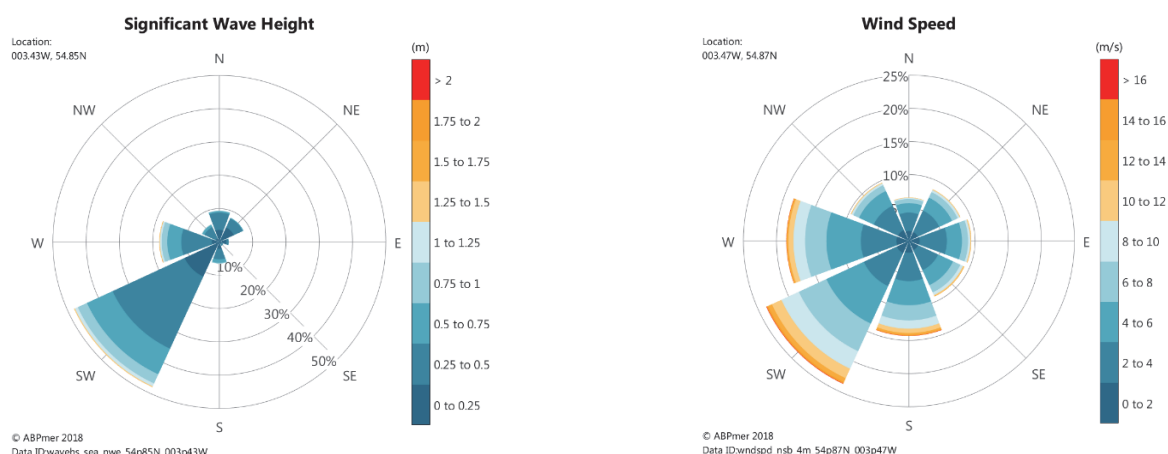
Figure 5.18: Nearshore wave and wind rose (Source: ABPmer, 2018).

The nearshore wave conditions (Fig. 5.18 (left)) were extracted for the area of the Solway Firth opposite the sand dune system, NGR NY 08283 51515. This data show that approximately 45 % of waves approach the shore from a south westerly direction with a significant wave height of up to 1.25 – 1.5 m, the majority of which fall between 0.25 – 0.5 m high. Approximately 17 % of waves approach the coast from the west with a significant wave height of up to 1.25-1.5 m, the majority of which fall between 0.25 – 0.5 m high. Waves also travel from, in descending order, the north (~9 %), northeast (~8 %), northwest (~5 %) and south (~5 %), and east (~2 %). The mean wave height of all the waves being 0.4 m. The corresponding wind rose (Fig. 5.18 (right)) describes the wind climate for the same area along the coast. Approximately 23 % of winds travel toward land from a south westerly direction with a maximum wind speed ranging from 0 to 16 m per second (m s^{-1}), with a small proportion exceeding 16 m s^{-1}. Winds also approach the coast from the west (~17 %), south (~14 %), the northwest (~9-10 %), the east (~9-10 %), the southeast (~8-10 %), and northeast (~ 7 %) and from the north (~6-7 %). The mean wind speed being 4.8 m s^{-1}.
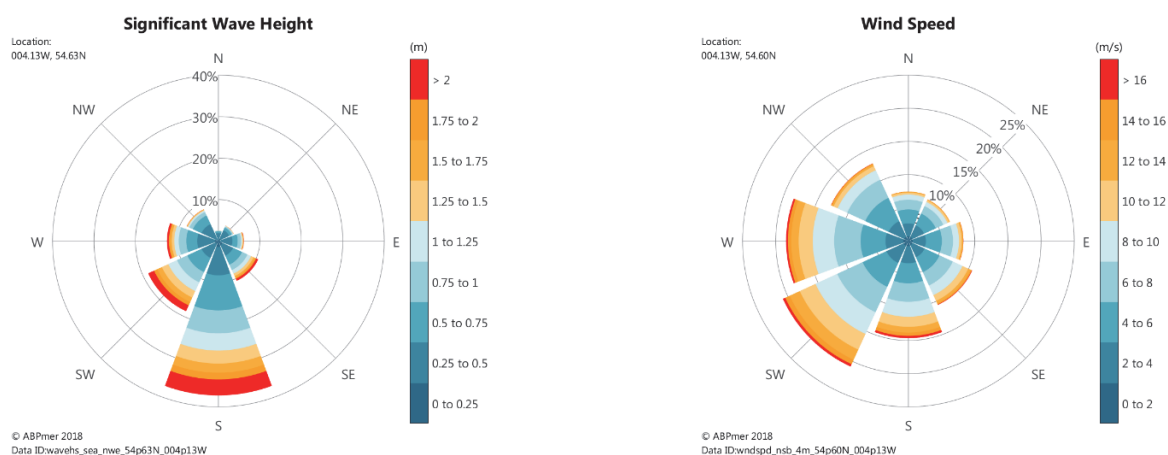
Figure 5.19: Offshore wave and wind rose (Source: ABPmer, 2018).

133

The offshore wave conditions (Fig. 5.19 (left)), centred on NGR NX 62600 28181, were located at the mouth of the Solway Firth where waters for the Irish Sea enter the estuary. Data from this area show that approximately 36 % of waves travel from the south and approximately 18 % from the southwest. These are followed by, in descending order, waves travelling from the west (~12 %), southeast (~11 %), northwest (~8 %), east (~5 %), and northeast (~ 3 %) and from the north (~2 %). The mean significant wave height was 0.9 m, however, waves were found to range from 0 to > 2 m high. The corresponding wind rose (Fig. 5.19 (right)) for the same area depicts approximately 24 % of wind travelling from the southwest followed by approximately 17 % of wind travelling from the west. Winds also travel from, in descending order, the south (~14 %), northwest (~9 %), east (~9 %), southeast (~9 %) and the north (~6 %). The mean wind direction is 6.7 m s^{-1} but can exceed 16 m s^{-1} on occasion.

The data analysed above appears to correspond with known wind data reports for the Solway Firth area. Solway Firth Partnership (1996, p. 42) also reported that wind data from Silloth demonstrated that winds are predominately from a south westerly direction. In addition, according to the Dubmill Point and Silloth Harbour Management Area summary approximately 45 % of winds come offshore from a south west to north direction (Allerdale Borough Council 2013, p. 3).

5.7.5 Coastal change at Beckfoot

The Beckfoot study area falls within the North West and North Wales Coastal Group – cell 11, sub-cell 11e (Jay, 2020, p. 19). Sub-cell 11e has been further sub-divided into eight policy areas. Policy area 11e5: Dubmill Point to Silloth covers the study area (Jay, 2020, p. 19). The priority unit is 11e5.1 (Jacobs, 2020, p. 17). According to the most recent Cumbrian Coastal Strategy the key risk to policy unit 11e5.1 was erosion, which could result in the loss of the B5300 coast road (Jay, 2020, p. 17). Erosion of the low cliffs and the sand dunes, identified at two pinch points has made this a priority unit (Jay, 2020, p. 17). The pinch points are located where the B5300 coast road is closest to the shoreline at Castle Corner, south of Beckfoot (within the Beckfoot study area) and at Dubmill Point (south of the Beckfoot study area) (Jay, 2020, p. 17). Both locations are currently defended.

A rock armour wall and apron was constructed between Beckfoot and Mawbray at Castle Corner in 2013 to protect the B5300 from coastal erosion in the short term (Coastal Engineering UK Ltd, 2015a, p. 40). Planning permission was granted for a 5 year period

(Jacobs, 2020b, p. 8). According to Eadie (2012, p. 319), preliminary construction work on the rock armour wall began in April 2012. The wall is near vertical and begins roughly at the location where the B5300 coast road bends landwards giving way to the wider dune system. The wall is reported to continue northwards for 500 m from NGR NY 08735 8609 to NGR NY 549062 (Coastal Engineering UK Ltd, 2014b, pp. 167 – 68). Its elevation was reduced in the middle of the frontage and further reduced to a single line of rocks that is flush with the beach level for at the northern end (Coastal Engineering UK Ltd, 2014b, pp. 167 – 68). The finishing point appears to have been incorrectly reported. The evidence from lidar and aerial photography suggests that the finishing point NGR NY 08942 49062, approximately 300m NNE of the starting point. The rock armour wall has been assessed regularly since its construction and was reported to be in a good condition with a residual life span of 10-20 years (Jacobs, 2020b, p. 5 - Table 2).

Location	Total historic change (m)	Historic rate (m/year)
Beckfoot north	+33.0 to +45.4	+0.30 to +0.41
Beckfoot centre	+61.8	+0.56
Beckfoot south	+55.7 to +59.0	+0.51 to +0.54
North of Castle Corner	+3.9 to +19.0	+0.04 to +0.17
South of Castle Corner	-33.9 to -44.8	-0.31 to -0.41
Mawbray north	+30.9 to +35.5	+0.28 to +0.32
Mawbray centre	+48.4	+0.44
Mawbray south	+61.1 to +79.9	+0.56 to +0.73

Table 5.3: Historic erosion rates, negative values represent erosion and positive values represent accretion (Source: Jacobs, 2020b, p 10 – Table 3).

In 2015, as part of the B5300 coastal defence appraisal, Capita undertook historic coastal change analysis providing erosion and accretion rates for this area (Capita, 2015). This appraisal was based on dune cliff line positions derived from historic maps and aerial photographs dating from 1891 to 2011. The results of this study were summarised in the Cumbria Coastal Strategy Technical Appraisal Report for Policy Area 11e5 Dubmill Point to Silloth (Jacobs, 2020b, p. 9 - 10). Table 5.3 presents the findings of locations relevant to the Beckfoot study area from the Capita 2015 analysis as reported by Jacobs (2020b, p. 10). The analysis states that the shoreline eroded by 33.9 to 44.8 m at a rate of 0.31 to 0.41 m/year for the land south of Castle Corner (Jacobs, 2020b, p. 10), where the Roman cremation cemetery is buried.

While much of the recent erosion has been attributed to the 2013/2014 winter storms, coastal erosion has been an ongoing problem at both Dubmill Point and at Castle Corner.

Jacobs (2020a, p. 10) states that sand dunes south of Beckfoot have receded by up to 14 m since 2004 and by 20 m between the 1950s and 1980s. Coastal change for policy unit 11e5.1 has been monitored on an annual basis using beach profiles surveyed from 2004 to 2015, however, no reports or data from 2004 to 2008 were available. Yearly surveys have recorded location and elevation points along ten beach profiles across the Beckfoot frontage, roughly perpendicular to the shoreline just north of the Rowanbank Caravan Park to north of Bank Mill Nurseries (Halcrow Group Limited, 2012a; Coastal Engineering UK Ltd, 2013; Coastal Engineering UK Ltd, 2014a; Coastal Engineering UK Ltd, 2015a; Coastal Engineering UK Ltd, 2016). Table 5.4 provides a summary of noted accretion and erosion from the annual monitoring reports in different sections of the study area. The Cell 11 Regional Monitoring Strategy (CERMS) 2009 Baseline Reporting notes that the southern half of the Beckfoot frontage was eroding while the northern half was accreting (Halcrow Group Limited 2010, 123). The report states that this was indicative of sediment not being replenished by the northerly drift from Dubmill Point (Halcrow Group Limited 2010, p. 123). The CERMS 2010 Monitoring Update Report for 2010 also reported the same pattern of accretion and erosion (Halcrow Group Limited, 2012a, p. 155).The annual local monitoring report for 2011 (Coastal Engineering UK Ltd, 2013, p. 3) found that erosion occurred along the southern part of the Beckfoot frontage and accretion along the northern part of the frontage. In 2012, the southern frontage continued to demonstrate erosion, while the northern frontage continued to accrete (Coastal Engineering UK Ltd, 2014a, p. 37). The 2013 findings were the same as the 2012 with the southern Beckfoot frontages eroding and the northern frontage accreting (Coastal Engineering UK Ltd, 2015a, p. 44).

The 2013 report noted the presence of erosion due to the 2013/2014 winter storms, causing the rock armour wall at Castle Corner to be overtopped (Coastal Engineering UK Ltd, 2015a, p. 39). This event caused erosion of the dunes behind the northern portion of the rock armour wall, and terminal erosion at the southern end of the wall, which continued to the south (Coastal Engineering UK Ltd, 2015a, p. 39). At this point, a reversal in trends was noted, reporting that the northern frontage eroded while the southern frontage accreted (Coastal Engineering UK Ltd, 2015a, p. 43). Between 2014 and 2015, erosion was noted along the southern Beckfoot frontages, while accretion was seen along the northern frontage (Coastal Engineering UK Ltd, 2016, p. 49).

Annual Local monitoring report year	Beckfoot frontage north	Terminal erosion north	Beckfoot frontage central/Rock armour wall post 2013	Terminal erosion south	Beckfoot frontage south	Source
2009	+	n/a	+/-	n/a	-	Halcrow Group Limited 2010
2010	+	n/a	+/-	n/a	-	Halcrow Group Limited 2014
2011	+	n/a	+/-	n/a	-	Coastal Engineering UK Ltd 2013
2012	+	n/a	+/-	n/a	-	Coastal Engineering UK Ltd 2014
2013	+	-	- (behind northern end of rock armour wall)	-	-	Coastal Engineering UK Ltd 2015
2014	-	-	- (behind northern end of rock armour wall)	-	+	Coastal Engineering UK Ltd 2015b
2015	+	n/a	n/a	n/a	+	Coastal Engineering UK Ltd 2016
2016	-	-	n/a	n/a	n/a	Jacobs 2020b
2017	-	-	n/a	-	n/a	Jacobs 2020b

Table 5.4: Evidence for erosion and accretion along Beckfoot coastline (+ represents accretion, - represents erosion, n/a is not applicable either due to no mention in report, or the fact that the rock armour wall was yet to be built).

The relevant reports were not available after 2015, however, coastal change for 2016 and 2017 for regions relevant to the Beckfoot study area was briefly described in Jacobs (2020b, p. 10) *Technical Appraisal Report for Policy Area 11e5 Dubmill Point to Silloth*. The 2015/2016 winter storms caused erosion within policy unit 11e5.1. Erosion was noted north of the rock armour wall along the southern part of Beckfoot village (Jacobs, 2020b, p. 10).

This was reported to be the same for 2017 although terminal erosion at the southern end of the rock armour wall was also pictured (Jacobs, 2020b, p. 10).

The National Coastal Erosion Risk Mapping (NCERM) 2018 – 2021 (Environment Agency, 2020) provides erosion extents and rates for three periods; short term (0 to 20 years); medium term (20 – 50 years); and long term (50 to 100 years). These rates were calculated at the fifth, 50th and 95th percentile confidence levels under two scenarios: no active intervention; and implementation of shoreline Management Plan (SMP) 2 Policy for this stretch of coastline. The upper and lower estimates of erosion according to NCERM for the study area are provided in table 5.5.

Location	Retreat distance (m) short term (up to year 2025)	Retreat distance (m) medium term (up to year 2055)	Retreat distance (m) long term (up to year 2105)
Between north end of rock armour wall and Silloth	0.68 to 1.32 m with no active intervention 0.68 to 1.32 m with SMP policy intervention	1.70 to 3.30 m with no active intervention 1.70 to 3.30 m with SMP policy intervention	3.40 to 6.60 m with no active intervention 3.40 to 6.60 m with SMP policy intervention
Along rock armour wall	4 to 6 m with no active intervention 4 to 8 m with SMP policy intervention	10 to 20 m with no active intervention 10 to 20 m with SMP policy intervention	20 to 40 m with no active intervention 20 to 40 m with SMP policy intervention
Between south end of rock armour wall and Mawbray	4 to 8 m with no active intervention 4 to 8 m with SMP policy intervention	10 to 20 m with no active intervention 10 to 20 m with SMP policy intervention	20 to 40 m with no active intervention 20 to 40 m with SMP policy intervention

Table 5.5: NCERM prediction rates of erosion (Source: Environment Agency, 2020).

The Capita (2015) coastal change study also looked at future rates of change over a 20 year, 50 year and 100 year period in accordance with the NCERM modelling temporal range (Table 5.6). The findings of this report showed erosion occurring south of Castle Corner of up to 41 m within 100 years' time, approximately matching the upper limit predicted by NCERM for the long-term period. This erosion would be located along the frontage where the Roman cremation cemetery is buried within the dunes and would therefore result in a major loss of the cemetery site.

Location	Predicted rate (m/year)	20 years (m)	50 years (m)	100 years (m)
Beckfoot north	+0.51 to +0.54	+10.2 to +10.8	+25.5 to +27	+51 to +54
Beckfoot centre	+0.56	+11.2	+28	+56
Beckfoot south	+0.30 to +0.41	+6 to +8.2	+15 to +20.5	+30 to +41
North of Castle Corner	+0.04 to +0.17	+0.8 to +3.4	+2 to +8.5	+4 to +17
South of Castle Corner	-0.31 to -0.41	-6.2 to -8.2	-15.5 to -20.5	-31 to -41
Mawbray north	+0.28 to +0.32	+5.6 to +6.4	+14 to +16	+28 to +32
Mawbray centre	+0.44	+8.8	+22	+44
Mawbray south	+0.56 to +0.73	+11.2 to +14.6	+28 to +36.5	+56 to +73

Table 5.6: Predicted rates of erosion/accretion according to Captia 2015 (Source: Jacobs, 2020, p. 10).

The Shoreline Management Plan 2 (SMP2) preferred mitigation strategy where coastal dunes exist, such as between Dubmill Point and Silloth, was managed realignment was selected over hold the line to allow the dunes to evolve unconstrained with minimal intervention (Halcrow Group Limited, 2012b, p. 7). This recommendation contrasts with the current practice at Dubmill Point and at Castle Corner, where rock armour walls have been constructed with the intention of holding the line (see above). The SMP2 accounts for these locations, which are currently defended. In these cases, monitoring cliff erosion is recommended with further intervention only occurring when assets are *sufficiently at threat* (Halcrow Group Limited, 2012b, p. 7). SMP2 was designed to allow for risk to heritage assets to be managed through short term mitigation and adaptation strategies (Halcrow Group Limited, 2012b, p. 41), however, in areas where the benefits of returning to a natural system, either through no active intervention or managed realinment, has been identified, this could result in increased flooding and erosion resulting in negative impacts to the historic environemt, including the schuled and unscheduled monuments of Hadrian's Wall WH site (Halcrow Group Limited, 2012b, pp. 23 – 24) . The *Cumbrian Coastal Strategy – Issues, Risks & Opportunities* Report (Jacobs, 2020a, pp. 14 - 15) recognises the archaeological sites associated with both Hadrian's Wall Coastal defence system and the Beckfoot Roman cremation cemetery, however, no real considerations of the impact to these sites have been made, stating instead that the risk to assets is limited.

The preferred strategic approach over the next ten years is to temporarily hold the line either through maintenance or reinforcement of the sea defences (Jay 2020, p. 66). At Castle

Corner this may require construction of sea defences with a more appropriate design and further planning permission (Jay 2020, p. 66). The preferred long-term solution (i.e. beyond 10 years) for shoreline management is realignment of the B5300 coast road and removal of the sea defences at Castle Corner and Dubmill Point to allow the coast to function as naturally as possible, however, it is stated that further research into this preferred long-term approach is required (Jay, 2020, p. 66).

5.8 Conclusions

This chapter provided justification for the choice of the Beckfoot study area for the proposed advanced geospatial framework for assessment of impacts from natural hazard on cultural WH. Through the identification of key sites within the study area and the detailed exploration of the current archaeological evidence it was possible to establish known extent, density and significance of the extensive archaeological.

In summary, there are three areas of archaeological interest within the Beckfoot study area: 1: Beckfoot Roman fort and extramural settlement; 2: The Roman cremation cemetery and the conjectured location of Milefortlet 15; and 3: Roman tower 15a. Destruction or deterioration of these sites would threaten the integrity of the stratigraphic resource and would ultimately result in a loss of archaeological knowledge. Based on our current knowledge of the archaeological remains in this area this resource includes information about how the people of the Roman military and extramural settlement lived, functioned, and interacted with each other as well as with the highly dynamic coastal landscape in which they lived and died. Moreover, as the coastal dunes erode, further evidence for mortuary beliefs and practices of these past peoples are also diminished, due to the direct impact that coastal processes have made on the cemetery site. Much of our current knowledge of the site comes from finds and deposits that were not recovered from stratigraphically secure deposits and as such their exact proveniences is not available. Erosion of the dune system has meant that the context of these archaeological finds and deposits has not been established, leading to the loss of valuable information about both the cremation burials and the wider cemetery site.

The situation of the above archaeological remains within the wider environmental and anthropogenic context has allowed the exploration of the influencing factors of the natural environmental in the Beckfoot study area, which makes the archaeological remains of the WH site particularly vulnerable to natural hazards. Supplemented by information about the

hydro and morpho-dynamics of this region it has been possible to determine the specific interaction between land and sea and understand the effect of specific processes on the archaeological record of the study area. These drivers of change along this highly dynamic coastline form, along with our detailed understanding of the archaeological evidence, the core basis of the conceptual model for this study area. Figure 5.20 provides a visual representative of this conceptual model for the Beckfoot study area. This map allows us to focus the analysis presented in chapter 6 specifically towards areas of concern and provide context for the past and future loss.
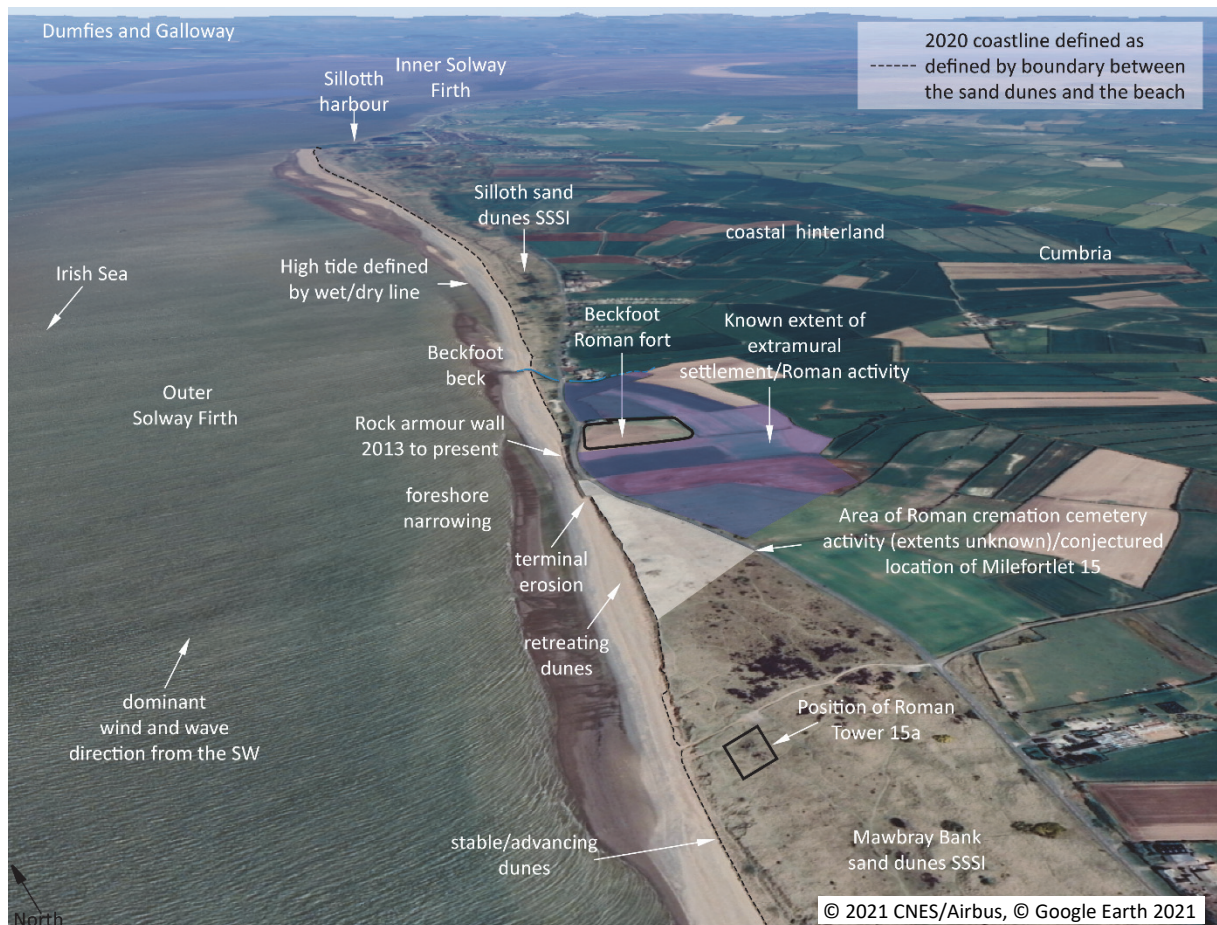
Figure 5.20: A conceptual understanding of the Beckfoot study area.

The following chapter presents the results of the 2D, 2.5D and 3D analysis of change within the study area to provide a deeper understanding of the pattern and rates of erosion of the coastal sand dunes. The chapter presents an extensive spatiotemporal time series, combined with a multi-modal approach that incorporates diverse datasets including historic maps, aerial photography and lidar data. This natural hazard impact assessment of the Beckfoot study area combines of change along the coastline with the detailed understanding archaeological record as outlined in this chapter to provide a full context to the loss suffered

in this region over more than 100 years. This approach allows the examination of past change and, through the application of several predictive models, the impact of future change on this diverse archaeological landscape.

Chapter 6: Natural hazard impact assessment for the Beckfoot study area

6.1 Introduction

This chapter presents the results of the impact assessment of coastal processes on the Beckfoot study area, using the methodology described in Chapter 4. The findings are presented across two sections. The first section, 6.2, focuses on the results of the various change detection methods that quantified past impact. Where possible, it includes evidence for erosion from the archaeological and historical records. The second section, 6.3, discusses the potential of predictive modelling to natural hazard impact assessment on WH sites. This was completed by comparing and contrasting the potential future outcomes as derived from the DSAS beta forecasting tool and the XBeach numerical model.

In order to compare diachronic change to the Earth's surface, resulting from natural processes and causing damage to the archaeological record of the Beckfoot study area, 5 coastal zones were defined which encompassed the coastline:

Zone 1: Opposite the remains of the **extramural settlement north** of the fort.

Zone 2: Opposite the remains of **Beckfoot Roman fort**.

Zone 3: Opposite the remains of the **extramural settlement south** of the fort.

Zone 4: Bordering the buried remains of the **Roman cremation cemetery/location of Milefortlet 15** (referred to as Roman cremation cemetery in the Figures). This extended south-westwards for approximately 430 m beyond the Oxford Archaeology evaluation trenches as the extent of the cemetery is unknown.

Zone 5: Opposite **Roman Tower 15a**.

The coastal zones were used to group together transects from the DSAS analyses for further statistical analyses. To calculate areal, volume and height changes from specific areas in the 2.5D change detection results, five budget segregation polygons were created, each of which encompassed a different topographical region and included: 1. Beach; 2. Sand dune cliff face; 3. Sand dunes; 4. Becks and; 5. Coastal hinterland (Figure 6.1 - right). Secondly, the sand dune cliff face budget segregation polygon was further subdivided into the five coastal zones defined above (Figure 6.1 - left) to provide finer detail of change comparable to the results derived from the 2D change detection analysis.
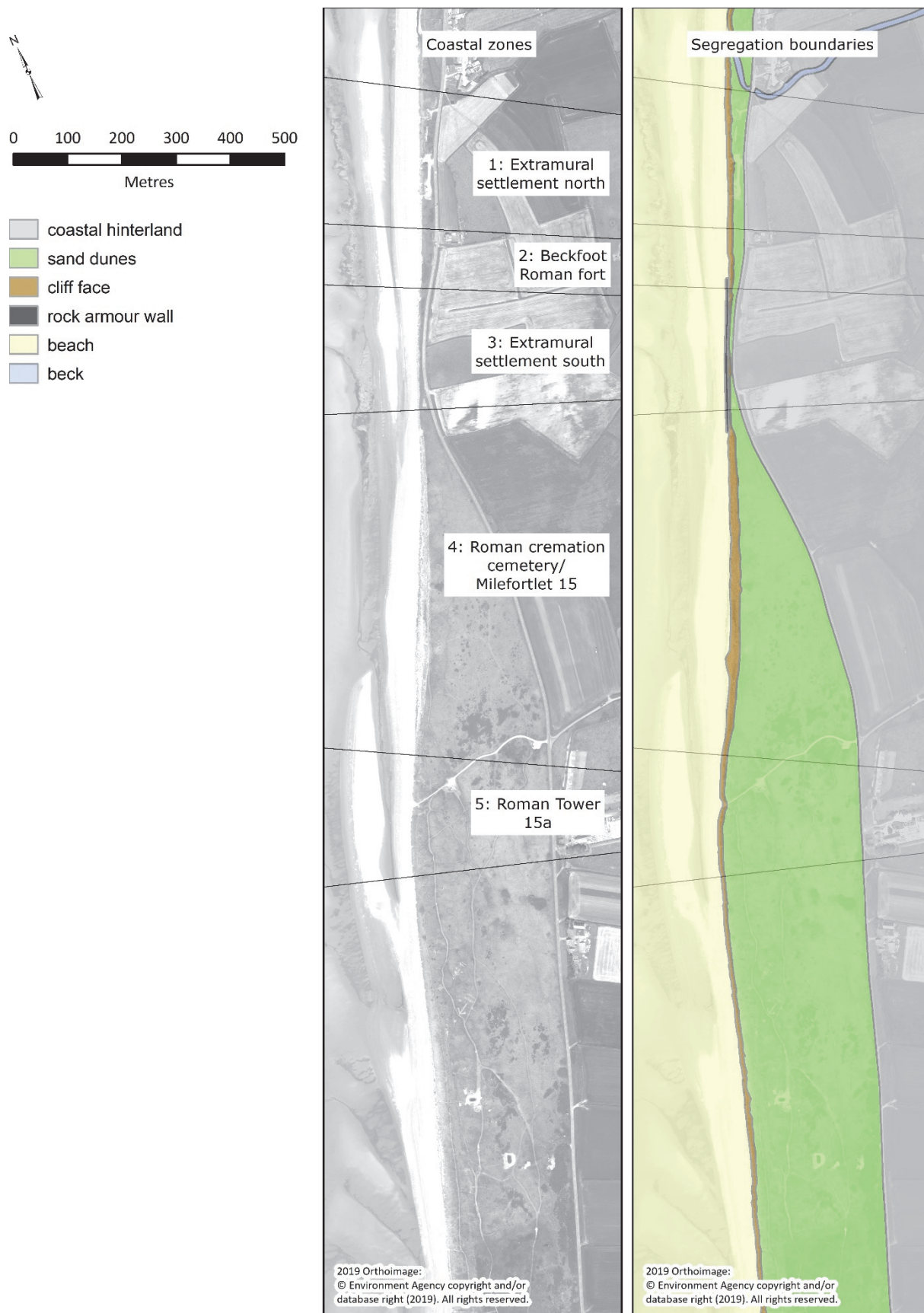
Figure 6.1: (left) Five coastal zones for 2D analysis; and (right) segregation boundaries for 2.5D analysis, these vary according to dune extent and presence/absence of rock armour wall.

6.2 Past impact

Past impact was calculated on 16 pairwise epochs, numbered 2 through 17 in table 6.1. The first change detection calculations were based on coastline positions from all epochs. Table 6.1 describes which change detection methods were applied to each pairwise epoch. In total 17 2D, six 2.5D and six 3D change detections were calculated.

The goal of the change detection analyses was to track past coastal change within the Beckfoot study area, focused on the Cumbrian coastline. For the purpose of this research, the coastline was defined by the boundary between the sand dune's seaward extent and the beach's landward extent for the 2D analyses and the sand dune cliff for the 2.5D and 3D analyses. The 2D analyses, which measured distances and rates of change between coastline positions, were conducted in ArcMap 10.6 using the Digital Shoreline Analysis AddIn (DSAS v. 5). The 2.5D analyses calculated Digital Elevation Models (DEMs) of Difference, (DoD) using the Geomorphic Change Detection Software ArcMap AddIn (GCD v. 7.5). Finally, the 3D analyses were conducted in CloudCompare using the Multi-scale-model-to-model-cloud-comparison (M3C2) plugin (Chapter 4).

	2D Change detection DSAS	2.5D change detection GCD	3D change detection M3C2
1	1866 to 2019*	N/A	N/A
2	1866 to 1899	N/A	N/A
3	1899 to 1923	N/A	N/A
4	1923 to 1948	N/A	N/A
5	1948 to 1957	N/A	N/A
6	1957 to 1991	N/A	N/A
7	1991 to 2009	$DoD_{2009\ minus\ 1991}$	$M3C2_{2009\ -1991}$
8	2009 to 2010	$DoD_{2010\ minus\ 2009}$	$M3C2_{2010\ -2009}$
9	2010 to 2013	$DoD_{2013\ minus\ 2010}$	$M3C2_{2013\ -\ 2010}$
10	N/A	$DoD_{2017\ minus\ 2013}$	$M3C2_{2017\ -\ 2013}$
11	2013 to 2014	N/A	N/A
12	2014 to 2015	N/A	N/A
13	2015 to 2017	N/A	N/A
14	April 2017 to Feb 2018	$DoD_{2018\ minus\ 2017}$	$M3C2_{2018\ -\ 2017}$
15	Feb 2018 to Sep 2018	N/A	N/A
16	Sep 2018 to Apr 2019	$DoD_{2019\ minus\ 2018}$	$M3C2_{2019\ -\ 2018}$
17	Apr 2019 to Jun 2019	N/A	N/A

Table 6.1: Summary of change detection methods employed per epoch pair (*calculations based coastline positions from all epochs).

Pairwise epochs	Extramural settlement north (zone 1)	Beckfoot Roman fort (zone 2)	Extramural settlement south (zone 3)	Roman Cremation cemetery/ Milefortlet 15 (zone 4)	Roman Tower 15a (zone 5)
1866 - 1899	100 %	82% 18 %	100 %	100 %	100 %
1899 - 1923	100 %	100 %	55% 45 %	92 % 8 %	56 % 44 %
1923 - 1948	96 % 4 %	100 %	100%	100 %	69 % 31 %
1948 - 1957	100 %	100 %	100%	100 %	100 %
1957 - 1991	100 %	100 %	100 %	100 %	100 %
1991 - 2009	100 %	100 %	71 % 29 %	14 % 86 %	100 %
2009 – 2010	100 %	9 % 91 %	81 % 14 %	63 % 37 %	100 %
2010 – 2013	10 % 90 %	100 %	75 % 25 %	90 % 9 % 1 %	46 % 54 %
2013 – 2014	100 %	100 %	39 % 61 %	83 % 17 %	30 % 70 %
2014 – 2015	68 % 32	56 % 11 % 2 %	82 % 17 % 1 %	82 % 16 % 2 %	30 % 70 %
2015 – 2017	96 % 4 %	45 % 55 %	86 % 14 %	87 % 12 % 1 %	8 % 92 %
2017 – 2018	98 % 2 %	82 % 18 %	57 % 43 %	37 % 63 %	46 % 54 %
2018 – 2018	2 % 98 %	100 %	24 % 76 %	84 % 16 %	100 %
2018 - 2019	N/A	N/A	2 % 98 %	92 % 8 %	62 % 36 % 2 %
2019 - 2019	N/A	N/A	58 % 42 %	2 % 98 %	51 % 49 %

Table 6.2: Direction and percentage of coastline movement in each of the five coastal zones (red = retreat, blue = advancement).

Table 6.2 presents a summary of coastline movement for each of the five coastal zones based on the percentage of transects, from the 2D analyses, experiencing either a landward (red font), seaward (blue font) or no change (black font) in coastline position. The landward movement of the coastline demonstrated that coastal erosion posed an increased threat to the archaeological remains within the study area due to a decrease in protective dunes, particularly in the location of the extramural settlement north, Beckfoot Roman fort,

extramural settlement south and Roman Tower 15a. In regard to the Roman cremation cemetery/Milefortlet 15, a landward movement of the coastline can be classed as a hazard as it has directly impacted upon the buried remains through erosive processes.

The following section presents the results for change detection analyses, starting with the results of the 2D change detection that used all epochs to derive coastline change statistics spanning 153 years. Following this, the results of each pairwise change epoch are discussed in turn beginning with the earliest epoch pair.

6.2.1 1866 to 2019

The 2D change detection was initially calculated using the coastline position from all epochs. This enabled further statistics to be calculated and trends to be identified that otherwise could not be calculated from a pairwise analyses. In total, 602 transects were cast from the baseline across the coastlines. The shoreline change envelope (SCE), net shoreline movement (NSM), end point rate (EPR) and EPR uncertainty values (ERPunc) were calculated for all transects. Linear regression rate (LRR), weighted linear regression (WLR) and the associated standard error, LSE and WSE, confidence interval, LCI95 and WSI95 and r-squared values, LR2 and WR2, were only calculated for 600 transects as two transects did not intersect three or more coastline positions, which is the minimum requirement for the regression statistics. Please refer to Chapter 4, Table 4.1, for an explanation of the statistical calculations. Table 6.3 summarises the NSM and EPR results for each of the five coastal zones.

A net movement landward has been identified in all 5 coastal zones, although to a lesser extent within coastal zones 1 and 5 - Roman Tower 15a and the extramural settlement north. The greatest impact was located in coastal zone 4 - Roman cremation cemetery/Milefortlet 15, where the linear regression rate (Figure 6.3) suggested a declining trend (i.e. the coastline is moving landwards). The declining trend was noted in all five coastal zones, however, this changed partially within coastal zones 1 and 5 - extramural settlement north and Roman Tower 15a to both the northern and southern extents, where the trend may be considered to have been favourable as the dunes appeared to be recovering.

Linear regression models were produced for three locations within zone 4 - Roman cremation cemetery /Milefortlet 15. Three transects were selected based on the known

extent of the buried remains of the Roman cremation cemetery. The intersect points from transects 347, 355 and 363 (Figure 6.2) gave measurements of distance (m) from the baseline to each of the coastline position. These measurements were plotted against date and fitted with a linear regression line. According to the three linear regression models the coastline demonstrated a trend toward a landward movement between 1866 and 2019, as indicated by the negative slope values, at a rate of 0.21 m/year, 0.27 m/year and 0.32 m/year respectively over the period of 153 years. The linear regression models showed that the dunes were eroding at a greater rate in the south of the area of proposed medium cemetery activity (Healey, 2007 – Figure 2) and to a lesser rate to the north of this same area.

Coastal zone	Direction of movement	Mean net movement (m)	Range net movement (m)	Mean EPR (m/year)	Range EPR (m/year)
Extramural settlement North (zone 1)	Landward (24 %)	2.97	0.83 – 4.99	0.02 +/- 0.02	0.01 – 0.03 +/- 0.02
	Seaward (76 %)	8.88	1.44 – 18.02	0.06 +/- 0.02	0.01 – 0.12 +/- 0.02
Beckfoot Roman Fort (zone 2)	Landward (100 %)	6.64	1.29 – 9.92	0.04 +/- 0.02	0.01 – 0.06 +/- 0.02
Extramural settlement South (zone 3)	Landward (95 %)	2.18	0.39 – 4.76	0.01 +/- 0.02	0.00 – 0.03 +/- 0.02
	Seaward (5 %)	1.39	0.85 – 1.93	0.01 +/- 0.02	0.01 – 0.01 +/- 0.02
Roman cremation cemetery/ Milefortlet 15 (zone 4)	Landward (100 %)	39.41	5.04 – 54.45	0.26 +/- 0.02	0.03 – 0.35 +/- 0.02
Roman Tower 15a (zone 5)	Landward (58 %)	9.11	0.36 – 16.57	0.06 +/- 0.02	0.00 – 0.11 +/- 0.02
	Seaward (42)	7.27	0.34 – 11.70	0.05 +/- 0.02	0.00 – 0.08 +/- 0.02

Table 6.3: Coastline change statistics for each of the coastal zones calculated using coastlines from all epochs (1866 to 2019).
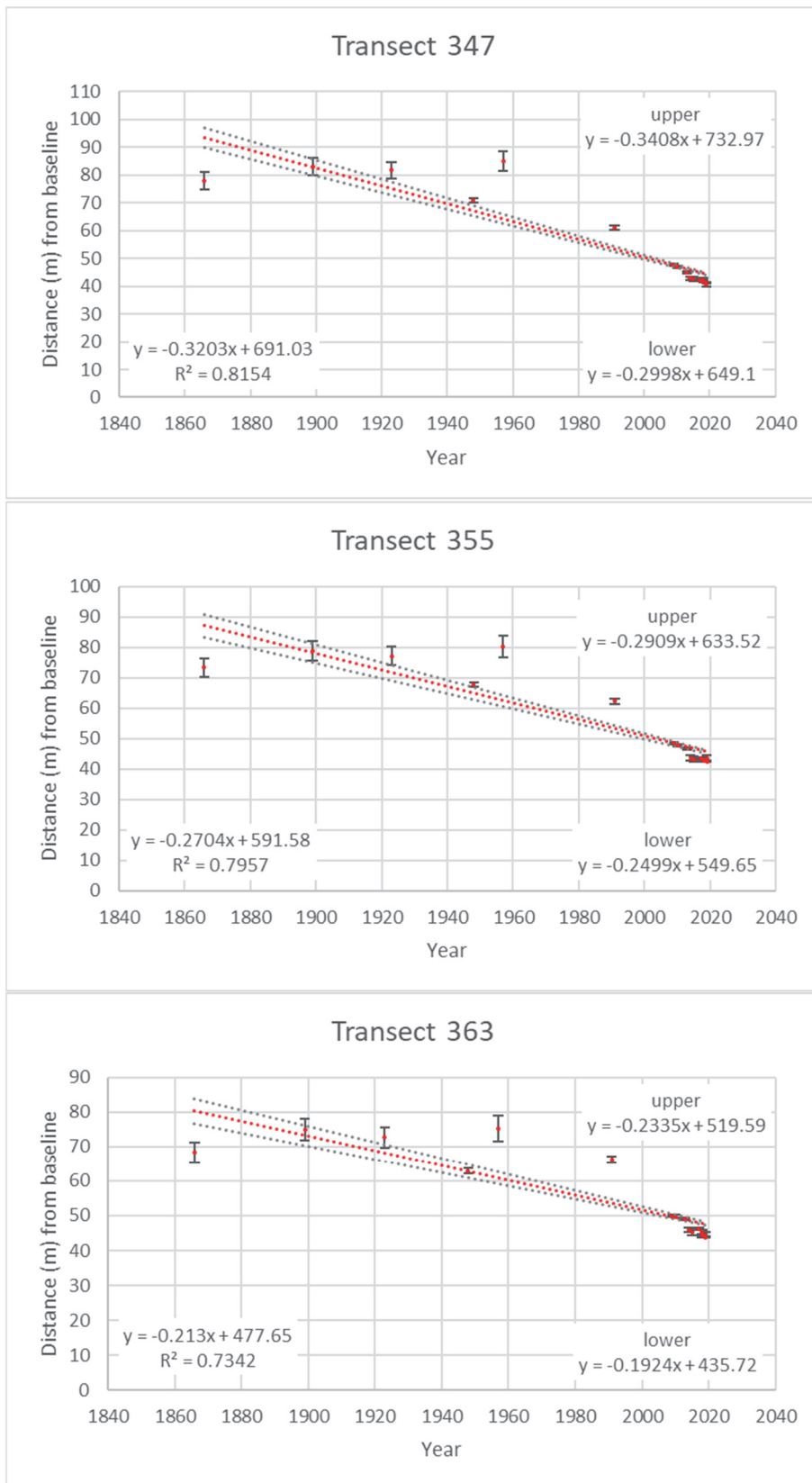
Figure 6.2: Graphs showing the linear regression models for transects 347, 355 and 363.
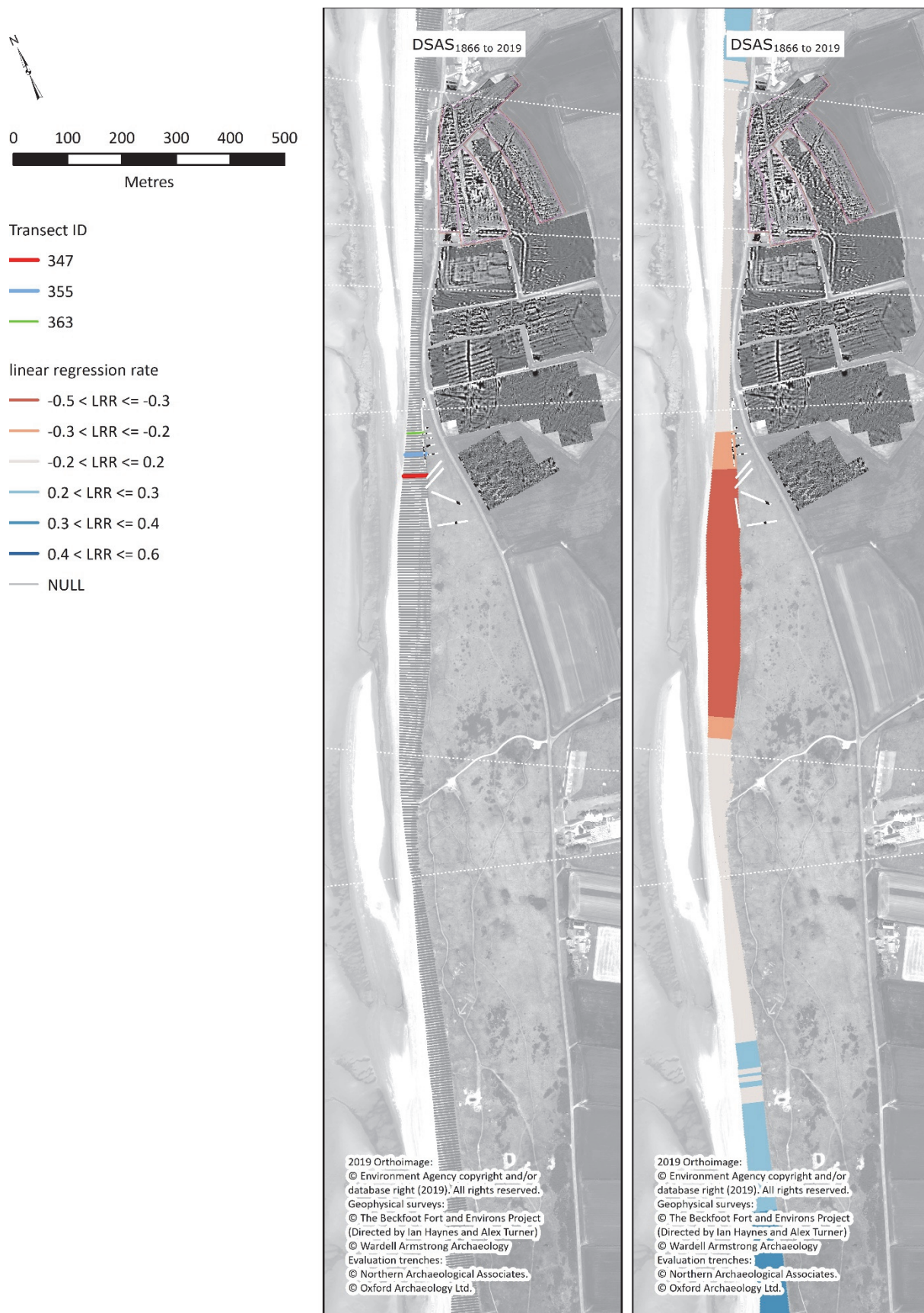
Figure 6.3: 1866 to 2019 transects displaying (left) transect locations for Figure 6.2; and (right) linear regression rate (m/year) calculated using coastline positions for all epochs.

While the linear regression rates provided details of the overall trends of the coastline moving either landward or seaward, coastal processes are not linear. The 2D change detection analysis, therefore was also conducted on a pairwise basis to give further insights into the evolution of the coastline within the study area and its impact on the archaeological record.

6.2.2 1866 to 1899

The results from the 2D change detection of the coastline position from 1866 to 1899 (Figure 6.4) show that the coastline experienced a landward movement in coastal zones 1 and 2 - extramural settlement north and Beckfoot Roman fort. The coastline beyond the beck to the northern extent of the study area also experienced a landward movement. Seaward movement of the coastline was noted in the coastal zones 3, 4 and 5 - extramural settlement south, the Roman cremation cemetery/Milefortlet 15 and Roman Tower 15a. The distances of seaward/landward movement, and rates of movement per year are provided in Table 6.4.

Coastal zone	Direction of movement	Mean net movement (m)	Range net movement (m)	Mean EPR (m/year)	Range EPR (m/year)
Extramural settlement north (zone 1)	Landward (100 %)	2.58	1.95 – 3.07	0.08 +/- 0.13	0.06 – 0.09 +/- 0.13
Beckfoot Roman Fort (zone 2)	Landward (82 %) Seaward (18 %)	2.43 4.91	0.86 – 2.93 2.56 – 5.89	0.07 +/- 0.13 0.15 +/- 0.13	0.03 – 0.09 +/- 0.13 0.08 – 0.18 +/- 0.13
Extramural settlement South (zone 3)	Seaward (100 %)	6.09	5.41 – 6.81	0.18 +/- 0.13	0.16 – 0.21 +/- 0.13
Roman cremation cemetery/ Milefortlet 15 (zone 4)	Seaward (100 %)	5.23	2.91 – 7.88	0.16 +/- 0.13	0.09 – 0.24 +/- 0.13
Roman Tower 15a (zone 5)	Seaward (100 %)	6.07	5.38 – 6.91	0.18 +/- 0.13	0.16 – 0.21 +/- 0.13

Table 6.4: Coastline change statistics for each of the coastal zones calculated using coastlines from epochs 1866 to 1899.
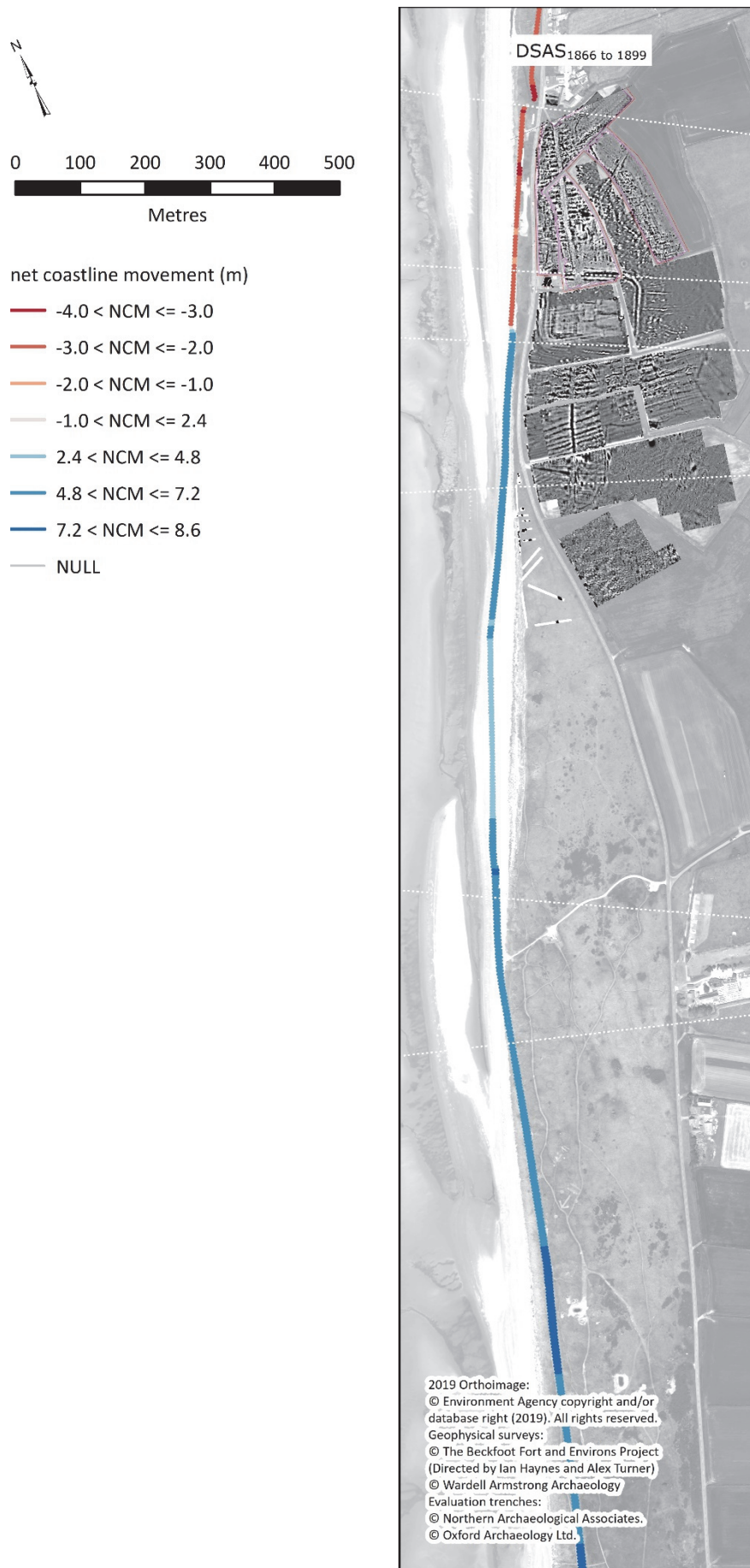
Figure 6.4: DSAS$_{1866\ to\ 1899}$ transects displayed by net coastline movement.

Erosion of the dunes between 1866 and 1899, indicated by the landward movement of the coastline position (indicated by the red transects), could have potentially destroyed archaeological evidence buried within the dunes associated with the Roman frontier, however, no evidence from early documentary sources was found to indicate destruction of the archaeological record due to erosion of the sand dune system.

The accretion of the coastal dunes, indicated by a seaward movement of the coastline position, would have provided protection to the remains of the Roman cremation cemetery/Milefortlet 15 and Roman tower 15a, through the accumulation of sediment and vegetation growth acting as a barrier.

6.2.3 1899 to 1923

The 2D change detection results for 1899 and 1923 coastline positions (Figure 6.5) demonstrated a contrast to the previous change detection results (1866 to 1899). The 1923 coastline position was further seaward than that of the 1899 position for coastal zones 1 and 2 - extramural settlement north and Beckfoot Roman fort. This seaward shift continued north-eastwards to the northern extent of the study area. The seaward movement could be evidence of dune recovery. Due to the accumulation of sediment any subsequent erosion would not have direct impact upon potential archaeological remains until the 1899 coastline position was surpassed in the landward direction.

The results also indicated a landward movement of the coastline in locations were the dunes had previously indicated a seaward movement. This landward movement mostly occurred in coastal zones 3, 4 and 5 - extramural settlement south, Roman cremation cemetery/Milefortlet 15 and Roman Tower 15a. This landward movement continued south-westwards for approximately 780 m. The remaining c. 230 m of the coastline demonstrated a seaward movement. Table 6.5 details the distances and rates of movement for the five coastal zones.

The landward movement of the coastline to the 1923 position did not exceed that of 1866 position in zone 4 - Roman cremation cemetery/Milefortlet 15. Erosion of the dunes, therefore, should not have directly impacted upon these archaeological remains. However, finds associated with the Roman cremation cemetery were discovered as early as 1908 and again in 1921 and c. 1923. This could indicate that dunes were eroded beyond the 1866 coastline position in 1908, 1921 and c. 1923, but may have also recovered at times before

eroding again to the 1923 coastline position, which was seaward of the 1866 coastline position.

Coastal zone	Direction of movement	Mean net movement (m)	Range net movement (m)	Mean EPR (m/year)	Range EPR (m/year)
Extramural settlement North (zone 1)	Seaward (100 %)	10.97	4.52 – 27.08	0.46 +/- 0.18	0.19 – 1.13 +/- 0.18
Beckfoot Roman Fort (zone 2)	Seaward (100 %)	5.28	4.07 – 7.4	0.22 +/- 0.18	0.17 – 0.31 +/- 0.18
Extramural settlement South (zone 3)	Landward (55%)	0.55	0.02 – 0.92	0.02 +/- 0.18	0.00 – 0.04 +/- 0.18
	Seaward (45 %)	3.27	0.15 – 6.56	0.14 +/- 0.18	0.01 – 0.27 +/- 0.18
Roman cremation cemetery/ Milefortlet 15 (zone 4)	Landward (92 %)	1.24	0.01 – 2.44	0.05 +/- 0.18	0.00 – 0.10 +/- 0.18
	Seaward (8 %)	0.43	0.01 – 0.72	0.02 +/- 0.18	0.00 – 0.03 +/- 0.18
Roman Tower 15a (zone 5)	Landward (56 %)	0.05	0.50 – 0.90	0.00 +/- 0.18	0.02 – 0.04 +/- 0.18
	Seaward (44 %)	0.32	0.06 – 0.90	0.01 +/- 0.18	0.00 – 0.04 +/- 0.18

Table 6.5: Coastline change statistics for each of the coastal zones calculated using coastlines from epochs 1899 to 1923.

In 1908 a cinerary urn containing cremated bone (Chapter 5, Table 5.2 - ID 1) was recovered (Caruana, 2004, p.136). In addition, Hope (1921, p.270) reported finds (Chapter 5, Table 5.2 - ID 2) discovered by Harold Duff from the dunes north of the fort 'where the encroachment of the Solway is now exposing remains long buried.' The location of these finds appeared to have been incorrectly reported. Bellhouse (1989, p.38) later confirmed with Duff that the finds, consisting of several fragments of Romano-British Castor ware including an almost complete cooking-pot (Hope 1921; pp.270-271), were retrieved from the dunes south of the fort. Hope (1923. p.295) reported further finds (Chapter 5, Table 5.2 - ID 3) that included roof-tiles, rims of mortaria and cooking-pots, fragments of Castor ware vases, part of a white clay flagon coated with black slip, charcoal, iron nails, silver finger ring which had
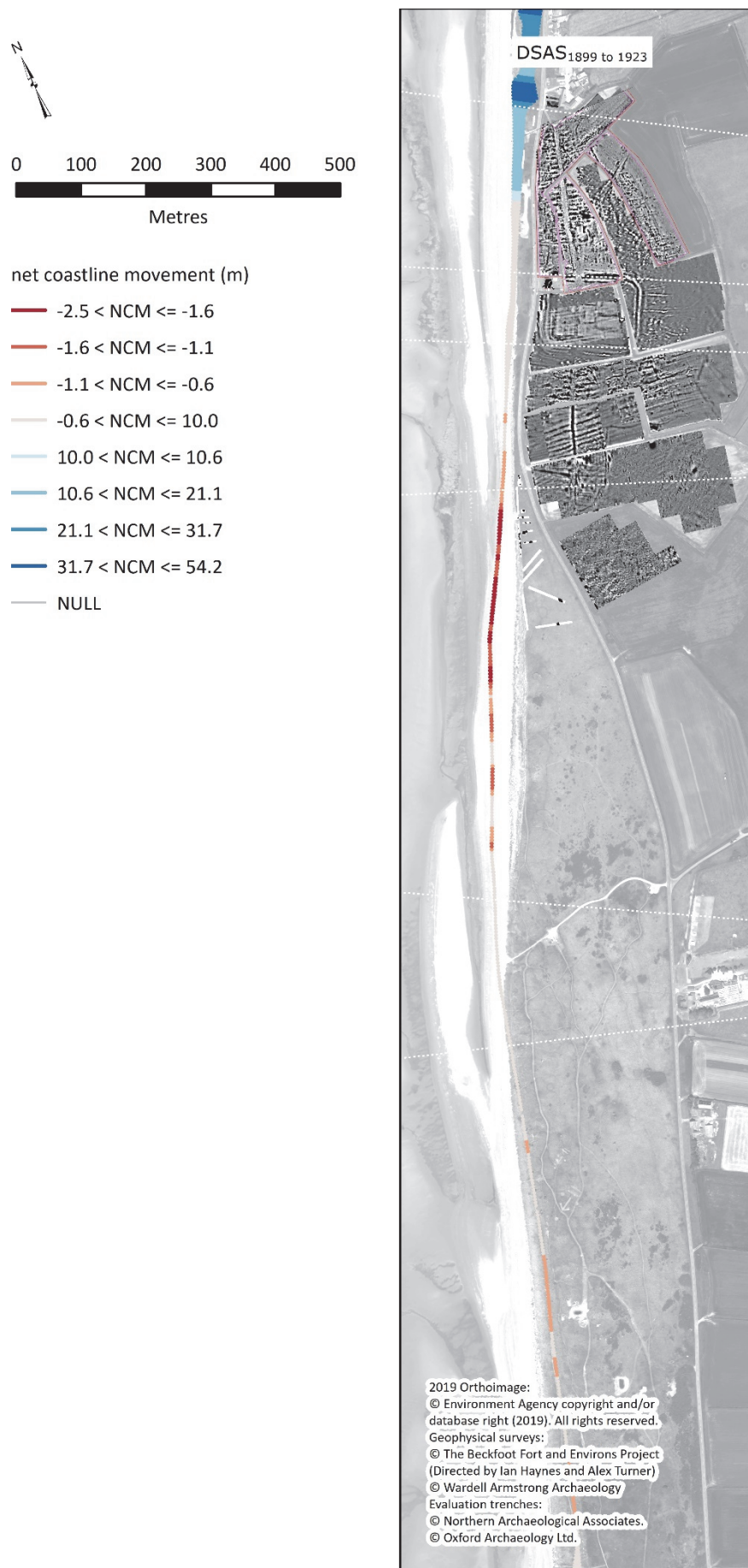
Figure 6.5: DSAS$_{1899 \text{ to } 1923}$ transects displayed by net coastline movement.

been subjected to fire, and a carved bone (potential knife handle), all retrieved by Harold Duff. In 1923, Duff stated: 'The continued erosion by the tide of the sand dunes opposite the site of the fort, discloses fragments of pottery and other debris, probably the remains of burials' (Hope, 1923, p.295). While the provenience of these finds are problematic as they were not precisely mapped, it is possible that they were discovered in this 700 m stretch of coastal dune erosion.

6.2.4 1923 to 1948

According to the 2D change detection results that compared the 1923 and 1948 coastline position, the coastline moved landward for all five coastal zones (Figure 6.6). The coastline from approximately the beck to the northern extent and c. 510 m of the southernmost transects from within the study area moved seawards. Note that the analyses did not extend fully to the southern extent of the study area due to lack of coverage provided by the 1948 orthomosaic. Table 6.6 provides details of distances and rates of movement.

Coastal zone	Direction of movement	Mean net movement (m)	Range net movement (m)	Mean EPR (m/year)	Range EPR (m/year)
Extramural settlement north	Landward (96 %)	2.39	0.29 - 5.14	0.09 +/- 0.12	0.01 – 0.20 +/- 0.12
	Seaward (4 %)	0.21	0.20 – 0.21	0.01 +/- 0.12	0.01 – 0.01 +/- 0.12
Beckfoot Roman Fort	Landward (100 %)	5.65	0.84 – 10.5	0.22 +/- 0.12	0.03 – 0.41 +/- 0.12
Extramural settlement south	Landward (100%)	10.51	9.08 – 12.89	0.41 +/- 0.12	0.50 – 0.36 +/- 0.12
Roman cremation cemetery/ Milefortlet 15	Landward (100 %)	21.86	8.95 – 32.53	0.86 +/- 0.12	0.35 – 1.27 +/- 0.12
Roman Tower 15a	Landward (69 %)	13.87	0.38 – 23.01	0.54 +/- 0.12	0.01 – 0.90 +/- 0.12
	Seaward (31 %)	4.33	0.46 – 7.38	0.17 +/- 0.12	0.02 – 0.29 +/- 0.12

Table 6.6: Coastline change statistics for each of the coastal zones calculated using coastlines from epochs 1923 to 1948.

The largest amount of landward movement measured 32.53 m. This occurred in coastal zone 4 - Roman cremation cemetery/Mileforlet 15 at a rate of up to 1.27 m/year +/- 0.12. This

landward movement of the coastline would have had a direct impact on the Roman cremation cemetery causing loss and destruction through the process of erosion. Between 1923 and 1948, Erosion of the sand dunes at this location resulted in the retrieval of material culture from the Roman cremation cemetery which included:

- A cremation urn containing bones was discovered by W. Armstrong c. 1940 (Chapter 5, Table 5.2 - ID 4) (Caruana, 2004, p.137).
- In 1945/1946 three boys from Abbeytown found a point in blown sand at a depth of 0.61 m approximately 1600 m south of the fort on the west side of the B5300 (Chapter 5, Table 5.2 - ID 5) (Caruana, 2004, p.137).
- A funeral bed and pyre excavated in April 1948 by Hogg and Hall (Chapter 5, Table 5.2 - ID 6) at NGR 094 499 (Caruarna, 2004, p.137; Hogg, 1949, p.32). This was found in the coastal dune cliff face approximately 365 m south west of the fort's south west corner (Hogg, 1949, p.34). Finds included an iron spear-head with an iron object fused to the socket, partially complete iron sword with a circular mass of iron fused to the blade (which had been bent), iron arrow-head with four barbs, 31 nails and fittings with evidence that they may have been gilded with gold leaf, two iron fittings, fragments of a blackened charred wooden structure, several pieces of a fragmentary bronze object – potentially a shield boss, and four fragments of calcined bone possible from a skull and part of a finger bone (Figure 6.7; Hogg, 1949, pp.34-35).

The funeral bed and pyre remains were discovered by Hall in a 'marine dissected coastal section' (Hogg, 1949, p.32). According to Hogg (1949, p.32) this is the first published report of the Roman cremation cemetery, although he does acknowledge that there have been numerous local reports of cremation urns and other cemetery remains having been washed out of the dunes by sea processes. In a footnote Hogg (1949, p.32) wrote that the cemetery site was now protected at the time of writing (1949) by a mass of gravel that lay above the mean high water mark of spring tides, that had accumulated as a result of a storm.

This finds discovered in c. 1940, 1945/1946 and 1948 help to understand coastal processes that took place during the intervening 25 years between the two epochs. As these were all discovered due to erosion of the coastal dunes, it may be suggested that the dunes were also eroding in 1940, 1945/1946 and 1948.
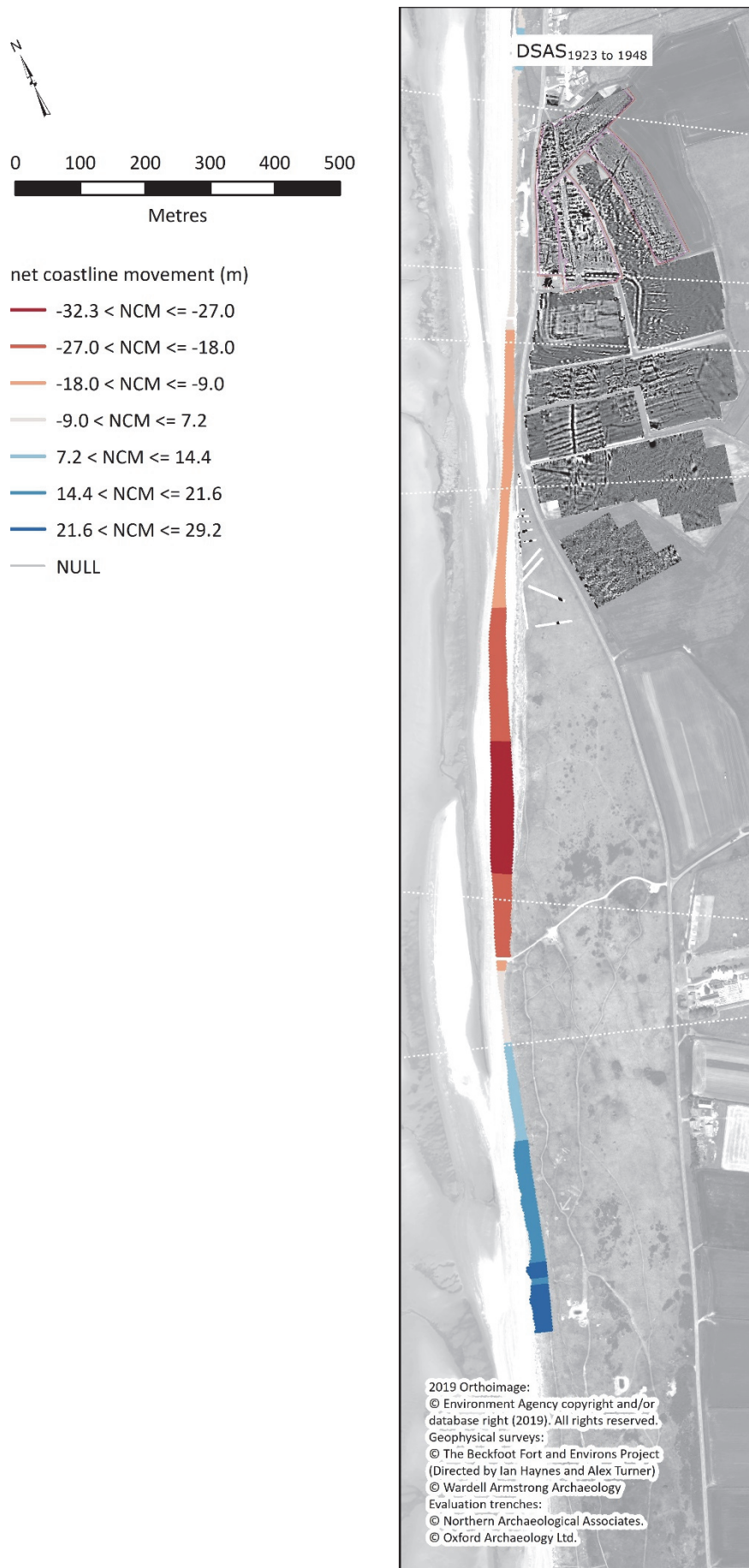
Figure 6.6: DSAS $_{1923\ to\ 1948}$ transects displayed by net coastline movement.
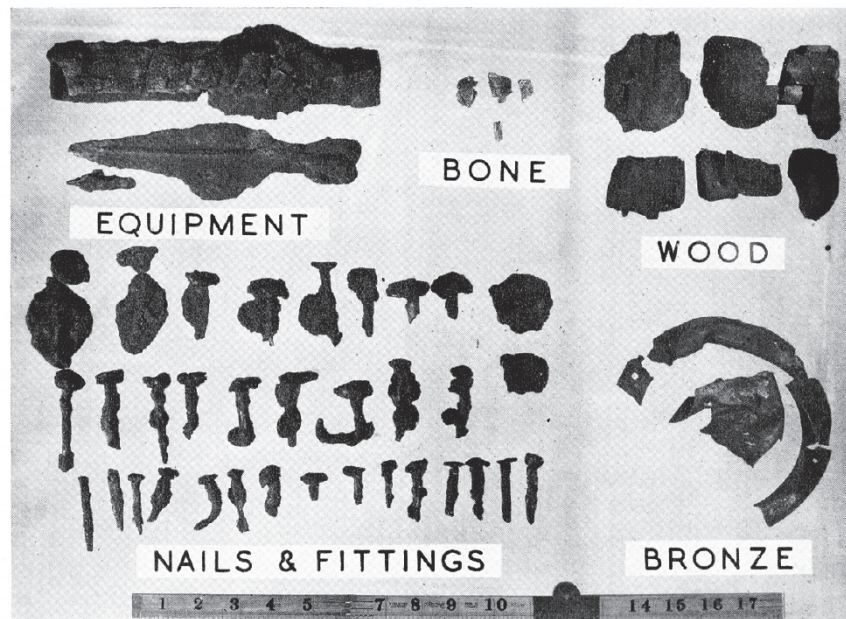
Figure 6.7: Objects from Beckfoot pyre discovered in the coastal cliff section in the location of Beckfoot Roman cremation cemetery (Source: Hogg 1949 p. 36).

Any subsequent erosion would have to have a landward movement beyond the 1948 coastline position for it to directly impact negatively upon the Roman cremation cemetery site, as this is the furthest landward position of the coastline within the time series thus far.

6.2.5 1948 to 1957

The 2D change detection results (Figure 6.8), which compared the 1948 and 1957 coastline positions, indicated that the reverse to the previous change detection (1923 to 1948) had occurred. The coastline position moved seaward for all five coastal zones where a landward movement was previously demonstrated. The sand dunes, therefore, appear to have went through a period of recovery. The 1957 coastline along this central stretch of the Beckfoot study area marked its furthest seaward limits out of all the recorded coastline positions from the Beckfoot time series. Any subsequent erosion along this stretch of coastal dunes would need to move landward beyond the 1948 coastline position in order to have a direct impact on the remains of the Roman cremation cemetery buried within the dunes.

Landward movements of the coastline occurred from the location of the beck to the northern extent of the study area and along the southernmost c. 410 m of the analysis. Like the previous change detection, coastal change was not calculated for the entire study area as the 1948 orthomosiac did not provide complete coverage. According to Haynes (2019) the

159

extramural settlement did not extend beyond the beck, therefore erosion of the dunes along the northern limit was not considered to have impacted the archaeological remains associated with Beckfoot Roman fort or its environs. This is also true for the area of erosion in the south as there is no evidence for Roman activity within this area of the dunes.

Coastal zone	Direction of movement	Mean net movement (m)	Range net movement (m)	Mean EPR (m/year)	Range EPR (m/year)
Extramural settlement north	Seaward (100 %)	3.36	1.64 – 5.45	0.40 +/- 0.45	0.19 – 0.65 +/- 0.45
Beckfoot Roman Fort	Seaward (100 %)	5.88	3.75 – 9.54	0.70 +/- 0.45	0.44 – 1.13 +/- 0.45
Extramural settlement south	Seaward (100%)	12.49	9.74 – 14.77	1.48 +/- 0.45	1.16 – 1.75 +/- 0.45
Roman cremation cemetery/ Milefortlet 15	Seaward (100 %)	24.67	11.26 – 33.56	2.92 +/- 0.45	1.34 – 3.98 +/- 0.45
Roman Tower 15a	Seaward (100 %)	15.71	0.76 – 30.90	1.86 +/- 0.45	0.09 – 3.66 +/- 0.45

Table 6.7: Coastline change statistics for each of the coastal zones calculated using coastlines from epochs 1948 to 1957.

While, the results of the 2D change detection for 1948 to 1957 showed advancement of the coastal dune system in the area of the Roman cremation cemetery, a number of finds were discovered. This could be an indication that the dunes were eroding in the intervening years between epochs.

- In March 1949 an inscribed fragment of a tombstone (Chapter 5, Table 5.1 - ID 7), likely dating to the 4th century was discovered by Hogg (Birley 1958). The inscription read '…]q(ui) vix(it) [annis…] I m(ensibus […' and has been translated by Birley (1958) as a 'memorial to someone who died at the age of so many years and months' (Birley 1958). While the fragments provenience was not detailed beyond being found at Beckfoot, based on the content of the inscription and dating method it was likely that this fragment of tombstone was retrieved from the Roman cremation cemetery.

Legend

net coastline movement (m)

- ▬ -27.8 < NCM <= -17.2
- ▬ -17.2 < NCM <= -11.5
- ▬ -11.5 < NCM <= -5.8
- ▬ -5.8 < NCM <= 10.0
- ▬ 10.0 < NCM <= 10.2
- ▬ 10.2 < NCM <= 20.4
- ▬ 20.4 < NCM <= 30.5
- ▬ 30.5 < NCM <= 33.6
- ▬ NULL

$DSAS_{1948\ to\ 1957}$

2019 Orthoimage:
© Environment Agency copyright and/or
database right (2019). All rights reserved.
Geophysical surveys:
© The Beckfoot Fort and Environs Project
(Directed by Ian Haynes and Alex Turner)
© Wardell Armstrong Archaeology
Evaluation trenches:
© Northern Archaeological Associates.
© Oxford Archaeology Ltd.

Figure 6.8: $DSAS_{1948\ to\ 1957}$ transects displayed by net coastline movement.

- Bellhouse (1954, p.28) recalled from a visit to Beckfoot in June 1954 '...raised beach deposits which were well displayed by recent erosion of the low cliffs thereabouts. Some 500 yards to the south of the hamlet, for a distance of about 300 yards, the spring tides had washed away the talus and brought down some of the cliff, leaving a nearly vertical section.' In the cliff south of the fort Bellhouse (1954 p. 28) discovered a patch of charcoal. Upon further investigation it became clear that this was the remains of a funerary pyre that included calcined human bones (Figure 6.9) (Chapter 5, Table 5.2 - ID 8).

- In 1956, a mortice and tennon joint, made of oak, possibly from a Roman bed was uncovered (Bellhouse and Moffat, 1958, p.61) (Chapter 5, Table 5.2 - ID 9).

- In 1957, a stone-lined grave, likely dating to the latter part of the Roman period, was found in the sand dune cliff face below the Roman levels (Bellhouse and Moffat, 1958, pp.61-62) (Chapter 5, Table 5.2 - ID 10).

- During Easter, 1957, while investigating funerary pyre remains located in close proximity to Milefortlet 15 , Moffat (1958, p.57) stated that the winter 'tides had exposed a long black line in the bank.' He troweled into this black layer to discover an urn-burial which consisted of partial remains of a samian ware bowl containing calcined bone (Bellhouse and Moffat, 1958). There were numerous pieces of bone under and around the bowl. A badly warped cooking-pot and some iron nails were also retrieved along side the burial (Bellhouse and Moffat, 1958) (Chapter 5, Table 5.2 - ID 11).

- Bellhouse (1958) also mentions finding at least 9 traces of creamtions located within the Roman level of the eroding sand dune face. While no specifics were given in regards to the exact date and location of his findings it can be safely assumed that these pre-dated his 1958 publication of these finds (Chapter 5, Table 5.2 - ID 12).

While the results of the 1948 to 1957 2D change detection results showed that the coastline in the area of the Roman cremation cemetery had been advancing, the archaeological evidence as described above adds additional details for the intervenening time between the two epochs. For example, the finds detailed in the above paragraph were all found during times when the dunes were eroding, which allowed for the Roman cremation cemetery material to be identifed in the cliff face. Therefore it can be deduced that while the results

showed an advancing coastline, that the sand dunes were in a state of retreat at the time the archaeological finds were recovered. This includes March 1949, June 1954, 1956 and springtime 1957.
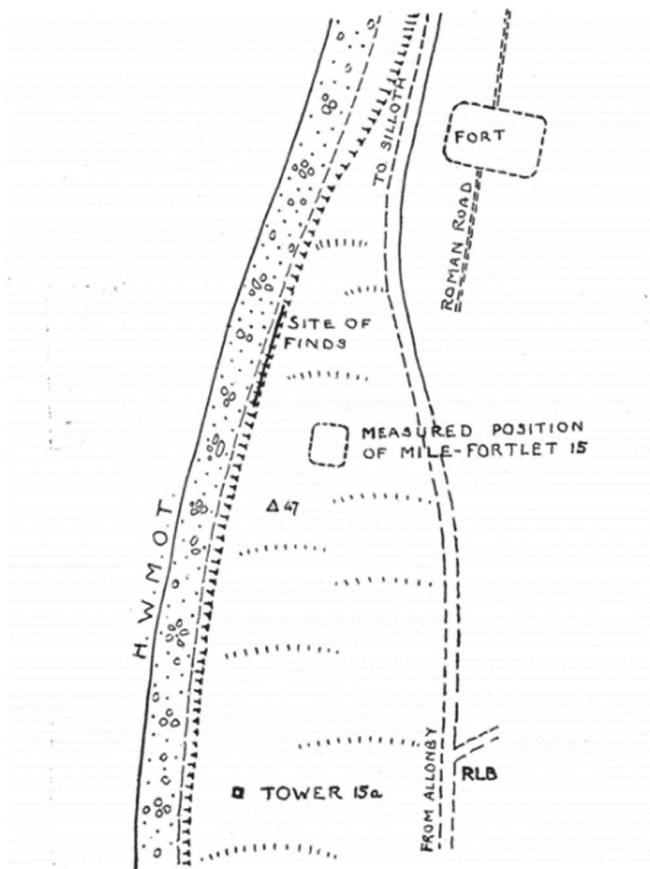
FIG. 6.—Sketch-plan (not to scale) of the cemetery site.
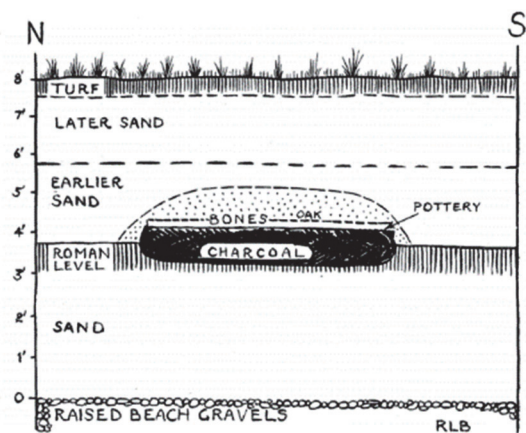
FIG. 7.—Section of the cremation pyre.

Figure 6.9: Location and section drawing of funerary pyre discovered by Bellhouse (1954).

6.2.6 1957 to 1991

According to the 1957 to 1991 2D change detection results (Figure 6.10), the position of the coastline moved landward for all coastal zones in contrast to the 1948 to 1957 results. While coastal erosion posed an increasing threat to the archaeological remains of Beckfoot Roman fort, the extramural settlement located both north and south of the fort and Roman Tower 15a, due to a decreasing of the distance to the coastline, these areas were not directly impacted upon. Erosion of the dunes occurring between 1957 and 1991, on the other hand, was hazardous to the Roman cremation cemetery. Removal of sediment through natural processes led to further partial destruction of the Roman cremation cemetery including the loss of material cultural as well as stratigraphic integrity.

Between 1957 and 1991, the coastline position moved seaward in two locations. These instances of seaward movement were from the location of the beck to the northern extent

163

of the study area and for the southernmost c. 125 m of the analysis. The 1991 orthmosaic did not provide full coverage, therefore change in the position of the coastline was not calculated for the entire study area.

Coastal zone	Direction of movement	Mean net movement (m)	Range net movement (m)	Mean EPR (m/year)	Range EPR (m/year)
Extramural settlement north	Landward (100 %)	9.11	6.43 – 10.64	12.88 +/- 0.11	0.19 – 0.31 +/- 0.11
Beckfoot Roman Fort	Landward (100 %)	8.88	7.87 – 9.69	0.26 +/- 0.11	0.23 – 0.28 +/- 0.11
Extramural settlement south	Landward (100%)	4.04	1.06 – 9.07	0.12 +/- 0.11	0.03 – 0.26 +/- 0.11
Roman cremation cemetery/ Milefortlet 15	Landward (100 %)	34.53	4.39 – 44.78	1.00 +/- 0.11	0.13 – 1.29 +/- 0.11
Roman Tower 15a	Landward (100 %)	27.59	15.55 – 43.89	0.80 +/- 0.11	0.45 – 1.27 +/- 0.11

Table 6.8: Coastline change statistics for each of the coastal zones calculated using coastlines from epochs 1957 to 1991.

This landward movement of the coastline has resulted in the loss of and destruction of the Roman cremation cemetery as the dunes retreated. Cemetery finds retrieved by enthusiasts, archaeologists and the local community during this 34 year period provided validation by attesting to the fact that the sand dunes having retreated as seen through the recovery of finds from the sand dune cliff face or from the beach frontage. Archaeological finds from up to sixteen entries from table 5.2 (ID 10-28) were recovered from the sand dune cliff face over the course of the 34 years. Although items 17, 16 and 22 may not have been found as the result of erosion of the sand dune cliff face.

Item 17 was a circular pit, possibly originally dug by Bellhouse while trying to locate Milefortlet 15 through a series of test pits (Bellhouse, 1957; Caruana, 2004, pp.138-9). This pit was discovered in 1985 because a 0.8m portion of dune had been dug into. If it were not for this purposeful removal of sediment the pit would have remained concealed by the dunes. Item 16, found in 1973 included a cooking pot with calcined bone fragments of animal origin, unidentified brushwood, charcoal and two beakers of cooking-pot form
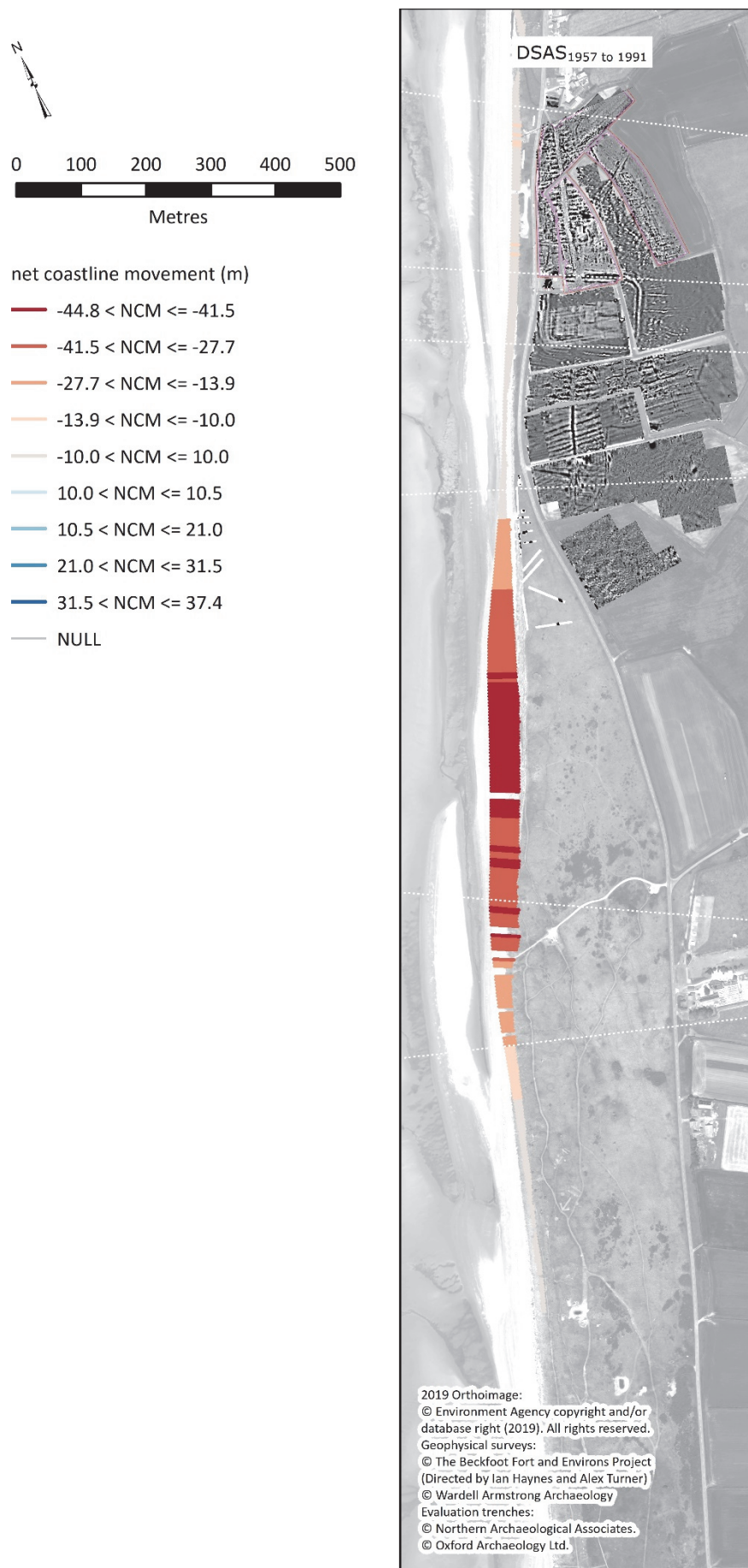
Figure 6.10: DSAS$_{1957 \text{ to } 1991}$ transects displayed by net coastline movement.

(Caruana, 2004, p.138). Caruana (2004, p.138) does not state the context in which Item 16 was discovered, therefore we do not know if it was due to erosion of the sand dunes. There were questions as to whether or not Item 22, discovered in 1952, was part of the collection of finds associated with Beckfoot Roman cremation cemetery. It was an early 4th century cooking pot used as an urn discovered 200 yards (182.9m) south of the south-west angle of the fort (Caruana, 2004, p.139). The vague description of the urns' location could place it in the fields east of the B5300. As the first three items were discussed in section 6.2.5, details of items 10, 11 and 12 are not provided again here.

Finds recovered from the sand dune cliff face and from the beach included:

- June 1960. A stone cist found in the sand dune cliff face 400 yards (365 m) south of Beckfoot Roman fort (Hogg, 1962). The seaward side of the cist was lost to erosion (Hogg 1962) (Chapter 5, Table 5.2 - ID 13).

- August 1961. A bronze disc brooch severely damaged by fire found within the Roman cremation cemetery horizon (Hogg, 1962) (Chapter 5, Table 5.2 - ID 14).

- 1972. A Roman-British olla type cinerary urn with calcined bones, iron nails and fittings were dug out of the sand dune cliff face 6 feet (1.83m) beneath the 1972 ground surface (Caruana, 2004, pp.137-8) (Chapter 5, Table 5.2 - ID 15).

- 1985. Located within a slumped dune opposite the fourth groyne an area of burning, which contained calcined bone was identified (Chapter 5, Table 5.2 - ID 18). Above this, located in the exposed roots was a fragment of charcoal, and recovered from the loose material below were more pieces of charcoal and two pieces of iron (Caruana 2004, p.139). South of the cremations was a flat feature composed of small shattered stones that measured 1.1 m long. The stones were mixed with black sand and charcoal (Caruana 2004) (Chapter 5, Table 5.2 - ID 27). Some un-stratified charcoal and one piece of calcined bone were also uncovered (Chapter 5, Table 5.2 - ID 20), as well as a disc-type brooch that would have held a glass insert or gemstone (Chapter 5, Table 5.2 - ID 19). The brooch appeared to have been subjected to heat and was discovered on the beach near the cemetery site by means of metal detecting (Richardson 1990). As the brooch was found on the beach and had evidence of burning, this could suggest that it had eroded from the sand dunes before being covered over by beach sediments.

- 1987. This was a fragmentary urn vessel found in a 'layer of black earth' at the Roman cremation cemetery (Richardson 1990). Caruana (2004, p.139) reported that the small pit containing the sherds of urn, bone, pottery and charcoal was discovered by Mr S.T. Collins and of the portion of pit that remained in situ was excavated by Alan James. The pit had been subjected to erosion and as such most of the pit fill had collapsed down the sand dune cliff face (Chapter 5, Table 5.2 - ID 21).

- 1956-57. Bellhouse (1958) mentions 'some small finds of 2nd and 4th-century pottery from the Roman levels in the area of the cemetery site (Bellhouse and Moffat 1958). Also mentions various pottery types collected since 1954, including early Hadrianic-Antonine cooking-pot, and pots of Gillam's types 147 and 148 dateable to ad 290-370, and a bowl to CINNAMUS (Bellhouse 1962) (Chapter 5, Table 5.2 - ID 23).

- 1971. A brooch found on April 15th 2 feet beneath the 1971 ground surface in an exposed section of coast due to erosion (Hogg 1972) (Chapter 5, Table 5.2 - ID 24).

- 1985 (May according to Caruana). Coin of Dupondius of Trajan (A.D 99 – 100) found on the beach near Beckfoot cemetery (Shotter 1986) (Chapter 5, Table 5.2 - ID 26).

- 1985 to 1987. Caruana (2004), along with Alan James and Derek Wellsby, discovered various un-stratified finds that included pottery, charcoal, a hobnail and calcined bone. Presumably these are the items discovered in the sand dune cliff face during visits from 1984 onwards, which Caruana (2004, p.134) referred to at the beginning of his article.

In addition to the above finds from the Roman cremation cemetery at Beckfoot, potential evidence for Milefortlet 15 was identified in the sand dune cliff edge (Bellhouse 1957; Bellhouse 1962). Bellhouse (1957) first reported discovering an exposed line of 'fossil' turf overlaid with sand and gravel, potentially representing ditch up-cast from Milefortlet 15 in August 1956 (Figure 6.11). Bellhouse later returned to the site on September 1st, 1960 with members of the Society and was able to point out this line of 'fossil' turf in the sand dune cliff face (Bellhouse 1962).

The archaeological evidence demonstrated further that the dunes had been experiencing erosion between at least 1957 and 1985 in the area of zone 4 - Roman cremation cemetery/Milfortlet 15. The eroding dunes had revealed archaeological evidence mostly relating to cemetery activity, but also possibly to Milefortlet 15. This discoveries were revealed during 1957, June 1960, August 1961, 1972, 1985, including August 23rd, 1987, April

15th 1971, and during 1985 to 1987. These dates are evidence of the coastline moving landward.
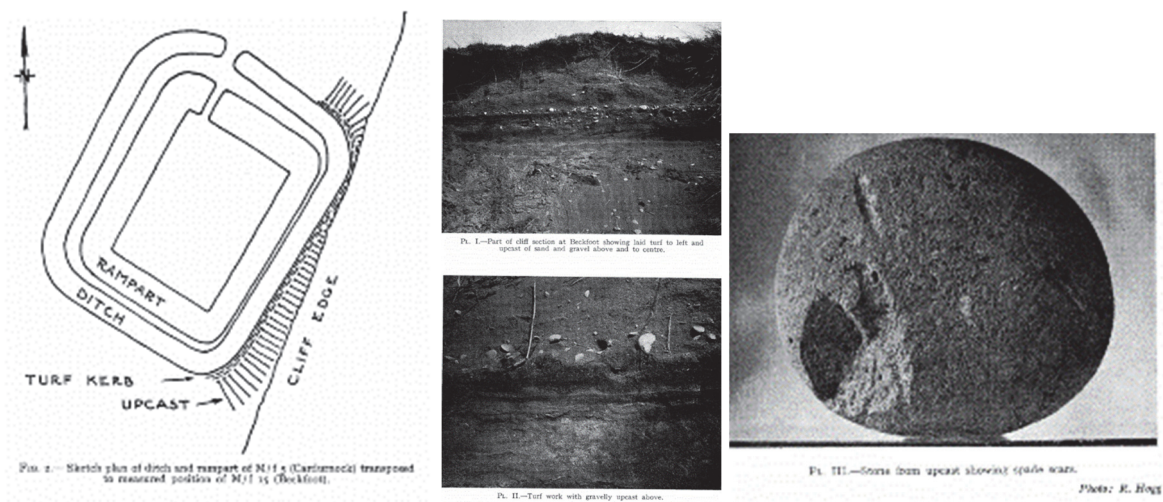
Figure 6.11: (left) Sketch plan of potential location of Milfortlet 15 based on (centre) potential ditch up-cast found in dune cliff face; and (right) stone with cut marks (Bellhouse 1962).

6.2.7 1991 to 2009

According to the 2D change detection results for 1991 to 2009, the 2009 coastline position moved seaward of the 1991 position in three locations and landward in two. Seaward movement took place in the coastal zones 1, 2 and 5 - extramural settlement north, Beckfoot Roman fort and Roman Tower 15a, with two small areas of seaward movement stretching into coastal zones 3 and 4 - extramural settlement south (29 %) and Roman cremation cemetery/Milefortlet 15 (14 %). This is in contrast to the previous change detection (1957 to 1991). The majority of the coastline opposite the extramural settlement south of the fort and along the Roman cremation cemetery/Milefortlet 15 moved landward. Details of seaward/landward movement are found in Table 6.9.

2.5D change detection was also undertaken. The distribution of erosion versus deposition can be seen on Figure 6.12. The results detected surface lowering in coastal zones 3 and 4 - of the extramural settlement south and Roman cremation cemetery/Milefortlet 15 as seen on the $DoD_{2009\ minus\ 1991}$ (Figure 6.13).

Additionally, 3D change detection was conducted for these pairwise epoch. The $M3C2_{2009\ -\ 1991}$ results (Figure 6.14) showed a similar pattern of deposition along the cliff dune face. While, some of the change detected by the M3C2 algorithm was likely owing to the noise present in the 1991 dense point cloud, the results provide a striking 3D visualisation of

coastal change, particularly in the vicinity of the coastal zone 4 - Roman cremation cemetery/Milefortlet 15.

Coastal zone	Direction of movement	Mean net movement (m)	Range net movement (m)	Mean EPR (m/year)	Range EPR (m/year)
Extramural settlement North (zone 1)	Seaward (100 %)	7.77	4.40 – 10.39	0.44 +/- 0.06	0.60 – 0.25 +/- 0.06
Beckfoot Roman Fort (zone 2)	Seaward (100 %)	8.57	6.54 – 9.70	0.49 +/- 0.06	0.38 – 0.56 +/- 0.06
Extramural settlement South (zone 3)	Landward (71 %)	11.23	0.85 – 16.14	0.64 +/- 0.06	0.05 – 0.92 +/- 0.06
	Seaward (29 %)	2.47	0.42 – 5.99	0.14 +/- 0.06	0.02 – 0.34 +/- 0.06
Roman cremation cemetery/ Milefortlet 15 (zone 4)	Landward (86 %)	9.36	0.97 – 16.36	0.54 +/- 0.06	0.06 – 0.94 +/- 0.06
	Seaward (14 %)	2.98	0.35 – 6.53	0.17 +/- 0.06	0.02 – 0.37 +/- 0.06
Roman Tower 15a (zone 5)	Seaward (100 %)	5.05	1.85 – 8.21	0.29 +/- 0.06	0.11 – 0.47 +/- 0.06

Table 6.9: Coastline change statistics for each of the coastal zones calculated using coastlines from epochs 1991 to 2009
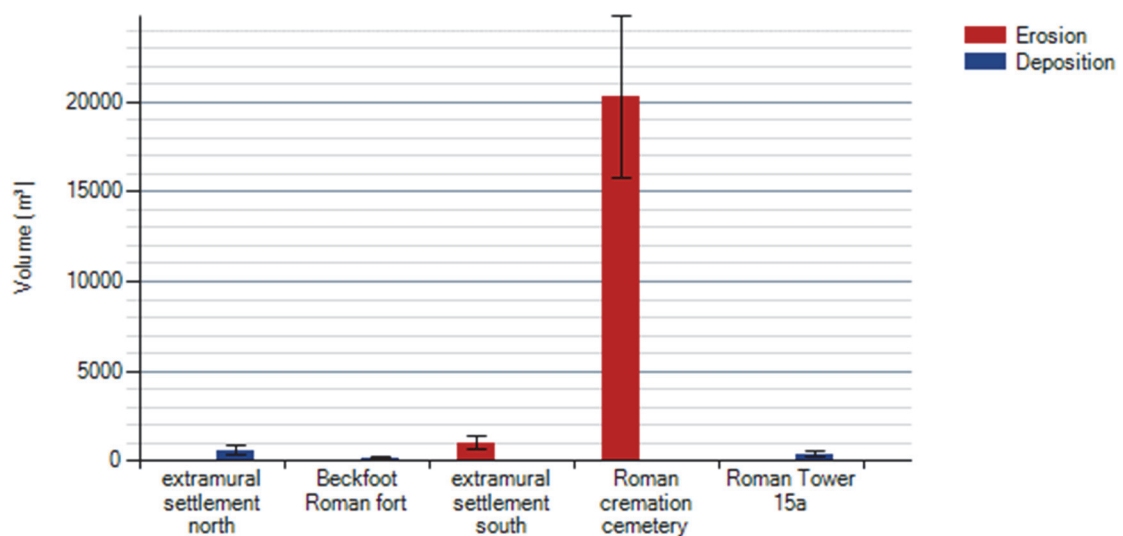
Figure 6.12: Erosion/deposition within each coastal zone of the sand dune cliff face quantified from the DoD$_{2009 \text{ minus } 1991}$.

Coastal zone	Measurement type	Surface raising (i.e. seaward movement)		Surface lowering (i.e. landward movement)	
		Raw	Thresholded	Raw	Thresholded
Extramural settlement north (zone 1)	Area (m^2)	2509	274	9	0
	Volume (m^3)	3625	572 +/- 261	1	0 +/- 0
	Average height/depth (m)	1.30	2.09 +/- 0.95	0	0 +/- 0
Beckfoot Roman Fort (zone 2)	Area (m^2)	1241	92	0	0
	Volume (m^3)	1843	182 +/- 87	0	0 +/- 0
	Average height/depth (m)	1.49	2.98 +/- 0.95	0	0 +/- 0
Extramural settlement south (zone 3)	Area (m^2)	673	0	1839	365
	Volume (m^3)	482	0 +/- 0	2266	1027 +/- 360
	Average height/depth (m)	0.72	0 +/- 0	1.23	2.82 +/- 0.99
Roman cremation cemetery/ Milefortlet 15 (zone 4)	Area (m^2)	2260	0	7788	4616
	Volume (m^3)	1012	0 +/-0	22974	20267 +/- 4547
	Average height/depth (m)	0.45	0 +/-0	2.95	4.39 +/- 0.98
Roman Tower 15a (zone 5)	Area (m^2)	2128	160	38	0
	Volume (m^3)	2352	360 +/- 154	4.53	0 +/- 0
	Average height/depth (m)	0.11	2.26 +/- 0.96	0.12	0 +/- 0

Table 6.10: Area, volume and height/depth of erosion and deposition from the sand dune cliff face quantified from the DoD$_{2009 \text{ minus } 1991}$.

Erosion of the coastline within the coastal zone 4 - Roman cremation cemetery/Milefortlet 15 would have had a negative impact on the archaeological remains buried within the dunes. The Roman cremation cemetery at Beckfoot made national news in October 2004 due to concerns that the sea was damaging the site. Community archaeologist from the Portable Antiquities Scheme (PAS), Faye Simpson, stated that the erosion was occurring 'at an amazing extent' (BBC News, 2004). On January 1st 2005 several cremated bones (PAS Unique ID: LANCUM-DD0B54) along with four nails and four sherds of pottery, were recovered from the sand dune cliff face in the area of Beckfoot Roman cremation cemetery (Boughton, 2005). In 2006 several finds were discovered at the foot of the eroding cliff in front of the Roman cremation cemetery and reported to the PAS (Bruns, 2006, p.14). These consisted mainly of black-burnished-ware cremation urns (Bruns, 2006, p.14).
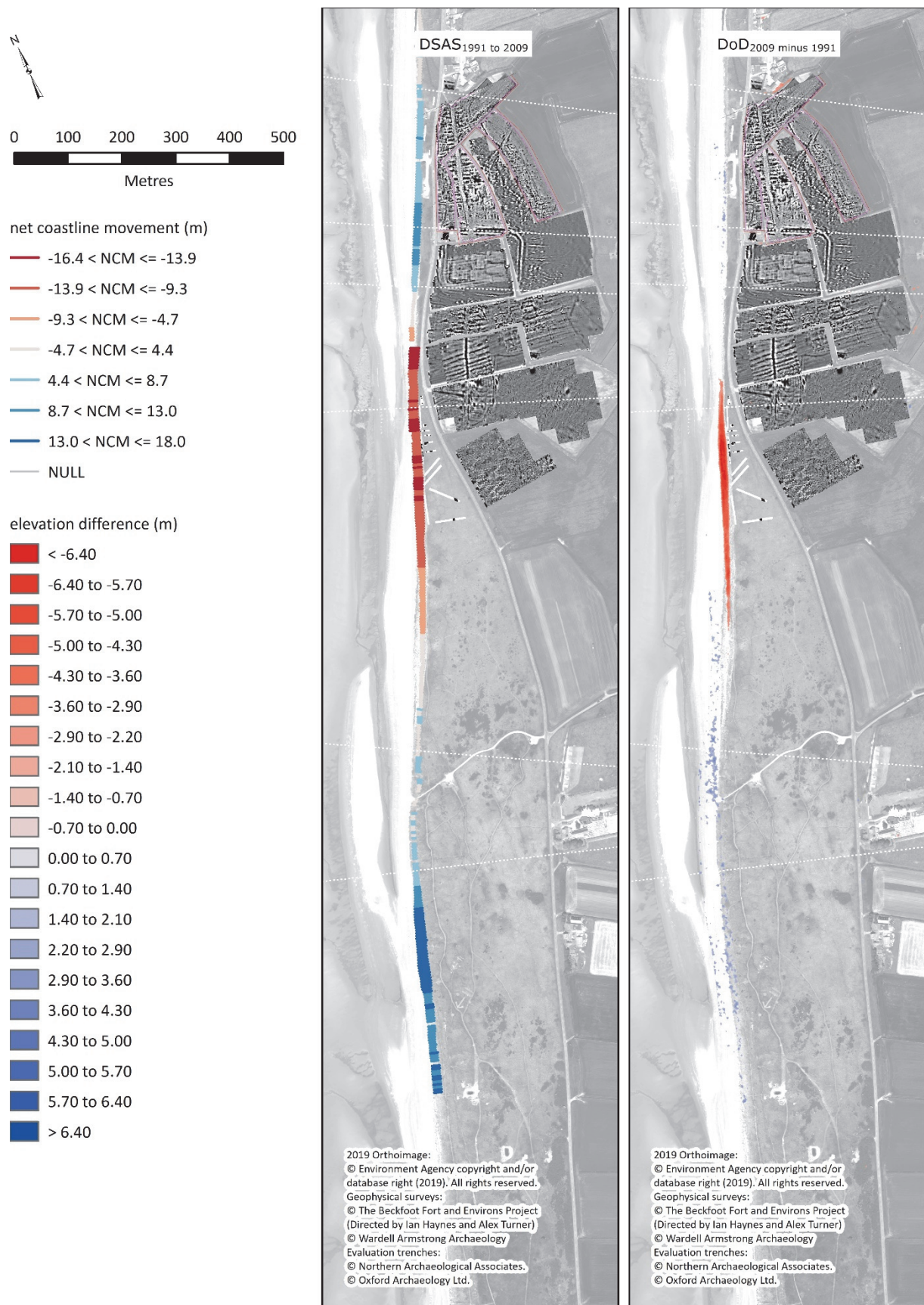
Figure 6.13: (left) DSAS$_{1991\ to\ 2009}$ transects displayed by net coastline movement; and (right) DoD$_{2009\ minus\ 1991}$ showing elevation difference.
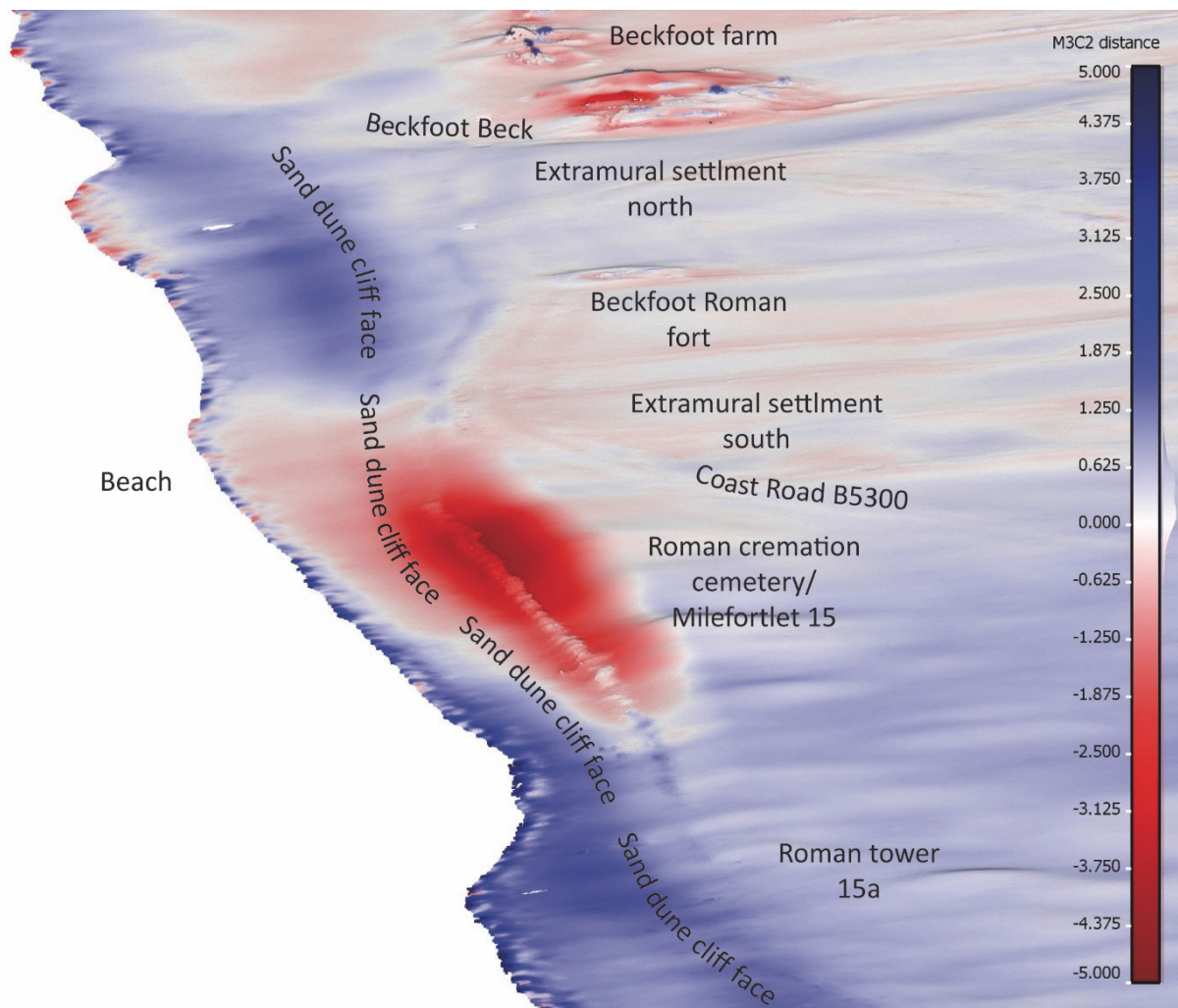
Figure 6.14: M3C2$_{2009 \text{ and } 1991}$ results, highlighting potential areas of erosion and deposition. These areas have likely been overestimated and underestimated due to error in the resulting 1991 point cloud.

6.2.8 2009 to 2010

A seaward movement of the coastline was detected for all five coastal zones on the 2D change detection results for 2009 to 2010. A landward movement of the coastline was also detected from within coastal zone 2, 3 and 4 - Beckfoot Roman fort (9 %), extramural settlement south (81 %) and Roman cremation cemetery/Milefortlet 15 (63%). Details for both the seaward and landward movement are provided in Table 6.11. Evidence for the landward movement of the coastline between 2009 and 2010 was also present on the DoD$_{2010 \text{ minus } 2009}$.

An area of 425 m^2 of surface lowering was detected from within the sand dune cliff face budget segregation polygon. This can be seen on the 2.5D change detection results in the coastal zones 3 and 4 - extramural settlement south and Roman cremation cemetery/Milefortlet 15. The total volume of surface lowering was 707.11 m^3 +/- 263.88 m^3

with an average depth of surface lowering of 1.66 m +/- 0.62 m. A detailed breakdown of surface change from the sand dune cliff face in each of the coastal zones is given in Table 6.12.

Coastal zone	Direction of movement	Mean net movement (m)	Range net movement (m)	Mean EPR (m/year)	Range EPR (m/year)
Extramural settlement North (zone 1)	Seaward (100 %)	3.77	1.76 – 7.52	3.37 +/- 0.51	1.57 – 6.73 +/- 0.51
Beckfoot Roman Fort (zone 2)	Landward (9 %)	0.22	0.04 – 0.4	0.2 +/- 0.51	0.04 – 0.36 +/- 0.51
	Seaward (91 %)	1.53	0.38 – 2.44	1.37 +/- 0.51	0.34 – 2.18 +/- 0.51
Extramural settlement South (zone 3)	Landward (81 %)	2.19	0.38 – 5.15	1.96 +/- 0.51	0.34 – 4.61 +/- 0.51
	Seaward (14 %)	0.45	0.16 – 0.87	0.40 +/- 0.51	0.14 – 0.78 +/- 0.51
Roman cremation cemetery/ Milefortlet 15 (zone 4)	Landward (63 %)	0.66	0.03 – 1.36	0.59 +/- 0.51	0.03 – 1.22 +/- 0.51
	Seaward (37 %)	1.46	0.02 – 5.03	1.30 +/- 0.51	0.02 – 4.5 +/- 0.51
Roman Tower 15a (zone 5)	Seaward (100 %)	3.18	0.56 – 9.44	2.84 +/- 0.51	0.5 – 8.44 +/- 0.51

Table 6.11: Coastline change statistics for each of the coastal zones calculated using coastlines from epochs 2009 to 2010.

The 2.5D change detection $DoD_{2010\ minus\ 2009}$ also revealed areas of detectable change from within the beach and the sand dunes budget segregation polygons. The surface raising from of the sand dunes appeared to be the result of misclassified ground points and represented the presence of vegetation rather than indications sediment deposition.

According to results from with the beach budget segregation polygon, the beach experienced both surface raising and surface lowering. This can be seen on the $DoD_{2010\ minus\ 2009}$ as alternating bands of blue and red, respectively (Figure 6.16). The pattern of surface raising and lowering is indicative of sediment transport driven by the tidal and wave regime.

Coastal zone	Measurement type	Surface raising (i.e. seaward movement)		Surface lowering (i.e. landward movement)	
		Raw	Thresholded	Raw	Thresholded
Extramural settlement north	Area (m^2)	1945	0	133	0
	Volume (m^3)	293	0 +/- 0	5.35	0 +/- 0
	Average height/depth (m)	0.15	0 +/- 0	0.04	0 +/- 0
Beckfoot Roman Fort	Area (m^2)	388	0	275	0
	Volume (m^3)	27	0 +/- 0	49	0 +/- 0
	Average height/depth (m)	0.07	0 +/- 0	0.18	0 +/- 0
Extramural settlement south	Area (m^2)	305	0	1519	317
	Volume (m^3)	25	0 +/- 0	1814	535 +/- 193
	Average height/depth (m)	0.08	0 +/- 0	0.78	1.69 +/- 0.61
Roman cremation cemetery/ Milefortlet 15	Area (m^2)	3470	0	2728	108
	Volume (m^3)	583	0 +/- 0	763	172 +/- 71
	Average height/depth (m)	0.17	0 +/ -0	0.28	1.59 +/- 0.66
Roman Tower 15a	Area (m^2)	1980	0	1606	0
	Volume (m^3)	120	0 +/- 0	75	0 +/- 0
	Average height/depth (m)	0.06	0 +/- 0	0.05	0 +/- 0

Table 6.12: Area, volume and height/depth of erosion and deposition from the sand dune cliff face quantified from the DoD$_{2010 \text{ minus } 2009}$.

The 3D change detection results, based on measurements taken along the surface normals, also indicated erosion within the coastal zones 3 and 4 - extramural settlement south and Roman cremation cemetery/Milefortlet 15 between 2009 and 2010 (Figure 6.15). This area of erosion along the cliff face extended for approximately 580m. The greatest amount of erosion was identified from where the dunes were the narrowest with the M3C2 distance measuring up to -1.41 m +/- 0.14 m. The M3C2 distance values from this 580 m stretch of erosion ranged between -0.05 m and -1.41 m with a distance uncertainty between 0.04 m and 0.61 m. Finer detail of the erosional process of the sand dunes cliff face was ascertained from the 3D change detection. For example, the erosion is seen at the top of the cliff face, while deposition has been identified at the bottom of the cliff face. This can be interpreted as slumping, or erosion from the upper levels being deposited on the lower levels of the cliff face.

Like the 2.5D geomorphic change detection results, evidence of sediment movement driven by tidal and wave action was present on the M3C2 results (Figure 6.17).

Figure 6.15: Erosion/deposition within each coastal zone of the sand dune cliff face quantified from the DoD$_{2010 \text{ minus } 2009}$.

According to a search of the Portable Antiquities Scheme one discovery event was reported to have been found at Beckfoot Roman cremation cemetery because of coastal erosion between 2009 and 2010. On May 5th 2009, two vessels (PAS Unique ID: LANCUM-413CA5) (Figure 6.18) dating to the Roman period were recovered by local archaeological enthusiasts, Jon Murray and Graham Ryan, from the dunes at Beckfoot Roman cremation cemetery (Pitts, 2009; Noon, 2010). One vessel was used as an urn and contained cremated human remains while the other was used as the urns lid (Pitts, 2009; Noon, 2010). This assemblage was reported to have washed out of the dune cliff due to the impact of heavy rains on the sand dunes (Pitts 2009, p.7).

net coastline movement (m)

— -9.4 < NCM <= -1.7
— -1.7 < NCM <= -1.1
— -1.1 < NCM <= -0.6
— -0.6 < NCM <= 1.6
— 1.6 < NCM <= 3.2
— 3.2 < NCM <= 4.7
— 4.7 < NCM <= 17.0
— NULL

elevation difference (m)

- < -2.50
- -2.50 to -2.20
- -2.20 to -1.90
- -1.90 to -1.60
- -1.70 to -1.40
- -1.40 to -1.10
- -1.10 to -0.80
- -0.80 to -0.50
- -0.60 to -0.30
- -0.30 to 0.00
- 0.00 to 0.30
- 0.30 to 0.60
- 0.60 to 0.90
- 0.80 to 1.10
- 1.10 to 1.40
- 1.40 to 1.70
- 1.70 to 2.00
- 1.90 to 2.20
- 2.20 to 2.50
- > 2.50

$DSAS_{2009 \text{ to } 2010}$

$DoD_{2010 \text{ minus } 2009}$

2019 Orthoimage:
© Environment Agency copyright and/or database right (2019). All rights reserved.
Geophysical surveys:
© The Beckfoot Fort and Environs Project (Directed by Ian Haynes and Alex Turner)
© Wardell Armstrong Archaeology
Evaluation trenches:
© Northern Archaeological Associates.
© Oxford Archaeology Ltd.

2019 Orthoimage:
© Environment Agency copyright and/or database right (2019). All rights reserved.
Geophysical surveys:
© The Beckfoot Fort and Environs Project (Directed by Ian Haynes and Alex Turner)
© Wardell Armstrong Archaeology
Evaluation trenches:
© Northern Archaeological Associates.
© Oxford Archaeology Ltd.

Figure 6.16: (left) $DSAS_{2009 \text{ to } 2010}$ transects displayed by net coastline movement; and (right) $DoD_{2010 \text{ minus } 2009}$ showing elevation difference.
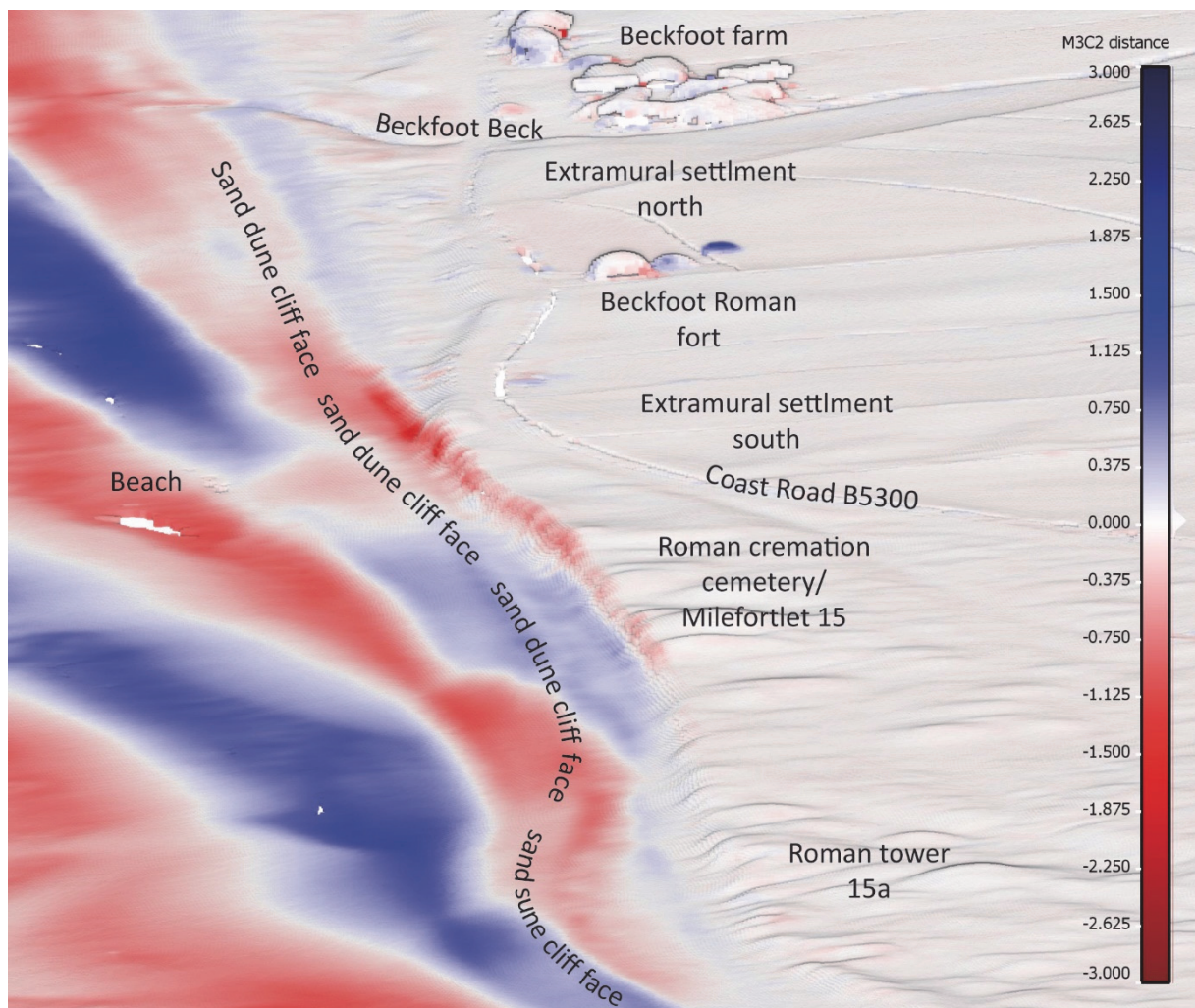
Figure 6.17: M3C2$_{2010 \text{ and } 2009}$ results, highlighting potential areas of erosion and deposition.

Figure 6.18: Urn containing cremated human remains discovered eroding from the dunes in May, 2009. LANCUM-413CA5 (Source: PAS https://finds.org.uk/database/artefacts/record/id/289313).

6.2.9 2010 to 2013

The 2010 to 2013 2D change detection results demonstrated a landward movement in all coastal zones, although to a far lesser extent from within zone 1 - extramural settlement north (Table 6.13). The areas with the greatest length of landward movement of the coastline were coastal zones 2, 3 and 4 - Beckfoot Roman fort (100 %), Extramural

177

settlement south (75 %) and Roman cremation cemetery/Milefortlet 15 (90 %). The greatest distance of landward movement was from within zone 5 - Roman Tower 15a coastal zone, which measured up to 9.83 m, followed by from within zone 4 - Roman cremation cemetery/Milfortelet 15 with a landward movement of up to 5.46 m recorded.

Coastal zone	Direction of movement	Mean net movement (m)	Range net movement (m)	Mean EPR (m/year)	Range EPR (m/year)
Extramural settlement North (zone 1)	Landward (10 %)	0.66	0.15 – 1.12	0.23 +/- 0.20	0.05 – 0.40 +/- 0.20
	Seaward (90 %)	2.93	0.32 – 5.21	1.05 +/- 0.20	0.11 – 1.86 +/- 0.20
Beckfoot Roman Fort (zone 2)	Landward (100 %)	3.58	1.33 – 5.06	1.28 +/- 0.20	0.48 – 1.81 +/- 0.20
Extramural settlement South (zone 3)	Landward (75 %)	1.39	0.09 – 3.56	0.50 +/- 0.20	0.03 – 1.27 +/- 0.20
	Seaward (25 %)	4.93	0.08 – 7.96	1.76 +/- 0.20	0.03 – 2.85 +/- 0.20
Roman cremation cemetery/ Milefortlet 15 (zone 4)	Landward (90 %)	1.41	0.01 – 5.46	0.50 +/- 0.20	0.00 – 1.95 +/- 0.20
	Seaward (9 %)	1.31	0.02 – 5.00	0.47 +/- 0.20	0.01 – 1.79 +/- 0.20
	No change (1 %)				
Roman Tower 15a (zone 5)	Landward (46 %)	5.88	0.52 – 9.83	2.10 +/- 0.20	0.18 – 3.51 +/- 0.20
	Seaward (54 %)	2.53	0.26 – 3.46	0.91 +/- 0.20	0.09 – 1.24 +/- 0.20

Table 6.13: Coastline change statistics for each of the coastal zones calculated using coastlines from epochs 2010 to 2013.

The 2.5D change detection result also detected surface lowering in coastal zones 2, 3 and 4 - Beckfoot Roman fort, extramural settlement south and Roman cremation cemetery/Milefortlet 15 (Figure 6.20). The results provided corresponding areal, volume and depth measurements (Table 6.14). No change was detected from within coastal zone 5 - Roman Tower 15a. Again, a typical pattern of erosion and deposition indicative of the tidal and wave regime can be seen on the DoD$_{2013\ minus\ 2010}$.

Coastal zone	Measurement type	Surface raising (i.e. seaward movement)		Surface lowering (i.e. landward movement)	
		Raw	Thresholded	Raw	Thresholded
Extramural settlement north (zone 1)	Area (m^2)	1602	0	301	0
	Volume (m^3)	376	0 +/- 0	49	0 +/- 0
	Average height/depth (m)	0.23	0 +/- 0	0.16	0 +/- 0
Beckfoot Roman Fort (zone 2)	Area (m^2)	128	0	575	78
	Volume (m^3)	16	0 +/- 0	300	106 +/- 43
	Average height/depth (m)	0.12	0 +/- 0	0.52	1.36 +/- 0.56
Extramural settlement south (zone 3)	Area (m^2)	810	5	722	157
	Volume (m^3)	321	6 +/- 3	468	248 +/- 94
	Average height/depth (m)	0.40	1.12 +/- 0.54	0.65	1.58 +/- 0.60
Roman cremation cemetery/ Milefortlet 15 (zone 4)	Area (m^2)	3017	9	3856	33
	Volume (m^3)	537	11 +/- 5	871	46 +/- 21
	Average height/depth (m)	0.18	1.21 +/- 0.58	0.23	1.38 +/- 0.62
Roman Tower 15a (zone 5)	Area (m^2)	2099	0	1696	0
	Volume (m^3)	301	0 +/- 0	145	0 +/- 0
	Average height/depth (m)	0.14	0 +/- 0	0.09	0 +/- 0

Table 6.14: Area, volume and height/depth of erosion and deposition from the sand dune cliff face quantified from the DoD$_{2013 \text{ minus } 2010}$.

The M3C2 results (Figure 6.21) also showed a pattern of sediment removal and deposition associated with the tidal regime and dominate wave direction as seen on the DoD$_{2013 \text{ minus } 2010}$ within the area of the beach as indicated by the red and blue bands. In addition, seen further seaward on the beach was a pattern of sediment removal and deposition corresponding to channels flowing from the beach to the sea in a dendritic configuration highlighted the water drainage network created by the ebb tidal current. The 2.5D results calculated at the 95th confidence interval did not detect this change corresponding to water drainage on the beach further from land where the dendritic pattern appeared. Less detail of the sediment was also detected by the 2.5D geomorphic change detection results.

Erosion was identified on the 3D change detection results in coastal zones 3, 4 and 5 - extramural settlement south, Beckfoot Roman fort and Roman cremation

cemetery/Milefortlet 15 (Figure 6.19). Beyond the fort and continuing north-eastwards, the coastline appeared to have been recovering as noted by the positive M3C2 distances.
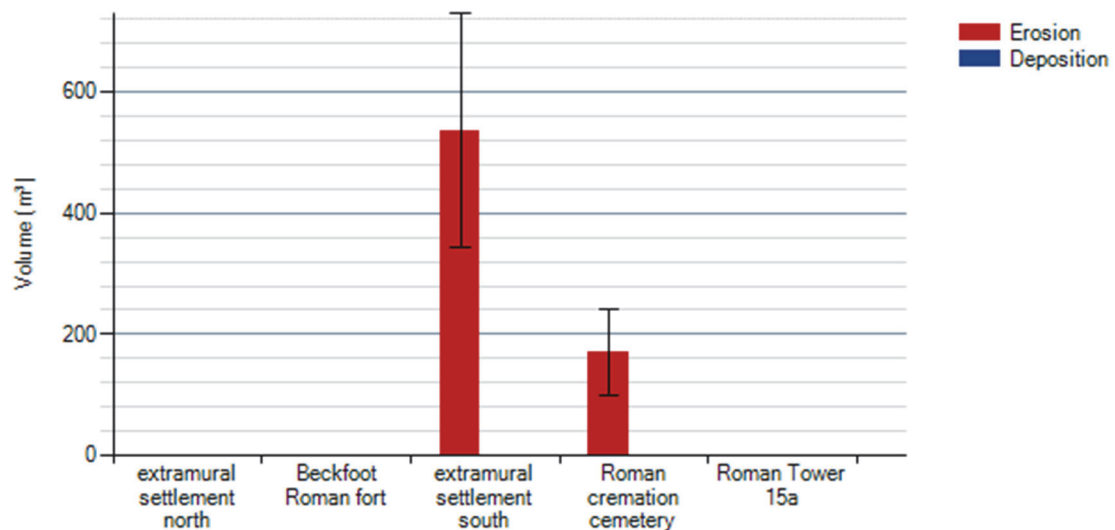

Figure 6.19: Erosion/deposition within each coastal zone within the sand dune cliff face quantified from the $DoD_{2013\ minus\ 2010}$.

From coastal zone 4 - Roman cremation cemetery/Milefortlet 15 the erosion appeared to be limited to the dune crest with deposition occurring on the dune cliff face below. The maximum M3C2 distance measured along the sand dunes indicating erosion was from coastal zone 2 - Beckfoot Roman fort which had a M3C2 maximum measurement of -1.55 m +/- 0.11 m (Figure. 6.21). The M3C2 distance ranged between -0.1 m and -1.56 +/- 0 m to 0.36 m.

In the location coastal zone 4 -Roman cremation cemetery/Milefortlet 15, the coastline continued to move landward by up to 1.84 m. The 2013 sand dune seaward extent was at this time more or less in line with Oxford Archaeology North 2006 western most evaluation trenches limit of excavation (LOE). Trench 3, orientated parallel to the coastline, contained features (306, 307 and 315), with extents that appeared to have continued beyond the LOE, therefore these features may have been visible in the cliff section or may have partially eroded from the cliff section prior to 2013 if not excavated in 2006. Two finds were reported to the PAS between 2010 and 2013, both were found on the 8th of May 2012. A fragment of oxidised coarse ware beaker including a small portion of the handle (PAS unique ID: LANCUM-546D25) dating to the 1st to 4th century AD (Noon, 2012a) and multiple fragments of a Bronze Age collared urn (PAS unique ID LANCUM-545A51) (Noon, 2012b)
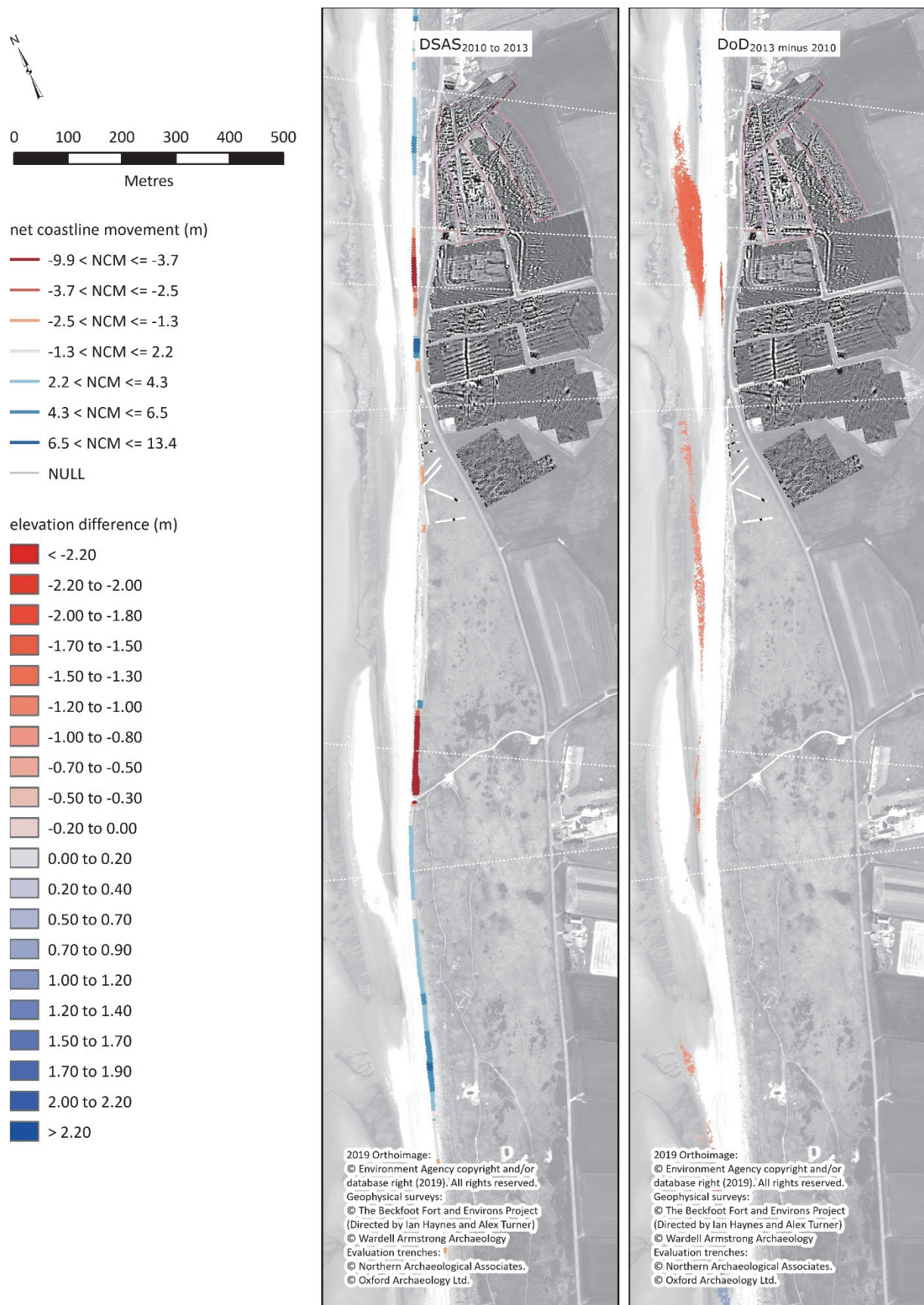
Figure 6.20: (left) DSAS$_{2010\ to\ 2013}$ transects displayed by net coastline movement; and (right) DoD$_{2013\ minus\ 2010}$ results showing elevation difference.
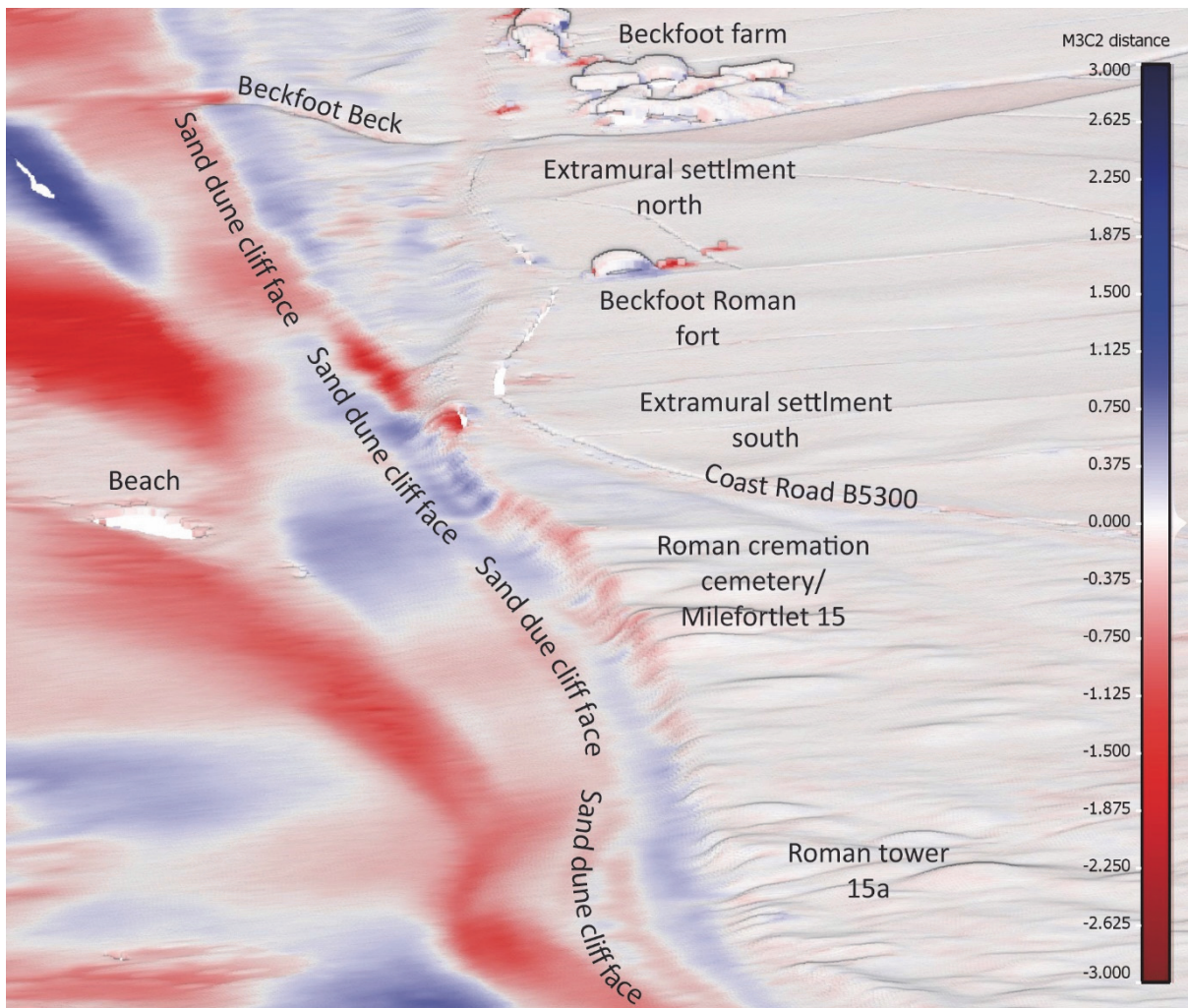
Figure 6.21: M3C2$_{2013 \text{ and } 2010}$ results, highlighting potential areas of erosion and deposition.

eroded out of the cliff at Beckfoot Roman cremation cemetery. The Bronze Age collard urn was of particular interest as it was potential evidence for a Bronze Age phase of cemetery activity, which was previously unknown at this site (Noon 2012b). Noon (2012b) argued that the Romans may have deliberately attempted to have appropriated the past through the re-use of the landscape as a cemetery site a thousand years later.

6.2.10 2013 to 2017 (including: 2013 to 2014, 2014 to 2015, and 2015 to 2017)

2.5D change detection was undertaken comparing the 2013 and 2017 epochs. For the intervening period (2013 to 2014, 2014 to 2015 and 2015 to 2017), 2D change detections of the coastline positions were also calculated as aerial imagery was available for 2014 and 2015.

The DoD$_{2017 \text{ minus } 2013}$ (Figure 6.34) compared two DEMs, one from pre (2013) and one from post (2017) construction of the rock armour wall at Castle Corners. The DoD$_{2017 \text{ minus } 2013}$ showed areas of surface raising and surface lowering of the beach (Table 6.15). The pattern

of deposition and erosion varied from the previous DoD's, which were indicative of the tidal and wave regime. Judging from the location of surface raising on the beach in relation sand dune cliff face, it may be that sediment that eroded from the dunes was deposited on the beach in front.

Coastal zone	Measurement type	Surface raising (i.e. seaward movement)		Surface lowering (i.e. landward movement)	
		Raw	Thresholded	Raw	Thresholded
Extramural settlement north (zone 1)	Area (m^2)	644	0	2730	1089
	Volume (m^3)	153	0 +/- 0	2564	1451 +/- 568
	Average height/depth (m)	0.24	0 +/- 0	0.94	1.33 +/- 0.52
Beckfoot Roman Fort (zone 2)	Area (m^2)	167	0	1377	839
	Volume (m^3)	30	0 +/- 0	1701	1349 +/- 450
	Average height/depth (m)	0.18	0 +/- 0	1.24	1.61 +/- 0.54
Extramural settlement south (zone 3)	Area (m^2)	759	0	1186	13
	Volume (m^3)	146	0 +/- 0	385	14 +/- 7
	Average height/depth (m)	0.19	0 +/- 0	0.32	1.05 +/- 0.51
Roman cremation cemetery/ Milefortlet 15 (zone 4)	Area (m^2)	1826	0	7451	4191
	Volume (m^3)	304	0 +/- 0	11566	10258 +/- 2492
	Average height/depth (m)	0.17	0 +/- 0	1.55	2.45 +/- 0.59
Roman Tower 15a (zone 5)	Area (m^2)	3946	3	571	0
	Volume (m^3)	1182	3 +/- 1.39	58	0 +/- 0
	Average height/depth (m)	0.30	1 +/- 0.46	0	0 +/- 0

Table 6.15: Area, volume and height/depth of erosion and deposition from the sand dune cliff face quantified from the DoD$_{2017 \text{ minus } 2013}$.

From the sand dune cliff face budged segregation polygon, an area measuring 11 m^2 demonstrated surface raising and an area measuring 6410 m^2 indicated surface lowering. The surface lowering equated to a total volume of 13344.83 m^3 +/- 3640.31 m^3 of removal of sediment from coastal zones 1, 2, 3 and 4 - extramural settlement north, Beckfoot Roman fort, Extramural settlement south and Roman cremation cemetery/Milefortlet 15 (Figure 6.22). Much of this erosion may have been episodic owing to the 2013-2014 winter storms. During the 2013-2014 winter storms waves were reported to have overtopped the rock

armour wall twice (Coastal Engineering UK Ltd, 2015a). The surge of water coupled with the force of the storms likely resulted in large volumes of sediment detaching from the from the sand dune cliff face and being carried cross shore, some of the which would have been deposited on the beach in front of the sand dunes opposite the area of erosion as the water moved seawards. Further investigation is required as these results calculated change for a three year period as there was no point cloud available immediately post-storm event.

The remains of Beckfoot Roman fort and extramural settlement north and south of the fort are located within the coastal hinterland and as such these areas were not under immediate threat from the erosion that occurred. Having said that, the dunes at this location were narrow and shallow. In 2013, at its narrowest (approximately opposite the fort), the sand dunes measured approximately 20m wide and at it widest, the sand dunes measured approximately 40m wide (approximately opposite the northern limit of the extramural settlement). In 2017 these widths were decreased to approximately 10 m and 30 m wide respectively providing less protection against ongoing and future threats of sea level rise and storm surges, to the archaeology remains within the coastal hinterland west of this area of erosion.
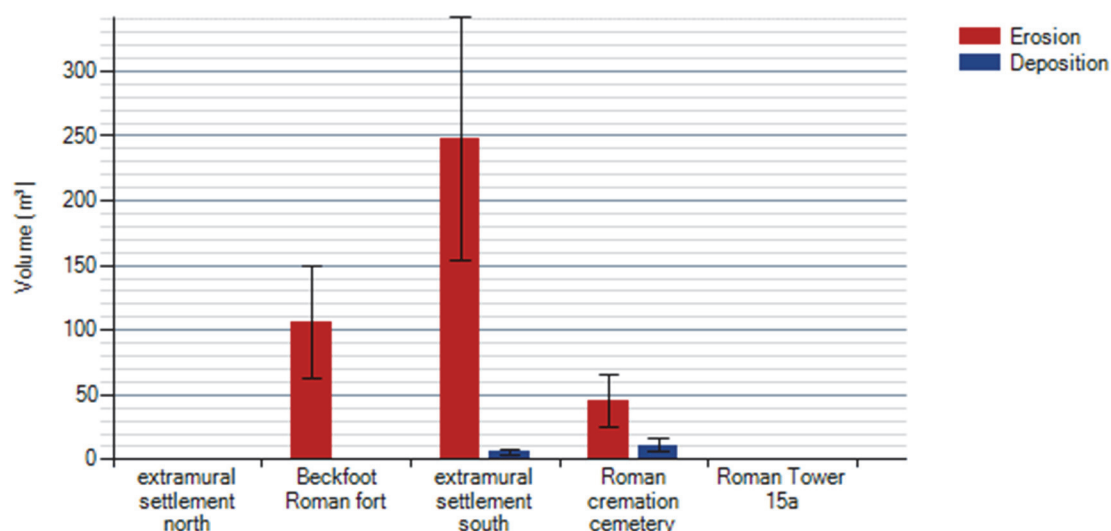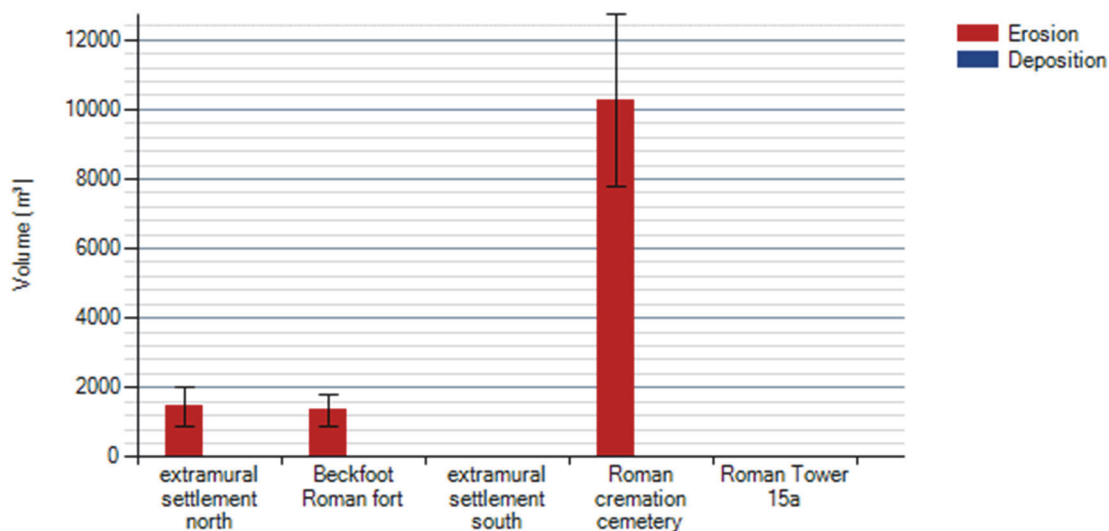

Figure 6.22: Erosion/deposition within each coastal zone of the sand dune cliff face quantified from the DoD$_{2017 minus 2013}$.
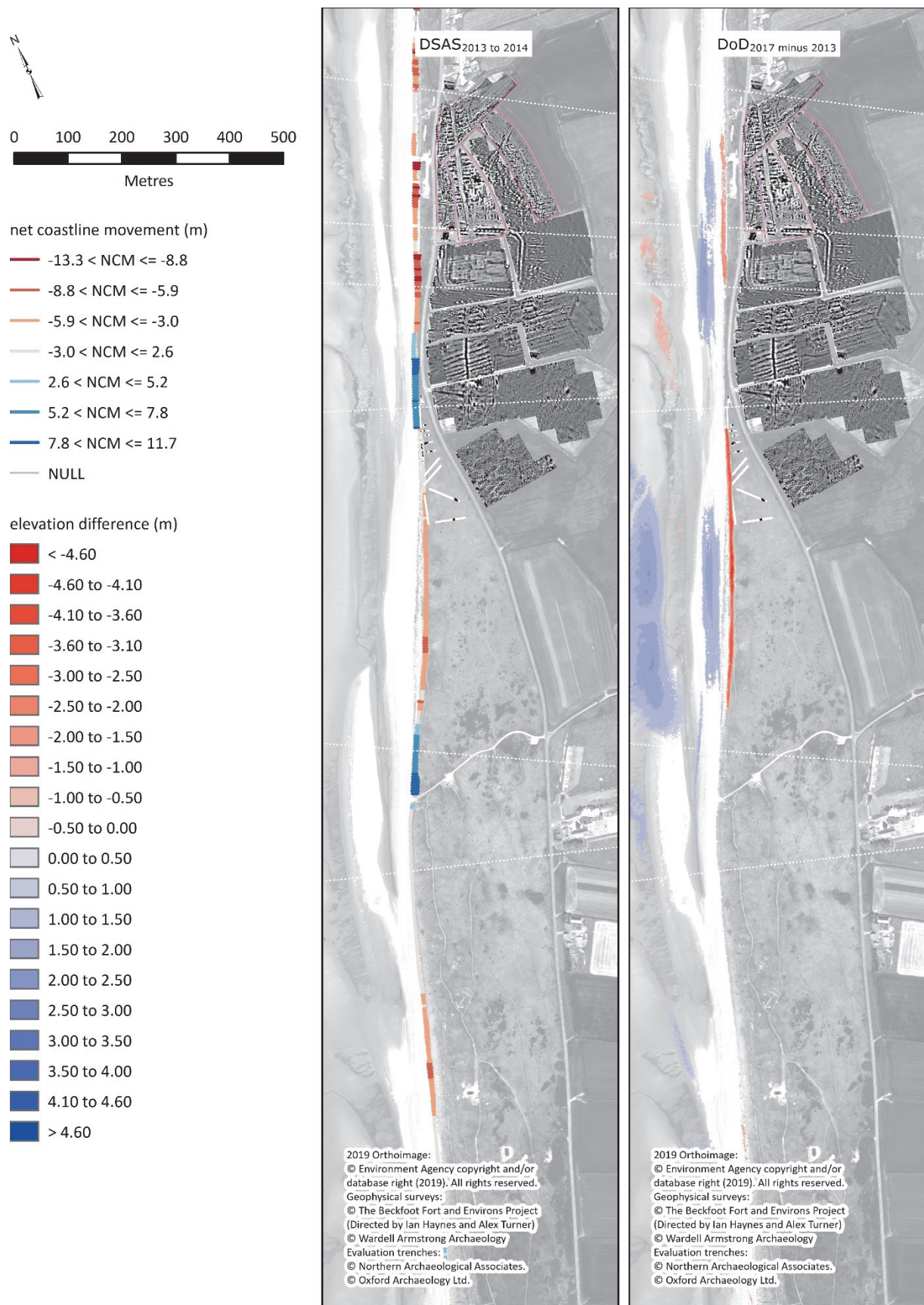
Figure 6.23: (left) DSAS$_{2013 \text{ to } 2017}$ transects displayed by net coastline movement; and (right) DoD$_{2017 \text{ minus } 2013}$ results showing elevation difference.

net coastline movement (m) - 2014 to 2015
— -10.3 < NCM <= -3.6
— -3.6 < NCM <= -2.4
— -2.4 < NCM <= -1.2
— -1.2 < NCM <= 1.0
— 1.0 < NCM <= 2.0
— 2.0 < NCM <= 2.9
— 2.9 < NCM <= 7.8
— NULL

net coastline movement (m) - 2015 to 2017
— -7.8 < NCM <= -3.2
— -3.2 < NCM <= -2.2
— -2.2 < NCM <= -1.1
— -1.1 < NCM <= 2.5
— 2.5 < NCM <= 5.0
— 5.0 < NCM <= 7.5
— 7.5 < NCM <= 11.0
— NULL
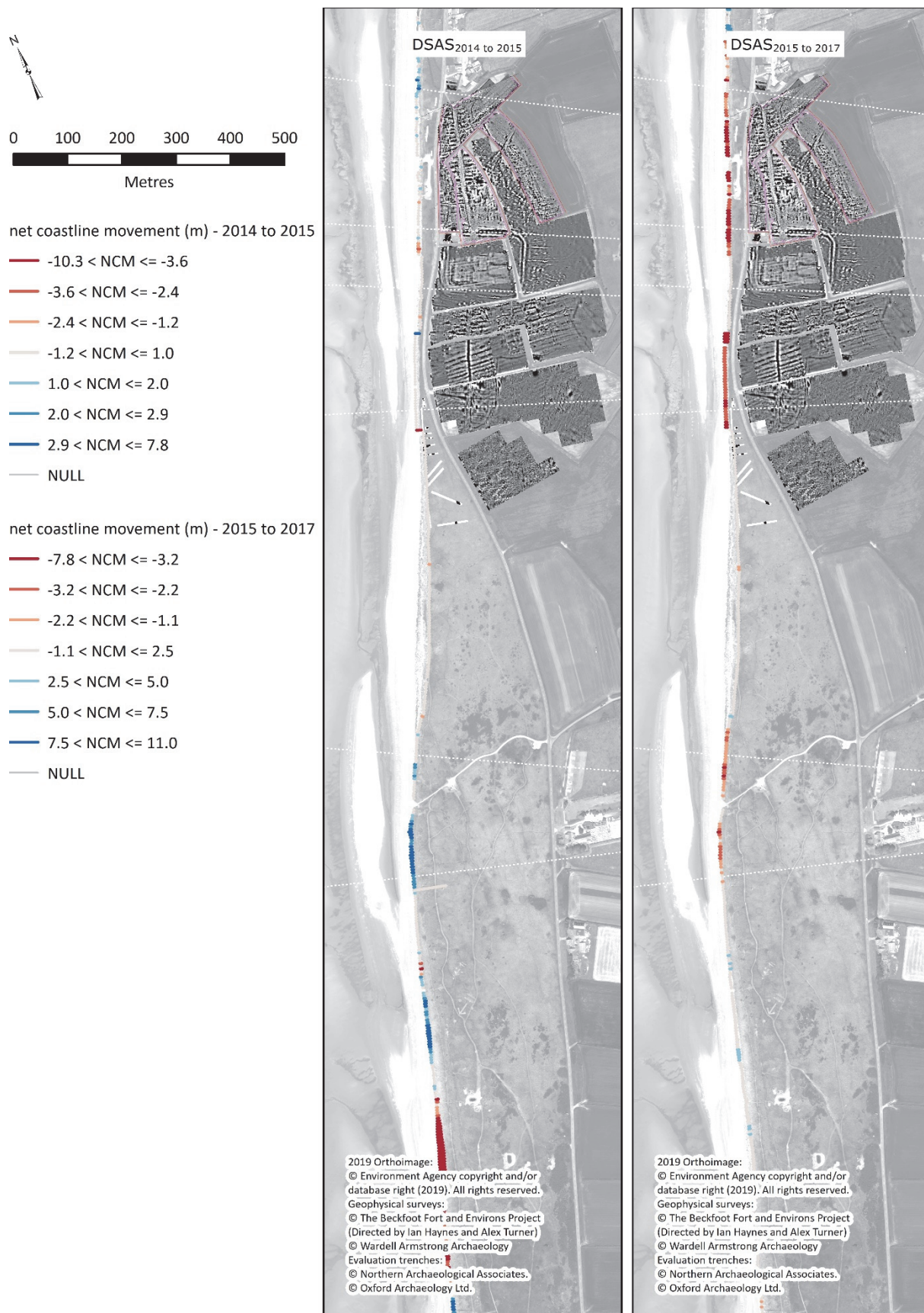
Figure 6.24: (left) DSAS$_{2014\ to\ 2015}$; and (right) DSAS$_{2015\ to\ 2017}$ transects displayed by net coastline movement for both.
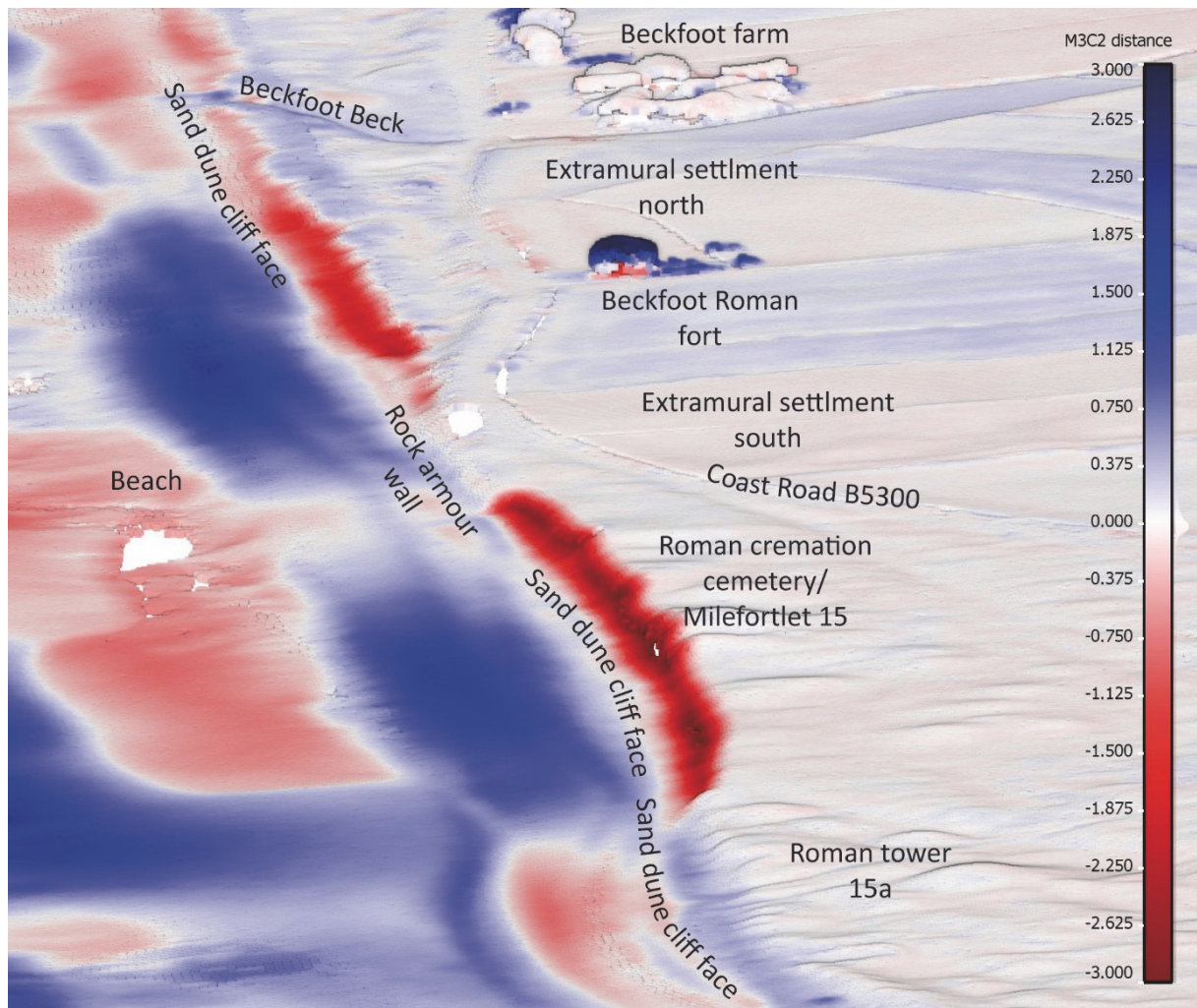
Figure 6.25: M3C2$_{2017 \text{ and } 2013}$ results, highlighting potential areas of erosion and deposition.

The 3D change detection results showed a pattern of erosion and deposition similar to that found on the DoD$_{2017 \text{ minus } 2013}$, although with far greater detail. According to the M3C2$_{2017 - 2013}$ results (Figure 6.25), the dunes experienced erosion for much of the coastline including in coastal zones 1, 2 and 4 - extramural settlement north, Beckfoot Roman fort and Roman cremation cemetery/Milefortlet 15. The rock armour wall afforded the coastal zone 3 - extramural settlement south some protection, although erosion was partially present within this zone to the North. Erosion also extended partially into coastal zone 5 - Roman Tower 15a. Most of the erosion came from two areas. The first was from the northern end of the rock armour wall to opposite the fields which contain the buried remains of the extramural settlement north of Beckfoot Roman fort. The M3C2 distances ranged between 0.3 m and 2.11 m +/- 0.33 m to 2.1m. The second was from the south terminal of the rock armour wall south westwards for approximately 550 m. The M3C2 distance measured between 0.1 m and 4.00 m +/- 0.04 m to 0.58 m.

Coastal zone	Direction of movement	Mean net movement (m)	Range net movement (m)	Mean EPR (m/year)	Range EPR (m/year)
Extramural settlement North (zone 1)	Landward (100 %)	4.51	0.55 – 11.05	2.73 +/- 0.52	0.33 – 6.71 +/- 0.52
Beckfoot Roman Fort (zone 2)	Landward (100 %)	6.13	2.32 – 9.86	3.73 +/- 0.52	1.41 – 5.99 +/- 0.52
Extramural settlement South (zone 3)	Landward (39 %)	4.98	3.64 – 7.38	3.03 +/- 0.52	2.21 – 4.48 +/- 0.52
	Seaward (61 %)	6.34	3.28 – 10.62	4.03 +/- 0.52	1.99 – 6.45 +/- 0.52
Roman cremation cemetery/ Milefortlet 15 (zone 4)	Landward (83 %)	3.88	0.64 – 6.59	2.36 +/- 0.52	0.39 – 4.01 +/- 0.52
	Seaward (17 %)	5.61	0.45 – 7.92	3.41 +/- 0.52	0.27 - 4.81 +/- 0.52
Roman Tower 15a (zone 5)	Landward (30 %)	1.38	0.04 – 2.67	0.84 +/- 0.52	0.02 – 1.62 +/- 0.52
	Seaward (70 %)	5.59	0.14 – 11.69	3.40 +/- 0.52	0.08 – 7.10 +/- 0.52

Table 6.16: Coastline change statistics for each of the coastal zones calculated using coastlines from epochs 2013 to 2014.

An analysis of the coastline position for the intervening years, from 2013 to 2014, 2014 to 2015 and 2015 to 2017 helped to further understand coastal change of the Beckfoot study area. Table 6.16, 6.17 and 6.18 presents the coastline statistics for these three 2D pairwise change detections. The results confirm that the majority of erosion across all coastal zones occurred between 2013 and 2014. The area of seaward movement from the coastal zones 3 and 4 - extramural settlement south and Roman cremation cemetery/Milefortlet 15 coincided with the location of the rock armour wall. While the greatest landward movement was from coastal zone 2 - Beckfoot Roman fort, coastal zone 4 - Roman cremation cemetery/Milefortlet 15 was impacted upon the most due to direct contact with the hazard.

Coastal zone	Direction of movement	Mean net movement (m)	Range net movement (m)	Mean EPR (m/year)	Range EPR (m/year)
Extramural settlement North (zone 1)	Landward (33 %)	0.49	0.04 – 7.35	0.07 +/- 1.83	0.07-2.55 +/- 1.83
	Seaward (67)	0.56	0.02 – 1.74	0.98 +/- 1.83	0.04 – 3.02 +/- 1.83
Beckfoot Roman Fort (zone 2)	Landward (68 %)	0.98	0.06 – 3.52	1.64 +/- 1.83	0.11 – 6.09 +/- 1.83
	Seaward (32 %)	0.50	0.06 – 1.37	0.87 +/- 1.83	0.14 – 2.63 +/- 1.83
Extramural settlement South (zone 3)	Landward (56 %)	0.28	0.02 – 1.51	0.48 +/- 1.83	0.04 – 2.61 +/- 1.83
	Seaward (11 %)	0.63	0.03 – 7.77	1.08 +/- 1.83	0.06 - 13.43 +/- 1.83
	No change (2 %)				
Roman cremation cemetery/ Milefortlet 15 (zone 4)	Landward (82 %)	0.52	0.01 – 8.72	0.89 +/- 1.83	0.01 – 15.08 +/- 1.83
	Seaward (17 %)	0.33	0.01 – 1.43	0.58 +/- 1.83	0.02 – 2.48 +/- 1.83
	No change (1 %)				
Roman Tower 15a (zone 5)	Landward (8 %)	0.19	0.02 – 0.28	0.33 +/- 1.83	0.04 – 0.49 +/- 1.83
	Seaward (92 %)	2.33	0.07-5.18	4.03 +/- 1.83	0.11 – 8.96 +/- 1.83

Table 6.17: Coastline change statistics for each of the coastal zones calculated using coastlines from epochs 2014 to 2015.

Eighty-two percent of transects from 2014 to 2015 2D change detection demonstrated continued erosion coastal zone 4 - Roman cremation cemetery/Milefortlet 15, with an average landward movement of 0.46 m ranging from 0.01 m to 8.72 m. While this was at a slower rate and decreased distance, any landward movement of the coastline would have resulted in erosion of the dunes at the location of the Roman cremation cemetery and therefore would have had a negative impact on the archaeological remains buried within the

dunes. The majority of the coastline along the extramural settlement also experienced a landward movement.

The 2D change detection results for 2015 to 2017 showed a dominant landward movement in coastal zones 1, 3, 4 and 5 - of the extramural settlement north, extramural settlement south, Roman cremation cemetery/Milefortlet 15 and Roman tower 15a (Table 6.18).

Coastal zone	Direction of movement	Mean net movement (m)	Range net movement (m)	Mean EPR (m/year)	Range EPR (m/year)
Extramural settlement North (zone 1)	Landward (96 %)	2.96	0.07 – 4.44	1.44 +/- 0.41	0.03 – 2.16 +/- 0.41
	Seaward (4 %)	0.52	0.36 – 0.68	0.26 +/- 0.41	0.18 – 0.33 +/- 0.41
Beckfoot Roman Fort (zone 2)	Landward (45 %)	3.40	1.18 – 5.33	1.66 +/- 0.41	0.58 – 2.59 +/- 0.41
	Seaward (55 %)	0.65	0.03 – 1.63	0.32 +/- 0.41	0.01 – 0.79 +/- 0.41
Extramural settlement South (zone 3)	Landward (86 %)	2.57	2.03 – 7.71	1.25 +/- 0.41	0.99 – 3.75 +/- 0.41
	Seaward (14 %)	0.83	0.04 – 2.03	0.40 +/- 0.41	0.02 – 0.99 +/- 0.41
Roman cremation cemetery/ Milefortlet 15 (zone 4)	Landward (87 %)	0.57	3.8 – 4.9	0.28 +/- 0.41	1.85 – 2.39 +/- 0.41
	Seaward (12 %)	0.56	0.01 – 4.9	0.28 +/- 0.41	0.01 – 2.39 +/- 0.41
	No change (1 %)				
Roman Tower 15a (zone 5)	Landward (98 %)	1.84	0.19 – 3.84	0.89 +/- 0.41	0.09 – 1.87 +/- 0.41
	Seaward (2 %)	0.63	0.63 – 0.63	0.31 +/- 0.41	0.31 – 0.31 +/- 0.41

Table 6.18: Coastline change statistics for each of the coastal zones calculated using coastlines from epochs 2015 to 2017.

The erosion of the sand dune cliff face as visible on the 2013 to 2017 results, including the intervening years, would have resulted in direct loss of material culture and associated contextual information from the proposed areas of cemetery activity. Fortunately, some of

the archaeological remains would have been recovered and preserved by record as part of the 2006 OA North evaluation (Healey 2006).

Evaluation trenches 2, 3, 8, 9 and 10 all intersected the area of erosion and would have experienced partial to complete destruction if they had not have been previously excavated and recorded. Four of these trenches (2, 3 8 and 9) listed above contained archaeological remains. The archaeological remains found within trench 3 would have been completely lost without prior archaeological intervention as the entire trench was located within the area of erosion. A cremation burial (315) of a probable female mature adult along with charcoal and some ironwork was recovered from an irregularly shaped pit cut into the Roman horizon within Trench 3 (Healey, 2007, p.23). A charcoal deposit 305 potentially from the remains of disturbed cremations and six instances of amorphous spread of dark material (306, 307, 308, 309, 310, 316), all possible cremation related deposits, were also recorded in Trench 3 along with another possible cremation 314. Trenches 8 and 9 also contained evidence for cemetery including a potential cremation pit 815, possible cremation deposits (804, 805, 812, 905, 906, 907, 908, 910) and a possible Roman ditch 816 (Healey, 2007, p.26). No detailed plans of these trenches were provided in the report, but the overall site plan overlaid with the results of the $DoD_{2017-2013}$ indicated that the erosion would have clipped the seaward end of these two trenches. While no archaeological remains were recovered from Trench 10, this trench was not fully excavated as the excavators reached the safe excavation limit before reaching the archaeological horizon or natural subsoil strata.

6.2.11 2017 to Sept 2018 (including 2017 to Feb 2018 and Feb 2018 to Sep 2018)

The 2D change detection results show mostly a landward movement of the coastline position within coastal zone 1 - extramural settlement north from 2017 to February 2018. The remaining coastal zones (zones 2 to 5 – Beckfoot Roman fort, extramural settlement south, Roman cremation cemetery/Milefortlet 15, and Roman tower 15a) demonstrated a mixture of both landward and seaward movement of the coastline position (Table 6.19). The greatest extent of landward movement occurred in coastal zone 1 - extramural settlement north with 98 percent of the transects indicating coastal retreat, followed by coastal zone 2 - Beckfoot Roman fort (57 %), coastal zone 3 - extramural settlement south (57 %), coastal zone 5 - Roman Tower 15 a (46%) and finally coastal zone 4 - Roman cremation cemetery/Milefortlet 15 (37 %). The furthest landward movement took place within coastal

zone 3 - extramural settlement south which measured a distance 7.14 m. The average rate of this movement was 3.73 m/year +/- 1.07 m.

Coastal zone	Direction of movement	Mean net movement (m)	Range net movement (m)	Mean EPR (m/year)	Range EPR (m/year)
Extramural settlement North (zone 1)	Landward (98 %)	2.37	0.45 – 4.63	2.98 +/- 1.07	0.56 – 5.81 +/- 1.07
	Seaward (2 %)	0.24	0.24 – 0.24	0.30 +/- 1.07	0.30 – 0.30 +/- 1.07
Beckfoot Roman Fort (zone 2)	Landward (82 %)	2.23	0.28 – 3.44	2.23 +/- 1.07	0.28 – 3.44 +/- 1.07
	Seaward (18 %)	0.78	0.43 – 1.47	0.98 +/- 1.07	0.54 – 1.85 +/- 1.07
Extramural settlement south (zone 3)	Landward (57 %)	2.97	0.10 – 7.14	3.73 +/- 1.07	0.03 – 1.27 +/- 1.07
	Seaward (43 %)	0.74	0.08 – 2.43	0.93 +/- 1.07	0.09 – 3.05 +/- 1.07
Roman cremation cemetery/ Milefortlet 15 (zone 4)	Landward (37 %)	0.43	0.01 – 5.58	0.54 +/- 1.07	0.01 – 7.00 +/- 1.07
	Seaward (63 %)	0.70	0.02 – 4.29	0.88 +/- 1.07	0.02 – 5.38 +/- 1.07
Roman Tower 15a (zone 5)	Landward (46 %)	0.68	0.01 – 1.98	0.85 +/- 1.07	0.02 – 2.49 +/- 1.07
	Seaward (54 %)	2.38	0.04 – 4.63	2.99 +/- 1.07	0.05 – 5.8 +/- 1.07

Table 6.19: Coastline change statistics for each of the coastal zones calculated using coastlines from epochs 2017 to February 2018.

Between February 2018 and September 2018, the 2D change detection results indicated dominant seaward movement of the coastline in coastal zones 1, 2, 3 and 5 - extramural settlement north, Beckfoot Roman fort, extramural settlement south and Roman Tower 15a. This change in direction of movement of the coastline was in contrast to the 2017 to February 2018 epoch and could be reflective of a change from a winter profile, in which the dunes may have been exposed to harsher weather conditions, to a summer profile, which allowed the dunes to recover due an improvement in weather conditions. In coastal zone 4 - Roman cremation cemetery/Milefortlet 15 a landward direction of coastline movement was

identified in 84 % of the transects demonstrating continued erosion of the coastal dune system at this vulnerable location.

Coastal zone	Direction of movement	Mean net movement (m)	Range net movement (m)	Mean EPR (m/year)	Range EPR (m/year)
Extramural settlement north (zone 1)	Landward (2 %)	0.48	0.48 – 0.48	0.80 +/- 1.40	0.80 – 0.80 +/- 1.40
	Seaward (98 %)	2.15	0.42 – 4.30	3.55 +/- 1.40	0.7 – 7.1 +/- 1.40
Beckfoot Roman Fort (zone 1)	Seaward (100 %)	1.78	1.06 – 2.38	2.95 +/- 1.40	1.75 – 3.93 +/- 1.40
Extramural settlement south (zone 3)	Landward (24 %)	1.24	0.03 – 3.39	0.05 +/- 1.40	0.05 – 5.61 +/- 1.40
	Seaward (76 %)	2.46	0.03 – 7.42	4.06 +/- 1.40	0.06 – 12.25+/- 1.40
Roman cremation cemetery/ Milefortlet 15 (zone 4)	Landward (84 %)	0.60	0.01 – 4.93	0.99 +/- 1.40	0.01 – 8.14 +/- 1.40
	Seaward (16 %)	0.38	0.03 – 1.56	0.63 +/- 1.40	0.06 – 2.58 +/- 1.40
Roman Tower 15a (zone 5)	Landward (100 %)	1.52	0.05 – 3.00	2.51 +/- 1.40	0.09 – 4.96 +/- 1.40

Table 6.20: Coastline change statistics for each of the coastal zones calculated using coastlines from epochs February 2018 to September 2018.

The 2.5D change detection results detected a surface lowering in four of the five coastal zones within the sand dune cliff face segregation polygon for coastal zones 1, 2, 4 and 5 - extramural settlement north, Beckfoot Roman fort, Roman cremation cemetery/Milefortlet 15 and Roman Tower 15a, with the greatest amount of erosion occurring within the first two zones (Figure 6.26). Erosion from these two coastal zones of the sand dune cliff face was limited to a stretch of coastline measuring approximately 100 m in length extending roughly from the northern end of the rock armour wall and contined north-eastwards. From within the coastal zone 4 - Roman cremation cemetery/Milefortlet 15, the surface lowering was concentrated to the southern end of the rock armour wall (Table 6.21). Localised erosion found at the terminal ends of seawalls is referred to as end scour, end effect, end-wall effect and flanking erosion.

Coastal zone	Measurement type	Surface raising (i.e. seaward movement)		Surface lowering (i.e. landward movement)	
		Raw	Thresholded	Raw	Thresholded
Extramural settlement north	Area (m^2)	996	0	1494	73
	Volume (m^3)	93	0 +/- 0	551	79 +/- 37
	Average height/depth	0.09	0 +/- 0	0.37	1.08 +/- 0.51
Beckfoot Roman Fort	Area (m^2)	506	0	460	75
	Volume (m^3)	49	0 +/- 0	191	102 +/- 42
	Average height/depth	0.10	0 +/- 0	0.41	1.36 +/- 0.55
Extramural settlement south	Area (m^2)	700	0	121	0
	Volume (m^3)	93	0 +/- 0	12	0 +/- 0
	Average height/depth	0.13	0 +/- 0	0.10	0 +/- 0
Roman cremation cemetery/ Milefortlet 15	Area (m^2)	6389	0	2193	10
	Volume (m^3)	673	0 +/- 0	408	14 +/- 6
	Average height/depth	0.11	0 +/- 0	0.12	1.24 +/- 0.56
Roman Tower 15a	Area (m^2)	1308	0	615	14
	Volume (m^3)	183	0 +/- 0	102	6 +/- 2.60
	Average height/depth	0.14	0 +/- 0	0.17	0.44+ +/- 0.19

Table 6.21: Area, volume and height/depth of erosion and deposition from the sand dune cliff face quantified from the DoDS$_{Sep\ 2018\ minus\ 2017}$.

Figure 6.26: Erosion/deposition within each coastal zone of the sand dune cliff face quantified from the DoD$_{Sep\ 2018\ minus\ 2017}$.
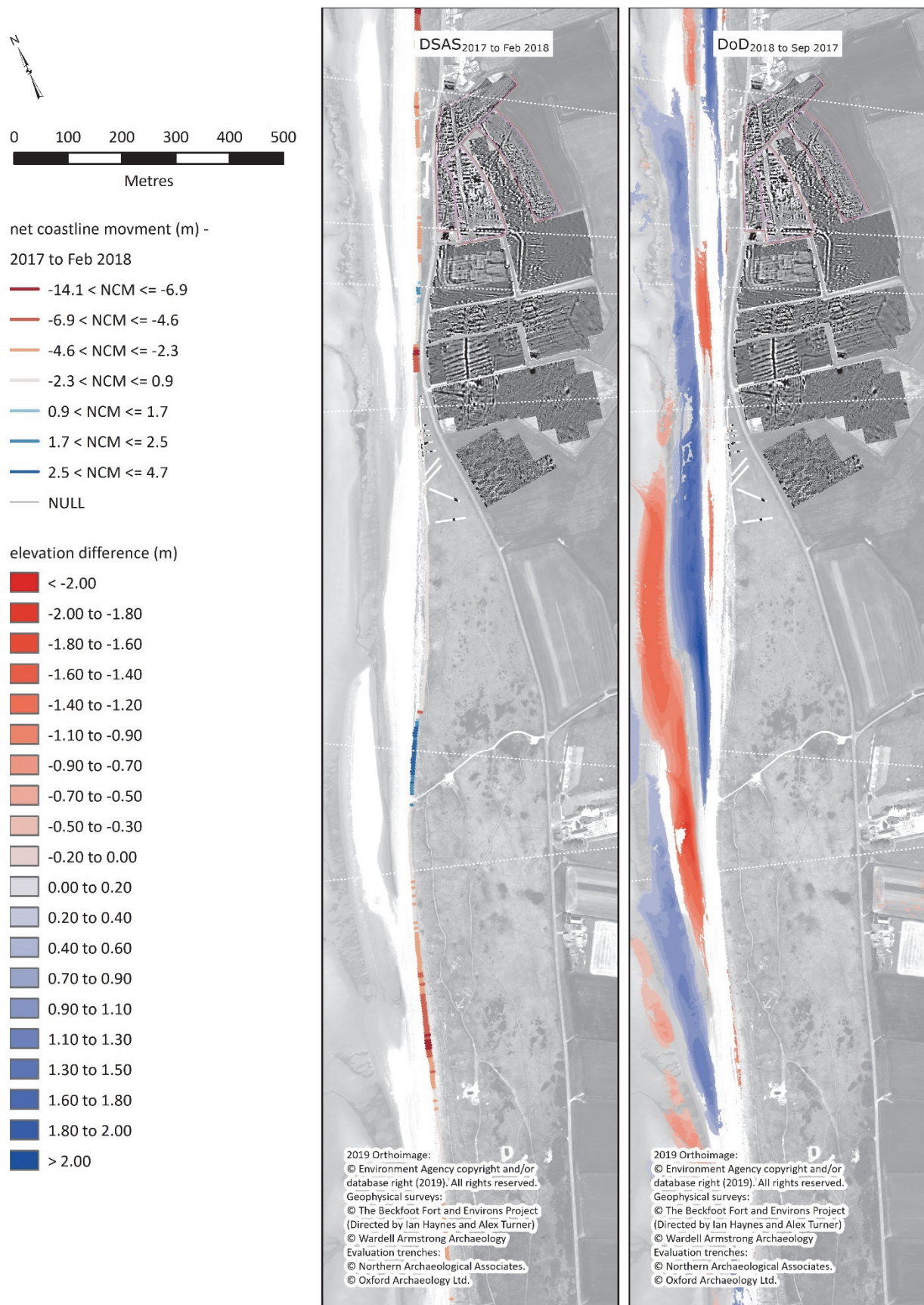
Figure 6.27: (left) DSAS$_{2017\ to\ Apr\ 2018}$ transects displayed by net coastline movement; and (right) DoD$_{2017\ minus\ Sep\ 2018}$ results showing elevation difference.

net coastline movment (m) -
Feb 2018 to Sep 2018

— -5.0 < NCM <= -1.0
— -1.0 < NCM <= -0.7
— -0.7 < NCM <= -0.4
— -0.4 < NCM <= 1.0
— 1.0 < NCM <= 1.9
— 1.9 < NCM <= 2.8
— 2.8 < NCM <= 7.6
— NULL

DSAS$_{Apr\ 2018\ to\ Feb\ 2018}$

2019 Orthoimage:
© Environment Agency copyright and/or
database right (2019). All rights reserved.
Geophysical surveys:
© The Beckfoot Fort and Environs Project
(Directed by Ian Haynes and Alex Turner)
© Wardell Armstrong Archaeology
Evaluation trenches:
© Northern Archaeological Associates.
© Oxford Archaeology Ltd.

Figure 6.28: DSAS$_{2018\ to\ Sep\ 2018}$ transects displayed net coastline movement
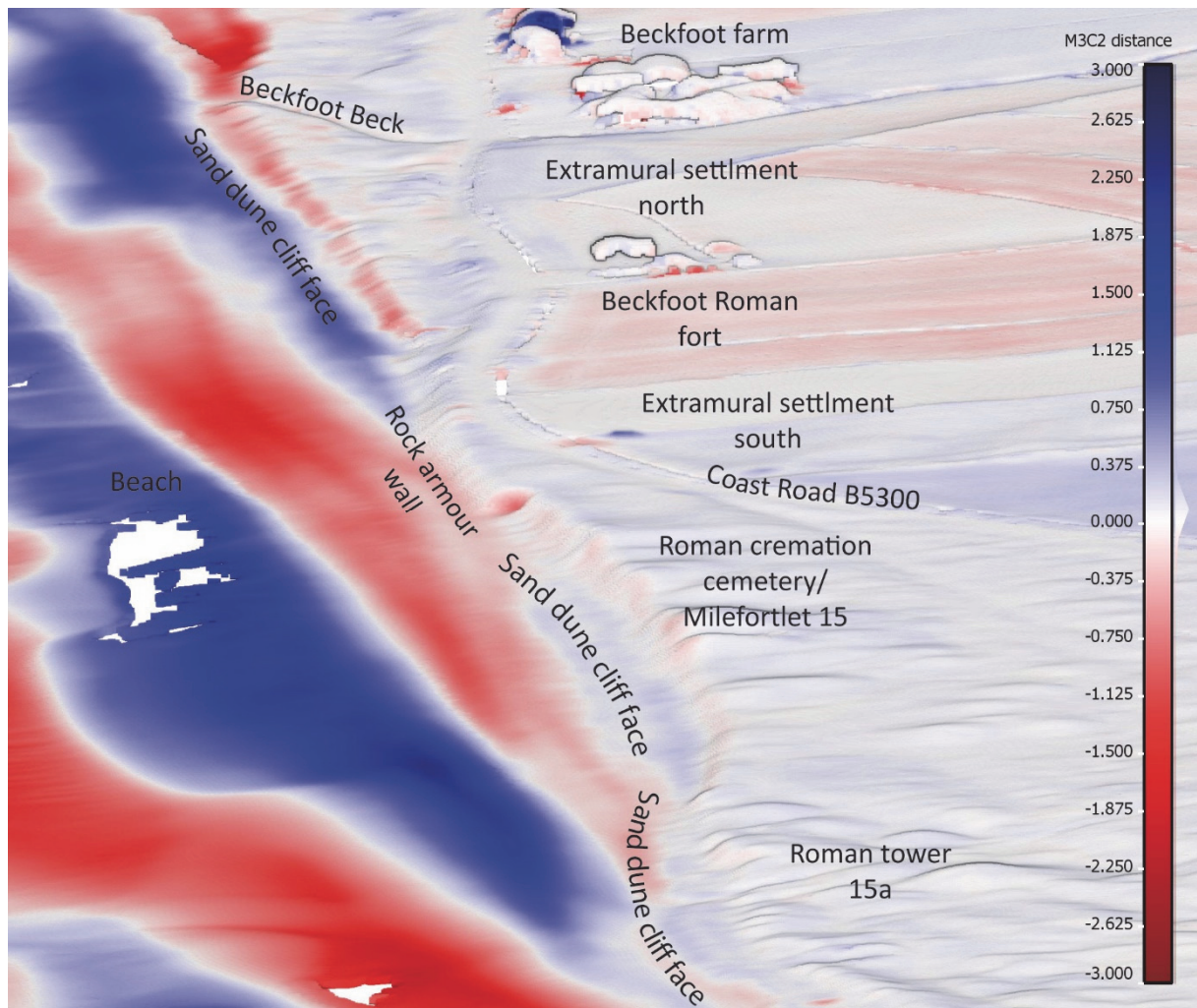
Figure 6.29: M3C2$_{2018 \text{ and } 2017}$ results, highlighting potential areas of erosion and deposition.

The 2018 to 2017 3D change detection results showed a pattern of sediment movement on the beach consistent with the tidal and wave regime. This is indicated by the alternating bands of blue (points with a positive M3C2 value) and red (points with a negative M3C2) representing deposition (blue) and erosion (red). In addition, the results also indicated erosion on the beach along the base of the rock armour wall (Figure 6.29). This evidence of beach lowering was potentially caused by the impact of waves with the structural feature driving the water downwards before returning to sea and picking up sediment along the way. Continued erosion at this location could undermine the rock armour wall eventually causing it to fail, putting any archaeological material buried within the dunes protected by the rock armour wall at risk.

Erosion can also be seen along the sand dune cliff face in coastal zones 1, 2, 4 and 5 - extramural settlement north, Beckfoot Roman fort, Roman cremations cemetery/Milefortlet 15 and Roman Tower 15a. As before, while the erosion of coastal zone 4 - Roman cremation cemetery/Milefortlet 15 may have occurred to a lesser magnitude to that within coastal

zones 1 and 2 - extramural settlement north and Beckfoot Roman fort, the impact is greater to coastal zone 4 - Roman cremation cemetery/Milefortlet 15, due to proximity of the erosion to buried remains. Erosion that occurred of the sand dune cliff face at this location Roman cremations cemetery. The results only show that sediment eroded from along the top of the cliff face and was deposit at its base, but they also further highlighted the flanking erosion that was identified in the 2.5D change detection results.

Located approximately 8 m inland from the rock armour wall where the flanking erosion was observed in the 3D change detection results, were the remains of a cremation burial enclosed by a ring ditch that contained cremated bone within the backfill recovered from trench 7 of the 2006 OA North archaeological evaluation (Healey, 2007, p.19). The cremation burial consisted of a ceramic vessel containing a small amount of bone which was discovered buried within a central pit that was filled with pyre debris. The OA North archaeological evaluation also revealed evidence for the Roman cremation cemetery from Trench 1. From Trench 1, multiple amorphous areas of dark subsoil were uncovered, one of which contained cremated bone. This trench was located parallel to and behind the rock armour wall and would have intersected the area of scour erosion at its southern extent. OA North also recorded an approximate extent of cemetery soil as observed in the sand dune cliff face which extended roughly 15m north-eastwards beyond the southern end of the rock armour wall. This extent of the Roman cemetery horizon along with the evidence for cemetery remains within trenches 1 and 7, allow for it to be deduced that the erosion at the southern terminal end of the rock armour wall had a direct impact on the remains of the Roman cemetery site.

6.2.12 Sep 2018 to Apr 2019 and Apr 2019 to Jun 2019

Transects displayed notable landward movement of the coastline between September 2018 and April 2019 within coastal zones 2, 4 and 5 - Beckfoot Roman fort (100 %), Roman cremation cemetery (92 %) and Roman Tower 15a (62 %). This was reduced to 54 percent, 2 percent and 51 percent landwards between April 2019 and June 2019. This reduction in landward movement demonstrated that the dunes may have been going through a period of recovery, particularly in coastal zone Roman cremation cemetery. Full details of distances and rates of change for both 2D pairwise change detections are provided in Table 6.22 and 6.23.

Coastal zone	Direction of movement	Mean net movement (m)	Range net movement (m)	Mean EPR (m/year)	Range EPR (m/year)
Extramural settlement North (zone 1)	Landward (10 %) Seaward (90 %)	N/A	N/A	N/A	N/A
Beckfoot Roman Fort (zone 2)	Landward (100 %)	N/A	N/A	N/A	N/A
Extramural settlement South (zone 3)	Landward (2 %) Seaward (98 %)	0.01 1.88	0.01 – 0.01 0.16 – 5.19	0.02 +/ 0.71 1.88 +/- 0.71	0.02 – 0.02 +/- 0.71 0.16 – 5.19 +/- 0.71
Roman cremation cemetery/ Milefortlet 15 (zone 4)	Landward (92 %) Seaward (8 %)	0.69 0.34	0.15 – 7.88 0.03 – 0.69	1.16 +/- 0.71 0.57	0.26 – 13.19 +/- 0.71 0.06 – 1.51 +/- 0.71
Roman Tower 15a (zone 5)	Landward (62 %) Seaward (36 %) No change (2 %)	0.84 0.77	0.21 – 2.41 0.03 – 1.50	1.40 +/- 0.71 1.30 +/- 0.71	0.34 – 4.03 +/- 0.71 0.06 – 2.52 +/- 0.71

Table 6.22: Coastline change statistics for each of the coastal zones calculated using coastlines from epochs Sep 2018 to Apr 2019.

The 2.5D change detection results detected change in coastal zone 4 - Roman cremation cemetery from within the sand dune cliff face segregation polygon (Table 6.24). This surface change, representing a surface lowering, was confined to the southern end of the rock armour wall indicating that flanking erosion was still ongoing between April 2019 and September 2019. This would have had a direct impact on the Roman cremation cemetery.

Also present on the DoD$_{\text{Apr 2019 minus Sep 2018}}$ was an area of surface lowering immediately in front of the southern portion of the rock armour wall within the beach segregation polygon. This was evidence of scour erosion at the base of the rock armour wall and was the first time this phenomenon presented itself in the 2.5D change detection results (Figure 6.31 and 6.32). Scour erosion at the base of a seawall is caused by increase wave reflection where

water meets the wall, is driven downwards and picks up sediment before returning out to sea. This type of erosion, as well as end scour, can overtime cause the seawall to become unstable and ineffective. A future failure of the seawall would result in a direct loss of the Roman cremation cemetery.

Coastal zone	Direction of movement	Mean net movement (m)	Range net movement (m)	Mean EPR (m/year)	Range EPR (m/year)
Extramural settlement North (zone 1)	N/A	N/A	N/A	N/A	N/A
Beckfoot Roman Fort (zone 2)	N/A	N/A	N/A	N/A	N/A
Extramural settlement South (zone 3)	Landward (58 %)	0.75	0.15 – 2.13	4.61 +/- 4.73	0.93 – 13.19 +/- 4.73
	Seaward (42 %)	2.53	1.92 – 3.43	15.65 +/- 4.73	11.9 – 21.22 +/- 4.73
Roman cremation cemetery/ Milefortlet 15 (zone 4)	Landward (2 %)	0.46	0.41 – 0.5	2.81 +/- 4.73	2.54 – 3.08 +/- 4.73
	Seaward (98 %)	1.44	0.06 – 8.83	8.89 +/- 4.73	0.39 – 54.64 +/- 4.73
Roman Tower 15a (zone 5)	Landward (51 %)	0.70	0.05 – 1.41	4.35 +/- 4.73	0.32 – 8.71 +/- 4.73
	Seaward (49 %)				

Table 6.23: Coastline change statistics for each of the coastal zones calculated using coastlines from epochs Apr 2019 to Jun 2019.

These 3D change detection results (Figure 6.33) also showed evidence for sediment movement on the beach indicative of the tidal and wave action. As per the 2.5D change detection results, the area of the beach in front of the rock armour wall demonstrated erosion. This continued around the southern extent of the rock armour wall up to the dune toe suggesting that the water level had progressed this far inland and removed sediment as it returned to the sea. The sand dune cliff face demonstrated deposition of the upper layers and erosion of the lower layers. While the remains of the Roman cremation cemetery are buried within the upper levels, if erosion of the lower level were to continue this would lead to collapse of the upper levels.

Coastal zone	Measurement type	Surface raising (i.e. seaward movement)		Surface lowering (i.e. landward movement)	
		Raw	Thresholded	Raw	Thresholded
Extramural settlement north	Area (m^2)	N/A	N/A	N/A	N/A
	Volume (m^3)	N/A	N/A	N/A	N/A
	Average height/depth (m)	N/A	N/A	N/A	N/A
Beckfoot Roman Fort	Area (m^2)	N/A	N/A	N/A	N/A
	Volume (m^3)	N/A	N/A	N/A	N/A
	Average height/depth	N/A	N/A	N/A	N/A
Extramural settlement south	Area (m^2)	538	0	741	0
	Volume (m^3)	46	0 +/- 0	80	0 +/- 0
	Average height/depth	0.09	0 +/- 0	0.11	0 +/- 0
Roman cremation cemetery/ Milefortlet 15	Area (m^2)	6532	0	4811	7
	Volume (m^3)	662	0 +/- 0	429	6 +/- 2
	Average height/depth	0.10	0 +/- 0	0.09	0.85 +/- 0.35
Roman Tower 15a	Area (m^2)	936	0	373	0
	Volume (m^3)	107	0 +/- 0	27	0 +/- 0
	Average height/depth	0.11	0 +/- 0	0.07	0 +/- 0

Table 6.24: Area, volume and height/depth of erosion and deposition from the sand dune cliff face quantified from the DoD$_{Apr\ 2019\ minus\ Sep\ 2018}$.
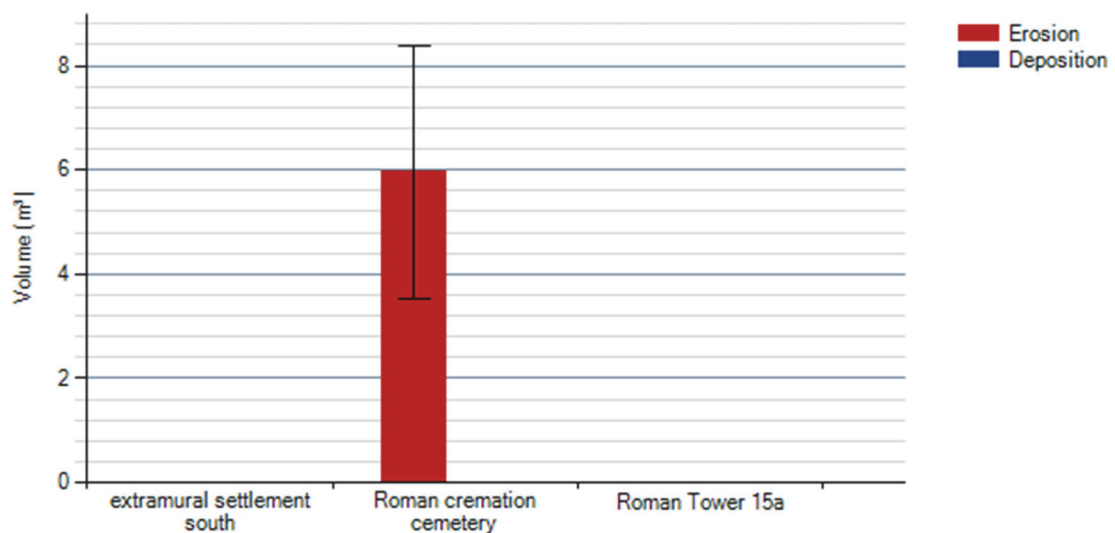
Figure 6.30: Erosion/deposition within each coastal zone within the sand dune cliff face quantified from the DoD $_{Apr\ 2019\ minus\ Sep\ 2018}$.
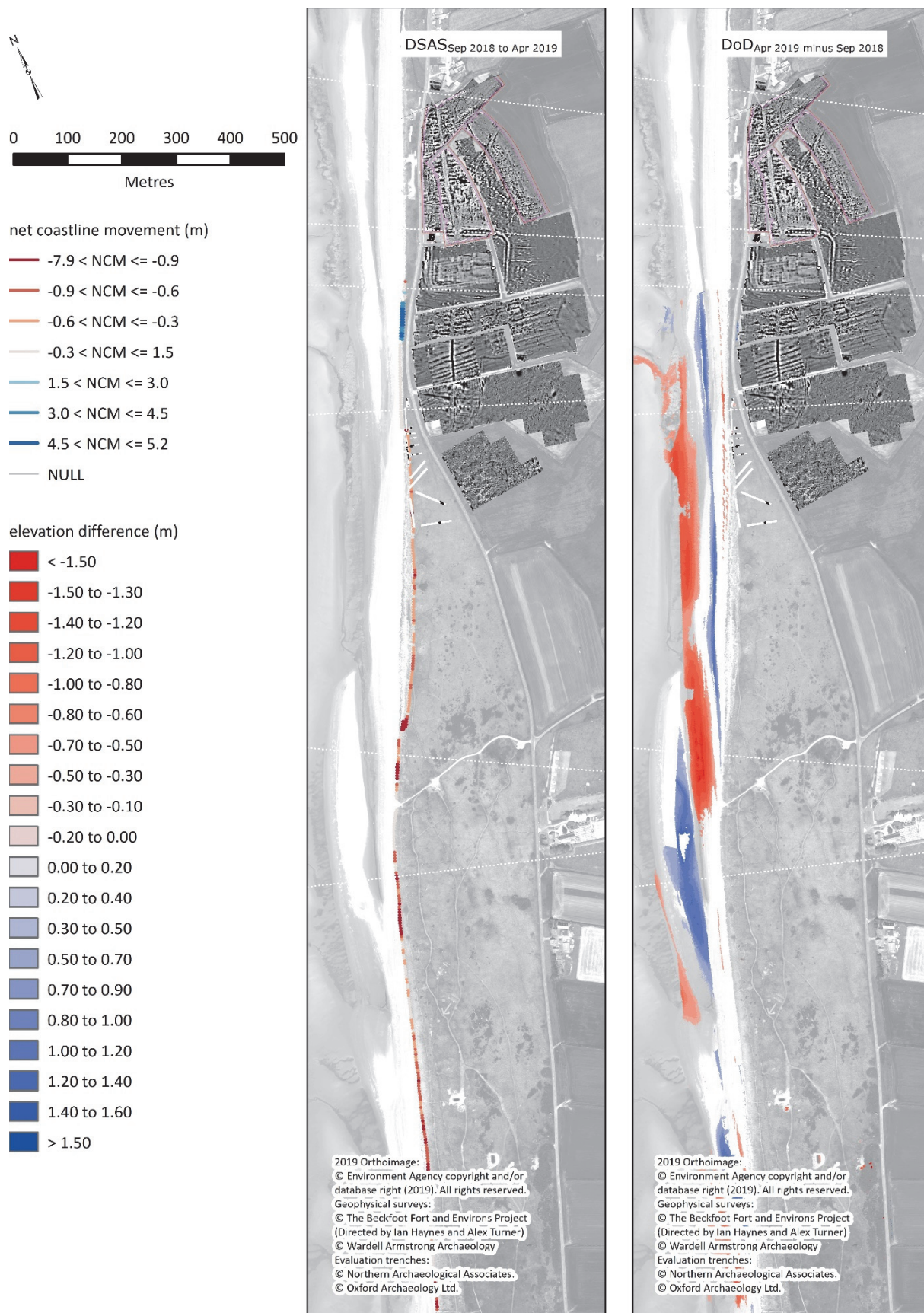
Figure 6.31: (left) DSAS$_{Sep\ 2018\ to\ Apr\ 2019}$ transects displayed by net coastline movement; and (right) DoD$_{Apr\ 2019\ minus\ Sep\ 2018}$ results showing elevation difference.
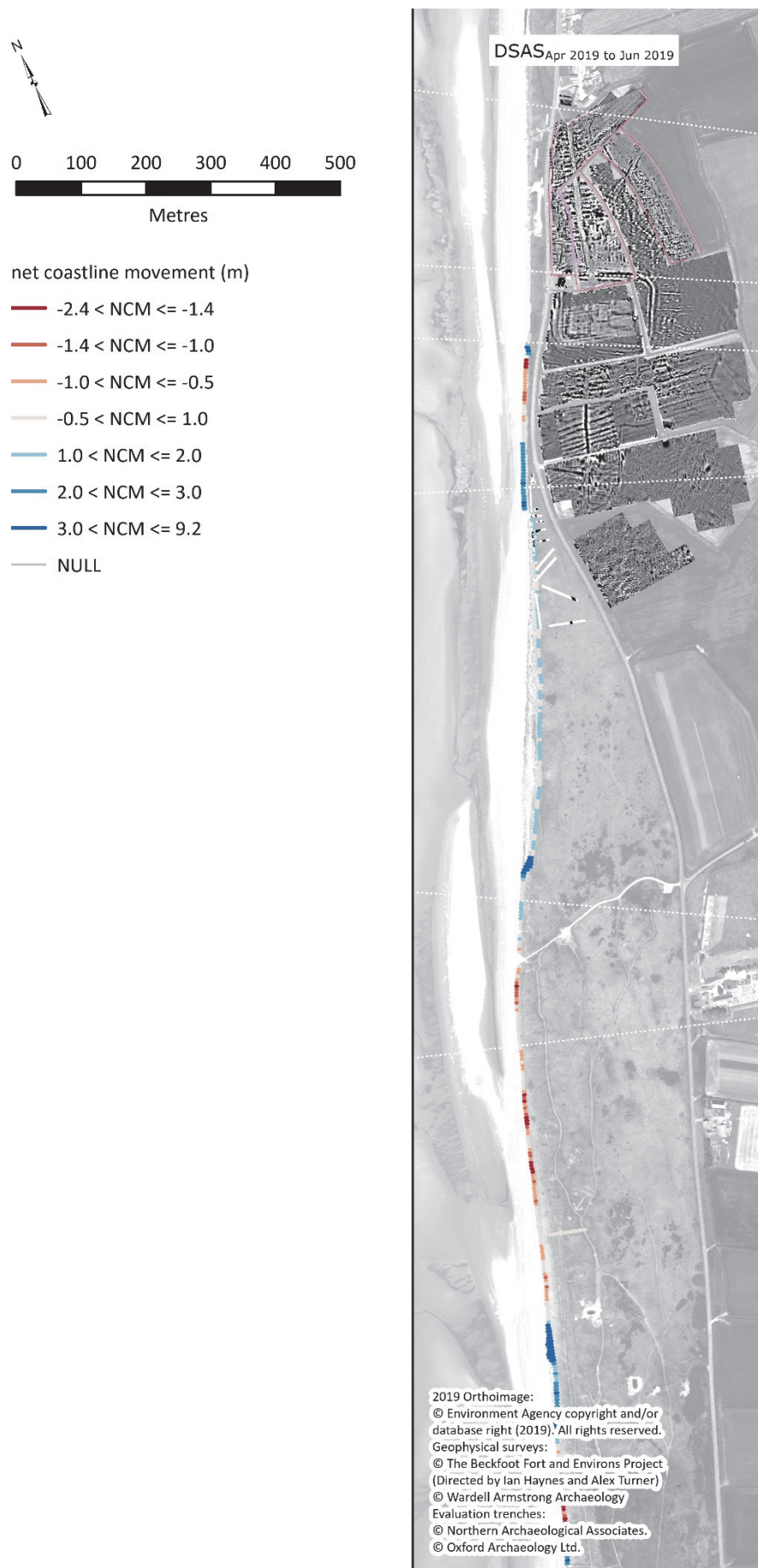
Figure 6.32: DSAS_{Apr 2019 to Jun 2019} transects displayed by net coastline movement.

Figure 6.32: DSAS$_{\text{Apr 2019 to Jun 2019}}$ transects displayed by net coastline movement.
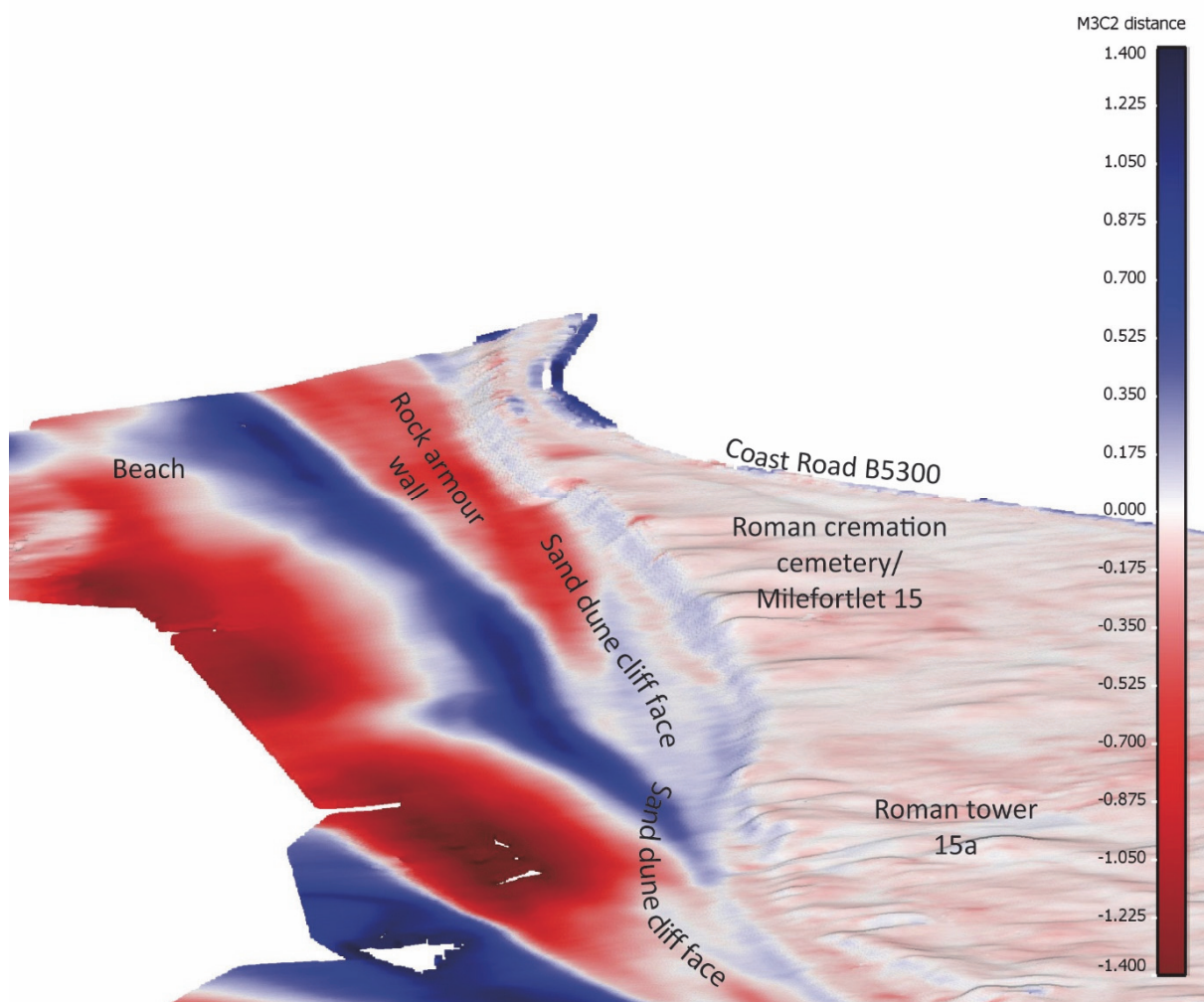
Figure 6.33: M3C2$_{\text{Sep 2018 to Apr 2019}}$ results, highlighting potential areas of erosion and deposition.

6.3 Future impact

Future impact was also assessed in order to provide proof of concept of the value of predictive modelling to natural hazard impact assessment of World Heritage properties. Two methods were employed. The first used linear regression to forecast future change 10 and 20 years into the future (section 6.3.1). The second was a complex numerical model which included a coastal dune avalanching algorithm and predicted surface change on the time scale of storm events (section 6.3.2)

6.3.1 DSAS beta forecasting tool

Three models were produced using the DSAS beta forecasting tool. The first provided a form of validation for the following two forecasts. This initial forecast was calculated using the coastline from epochs 1 – 7, which dated to 2009 and earlier. The output of this analysis was a forecasted 2019 coastline position and uncertainty buffer zone. The position of the

forecasted 2019 coastline position and buffer zone was then compared to the known 2019 coastline position derived from the 2019 orthomosaic.

Results of the validation show that the beta forecasting tool both under and over predicted the coastline 2019 positon. The values of over/under prediction are reported in Table 6.25. However, the uncertainty associated with the forecasted location most often encompassed the known 2019 coastline position as seen on Figure 6.35, particularly in the area of coastal zone of the Roman cremation settlement/Milefortlet 15. Forecasting of the 2029 and 2039 coastline positions was also completed with this awareness of over/under prediction in mind.

Coastal zone	Over/under prediction of landward movement	Mean net movement (m)	Range net movement (m)
Extramural settlement North	Over (33 %)	3.07	0.49 – 7.47
(zone 1)	Under (67 %)	6.66	0.14 – 15.21
Beckfoot Roman Fort (zone 2)	Under (100 %)	16.45	13.46 – 18.83
Extramural settlement South	Over (50 %)	11.21	9.15 – 12.68
(zone 3)	Under (50 %)	6.35	0.58 – 12.96
Roman cremation cemetery/ Milefortlet 15 (zone 4)	Over (100 %)	8.35	1.57 – 20.92
Roman Tower 15a (zone 5)	Over (98 %)	15.38	8.05 – 26.08
	Under (2 %)	11.94	11.94 – 11.94

Table 6.25: DSAS beta forecasting - quantity of over/under prediction.

The forecasted 2029 coastline position moved landward in all coastal zones (Table 6.26). The amount of transects demonstrated a landward movement was 100 percent for coastal zones 3, 4 and 5 - Beckfoot Roman fort, extramural settlement south and Roman cremation cemetery/Milefortlet 15. In the case of extramural settlement north (coastal zone 1) and

Roman Tower 15a (coastal zone 5) this was reduced to 51 percent and 27 percent
respectively. The greatest amount of landward movement was from coastal zone 4 - Roman
cremation cemetery/Milefortlet 15, which ranged between 1.40 m – 11.05 m. These figures
do not include the buffer distance as it varied at each transect, however, the forecasted
2029 coastline position along with its buffer zone can be seen on Figure 6.35.

Coastal zone	Direction of movement	Mean net movement (m)	Range net movement (m)
Extramural settlement North (zone 1)	Landward (51 %) Seaward (49 %)	1.91 3.60	0.32 – 4.28 1.09 – 5.99
Beckfoot Roman Fort (zone 2)	Landward (100 %)	3.51	1.40 – 5.64
Extramural settlement South (zone 3)	Landward (100 %)	4.58	0.83 – 7.92
Roman cremation cemetery/ Milefortlet 15 (zone 4)	Landward (100 %)	8.01	1.40 – 11.05
Roman Tower 15a (zone 5)	Landward (27 %) Seaward (73 %)	1.50 3.57	0.07 – 3.49 0.04 – 5.82

Table 6.26: DSAS beta forecasting - 10 year prediction.

The forecasted 2039 position also moved landward in all coastal zones (Table 6.27). Again
this was mostly concentrated to the three central coastal zones (coastal zones 2, 3 and 4 -
Beckfoot Roman fort, extramural settlement south and Roman cremation
cemetery/Milefortlet15). The forecasted landward movement extended into coastal zone 1 -
extramural settlement north by 49 percent and into coastal zone 5 - Roman Tower 15a by 12
percent. The greatest amount of landward movement was also forecasted to be within
coastal zone 4 - Roman cremation cemetery/Milefortlet 15 (Figure 6.36). This landward
movement ranged between 0.50 m and 18.62 m.

Figure 6.35 depicts the 2029 and 2039 forecasted positions along with associated
uncertainty buffer zone. In addition, the Oxford Archaeology North trenches have been
included to provide a visual of the potential for loss of the archaeological record. The

evaluation only recovered a small sample of data from across the dunes. The dunes likely hold a wealth of information, particularly in the area of proposed medium and dense cemetery activity, which if preserved in situ, would result in a significant loss of the cemetery remains if the forecasted scenario were to occur.

Coastal zone	Direction of movement	Mean net movement (m)	Range net movement (m)
Extramural settlement North (zone 1)	Landward (49 %)	4.26	1.74 – 7.55
	Seaward (51 %)	5.14	0.87 – 8.90
Beckfoot Roman Fort (zone 2)	Landward (100 %)	8.07	5.37 – 10.53
Extramural settlement South (zone 3)	Landward (100 %)	6.43	0.71 – 12.20
Roman cremation cemetery/ Milefortlet 15 (zone 4)	Landward (98 %)	13.51	0.50 – 18.62
	Seaward (2 %)	0.09	0.06 – 0.12
Roman Tower 15a (zone 5)	Landward (12 %)	2.19	0.35 – 5.50
	Seaward (88 %)	6.30	0.33 – 10.31

Table 6.27: DSAS beta forecasting tool - 20 year prediction.

In the worst case scenario, if the coastline reaches the landward edge of the 20 year forecast, coastal zones 2 and 3 - Beckfoot Roman Fort and the extramural settlement south, would be in a similar situation to Roman cremation cemetery/Milefortlet 15. The coastline would be located on the seaward limit of the known archaeological remains buried within the fields of the coastal hinterland. Coastal erosion would no longer be a threat. Instead coastal erosion would present itself as a hazard causing loss and destruction to the archaeological record or the Roman fort and extramural settlement.

While this model provided a straight forward method for quickly forecasting future coastline positions, it relied solely on the input of past coastline positions. In addition it treated coastal change as a linear process. In reality, this is not the case. Various hydrodynamic
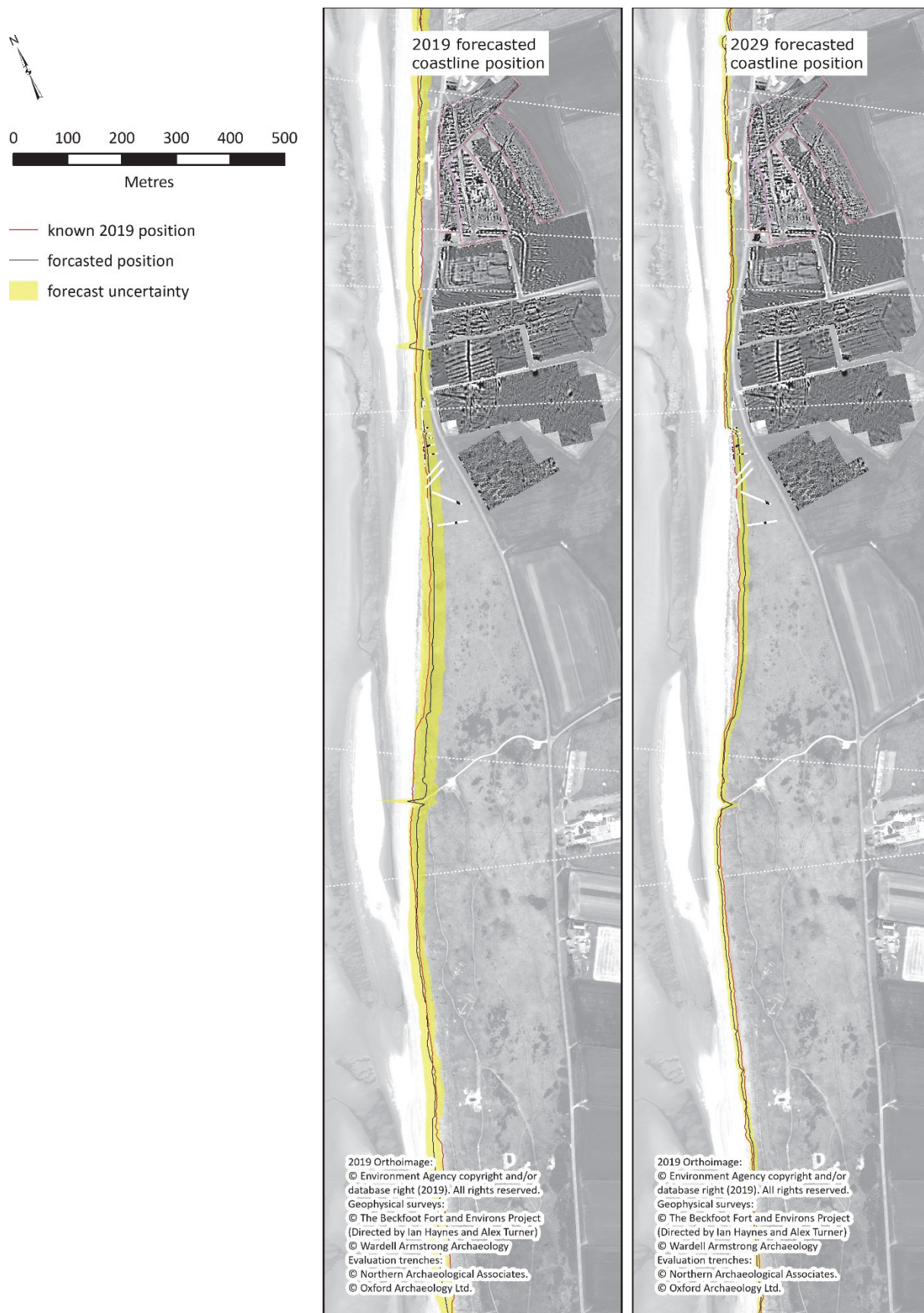
Figure 6.34: (left) forecasted 2019 coastline position to assess accuracy of method; and (right) 2029 forecasted coastline position.

Figure 6.35: 2039 forecasted coastline position.

processes such as waves, tides and currents all influence coastline morphology. Weather

also plays a role as demonstrated by the 2D and 3D 2013 to 2014 change detection results,

in which the winter storms of 2013/2014 likely were the cause of erosion north and south of the rock armour wall. In addition, human actions can shape the coastline, through coastal management strategies, such as the construction of a hard coastal defence to protect the hinterland. Due to the complexities of the coastal system, there is also a need for more complex modelling. In regards to the Beckfoot study area XBeach was identified as an appropriate model as it is capable of modelling coastal dune erosion.

6.3.2 XBeach

As discussed in Chapter 4, section 4.4.2 two simulations were produced using the XBeach numerical model. The first simulated coastal hydro- and morpho-dynamics of the Beckfoot study area under the current mitigation strategy which includes a hard coastal structure to protect the Coast road B5300 from erosion. In the second simulation the rock armour wall was removed in order to see how the coastline would have potentially responded if not protected.

Results from the first model (Figure 6.36) demonstrated coastal dune erosion in all coastal zones. However, no erosion of the dunes occurred in the area of the rock armour wall. The material that eroded from the dunes was deposited on the beach frontage similar to that seen in the 2.5D change detection results (DoD$_{2017\ minus\ 2013}$). Results from the second model (Figure 6.36) demonstrated coastal dune erosion along the entire length of the coastline from within the Beckfoot study area. Erosion was most intense in coastal zones (listed in order of intensity) 4, 3 and 2 - Roman cremation cemetery/Milefortlet 15, extramural settlement south and Beckfoot Roman fort. The eroded sediment from the coastal dunes was also been deposited on the beach frontage.

These models appear to have over predicted the amount of erosion. Further refinement of input parameters in addition to coupling with a more appropriate wave model, such as the SWAN (Simulating Waves Nearshore) wave model is likely required to produce results that closely match what was revealed in the change detection analyses. Once ideal parameters have been defined, the model can then be run using the most recent topobathy (a seamless surface model produced by combining topographic and bathymetric data) of the study area in order to predict future coastal morphological change. In addition, modelling a variety of scenarios including climate change projections such as sea level rise can give a better understanding of a range of future outcomes to assess future impact from natural hazards.
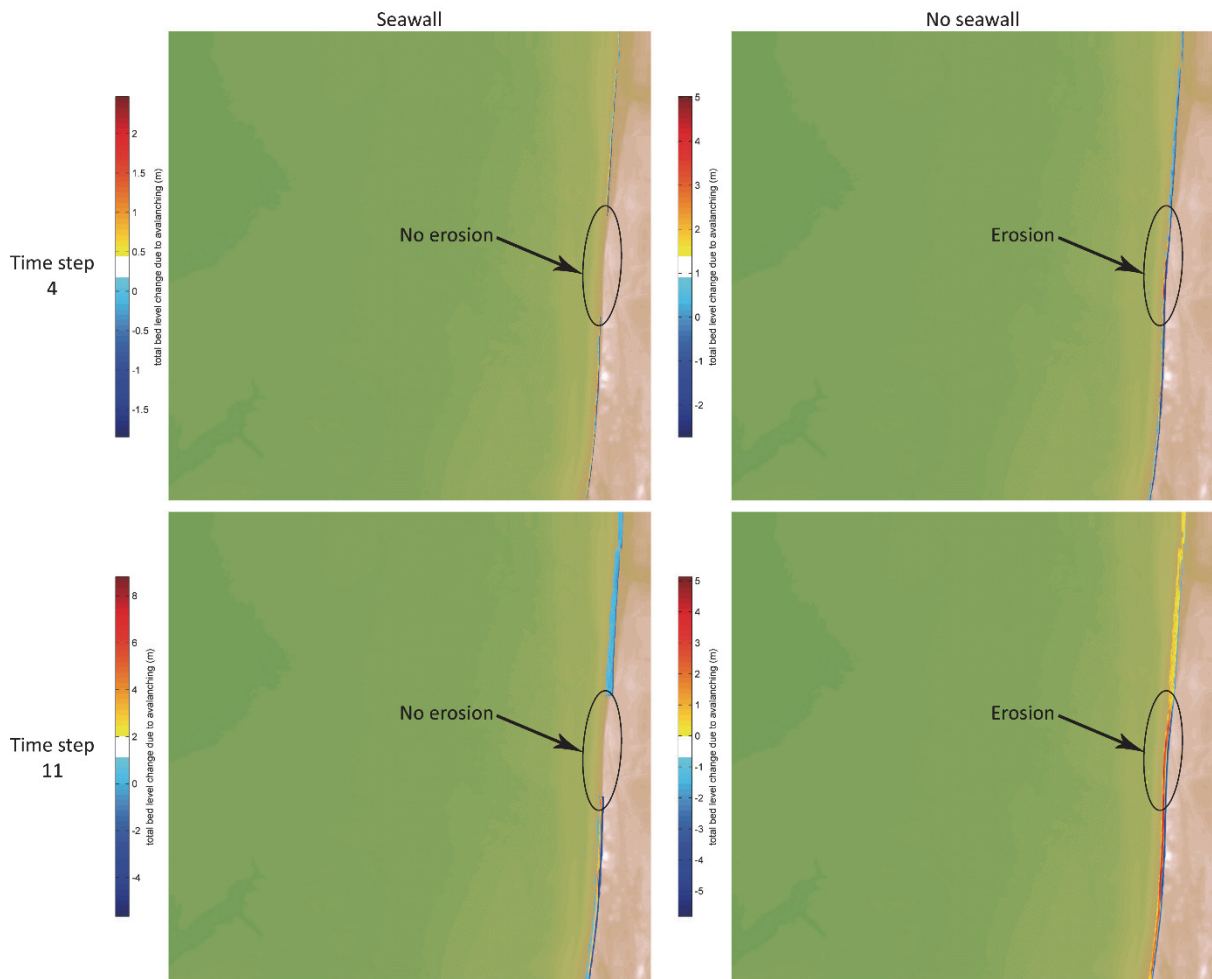
Figure 6.36: XBeach results showing erosion and deposition due to coastal dune avalanching (top left) time step 4, no seawall, (top right) time step 4 with seawall, (bottom left) time step 11, no seawall; and (bottom right) time step 11 with seawall. All results were displayed overlying 2013 DEM.

6.4 Key findings

The following presents the key findings from the past and future impact analysis:

- Erosion was first detected between 1866 and 1899 in coastal zones 1 and 2 - extramural settlement north and Beckfoot Roman fort.

- For the coastal zones 3, 4 and 5 - extramural settlement south, Roman cremation cemetery/Milefortlet 15 and Roman tower 15a erosion was first detected between 1899 and 1923. This date was further refined with evidence from the historical sources, which suggested that erosion began as early as 1908. This erosion was likely in coastal zone 4 - Roman cremation cemetery/Milefortlet 15 as a Roman cinerary urn was recovered. Whether or not erosion occurred between 1899 and 1908 is unknown.

- Erosion in the coastal zone 4 - Roman cremation cemetery/Milefortlet 15, according to the past change detection results and evidence from the archaeological record, appears to have been ongoing since 1908. While the result from the change detection analyses show one period of recovery (1948 to 1957), the archaeological evidence contradicted these findings suggesting coastal dune erosion was occurring during the intervening years with finds discovered in 1948, 1949, 1952, 1954, 1956 and 1957.

- Most of the erosion, as suspected, occurred along coastal zone 4 - Roman cremation cemetery/Mileforlet 15. The total volume of sediment that eroded from the dunes between 1991 and 2019 from within this coastal zone was 30763 m^3 +/- 7139 m^3. This would have had a direct impact to the Roman cremation cemetery, as demonstrated by the finds discovered either on the beach or eroding from the dune cliff face. Stray finds found due to coastal erosion resulted in the loss of provenience and important contextual information due to being unstratified and through the destruction of stratigraphic integrity.

- The greatest net landward movement between 1866 and 2019, according to the results, was 54.45 m which was recorded in coastal zone 4 - Roman cremation cemetery/Milefortlet 15. On average the landward movement within this coastal zone was 39.41 m and occurred at an average rate of 0.26 m/year +/- 0.02 m.

- While the coastline from within the Beckfoot study area has gone through periods of both coastal retreat and advancement, the trend based on an analyses of past coastline positions dating back to 1866 was a landward movement.

- Some of the erosion that occurred was likely the result of the 2013/2014 storm event. The impact of erosion may have been exacerbated by the rock armour wall, although further modelling is needed to confirm this point.

- Future prediction show that the coastline is going to continue to retreat over the next 20 years.

- The future prediction modelling demonstrates the potential of this approach, however, this methodology requires further research to refine the model inputs to produce a more detailed and accurate output.

6.5 Conclusion

This chapter applied the methodology for natural hazard impact assessment outlined in Chapter 4 to an at-risk archaeological site from the Hadrian's Wall WH site. The site that was selected was that of Beckfoot Roman fort and its' environs which encompassed the fort, the extramural settlement, the Roman cremation cemetery/Milefortlet 15 and Roman Tower 15a. This site was chosen due to ongoing coastal processes threatening the buried archaeological remains associated with the Roman fort at Beckfoot. The Natural Hazard Impact Assessment allowed for an in-depth analysis of the impacts from natural hazards to the archaeological record which quantified loss of the sand dune system. Details of past coastal change was tracked over 153 year period for the Beckfoot study area. It is believed that Milefortlet 15 has already succumbed to coastal erosion as no definitive evidence for its remains in the conjectured location has been found. While all areas are at risk of loss from the threat of coastal erosion, the Roman cremation cemetery has, for the most part, been subjected to what appears to have been continued erosion since as early as 1908 according to the documentary evidence and 1899 to 1923 according to the change detection analysis. Therefore coastal erosion is considered a hazard, resulting not only in the loss of the protective dune system, but also in a loss of the archaeological record. Modelling was also undertaken in order to forecast future coastal change.

The following chapter, Discussion and conclusion, critically explores the findings of the research presented for the Beckfoot case study. This chapter also explores the wider contribution that this research has measuring the impact of natural hazards on World Heritage sites. This will be accomplished by revisiting the aims and objectives, as presented in Chapter 1, and details how each was fulfilled throughout this research.

Chapter 7: Discussion and conclusion

7.1 Introduction

This chapter provides a critical discussion of the research presented in this thesis. The chapter begins by revisiting the aims and objectives to demonstrate how each has been achieved through the completion of this thesis. Next the key findings from the natural hazard impact assessment for the Beckfoot study area are presented. This is followed by the limitations encountered in undertaking the impact assessment. The chapter concludes by providing suggestions for future avenues of research.

7.2 Revisiting aims and objectives

7.2.1 Aims

The aim of this research was to develop a geospatial framework for quantitative impact assessment of natural hazards on cultural WH properties. The framework comprised of methods for assessing past geomorphic change as well as predicting future geomorphic change. Where possible it incorporated evidence from the archaeological record into the impact assessment. This approach was demonstrated on a world-renowned archaeological site using a spatiotemporal time series combined with multi-modal geospatial methods, with each epoch in the time series representing the topographic conditions at specific points in time. The approach was applied successfully to the Beckfoot study area from Hadrain's Wall WH site, due to threats from historic and ongoing coastal erosion. The spatiotemporal time series for the study area was composed of data derived from Ordnance Survey (OS) historic maps, archived and modern aerial imagery, and airborne and remotely piloted aircraft systems (RPAS) lidar. The techniques included 2D, 2.5D and 3D geomorphic change detection methods to detect past surface changes that could be attributed to natural hazards impacting a cultural heritage landscape. Through the combination of these methods, distances, areal, volumetric and rates of past coastal change were calculated. Future geomorphic change was demonstrated through the application of two predictive models created specifically for modelling coastal change. Their applications demonstrated the potential to enhance natural hazard impact assessments by providing scenarios of future change that may cause loss and destruction to WH properties.

7.2.2 Objectives

The aim of this thesis was accomplished through addressing five objectives. Below, each of the objectives is discussed in turn, showing how they have been met.

7.2.2.1 Objective 1

Critically evaluate impact assessment practices regarding natural hazards on WH properties and provide a comprehensive review of threats to at risk heritage from Hadrian's Wall WH site.

The first part of Objective 1, to *critically evaluate impact assessment practices regarding natural hazards on WH properties*, was addressed in Chapter 2, section 2.2. Firstly, the importance of WH was established to demonstrate the necessity of a natural hazard impact assessment. This was accomplished through a synopsis of the history of the creation of the WH Convention, the definition of key terms (i.e. authenticity, integrity, hazard, and natural hazard), discussing threats to WH and outlining the responsibilities of the State Parties. The Convention is a testament to the global importance of cultural and natural sites given WH status, as agreed by the WH Committee and the State Parties who have each ratified the Convention. Through ratification, the State Parties agree to uphold the integrity and authenticity of the WH properties - the values in which a sites Outstanding Universal Value (OUV) is determined. The two values of OUV need to be maintained or else the property's prestigious status may be put in danger of being revoked due to the degradation of OUV. Three former WH sites have been delisted due to impacts driven by human actions, resulting in negative consequences to integrity and authenticity. To date, there has been no precedence of a WH property losing its status because of natural processes, however, these processes, which manifest as natural hazards, can cause loss and destruction and therefore are considered a threat to a properties OUV. Negative impacts, whether the results of human actions or natural hazards, are further exacerbated by the climate crises. The methods in which a WH property is protected and managed is ultimately the responsibility of the State Party in which the property resides.

Secondly, a review of guidance for impact assessment methods were also presented, which highlighted their inadequacies for assessing impact resulting from natural hazards. UNESCO has published a number of guidance documents regarding the protection and management of WH properties in order to uphold OUV. The two main guidance documents are the Heritage Impact Assessment (HIA) (ICOMOS 2011) and *Managing Disaster Risks for World*

Heritage (UNESCO 2010). The HIA is triggered by proposals for development and is therefore applicable to human-driven change that may pose a threat to a WH property. The latter, is guidance on disaster risk reduction associated with catastrophic events such as an earthquake and as such gradual, cumulative processing may be overlooked. Neither of these documents were therefore sufficient for assessing impacts from natural hazards, particularly in the face of the changing climate regime. Recently, UNESCO published the Draft Policy Document on the Climate Action for World Heritage, in which it was stressed the need for rigorous impact assessments on potential threats from climate change to OUV (UNESCO and WHC, 2021, p. 5). This policy document, however, provided no detailed approaches for undertaking rigorous impact assessment of natural hazards. The recently developed Climate Vulnerability Index (CVI)(Day *et al.*, 2019), is gradually being employed as a rapid impact assessment tool for cultural and natural WH sites from around the world. The CVI provides a method for assessing the impact from climate change to OUV, as well as to community value of a WH property based on a risk matrix. As the CVI is a rapid assessment tool, it only provides a broad conceptual understanding of impact based on expert observation in consultation with the community. A need for a detailed natural hazard impact assessment method was therefore evident.

The second part of objective 1, to *provide a comprehensive review of threats to at risk heritage from Hadrian's Wall WH site*, was addressed in Chapter 2, section 2.3. This section provided an introduction to Frontiers of the Roman Empire: Hadrian's Wall WH site (FRE), to provide context of its uniqueness in terms of heritage management. The management of Hadrian's Wall WH site is unique due to its shear expanse, crossing multiple environmental, geological, topographical, designated and administrative boundaries, each of which contribute to site survival through potentially conflicting agendas. It is composed of 190 Scheduled Monuments (SM), which consists of buried archaeological remains, earthwork monuments and built heritage with varying exposures and vulnerabilities to hazards. In addition, there are many key stakeholders and approximately 1000 landowners with vested interests in the Hadrian's Wall WH site. Finally, the WH is protected by the Ancient Monuments and Archaeological Areas Act of 1979 as well as several other legislations. All these aspects pose management issues on top of those introduced by the climate crisis.

Next, this section assessed the literature for at risk sites from Hadrian's Wall WH site, as a means of collating past and present threats to this WH site. Hadrian's Wall WH site has been

subjected to periods of destruction from deliberate human actions, such as pillaging of the stone material for construction elsewhere, in addition to areas where the site suffered total destruction from roadworks, pipelines and quarrying. While the Hadrian's Wall WH site is now protected through legislation, ongoing arable ploughing poses a major threat at numerous locations, as this was the most often cited reason for inclusion on Historic England's Heritage at Risk Register (Historic England, 2021). Natural hazards have also caused, and are continuing to cause, damage at a number of locations across Hadrian's Wall WH site through the destruction of bridges from river migration to coastal erosion, cliff instability and changes to the water table. Legislation, however, does not account for threats from natural hazards.

Finally, this chapter concluded with a review of geospatial methods employed at sites from Hadrian's Wall WH site. Those focusing on land surface dynamics was limited to three projects; CHT2 (Peppa *et al.*, 2018), Magna Roman fort (Guiney *et al.*, 2021) and the vulnerability index for coastal heritage assets (LUC, 2019). The first attempted to quantify landscape change based on DEMs derived from archived and digital aerial image using a SfM-MVS workflow (Peppa *et al.*, 2018). The second used the Revised Universal Soil Loss Equation (RUSLE) to predict soil erosion (Guiney *et al.*, 2021) and the third resulted in a vulnerability index of coastal sites around England, for which Hadrian's Wall provided a case study (LUC, 2019).

7.3.2.2 Objective 2

Review current spatiotemporal data and methods for quantifying impact from natural hazards.

Addressing Objective 2 was central to Chapter 3, in which spatiotemporal data and methods for quantify change to the Earth's surface were critically reviewed.

The chapter began by reviewing methods of identifying change in the Earth's Surface, by first providing a definition for change detection (section 3.2.1). The chapter highlighted the necessity of co-registration (section 3.2.2), particularly, the implementation of fine registration prior to undertaking 2.5D and 3D change detection. Fine registration, such as iterative closest point (ICP), is an essential step as it reduces the space between point cloud epochs due to registration error, thereby minimising surface change attributed to misaligned epochs.

The chapter also evaluated several change detection methods (section 3.2.3) which provided a means of assessing past deformation to the Earth's surface. The chapter included a brief discussion about 2D image based methods for satellite imagery and more in-depth review of 2D (historical trend analysis), 2.5D (DEM differencing) and 3D (change detection in 3D space) vector and raster based methods. While each change detection method has strengths and weaknesses, the chapter argues in favour of a multi-modal approach. By undertaking a 2D historic trend analysis of the planar position of a boundary feature, evidence from historic maps were included in the spatiotemporal time series. In addition archived aerial photographs that were deemed insufficient for accurate 3D reconstruction of the topography, but had acceptable horizontal accuracy for the 2D orthomosaic, could also be included in such an analysis. The addition of elevation data made it possible to calculate areal and volumetric quantification of sediment erosion/deposition through 2.5D change detection. In contrast to 2.5D change detection which measured change vertically, 3D change detection calculated change along the surface normals of each of the points within the reference point cloud to the corresponding point in the compared cloud. In addition, interpolation to a raster DEM was not required as calculations were completed using the point clouds in the 3D change detection analysis. Change detection in 3D space allowed for more nuanced evidence for change to be identified which otherwise would have gone undetected.

The chapter then discussed the three main data types composing the spatiotemporal time series (section 3.2.4). These were historic maps, archived aerial imagery and airborne lidar. These data types were addressed as each represented a useful source of topographic information, which could specifically provide evidence of geomorphic change associated with natural hazards, particularly when compared to one another.

Chapter 3 also demonstrated the benefits of constructing a spatiotemporal time series by combining heterogeneous geospatial data. The primary benefit in doing so was the extension of the temporal range, which allowed for a longer timespan to potentially establish trends. Extension of the time series was achieved through the incorporation of historic maps, as they are the oldest depiction of topography. Analysis of mapping techniques in Chapter 3 led to the recommendation that the earliest maps used in a spatiotemporal time series were those that were mapped using accurate mapping techniques. In the UK such accurate mapping can be traced back to the origins of OS. While

the first published OS map was the one-inch Map of Kent dating to 1801, greater accuracy was achieved with the introduction of the 6 inch and 25 inch maps, beginning in 1846 and 1854 respectively.

Additionally, Chapter 3 demonstrated the value of including archived aerial photographs in a spatiotemporal time series. The strength of archived aerial photographs, particularly those captured by the Royal Air Force and the Ordnance Survey, lies in data collection methodology for the purpose of mapping, which captured images as near verticals imagery in overlapping pairs. The fact that these photographs were taken in stereo pairs has made them potentially suitable for 3D topographic reconstruction using a SfM-MVS workflow, which requires overlapping photographs from multiple viewpoints to reconstruct geometry. This chapter also demonstrated the fact that archived aerial photographs require special considerations when using this type of workflow as SfM-MVS algorithms were not originally developed for working with analogue imagery. Considerations include analogue to digital conversion, cropping to film size, determining the presence/absence of a camera calibration certificate and fiducial marks, the addition of ground control points to provide geospatial alignment and scale, and the assessment of horizontal and vertical accuracy of the output products. These considerations are particularly important for the determination of inclusion in subsequent change detection analysis. For example, the 1948 SfM-MVS horizontal accuracy was sufficient for inclusion in the 2D change detection analysis, however, the 3D accuracy resulted in a noisy dense point cloud, and therefore this epoch was not included in the 2.5D and 3D change detection analyses.

Chapter 3 also discussed the incorporation of airborne lidar into a spatiotemporal time series. The nature of this data, a 3D point cloud representing the Earth's surface, makes it an ideal source for change detection purposes. In addition, the advantages of lidar over aerial imagery were discussed. Unlike optical imagery, lidar can return ground points in wooded areas and therefore, bare earth DEM's of wooded areas can be derived from lidar, although at a reduced resolution in comparison to open areas. The chapter also warned, however, that lidar data often comes pre-classified using semi-automatic classification routines, which can lead to misclassification. It is therefore important to assess point cloud for classification error, particularly along breaks of slope and beneath vegetated areas to ensure an accurate re-classification of ground points.

Following on from the discussion on the spationtemporal time series and appropriate data for inclusion in such a time series, Chapter 3 also presented a discussion on modelling, which offers powerful tools for predicting future changes to the Earth's surface. There are a variety of models available to Earth scientists, which can be exploited within the heritage sector. Mathematical models in particular, can help inform decisions regarding mitigation procedures to protect heritage assets from natural hazards. Modelling can allow for the exploration of various land management practices to be modelled under varying climate projections in order to present a range of potential future results. However, as the Chapter points out, predictive modelling, as well as geomorphic change detection, is underutilised in the heritage sector for this purpose.

7.3.2.3 Objective 3

Develop an innovative geospatial framework for assessing impact from natural hazards on WH sites, using a fully integrated spatiotemporal time series.

Objective 3 was addressed in chapter 4 in which the methods for undertaking the proposed innovative geospatial framework for assessing impact from natural hazards on cultural WH sites was presented. The framework used a spatiotemporal time series combined with a multi-modal geospatial approach for assessing past and future geomorphic change.

Chapter 4, first provided a brief introduction to the study area (section 4.2), which was focused on Beckfoot Roman fort and its environs.

Next, in section 4.3.1, the steps for measuring past geomorphic change were described in detail. The geomorphic change detection in the framework included 2D, 2.5D and 3D methods to provide comprehensive measurements geomorphic change. Each method was described in turn. The 2D method used the Digital Shoreline Analysis System (DSAS) ArcMap AddIn, developed by the USGS to measure the difference in the planar position of a time series of vectorised coastlines and to provide rates of change measurements. For the 2.5D geomorphic change detection analysis, DEM differencing was completed using the Geomorphic Change Detection (GCD) ArcMap AddIn developed by Riverscape Consortium. Undertaking GCD on a pairwise basis, resulted in a series of raster images representing elevation change as either surface raising (deposition, accretion or advance) or surface lowering (erosion or retreat). The areas of raising and lowering were then segregated by polygons representing physical characteristics (beach, sand dune cliff face, sand dunes, and

221

coastal hinterland) to calculate areal and volumetric measurements of sediment loss and gain. Finally, in section 4.3.1, the steps for undertaking 3D geomorphic change detection using the Multiscale Model to Model Cloud Comparison (M3C2), a plugin offered in Cloud Compare, were described. This method allowed for distance measurements between two point clouds without the need to interpolate to raster DEM as calculations were performed in 3D space.

The main reasons for employing three kinds of geomorphic change detection were: the 2D geomorphic change detection extended the temporal range into the past through the inclusion of information derived from OS historic maps, and orthomosaics created using a SfM-MVS workflow applied to archived aerial photographs; the 2D method was the only method to provide rates of change statistics; the 2.5D geomorphic change detection enabled areal and volumetric measurements to be calculated; and the 3D change detection method which measured changed in 3D space, detected more nuanced change that could be missed by the vertical calculation offered by the DEM differencing method.

Details of the data used in the various change detection analyses were then provided in section 4.3.2. The spatiotemporal time series for the Beckfoot study area was compiled from both analogue and digital representations of topography and included the main data sources discussed in chapter 3, namely OS historic maps, archived aerial photographs and airborne lidar. This data was supplemented by orthophotographs and RPAS lidar to fill the temporal gaps between epochs derived from the main three sources of topographic data and to bring the temporal range forward to the present.

The chapter demonstrated that prior to completing an analysis of geomorphic change, several pre-processing steps (section 4.3.3) needed to be completed, which, due to the heterogeneity of the data, vary according to data type. The analogue data needed to be converted to digital data. This was done by scanning at a high resolution. In regards to the archived aerial photographs, it has been recommended that scanning be carried out with a photogrammetric scanner to reduce introducing scanner error. In this research, due to a lack of access to equipment, photogrammetric scanning was not possible. Moreover, OS historic maps require alignment to a geospatial referencing system, which was completed through georeferencing to a modern map with an affine transformation. Spatial alignment was also a requirement of the archived aerial photographs. For archived aerial photographs this was completed during the SfM-MVS workflow through the addition of GCPs. For airborne lidar, it

was suggested in that the classification of points should be assessed when working with data from a third party. Misclassified points where found to be along breaks of slope and under tree canopies where physical characteristics of geomorphic features were falsely classified as above ground points, or erroneous features being included in the ground point class.

As argued for in chapter 3, fine registration, described in section 4.3.4, was an essential pre-requisite of point cloud data prior to undertaking 3D geomorphic change detection in order to minimise misalignment error between epochs. This step was completed prior to interpolation from point cloud to DEM for inclusion in 2.5D geomorphic change detection. While there are multiple methods of fine registration, this research used the ICP algorithm, as it has gone through numerous improvements and is the most commonly used algorithm for fine co-registration of point clouds.

Once all epochs in the time series were co-registered, either by means of georeferencing or through the application of the ICP algorithm, further processing steps were required for the 2D and 2.5D change detection analysis. These steps included defining and boundary feature as described in section 4.3.5 for the 2D analysis and interpolation from point cloud to raster DEM as described in section 4.3.6 for the 2.5D analysis.

Chapter 4 also addressed the importance of assessing uncertainty in section 4.3.7. Uncertainty, or error, should be measured for each epoch and incorporated into the change detection analyses, as error within the results could over estimate or underestimate change. Misestimating geomorphic change could lead to an unrealistic assessment of impact.

Finally, chapter 4 discussed the two models used to predict future impact from natural hazards. The models, DSAS beta forecasting tool and XBeach, were selected, as both were developed for the purpose of coastal change studies. The first, the DSAS beta forecasting tool was a relatively straightforward model, which predicted future coastline positions in 10 and 20 years' time based on past rates of coastal change. The second, XBeach, was a complex process based model requiring expert knowledge of hydro- and morpho-dynamic systems. XBeach was developed to predict coastal dune erosion on the time scale of storm events, but has since been further developed to work on a wider range of time scales and on a variety of beach types. The model was calibrated for two coastal management scenarios – current management practice (i.e. rock armour wall), and no active intervention (i.e. no rock armour wall). While further work is required using this model, it was presented in this thesis

to demonstrate the potential of numerical modelling to natural hazard impact studies at cultural WH properties.

7.3.2.4 Objective 4

Provide a conceptual understanding of the impact of natural hazards on the archaeological record of an at risk site from the Hadrian's Wall WH site.

Objective 4 was addressed in Chapter 5, in which a conceptual model of the Beckfoot study area was presented. This chapter demonstrated the importance of drawing together both the archaeological and natural environmental evidence to provide an understanding of how natural processes interact with the archaeological record. This understanding was achieved by creating a fully integrated GIS for the Beckfoot study area. Archaeological evidence was provided in the form of geophysical survey results, archaeological evaluation results, Aerial Investigation and Mapping data, Historic Environment Record data and data from Historic England's National Heritage List for England. In addition, the Portable Antiquities Scheme as well as textual records were consulted with a specific focus on uncovering details of eroding archaeological remains and artefacts. OS historic maps, aerial imagery and the results from CHT2 project were also compiled within the GIS. Environmental data included bedrock and superficial geology, topography, wind, tide and wave data, as well as GIS data on coastal behaviour created as part of the futurecoasts project. The shoreline management plans (SNPs) were also consulted to provide additional details regarding coastal processes of the Solway Firth.

Chapter 5 provided justification (section 5.2) for the choice of the Beckfoot study area as the subject of the proposed natural hazard impact assessment framework. The chapter listed the relevant designations (section 5.3) In addition, Chapter 5 also situated the archaeological remains within its natural environmental and anthropogenic context. This was completed through an analysis of topographic and geographic (section5.4) in which the study areas location, topography and geology were described.

Next, a brief introduction to the FRE was provided followed by details of the key archaeological sites from within the Beckfoot study area, which form part of the Hadrian's Wall WH site (section 5.5). In section 5.6, the evidence for each of the key archaeological sites (i.e. Beckfoot Roman fort and extramural settlement, the Roman cremation cemetery and the conjectured location of Milefortlet 15, and Roman tower 15a) derived from historic

maps, aerial photographs, airborne lidar and archaeological investigations was presented. In doing so, the chapter established the current knowledge of the extent, density and significance of the extensive archaeological remains within the study area.

 A thorough analysis of the eroding archaeology of the Beckfoot study area was also presented in section 5.6.4. Compelling evidence for the erosion of the Roman cremation cemetery was highlighted, which provided further testament to the urgency of the need for a natural hazard impact assessment. Evidence of erosion of the archaeological record was established through an in-depth review of the relevant literature, such as antiquarian accounts, archaeological publications and excavation reports. Of particularly importance was Caruana's publication: *Romans on the Solway: essays in honour of Richard Bellhouse,* in which a schedule of finds from the Roman cremation cemetery was presented providing valuable information regarding the erosion of the coastal dunes. Information from this publication was summarised and updated with information from the PAS in Table 5.2.

Chapter 5 stressed influencing factors impacting upon the Beckfoot study area, making the archaeological remains of the WH site vulnerable to natural hazards by turning the focus to the hydro-dynamics of the Solway Firth (section 5.7). This discussion allowed for the interaction between sea and the cultural heritage landscape to be understood. The reader's attention was drawn to the potential drivers for change of the highly dynamic coastal zone and the potential impacts on the archaeological record.

Finally a conceptual framework was presented drawing together the evidence from the archaeological record, with the hydro- and morpho-dynamics of the Solway Firth. This conceptual model demonstrated the vulnerability of the archaeological record from within the Beckfoo study area by: determining the proximity of the archaeological remains to be within 200 m of the coastline – the area deemed to be at risk from coastal flooding and erosion (CH2M, 2018). Coastal flooding and erosion could result in an impact on the stratigraphic integrity and preservation of archaeological remains, which could lead to total destruction through erosional processes; and highlighting that the remains of the Roman cremation cemetery and conjectured location of Milefortlet 15 which are located within the Mawbray Bank sand dunes Site of Special Scientific Interest (SSSI), are most susceptible to loss and destruction from erosion. The chapter attempted to define the extents of the Roman cremation cemetery remains. However, this cannot truly be determined as it

seaward limits have been truncated through dune erosion since at least as early as the 1900's.

7.3.2.5 Objective 5

Quantify impact from natural hazards for an at risk site from the Hadrian's Wall WH site and interpret results incorporating archaeological evidence.

Results of the natural hazard impact assessment for the Beckfoot study areas were presented in Chapter 6, thereby fulfilling objective 5. Through the application of 2D, 2.5D and 3D geomorphic change detection methods to a long spatiotemporal time series, the chapter provided a diachronic analysis of past landscape change. The chapter detailed the evolving coastline, as defined by the sand dune seaward boundary over a 153 year period between 1866 and 2019. Evidence for the movement of the coastline was further refined by the archaeological record. According to the 2D change detection analysis, erosion in and around the Roman cremation cemetery began as early as 1899 to 1923. However, this date range could potentially be narrowed, albeit with caution. In 1908 the first known archaeological find from the Roman cremation cemetery was discovered in this area and as such this erosion date range could potentially be narrowed to sometime between 1899 and 1908.

The results presented in Chapter 6 also reiterate the importance of including OS historic maps into the impact analysis. The incorporation of the OS historic maps, along with the orthomosaic of aerial imagery dating to 1948, enabled 5 additional pairwise 2D change detections covering a period of 125 years. If these pairwise change detections were excluded, along with the 2D change detection analysis, coastal change of the Beckfoot study area would have been limited to just a 28 year period. However, it should be stated that the inclusion of the 2.5D and 3D change detection analysis, provided additional details regarding areal, volumetric and nuanced change that otherwise would not have been possible. This chapter therefore demonstrated the significance of a multi modal approach that provided a complete and holistic analysis of shoreline change.

Areal and volumetric values were calculated using 2.5D geomorphic change detection on a pairwise basis from 1991 to 2019. The corresponding results of the 3D change detection uncovered additional details that would have otherwise gone undetected in the 2D and 2.5D analyses. For example, terminal erosion located at the southern end of the rock armour wall

was present on the 3D change detection results that compared the 2017 to 2018 lidar point clouds, but was not detected on the $DoD_{2018\ minus\ 2017}$. This discrepancy was due to the distances between point clouds that were measured along the surface normals of the points, rather than a vertical measurement as per the 2.5D geomorphic change detection analysis that utilised the DoD method.

While understanding past change is important for multiple reasons, such as assessing impact, the importance of understanding future change should not be underestimated. Predictive modelling can inform mitigation strategies for safeguarding WH properties. The results from the past geomorphic change detection were used to inform/validate models to study future change, as demonstrated in Chapter 6. Two models were employed for the case study area. The first was a simple model, provided by the DSAS ArcMap AddIn that used the rates of change statistics, linear regression and a kalman filter to forecast future positions of the coastline in 10 and 20 years' time. To assess the accuracy of the model, the DSAS Beta forecasting tool was first run using only the coastline positions up to 2009. This resulted in the predicted position of the 2019 coastline. The predicted 2019 position was then compared to the recorded 2019 position, to ascertain whether the tool was over or under predicting results. The second model utilising the XBeach software, was employed to simulate the hydro- and morpho-dynamics of the dunes over the period of a storm. This demonstrated the use of such a model under different coastal management scenarios.

7.3 Key findings

There were a number of key findings identified as a result of this research. The following details those findings from the application of a natural hazard impact assessment of the Beckfoot study area:

1. Current methods for assessing impact on cultural WH properties, and heritage properties in general, are inadequate for producing quantifiable measurements of change caused by natural hazards. This is because such assessments:
    a. Tend to be triggered by proposals for development rather than the existence of natural phenomenon threatening the survival of our heritage sites.
    b. Are used to create strategies for disaster risk reduction in response to potential sudden onset threats of catastrophic nature rather than gradual slow accumulation of change over time.

c. Include guidance which is purposefully vague so as not to impose methods which may not be achievable due to lack of access to resources or technical expertise.

d. Are used as a rapid assessment tool based on expert judgement in consultation with the local community to produce a conceptual understanding or risk and vulnerability.

2. Historical analogue data can and should be combined with modern digital remote sensing data to assess impact from natural hazards over a longer period of time. Combining the heterogeneous data types can be optimally achieved through a number of pre-processing steps. Firstly, digitisation of the analogue data. This is done through scanning negatives, slides, and paper copies at a high resolution. Where possible scanning of aerial photographs should be carried out on a photogrammetric scanner as recommended by Sevara *et al.* (2017, p. 614 - 615). Secondly, each epoch will need to be aligned to a projected coordinate system either through the use of GCPs or through direct georeferencing means. Thirdly, for archived aerial photographs, a SfM-MVS workflow is used to produce orthomosaics and 3D dense point cloud. In addition, point clouds derived from airborne and RPAS lidar require semantic labelling to extract ground points. Next epochs containing elevation data will need to be co-registered to one another in order to reduce alignment error. This step may be completed using the ICP algorithm. Once co-registration is completed, interpolation to a raster DTM surface. The resulting DTM and error surface can then be used for 2.5D geomorphic change detection analysis. Boundary features will need to be digitised from historic maps, orthophotographs, and lidar for incorpation, along with uncertainty values, in the 2D geomorphic change detection analysis. The dense point cloud produced using the arhived aerial photographs and SfM-MVS along with the lidar ground points the input data for the 3D geomorphic change detection analysis.

3. Geomorphic change detection methods have been developed for the purpose of studying past deformation of the Earth's surface. These include methods created with specific applications in mind such as for coastal monitoring, understanding river dynamics and more generally to track the development of natural surfaces. These methods, as demonstrated in this thesis, can be employed for purposes which they

228

were not originally intended. For example, the DSAS, which was developed to measure the difference in planar position of the coastline, commonly defined by the Mean High Water Mark or the Mean Low Water Mark, was used to track the retreat and advancement of the coastal sand dunes over time. Also, in this thesis, the Geomorphic Change Detection software was employed in a coastal setting rather than to measure topographic change in rivers - the intended application of the software.

Geomorphic change detection methods can be 2D, 2.5D and 3D. As mentioned above, 2D methods measure the change in the planar position of a boundary feature represented by vector polylines, while 2.5D methods calculate the difference in elevation between two raster DEM surfaces and 3D methods measure change in 3D space using two point clouds. All three methods should be employed where possible. This allows for a variety of heterogeneous geospatial data representing topography to be exploited in the analysis resulting in deformations to the Earth's surface being tracked over a greater period of time. In addition, the multimodal methods allow for multiple variables to be measured including distances in 2D and 3D space, areal and volumetric measurements and rates of change statistics.

Measuring impact of natural hazards by diachronically quantifying geomorphic change can be employed to assess past and future impacts from natural hazards on cultural WH properties. The framework for natural hazard impact assessment for cultural WH should be triggered when natural hazards present themselves as deformation to the Earth's surface in locations that intersect with cultural WH properties. The benefit in doing so gives those who manage the historic environment robust knowledge of damage incurred by the property as well as an understanding of potential future impacts. This knowledge can aid in the creation and implementation of informed mitigation strategies to better safeguard cultural WH for future generations.

4. The archaeological record should form a key component of the natural hazard impact assessment for cultural WH properties. Archaeological data, such as excavation/evaluation plans, geophysical survey plots, aerial investigation and mapping results, Historic Environment Record data and Portable Antiquities Scheme data should be complied into a GIS for spatial comparison to the geomorphic change

detection and predictive modelling results. This information should be set alongside the natural environmental setting of the property. In doing so a conceptual understanding of the natural and anthropogenic system and how it interacts with the cultural WH property is achieved and the extents of the cultural WH property, based on current knowledge, is defined. In addition, documentary sources should be consulted to identify historic narratives of erosion of the archaeological record. This evidence of documented erosion can aid in the interpretation of the results, through providing evidence for direction of change (i.e. erosion/retreat versus deposition/advancement) which may have occurred in the intervening years for which there is no topographic data available (i.e. between epoch pairs). It also provides additional information regarding the level of destruction already incurred.

7.4 Limitations

There were some limitations to be aware of. These were as follows:

1. The analogue to digital conversion of the archived aerial photographs was not optimal. Historic England did not have the expertise for photogrammetric scanning at the time that the legacy data was collected. In addition, the photographs were not permitted to leave the Historic England Archive for scanning at a secondary location. Therefore, the archived aerial photographs could not photogrammetrically scanned as part of this research, likely resulting in poorer results from the SfM-MVS workflow. Photogrammetric scanning of these photographs would have likely improved the output from the SfM-MVS workflow, as demonstrated by research undertaken by Sevara *et al.* (2017) and by (Feurer and Vinatier, 2018), both of which were discussed in Chapter 3, 3.2.5.2.

2. The uncertainty analysis conducted within this research could be improved in some instances. For example, the epochs derived from archived aerial photographs used a uniform error surface for the 2.5D geomorphic change detection. This was based on RMSE results from SfM-MVS workflow. The 3D geomorphic change detection based uncertainty on surface roughness of the point clouds, derived from both archived aerial photographs and from lidar. James et al (2017) has created a method for producing 3D uncertainty values that results in a precision map that can be incorporated into the 3D geomorphic change detection analysis. Precision maps provide an error value for every point in the point cloud for incorporation in the

M3C2 algorithm. This method was developed for digital photographs taken from a UAV platform for the purpose of 3D topographic reconstruction using SfM-MVS, although the method can also be applied to terrestrial-acquired data. While the validity of this approach applied to archived aerial photographs needs to be assessed, there is potential that it can be applied or adapted for analogue photographs. Furthermore, since the completion of the various analyses of the research presented in this thesis, Winiwarter et al (2021) have devised a method, called M3C2-EP, for assessing propagated error within point clouds collected by terrestrial laser scanning systems. Again, this method has not been tested against airborne/RPAS lidar and therefore would require validation for working with datasets used in this research. Alternatively, potentially the error surface created for the 2.5D change detection could be sampled to the lidar point cloud for incorporation in the M3C2 analysis.

3. Satellite imagery did not form part of the spatiotemporal time series. Due to the prohibitive costs of high resolution imagery, this data type was ruled out from the beginning of this research. If available, this imagery may have provided epochs for intervening years where other data types did not exist, however, the largest gaps present in the time series of the Beckfoot study area that would have benefited from additional intervening epochs were from a time prior to the existence of satellite imagery. That being said, the incorporation of high resolution imagery could potentially have resulted in an even more robust spatiotemporal time series.

4. Forecasting future change conveyed potential future impact that would result in further loss of the Roman cremation cemetery. The complex modelling that was undertaken simulated coastal dune hydro- and morpho-dynamics under storm conditions both with the presence and absence of the rock armour wall. This demonstrated the potential of such an application to the study of impact of natural hazards on cultural WH properties. While various management strategies were modelled, to add scientific rigour to the simulation of hydro- and morpho-dynamics under storm conditions, further modelling using XBeach is required. This further modelling should consider a multitude of future scenarios, including more mitigation strategies and climate change projections such as sea level rise. In addition, coupling the model with a more appropriate wave model such as the SWAN wave model may improve results.

5. The past geomorphic change detection techniques presented detect surface change. Therefore these methods may not be suitable for all types of natural hazards. The natural hazards must interact with the landscape in a way which results in a surface change for deformation to be measureable through these techniques. Furthermore, the surface change must be greater than the noise in the data in order for that change to be deemed real change. An example of when this methodology would not be suitable is when researching the impact on the buried archaeological record caused by changes in water table levels, as these changes do not manifest as topographic change.

6. The modelling presented in this research is not universal across WH properties. Predictive models have been carefully constructed to answer particular research questions based on specific physical processes. The DSAS beta forecasting tool and the XBeach models used for this research may be inappropriate choices for applications where a WH site is under threat from landslide. In addition, the DSAS beta forecasting tool is based on linear regression, however coastal change is not linear. Erosion can be episodic. Furthermore, XBeach is not ideal for all coastal applications as it was developed to be applied to sandy beaches (Roelvink *et al.*, 2009). XBeach-G (Gravel) was subsequently developed for simulating gravel beach processes, while the SCAPE+ model, developed by Walkden and Hall (2004 A predictive mesoscale model of the erosion and profile development of soft rock shores) can be applied in the context of Soft Cliff And Platform Erosion where the cliff is composed of soft rock geology.

7.5 Future research

Below, a number of avenues for future research are suggested, which include both those specific to the Beckfoot study area and more generally to cultural WH sites across the world and heritage management strategies.

In regards to the Beckfoot study area, this research should continue to be updated as relevant datasets become available. When the most recent aerial imagery becomes freely available, the rates of change statistics should be adjusted with the corresponding coastline information. In 2019, the dunes along coastal zone of the Roman cremation cemetery/Mileforlet 15, with the exception of terminal erosion, appears to potentially be recovering, as seen in the April 2019 to June 2019 results. This was supported by vegetation

growth on the collapsed sediment that accumulated at the foot of the dune. From consulting Google Earth (2021) imagery of the study area, the dune system at the same location in April 2020 appears to be in a state of erosion. This can be seen by the steep cliff face free of vegetation growth and the lack of vegetated sand at the foot of the dune. By updating the natural hazard impact assessment, heritage managers will be better informed to react to the changing conditions impacting site survival.

More rigourous modelling of the Beckfoot study area should also be conducted to give a range of potential outcomes under different scenarios. These scenarios should include the various proposed coastal management strategies as discussed in Chapter 5 (section 5.7.5). Models should also consider an extension of the rock armour wall to understand if this strategy could proctect the Roman cremation cemetery and how this would affect the coastline beyond the study area. In addition, these models should also consider the climate change projections particularly regarding sea level rise and storm conditions, to provide a better understanding of coastal dune reaction to an increase in the volume of water.

Figure 7.1: Coastal change of the Bekcfoot Study area in coastal zone Roman cremation cemetery/Milefortlet 15 between (left) June 2019 and (right) April 2021.

Alternative ways of safeguading the coastal sites of the Hadrian's Wall WH site should be explored, with the coastal zone Roman cremation cemetery/Milefortlet 15 being a priorty area. Heritage managers should be involved in coastal management decision making where heritage sites are being impacted upon. If the preferred coastal management strategy is to let nature take its course through no active intervention, then preservation by record needs

to become a viable and preferred method for passing the information gathered from sites onto future generations. This should be a favoured option where physical protective measures are not viable, over the acceptance of loss especially for sites of Outstanding Universal Value.

Other at risk WH properties could benefit from the application of the natural hazard impact assessment developed as part of this research, especially in those instances where the physical remains of the archaeological record have been, or are being, impacted upon by forces of nature. For example, the natural hazard impact assessment framework outlined in this research could follow on from the Climate Impact Assessment undertaken at Skara Brae. The ongoing situation at Skara Brae closely parallels that of the Beckfoot study area in regards to hydro- and morpho-dynamics and coastal management strategies. Both locations are coastal, both contain archaeological remains buried within sand dunes, a seawall has been erected in both locations, and erosion is present at the terminal ends of the seawall at Skara Bare, similar to that seen within the Beckfoot study area.

The application of the natural hazard impact assessment from this research could also be implemented in other topographical and geographical contexts. The methods proposed within the natural hazard impact assessment framework have wider applicability beyond coastal heritage landscapes. The various change detection analyses utilised as part of this research are not limited by geographical factors. The 2D change detection analysis can be applied to any natural phenomena that can be represented as a series of vector polylines. Therefore it can be used to track historic river migration, lake extents, and cliff top and toe positions through time. In regards to the 2.5D and 3D change detection methods, these rely on 3D representation of the earth surface, as both measure elevation difference that can be attributed to surface deformation. As long as access to relevant data is available, and geomorphic change has occurred, these two methods can also be applied to detect that change. Predicative modelling can also be utilised in other contexts, however, model choice will need to be site specific, dependent upon the physical processes impacting upon the landscape.

The 2D change detection and forecasting method could be extended and applied to the entirety of the UK coastline and would be beneficial not only to coastal stakeholders, but also to heritage managers. This expanded approach is achievable on a large scale, as demonstrated by the Dynamic Coast (2021) project, which has produced a national database

for historic coastal change the coastline of Scotland. The output of this project has provided an overview of past and future coastal change and can also be used to identify areas for more in-depth analysis using the natural hazard impact assessment framework proposed in this thesis. While extension of the 2D analysis would require the analysis to be conducted at a lower resolution, the outputs can be used to identify areas for targeted detailed analysis.

8.0 References

Abarquez, I. and Murshed, Z. (2004) *Field Practitioners' Handbook: Community-based Disaster Risk Management*. Bangkok: Asian Disaster Preparedness Centre.

Aber, J.S., Marzolff, I., and Ries, J.B. (2010) 'Chapter 1 – Introduction to small-format aerial photography,' in Aber, S., Marzolff, I., and Ries, J.B (eds.) *Small-format aerial photography* pp. 1 – 13. doi: https://doi.org/10.1016/B978-0-444-53260-2.10001-8

ABPmer (2018). *SEASTATES: Data Explorer*. Available at: https://www.seastates.net/explore-data/ (Accessed 20 May 2021)

ABPmer (2021). *What is SEASTATES*? Available at: https://www.seastates.net/about/ (Accessed 20 May 2021)

Adams, Brian, 2005. *Projections and origins*, London: Charles Close Society.

Agapiou, A. (2020) 'Detecting Looting Activity through Earth Observation Multi-Temporal Analysis over the Archaeological Site of Apamea (Syria) during 2011–2012', *Journal of Computer Applications in Archaeology*, 3, pp. 219-237. doi: http://doi.org/10.5334/jcaa.56

Agisoft (2021) 'Agisoft Metashape User Manual Professional Edition, Version 1.8.' Available at: https://www.agisoft.com/downloads/user-manuals/

Air Ministry, Assistant Chief of the Air Staff. (1945) *Evidence in Camera 1939 – 1944: Special Edition on Photographic Reconnaissance and Photographic Intelligence - March 1945*. Reprint. Cambridge: The GeoInformation Group, 2003.

Alberts, H.C. and Hazen, H.D. (2010) 'Maintaining authenticity and integrity at cultural World Heritage sites', *Geographical Review*, 100(1), pp. 56-73. doi: https://doi.org/10.1111/j.1931-0846.2010.00006.x

Alcaíno-Olivares, R., Perras, M.A., Ziegler, M. and Leith, K. (2021) 'Thermo-Mechanical Cliff Stability at Tomb KV42 in the Valley of the Kings, Egypt', in Sassa, K., Mikoš, M., Sassa, S., Bobrowsky, P.T., Takara, K. and Dang, K. (eds.) *Understanding and Reducing Landslide Disaster Risk: Volume 1 Sendai Landslide Partnerships and Kyoto Landslide Commitment.* WLF 2020. ICL Contribution to Landslide Disaster Risk Reduction. Cham: Springer, pp. 471-478.

Allerdale Borough Council (2013). *Dubmill Point to Silloth Harbour Management Area Summary 2013*, Available at https://www.coastalmonitoring.org/pdf_download/?metadata_id=421637 (Accessed 26 March 2021).

Ames, C.J.H., Chambers, S., Shaw, M., Phillips, N., Jones, B.G. and Mackay, A. (2020) 'Evaluating erosional impacts on open-air archaeological sites along the Doring River, South Africa: methods and implications for research prioritization', *Archaeological and Anthropological Sciences*, 12(5). doi: https://doi.org/10.1007/s12520-020-01061-x

Ancient Monuments and Archaeological Areas Act (1979) Chapter 46. Available at: https://www.legislation.gov.uk/ukpga/1979/46/introduction (Accessed: 27 November 2017).

Anon (1921) 'Proceedings', *Transactions of Cumberland & Westmorland Antiquarian & Archaeological Society* (series 2), 21, pp. 257-272.

Anon (1923) 'Proceedings', *Transactions of Cumberland & Westmorland Antiquarian & Archaeological Society* (series 2), 23, pp. 277-296.

Asăndulesei, A., Tencariu, F.A. and Nicu, I.C. (2020) 'Pars pro toto—Remote Sensing Data for the Reconstruction of a Rounded Chalcolithic Site from NE Romania: The Case of Ripiceni–Holm Settlement (Cucuteni Culture)', *Remote Sensing*, 12, 887. doi: https://doi.org/10.3390/rs12050887

Baas, A.C.W. (2013) '2.1 Quantitative Modeling of Geomorphology', in Shroder, J.F. (ed.) *Treatise on Geomorphology*. San Diego: Academic Press, pp. 1-5. doi: https://doi.org/10.1016/B978-0-12-374739-6.00023-3

Baas, A.C.W. (2017) 'Models in Geomorphology', in Richardson, D., Castree, N., Goodchild, M.F., Kobayashi, A., Liu, W. and Marston, R.A. (eds.) *International Encyclopedia of Geography: People, the Earth, Environment and Technology*. pp. 1-6. doi: https://doi.org/10.1002/9781118786352.wbieg0882

Badillo-Almaraz, H., Orduña-Bustamante, A., Quintero-Sifuentes, O. and Orozco-Rojas, J. (2018) 'Assessment of the Structural Damage on the Former San Agustin Temple Using Numerical Modelling', in Aguilar, R., Torrealva, D., Moreira, S., Pando, M.A. and Ramos, L.F.

(eds.) *Structural Analysis of Historical Constructions: An Interdisciplinary Approach.* Cham: Springer International Publishing, pp. 938-946.

Barber, M. (2011) *A History of Aerial Photography and Archaeology: Mata Hari's Glass Eye and Other Stories*. Swindon: English Heritage.

Barnhart, T.B. and Crosby, B.T. (2013) 'Comparing Two Methods of Surface Change Detection on an Evolving Thermokarst Using High-Temporal-Frequency Terrestrial Laser Scanning, Selawik River, Alaska', *Remote Sensing*, 5(6), pp. 2813-2837. doi: http://dx.doi.org/10.3390/rs5062813

Bartoli, G., Betti, M. and Borri, C. (2015) 'Numerical Modeling of the Structural Behavior of Brunelleschi's Dome of Santa Maria del Fiore', *International Journal of Architectural Heritage*, 9(4), pp. 408-429. doi: https://doi.org/10.1080/15583058.2013.797038

BBC News (2004). 'Sea damaging Roman burial site', BBC *News*, 26 October. Available at: http://news.bbc.co.uk/1/hi/england/cumbria/3954079.stm (Accessed: 9 September 2020).

Bellhouse, R. L. (1954). 'Roman sites on the Cumberland coast, 1954'. *Transactions of the Cumberland & Westmorland Antiquarian & Archaeological Society*, series 2, 54, pp. 28-55.

Bellhouse, R. L. (1957). 'Roman sites on the Cumberland coast, 1954'. *Transactions of the Cumberland & Westmorland Antiquarian & Archaeological Society*, series 2, 57, pp. 18-26.

Bellhouse, R.L. (1962a) 'Moricambe in Roman times and Roman sites on the Cumberland coast', *Transactions of Cumberland & Westmorland Antiquarian & Archaeological Society*, series 2, 62, pp. 56 - 72.

Bellhouse, R.L. (1962b) 'Appendix: The cliff section at the measured position of Mile-fortlet 15 (Beckfoot)', *Transactions of Cumberland & Westmorland Antiquarian & Archaeological Society*, 62 (series 2), pp. 71-72.

Bellhouse, R.L. (1989) *Roman sites on the Cumberland coast: a new schedule of coastal sites.* Cumberland & Westmorland Antiquarian & Archaeological Society Research Series vol 3.

Bellhouse, R. (1992). *Joseph Robinson of Maryport: Archaeologist extraordinary*. Smith Settle: Otley, West Yorkshire.

Bellhouse, R.L. and Moffat, I. (1958) 'Further Roman finds in the Beckfoot cemetery site', *Transactions of the Cumberland & Westmorland Antiquarian & Archaeological Society*, series 2, 58 pp. 57-62.

Besl, P.J. and McKay, N.D. (1992) 'A Method for Registration of 3-D Shapes', *IEEE Transactions on Pattern Analysis and Machine Intelligence*, 14(2), pp. 239-256. doi: 10.1109/34.121791.

Bidwell, P.T. and Holbrook, N. (1989) *Hadrian's Wall Bridges*. English Heritage Archaeological Report no 9. London: Historic Buildings & Monuments Commission for England.

Bird, E. (2001) *Coastal Geomorphology An Introduction*. 2nd edition. England: John Wiley & Sons Ltd.

Blott, S.J., Pye, K., van der Wal, D. and Neal, A. (2006) 'Long-term morphological change and its causes in the Mersey Estuary, NW England', *Geomorphology*, 81(1), pp. 185-206. doi: https://doi.org/10.1016/j.geomorph.2006.04.008

Bokwa, A. (2013) 'Natural Hazard', in Bobrowsky P.T. (ed) *Encyclopedia of Natural Hazards*. Encyclopedia of Earth Sciences Series. Springer, Dordrecht., pp. 711-718. doi: https://doi.org/10.1007/978-1-4020-4399-4_248

Boughton, D. (2005). *LANCUM-DD0B54: A ROMAN HUMAN REMAINS.* Available at: https://finds.org.uk/database/artefacts/record/id/88295 (Accessed: 31 May 2021).

Breeze, D.J. (2004) 'Roman military sites on the Cumbrian coast', in Wilson, R.J.A. and Caruana, I.D. (eds.) *Romans on the Solway: essays in honour of Richard Bellhouse*, Kendal: Cumberland & Westmorland Antiquarian & Archaeological Society Extra Series 31, pp. 66-94.

British Geological Survey (2021) *Geology of Britain viewer (classic)*. Available at: https://mapapps.bgs.ac.uk/geologyofbritain/home.html (Accessed: 21 July 2021).

British Oceanographic Data Centre (2021) *Search the data BODC Database*. Available at: https://www.bodc.ac.uk/data/all-data.html (Accessed: 07 December 2021).

Bruce, J.C. and Daniels, M.C. (1978) *J. Collingwood Bruce's Handbook to the Roman Wall Thirteenth Edition.* [edited] by Charles M. Daniels, Harold Hill & Son, Scotland.

Bruce, J.C. and Breeze, D.J. (2006) *J. Collingwood Bruce's Handbook to the Roman Wall Fourteenth Edition.* [edited] by David J. Breeze, Newcastle upon Tyne: Society of Antiquaries of Newcastle upon Tyne.

Bruns, D. (2006). 'Roman Objects from Lancashire and Cumbria: A Round-Up of Finds Reported via the Portable Antiquities Scheme in 2006', *Contrebis,* 31, pp.13-22.

Burnham, B.C., Keppie, L.J.F., Esmonde Cleary, A.S., Hassall, M.W.C. and Tomlin, R.S.O. (1996) 'Roman Britain in 1995', *Britannia*, 27, pp. 389-457.

Campiani, A., Lingle, A. and Lercari, N. (2019) 'Spatial analysis and heritage conservation: Leveraging 3-D data and GIS for monitoring earthen architecture', *Journal of Cultural Heritage*, 39, pp. 166-176. doi: https://doi.org/10.1016/j.culher.2019.02.011

Capita (2015) *B5300 Coastal Defence Appraisal. Final Appraisal Report*. Prepared for Cumbria County Council. June 2015.

Capper, J.E. (1907) 'XXIII.—Photographs of Stonehenge, as seen from a War Balloon', *Archaeologia*, 60(2), pp. 571.

Carr, A.P. (1962) 'Cartographie Record and Historical Accuracy', *Geography*, 47(2), pp. 135-144.

CAT (2021) *Glasgow's 2030 credibility gap: net zero's lip service to climate action*. Available at: https://climateactiontracker.org/publications/glasgows-2030-credibility-gap-net-zeros-lip-service-to-climate-action/ (Accessed: 20 December 2021).

Caruana, I.D. (2004) 'The cemetery at Beckfoot Roman Fort', in Wilson, R.J.A. and Caruana, I.D. (eds.) *Romans on the Solway: essays in honour of Richard Bellhouse*, Kendal: Cumberland & Westmorland Antiquarian & Archaeological Society Extra Series 31, pp. 134-173.

Cassetari, S. (2004) 'Photo Mapping of Great Britain: A Growing Opportunity?', The Cartographic Journal, 41(2), pp. 95 – 100. doi: https://doi.org/10.1179/000870404X12824

Cerra, D., Plank, S., Lysandrou, V. and Tian, J. (2016) 'Cultural Heritage sites in danger-Towards automatic damage detection from space', *Remote Sensing*, 8(9), 781. doi: http://dx.doi.org/10.3390/rs8090781

Chen, Y. and Medioni, G. (1991) 'Object Modeling by Registration of Multiple Range Images', *Proceedings of the 1991 IEEE International Conference on Robotics and Automation, Sacramento, California - April 1991*, vol 3, pp. 2724-2729. doi: https://doi.org/10.1109/ROBOT.1991.132043

CH2M (2018) *Strategic Environmental Assessment Scoping Report: Cumbria Coastal Strategy.* [Online]. Available at: https://www.cumbria.gov.uk/eLibrary/Content/Internet/544/17312/43108154059.pdf (Accessed: 30 April 2018).

Cheng, L., Chen, S., Liu, X., Xu, H., Wu, Y., Li, M. and Chen, Y. (2018) 'Registration of Laser Scanning Point Clouds: A Review', *Sensors*, 18(5). doi: https://doi.org/10.3390/s18051641

CHERISH (2021) *CHERISH Climate Change & Coastal Heritage.* Available at: http://cherishproject.eu/en/ (Accessed: 26 November 2021).

Chughtai AH, Abbasi H, Karas I.R. (2021) 'A review on change detection method and accuracy assessment for land use land cover', *Remote Sensing Applications: Society Environment,* 22, 100482. doi: https://doi.org/10.1016/j.rsase.2021.100482

Chyla, J.M. (2017) 'How Can Remote Sensing Help in Detecting the Threats to Archaeological Sites in Upper Egypt?', *Geosciences*, 7(4), p. 97. doi: https://doi.org/10.3390/geosciences7040097

CHT2 (2019) *CHT2 Project Cultural Heritage Through Time*. Available at: http://cht2-project.eu/ (Accessed: 26 November 2021).

Cigna, F., Tapete, D., Lasaponara, R. and Masini, N. (2013) 'Amplitude Change Detection with ENVISAT ASAR to Image the Cultural Landscape of the Nasca Region, Peru', *Archaeological Prospection*, 20(2), pp. 117-131. doi: https://doi.org/10.1002/arp.1451

Clemente, P., Delmonaco, G., Puzzilli, L. and Saitta, F. (2019) 'Seismic Analysis of the Stylite Tower at Umm ar-Rasas', in Rafael, A., Torrealva, D., Moreira, S., Pando, M.A. and Ramos, L.F. (eds.) *Structural Analysis of Historical Constructions*. Cham: Springer International Publishing, pp. 1780-1788.

CLIMA (2021) *CLIMA Cultural Landscape risk Identification Management and Assessment*. Available at: http://www.clima-project.eu/the-project/ (Accessed: 26 November 2021).

Climate Analytics and New Climate Institute (2021) *Climate Action Tracker - Warming Projections Global Update, November 2021.* Available at: https://climateactiontracker.org/documents/997/CAT_2021-11-09_Briefing_Global-Update_Glasgow2030CredibilityGap.pdf (Accessed: 26 November 2021).

Close, C.F. (1969) *The early years of the Ordnance Survey.* Newton Abbot: David & Charles Reprints.

Coastal Engineering UK Ltd (2013) *Allerdale and Carlisle: Annual Local Monitoring Report 2011: Final Report.* Allerdale Borough Council report.

Coastal Engineering UK Ltd (2014a) *Allerdale and Carlisle Annual Local Monitoring Report 2012: Final Report*. Allerdale Borough Council report.

Coastal Engineering UK Ltd (2014b) *Allerdale Borough Council Annual Coastal Monitoring Inspection - February 2014: Inspection Report.* Allerdale Borough Council report.

Coastal Engineering UK Ltd (2015a) *Allerdale and Carlisle Annual Local Monitoring Report 2013: Final Report.* Allerdale Borough Council report.

Coastal Engineering UK Ltd (2015b) *Allerdale and Carlisle Annual Local Monitoring Report 2014: Final Report.* Allerdale Borough Council report.

Coastal Engineering UK Ltd (2015c) *Sefton Council: North West Strategic Monitoring Programme Regional Sediment Analysis and Reporting Inter-tidal Report - November 2015*. Sefton Council report.

Coastal Engineering UK Ltd (2016) *Allerdale and Carlisle Annual Local Monitoring Report 2015: Final Report.* Allerdale Borough Council report.

Colette, A. (2007) *Case studies on Climate Change and World Heritage*. Paris, France: UNESCO World Heritage Centre. Available at: http://whc.unesco.org/document/106621 (Accessed: 27 November 2017).

Collingwood, R.G. (1936) 'The Roman Fort at Beckfoot', *Transactions of Cumberland & Westmorland Antiquarian & Archaeological Society*, series 2, 36, pp. 76-84.

Collins, B.D., Corbett, S.C., Fairley, H.C., Minasian, D., Kayen, R., Dealy, T.P. and Bedford, D.R. (2012) *Topographic change detection at select archeological sites in Grand Canyon National Park, Arizona, 2007–2010*: U.S. Geological Survey Scientific Investigations Report 2012–5133. Available at: http://pubs.usgs.gov/sir/2012/5133/ (Accessed: 22 November 2020).

Collins, B.D., Minasian, D. and Kayen, R. (2009) *Topographic change detection at select archeological sites in Grand Canyon National Park, Arizona, 2006-2007*: U.S. Geological Survey Scientific Investigations Report 2009-5116. Available at: http://pubs.usgs.gov/sir/2009/5116 (Accessed: 22 November 2020).

Collins, M., Knutti, R., Arblaster, J., Dufresne, J.-L., Fichefet, T., Friedlingstein, P., Gao, X., Gutowski, W.J., Johns, T., Krinner, M., Shongwe, M., Tebaldi, C., Weaver, A.J. and Wehner, M. (2013) 'Long-term Climate Change: Projections, Commitments and Irreversibility. ', in Stocker, T.F., Qin, D., Plattner, G.-K., Tignor, M., Allen, S.K., Boschung, J., Nauels, A., Xia, Y., Bex, V. and Midgley, P.M. (eds.) *Climate Change 2013: The Physical Science Basis. Contribution of Working Group I to the Fifth Assessment Report of the Intergovernmental Panel on Climate Change*. Cambridge, United Kingdom and New York, NY, USA: Cambridge University Press, pp. 1029-1136.

Collins, M. (2005) *Beckfoot Roman cemetery and milefortlet: specification for archaeological evaluation works.* Unpublished English Heritage report.

Collins, M. (2009) 'Case Study: Beckfoot Roman Cemetery', in Symonds, M.F.A. and Mason, D.J.P. (eds) (2009a) *Frontiers of Knowledge: A research framework for Hadrian's Wall, Part of the Frontiers of the Roman Empire World Heritage Site, Volume I: Resource Assessment.* Durham: Durham County Council, pp. 163-164.

Collins, R. (2015) *Hadrian's Wall and LiDAR: New features in an ancient frontier landscape*. FREDHI (Frontiers of the Roman Empire Digital Humanities Initiative) Report 1. Newcastle: Newcastle University.

Collins, R. and Symonds, M. (eds) (2019) *Hadrian's Wall 2009-2019: A Summary of Excavation and Research, prepared for the Fourteenth Pilgrimage of Hadrian's Wall, 20-28 July 2019*. Kendal: Cumberland & Westmorland Antiquarian & Archaeological Society and Society of Antiquaries of Newcastle upon Tyne.

Collins, R., Shaw, K., Garland, N., Kille, I., Frodsham, P., Bell, E., Watson, F., and Clasper, A. (2018 Hadrian's Wall Community Archaeology Project (WallCAP) HG-16-08924 Activity Plan. Unpublished report, submitted 14 June 2018 To Heritage Lottery Fund National Committee

Collison, S. (2019) *Land South of Beckfoot. Archaeological Evaluation Final Report*. Barnard Castle: Northern Archaeological Associates. doi: https://doi.org/10.5284/1089471.

Cowley, D., Ferguson, L. and Williams, A. (2013) 'The Aerial Reconnaissance Archives: A Global Aerial Photographic Collection', in Hanson W., Oltean I. (eds) Archaeology from Historical Aerial and Satellite Archives. Springer, New York, NY, pp. 13-30. doi: https://doi.org/10.1007/978-1-4614-4505-0_2

Croft, A. (2013) *Assessment of Heritage at Risk from Environmental Threat: Key messages report in partnership with English Heritage*. Birmingham: Atkins. Available at: https://historicengland.org.uk/images-books/publications/assessment-heritage-at-risk-from-environmental-threat/ (Accessed: 27 November 2017).

CSDMS (2021) *Search the community model repository.* Available at: https://csdms.colorado.edu/wiki/Model_download_portal (Accessed: 7th June 2018).

Cutajar, D., Farrugia, P.-S. and Micallef, A. (2019) 'An integrated approach to the study of heritage sites', *Journal of Cultural Heritage*, 37, pp. 1-8. dDoi: https://doi.org/10.1016/j.culher.2018.10.014

CVI Heritage (2021) *CVI Update #7 July 2021*. Available at: https://www.jcu.edu.au/__data/assets/pdf_file/0008/1905623/Update_7_FINAL_July2021.pdf (Accessed: 27 August 2021).

Day, J.C., Heron, S.F. and Markham, A. (2019) *Climate Vulnerability Index - two-page information sheet.* Available at: https://www.jcu.edu.au/__data/assets/pdf_file/0003/867054/Climate-Vulnerability-Index-flyer_web2.pdf (Accessed: 26 November 2021).

Day, J.C., Heron, S.F., Markham, A., Downes, J., Gibson, J., Hyslop, E., Jones, R. and Lyall, l. (2019a) *Climate risk assessment for Heart of Neolithic Orkney World Heritage Property - An application of the Climate Vulnerability Index.* Edinburgh: Historic Environment Scotland.

de Beer, J., Price, S.J. and Ford, J.R. (2012) '3D modelling of geological and anthropogenic deposits at the World Heritage Site of Bryggen in Bergen, Norway', *Quaternary International*, 251, pp. 107-116. doi: https://doi.org/10.1016/j.quaint.2011.06.015

DEFRA (2020) DEFRA survey data download portal. Available at: Defra Survey Data Download (Accessed 12th December 2020).

DEFRA (2021) *Multi-Agency Geographic Information for the Countryside (MAGIC).* Available at: https://magic.defra.gov.uk/home.htm (Accessed: 21 July 2021).

Deltares (2018) *XBeach Documentation Release XBeach v1.23.5527 XBeachX FINAL*.

Department for Environment Food and Rural Affairs (2021) *National Lidar Programme*. Available at: https://environment.data.gov.uk/dataset/2e8d0733-4f43-48b4-9e51-631c25d1b0a9 (Accessed: 5 May 2021).

Dong, P. and Chen, Q. (2017) *LiDAR Remote Sensing and Applications*. 1st edition. Boca Raton: CRC Press.

Dynamic Coast (2021a) *About*. Available at: https://www.dynamiccoast.com/about (Accessed: 11 November 2021).

Dynamic Coast (2021b) *Webmaps.* Available at: https://www.dynamiccoast.com/webmaps (Accessed: 11 November 2021).

Eadie, G. (2012) *The North West Rapid Coastal Zone Assessment (NWRCZA) Phase 2 Project Report*. Bakewell: UK. Archaeological Research Services. ARS Ltd Report No. 2012/769

Edina Digimap (2021a) *Digimap - Aerial*. Available at: https://digimap.edina.ac.uk/aerial (Accessed: 09 September 2021).

Edina Digimap (2021b) *Digimap - FAQs*. Available at: https://digimap.edina.ac.uk/help/faqs/aerial/#faq-8 (Accessed: 09 September 2021).

Elnabawi, M.H., Hamza, N. and Dudek, S. (2015) 'Numerical modelling evaluation for the microclimate of an outdoor urban form in Cairo, Egypt', *HBRC Journal*, 11(2), pp. 246-251. doi: https://doi.org/10.1016/j.hbrcj.2014.03.004

Environment Agency (2019a) *Remote Sensing and Surveying in the Environment Agency: Surveying & Analysis - Accuracy & Resolution.* Available at: https://experience.arcgis.com/experience/753ad2ebd3554fa696885b8c366c3049/page/LIDAR/ (Accessed: 9th September 2021).

Environment Agency (2019b) *Remote Sensing and Surveying in the Environment Agency: Surveying & Analysis - DSM & DTMs.* Available at: https://experience.arcgis.com/experience/753ad2ebd3554fa696885b8c366c3049/page/LIDAR/?views=DSM-%26-DTMs (Accessed: 9th September 2021).

Environment Agency (2019c) *Remote Sensing and Surveying in the Environment Agency: Surveying & Analysis - Point Cloud.* Available at: https://experience.arcgis.com/experience/753ad2ebd3554fa696885b8c366c3049/page/LIDAR/?views=Point-Cloud(Accessed: 9th September 2021).

Environment Agency (2019d) *Remote Sensing and Surveying in the Environment Agency: Surveying & Analysis – Composite.* Available at: https://experience.arcgis.com/experience/753ad2ebd3554fa696885b8c366c3049/page/LIDAR/?views=Composite(Accessed: 9th September 2021).

Environment Agency (2019e) *Remote Sensing and Surveying in the Environment Agency: Surveying & Analysis - LIDAR Home.* Available at: https://experience.arcgis.com/experience/753ad2ebd3554fa696885b8c366c3049/page/LIDAR/?views=LIDAR-Home(Accessed: 9th September 2021).

Environment Agency (2019f) *Remote Sensing and Surveying in the Environment Agency: Surveying & Analysis – National LIDAR Programme.* Available at: https://experience.arcgis.com/experience/753ad2ebd3554fa696885b8c3049/page/LIDAR/?views=National-LIDAR-Programme (Accessed: 9th September 2021).

Environment Agency (2019g*) Remote Sensing and Surveying in the Environment Agency: Surveying & Analysis - Time Series.* Available at: https://experience.arcgis.com/experience/753ad2ebd3554fa696885b8c366c3049/page/LIDAR/?views=Time-Series(Accessed: 9th September 2021).

247

Environment Agency (2020). *National Coastal Erosion Risk Map*. Available at: https://www.arcgis.com/apps/webappviewer/index.html?id=9cef4a084bbb4954b970cd35b099d94c (Accessed 14 April 2020).

ESRI (2021) *ArcGIS Pro - Overview of Georeferencing*. Available at: https://pro.arcgis.com/en/pro-app/latest/help/data/imagery/overview-of-georeferencing.htm (Accessed: 09 September 2021).

Fieber, K.D., Mills, J.P., Peppa, M.V., Haynes, I., Turner, S., Turner, A., Douglas, M. and Bryan, P.G. (2017) 'Cultural Heritage Through Time: A case study at Hadrian's Wall, United Kingdom', *The International Archives of the Photogrammetry, Remote Sensing and Spatial Information Sciences.* XLII-2/W3, pp. 297–302. Available at: https://doi.org/10.5194/isprs-archives-XLII-2-W3-297-2017 (Accessed: 15 November 2021).

Ferguson, R.S. (1878) ' An attempt at a Survey of Roman Cumberland and Westmorland; with remarks on Agricola's Line of March, and on the importance of the Camp at Old Carlisle, and on the loth Iter of Antoninus', *Transactions of Cumberland & Westmorland Antiquarian & Archaeological Society*, series 1, 3, pp. 64-94.

Feurer, D. and Vinatier, F. (2018) 'Joining multi-epoch archival aerial images in a single SfM block allows 3-D change detection with almost exclusively image information', *ISPRS Journal of Photogrammetry and Remote Sensing*, 146, pp. 495-506. doi: https://doi.org/10.1016/j.isprsjprs.2018.10.016

Fluck, H. and Wiggins, M. (2017) 'Climate Change, Heritage Policy and Practice in England: Risk and Opportunities', *Archaeological Review from Cambridge*, 32(2), pp. 159 - 181. Ddoi: https://doi.org/10.17863/CAM.23646

Fookes, P.G., Lee, M.R. and Griffiths, J.S. (2006) *Engineering geomorphology: theory and practice*. Dunbeath: Whittles.

Frere, S.S. and St Joseph, J.K.S. (1983) *Roman Britain from the Air*. Cambridge: Press Syndicate of the University of Cambridge.

Getmapping Plc (2021) *Getmapping - Products and Services*. Available at: https://www.getmapping.com/products-and-services (Accessed: 09 September 2021).

Girardeau-Montaut, D., Roux, M., Marc, R. and Thibault, G. (2005). 'Change detection on points cloud data acquired with a ground laser scanner'. *International Archives of Photogrammetry, Remote Sensing and Spatial Information Sciences,* 36(3), pp.30–35.

Glira, P., Pfeifer, N., Briese, C. and Ressl, C. (2015) ' A Correspondence Framework for ALS Strip Adjustments based on Variants of the ICP Algorithm', *Photogrammetrie - Fernerkundung - Geoinformation*, 4, pp. 275-289. doi: http://dx.doi.org/10.1127/pfg/2015/0270

Google (2018) *Beckfoot*. Available at: https://earth.google.com/web/ (Accessed: 5 July 2018).

Grady, D. (2019) *A Brief History of the Historic England Archive of Aerial Photographs.* Available at: https://historicengland.org.uk/whats-new/research/50-years-flying/history-of-the-historic-england-aerial-photo-archive/ (Accessed: 05 May 2019).

Green, D. (2014) 'Modelling Geomorphic Systems: Scaled Physical Models', in Cook, S.J., Clarke, L.E. and Nield, J.M. (eds.) *Geomorpholoigcal Techniques (Online Edition)*. London, UK: British Society for Geomorphology.

Guidi, G., Beraldin, J-A., Atzeni, C. (2007) 'Wood artworks monitoring through high-resolution 3D cameras' *Proceedings SPIE 6491 Videometrics IX 64910T*. pp. 1 – 7. doi: https://doi.org/10.1117/12.705332

Guidi, G., Atzeni, C., Seracini, M., and Lazzari, S., (2004) 'Painting Survey by 3D Optical Scanning: The Case of "Adoration of the Magi" by Leonardo da Vinci', Studies in Conservation, 49(1), pp. 1 – 12. Available at: https://www.jstor.org/stable/1506926

Guiney, R., Santucci, E., Valman, S., Booth, A., Birley, A., Haynes, I., Marsh, S. and Mills, J. (2021) 'Integration and Analysis of Multi-Modal Geospatial Secondary Data to Inform Management of at-Risk Archaeological Sites', *ISPRS International Journal of Geo-Information*, 10(9), 575. doi: https://doi.org/10.3390/ijgi10090575

Hadrian's Wall Country (2008) *Frontiers of the Roman Empire World Heritage Site: Hadrian's Wall Management Plan 2008 - 2014*. Available at: https://www.nationaltrail.co.uk/sites/default/files/1._hadrians_wall_management_plan_2008-2014_-_text.pdf (Accessed: 27 November 2017).

Hadrian's Wall Country (2018a) *Hadrian's Wall Management Plan*. Available at:

https://hadrianswallcountry.co.uk/hadrians-wall-management-plan (Accessed: 12 November

2021).

Hadrian's Wall Country (2018b) *Hadrian's Wall Management Plan - Description*. Available at:

https://hadrianswallcountry.co.uk/hadrians-wall-management-plan/description (Accessed:

12 November 2021).

Hadrian's Wall Country (2018c) *Hadrian's Wall Management Plan - Hadrian's Wall*

Significance. Available at: https://hadrianswallcountry.co.uk/hadrians-wall-management-

plan/hadrians-wall-significance (Accessed: 12 November 2021).

Hadrian's Wall Country (2018d) *Hadrian's Wall Management Plan - Attributes*. Available at:

https://hadrianswallcountry.co.uk/hadrians-wall-management-plan/attributes (Accessed: 12

November 2021).

Halcrow Group Limited (2010) *Cell 11 Regional Monitoring Strategy (CERMS) 2009 Baseline*

Reporting. Swindon, Wiltshire. Available at

https://www.coastalmonitoring.org/pdf_download/?metadata_id=408930 (Accessed: 15

November 2021).

Halcrow Group Limited (2012a) *Cell 11 Regional Monitoring Strategy (CERMS) 2010*

Monitoring Update Report. Swindon, Wiltshire. Available at:

https://www.coastalmonitoring.org/pdf_download/?metadata_id=408059 (Accessed: 15

November 2021).

Halcrow Group Limited (2012b) *North West & North Wales Coastal Group: North West*

England and North Wales Shoreline Management Plan SMP2 - Main SMP2 Document.

Swindon. Swindon, Wiltshire. Available at: http://www.hoylakevision.org.uk/wp-

content/uploads/2012/11/SMP2Main.pdf

Harkin, D., Davies, M., Hyslop, E., Fluck, H., Wiggins, M., Merritt, O., Barker, L., Deery, M.,

McNeary, R. and Westley, K. (2020) 'Impacts of climate change on cultural heritage', *MCCIP*

Science Review 2020, pp. 616-641. https://doi.org/10.14465/2020.arc26.che.

Harley, J.B. (1964) *The historian's guide to Ordnance Survey maps: reprinted from the 'Amateur Historian' with additional material*. London: Published for the Standing Conference for Local History by the National Council of Social Service.

Harley, J.B. (1975) *Ordnance Survey maps: a descriptive manual*. Southampton: Ordnance Survey.

Hassan, F.A. (2007) 'The Aswan High Dam and the International Rescue Nubia Campaign', *African Archaeological Review* 24, pp. 73-94. doi: https://doi.org/10.1007/s10437-007-9018-5

Haynes, I. (2019) 'Beckfoot Fort (?Bibra)', in Collins, R. and Symonds, M. (eds) *Hadrian's Wall 2009-2019: A Summary of Excavation and Research, prepared for the Fourteenth Pilgrimage of Hadrian's Wall, 20-28 July 2019*. Kendal: Cumberland & Westmorland Antiquarian & Archaeological Society and Society of Antiquaries of Newcastle upon Tyne, pp. 201-204.

Haynes, I. and Arbuthnot, S. (2016) *Written Scheme of Investigation: Beckfoot Roman Fort, Geophysical Survey*. Unpublished report. Newcastle upon Tyne: Newcastle University.

Healey, C. (2007) *Beckfoot Roman Cemetery and Milefortlet, Cumbria. Archaeological Evaluation Assessment Report*. Lancaster: Oxford Archaeology (North).

Higley, C. (2011) *Old Series to Explorer: A field guide to the Ordnance map*. London: The Charles Close Society.

Hil, G. (2020) 'Better Management Through Measurement: Integrating Archaeological Site Features into a GIS-Based Erosion and Sea Level Rise Impact Assessment—Blueskin Bay, New Zealand', *The Journal of Island and Coastal Archaeology*, 15(1), pp. 104-126. doi: https://doi.org/10.1080/15564894.2018.1531331

Himmelstoss, E.A., Henderson, R.E., Kratzmann, M.G., and Farris, A.S. (2021) *Digital Shoreline Analysis System (DSAS) Version 5.1 User Guide* US Geological Survey Open-File Report 2021-1091. Available at: https://doi.org/10.3133/ofr20211091

Historic England (2017a) *Research Agenda*. Swindon: Historic England. Available at: https://content.historicengland.org.uk/images-books/publications/he-research-agenda/research-agenda.pdf/ (Accessed: 27 November 2017).

Historic England (2017b) *Heritage at Risk: North West Register 2017.* London, UK: English Heritage. Available at: https://content.historicengland.org.uk/images-books/publications/har-2017-registers/nw-har-register2017.pdf/ (Accessed: 27 November 2017).

Historic England (2020) *Heritage at Risk: North West Register 2020*. London, UK: English Heritage Available at: https://historicengland.org.uk/images-books/publications/har-2020-registers/nw-har-register2020/ (Accessed: 27 November 2017).

Historic England (2021a) *Heritage at Risk: North East & Yorkshire Register 2021.* London, UK: English Heritage. Available at: https://historicengland.org.uk/images-books/publications/har-2021-registers/ne-yo-har-register2021/ (Accessed: 27 November 2021).

Historic England (2021b) *Heritage at Risk North West Register 2021*. London: Historic England. Available at: https://historicengland.org.uk/images-books/publications/har-2021-registers/nw-har-register2021/ (Accessed: 27 November 2021).

Historic England (2022) *Download Listing Data*. Available at: https://historicengland.org.uk/listing/the-list/data-downloads/ (Accessed: 21 November 2019).

Hogg, R. (1949) 'A Roman cemetery site at Beckfoot, Cumberland', *Transactions of the Cumberland & Westmorland Antiquarian & Archaeological Society*, series 2, 49, pp. 32-37.

Hogg, R. (1962) 'Beckfoot fort, cemetery site', *Transactions of Cumberland & Westmorland Antiquarian & Archaeological Society*, series 2, 62, pp. 323 - 324.

Hooke, R.L. (2003) 'Predictive Modeling in Geomorphology: An Oxymoron?', in Wilcock, P.R. and Iverson, R.M. (eds) *Prediction in Geomorphology*, Geophysical Monograph series 135, pp. 51-61. doi: https://doi.org/10.1029/135GM05

Howard, A.J. (2013) 'Managing global heritage in the face of future climate change: the importance of understanding geological and geomorphological processes and hazards', *International Journal of Heritage Studies*, 19(7), pp. 632-658. doi: https://doi.org/10.1080/13527258.2012.681680

Howard, A.J., Coulthard, T.J. and Knight, D. (2017) 'The potential impact of green agendas on historic river landscapes: Numerical modelling of multiple weir removal in the Derwent Valley Mills world heritage site, UK', Geomorphology, 293, Part A, pp. 37-52. doi: https://doi.org/10.1016/j.geomorph.2017.05.009

Howard-Davis, C., Leary, R., and Ward, M. (2017) 'Evaluation of Beckfoot Roman Cemetery, 2006', *Transactions of Cumberland and Westmorland Antiquarian and Archaeological Society*, CW3(17), pp. 43 – 84.

Howland , M.D., Jones, I.W.N, Najjar, M., and Levy, T.E. (2018) 'Quantifying the effects of erosion on archaeological sites with low-altitude aerial photography, structure from motion, and GIS: A case study from southern Jordan.' *Journal of Archaeological Science* 90 pp. 62 – 70. doi: https://doi.org/10.1016/j.jas.2017.12.008

HR Wallingford, ABPmer and Pethick, J. (2006) *Review and formalisation of geomorphological concepts and approaches for estuaries*. London: FM R&D Dissemination, D.-F.M.D.

Hussain, M., Chen, D., Cheng, A., Wei, H. and Stanley, D. (2013) 'Change detection from remotely sensed images: From pixel-based to object-based approaches', *ISPRS Journal of Photogrammetry and Remote Sensing*, 80, pp. 91-106. doi: https://doi.org/10.1016/j.isprsjprs.2013.03.006

Hutchinson, W. (1794) *The History of the County of Cumberland*. Carlisle: F. Jollie.

Hutton, C. (2012) 'Modelling Geomorphic Systems: Numerical Modelling', in Clark, L.E., Cook, S.J. and Nield, J.M. (eds.) *Geomorphological Techniques (Online Edition)*. London, UK: British Society for Geomorphology.

ICOMOS (2011) *Guidance on Heritage Impact Assessments for Cultural World Heritage Properties - A publication of the International Council on Monuments and Sites*, ICOMOS: Paris. Available at: http://openarchive.icomos.org/id/eprint/266/ (Accessed: 22 November 2020).

IEMA (2021) *Principles of Cultural Heritage Impact Assessment in the UK*. Available at: https://www.archaeologists.net/sites/default/files/j30361_iema_principlesofchia_v8.pdf (Accessed: 27 November 2017).

IPCC (2021) 'Summary for Policymakers', in Masson-Delmotte, V., Zhai, P., Pirani, S., Connors, S.L., Péan, C., Berger, S., Caud, N., Chen, Y., Goldfarb, L., Gomis, M.I., Huang, M., Leitzell, K., Lonnoy, E., Matthews, J.B.R., Maycock, T.K., Waterfield, T., Yelekçi, O., Yu, R. and Zhour, B. (eds.) *Climate Change 2021: The Physical Science Basis. Contributions of Working Group I to the Sixth Assessment Report of the Intergovernmental Panel on Climate Change.* IPCC: Switzerland.

Jacobs (2020a) *Cumbria Coastal Strategy: Issues, Risks and Opportunities report.* Cumbrian County Council Report.

Jacobs (2020b) *Cumbria Coastal Strategy: Technical Appraisal Report for Policy Area 11e5 Dubmill to Silloth*. Cumbrian County Council Report.

James, L.A., Hodgson, M.E., Ghoshal, S. and Latiolais, M.M. (2012) 'Geomorphic change detection using historic maps and DEM differencing: The temporal dimension of geospatial analysis', *Geomorphology*, 137(1), pp. 181-198. doi: https://doi.org/10.1016/j.geomorph.2010.10.039

James, M.R., Robson, S. and Smith, M.W. (2017) '3-D uncertainty-based topographic change detection with structure-from-motion photogrammetry: precision maps for ground control and directly georeferenced surveys', *Earth Surface Processes and Landforms*, 42(12), pp. 1769-1788. doi: https://doi.org/10.1002/esp.4125

Jay, H. (2020) *Cumbria Coastal Strategy - Main Document*. Cumbrian County Council Report. Swindon: Jacobs Consultancy Ltd.

Johnson, B. (2009) *North West Rapid Coastal Zone Assessment (NWRCZA) Final SMP2 version.* Gateshead: Archaeological Research Services.

Jones, R.H., Davies, M.H., Day, J.C. and Heron, S.F. (2022) 'Developing Climate Risk Assessments for World Heritage: the Climate Vulnerability Index', Internet Archaeology, 60. doi: https://doi.org/10.11141/ia.60.3

Kincey, M., Batty, L., Chapman, H., Gearey, B., Ainsworth, S. and Challis, K. (2014) 'Assessing the changing condition of industrial archaeological remains on Alston Moor, UK, using multisensor remote sensing', *Journal of Archaeological Science*, 45, pp. 36-51. doi: https://doi.org/10.1016/j.jas.2014.02.008

Kincey, M., Gerrard, C. and Warburton, J. (2017) 'Quantifying erosion of 'at risk' archaeological sites using repeat terrestrial laser scanning', *Journal of Archaeological Science: Reports*, 12, pp. 405-424. doi: https://doi.org/10.1016/j.jasrep.2017.02.003

Kościuk, J. and Kogut, J. (2019) 'Numerical Modelling of Hypothetical Quincha Walls on Samaipata Rock', in Aguilar R., Torrealva D., Moreira S., Pando M.A., Ramos L.F. (eds) Structural Analysis of Historical Constructions. RILEM Bookseries, vol 18. Cham. Springer International Publishing. doi: https://doi.org/10.1007/978-3-319-99441-3_90

Lague, D., Brodu, N. and Leroux, J. (2013) 'Accurate 3D comparison of complex topography with terrestrial laser scanner: Application to the Rangitikei canyon (N-Z)', *ISPRS Journal of Photogrammetry and Remote Sensing*, 82, pp. 10-26. doi: https://doi.org/10.1016/j.isprsjprs.2013.04.009

Land Use Consultants (2010) *The Solway Coast Area of Outstanding Natural Beauty: Landscape and Seascape Character Assessment.* Edinburgh: LUC Services

Land Use Consultants (2019) *Coastal Risk and Priority Places: The development of an interactive map resource.* Report 37/2019. Historic England. Available at: https://historicengland.org.uk/research/results/reports/37-2019 (Accessed: 11/07/2020).

Lane, S.N., Richards, K.S. and Chandler, J.H. (1994) 'Developments in monitoring and modelling small-scale river bed topography', *Earth Surface Processes and Landforms*, 19(4), pp. 349-368. doi: https://doi.org/10.1002/esp.3290190406

Lasaponara R., Elfadaly A. and Attia W. (2016) 'Low Cost Space Technologies for Operational Change Detection Monitoring Around the Archaeological Area of Esna-Egypt', in Gervasi O., Murgante, B., Misra, S., Rocha, A.M.A.C., Torre, C.M., Taniar, D., Apduhan, B.O., Stankova, E. and Wang, S. (eds) *Computational Science and Its Applications – ICCSA 2016*. ICCSA 2016. Lecture Notes in Computer Science, vol 9787. Springer, Cham. doi: https://doi.org/10.1007/978-3-319-42108-7_48

Lasaponara, R. and Masini, N. (2018) 'Space-Based Identification of Archaeological Illegal Excavations and a New Automatic Method for Looting Feature Extraction in Desert Areas', *Surveys in Geophysics*, 39, pp. 1323-1346. doi: https://doi.org/10.1007/s10712-018-9480-4

Leisz, S.J. (2013) 'An Overview of the Application of Remote Sensing to Archaeology During the Twentieth Century', in Comer, D.C. and Harrower, M.J. (eds) *Mapping Archaeological Landscapes from Space*. New York, NY: Springer New York, pp. 11-19.

Lercari, N. (2019) 'Monitoring earthen archaeological heritage using multi-temporal terrestrial laser scanning and surface change detection', *Journal of Cultural Heritage*, 39, pp. 152-165. doi: https://doi.org/10.1016/j.culher.2019.04.005

Li, H., Sumner, R., and Pauly, M. (2008) 'Global Correspondence Optimization for Non-Rigid Registration of Depth Scans', *Computer Graphics Forum*, 27(5), pp. 1421 – 1430. doi: https://doi.org/10.1111/j.1467-8659.2008.01282.x

Li, P., Wang, R., Wang, Y. and Tao, W. (2020) 'Evaluation of the ICP Algorithm in 3D Point Cloud Registration', *IEEE Access*, 8, pp. 68030-68048. doi: https://doi.org/10.1109/ACCESS.2020.2986470

Lowe, J.A., Bernie, D., Bett, P., Bricheno, L., Brown, S., Calvert, D., Clark, R., Eagle, K., Edwards, T., Fosser, G., Fung, F., Gohar, L., Good, P., Gregory, J., Harris, G., Howard, T., Kaye, N., Kendon, E., Krijnen, J., Maisey, P., McDonald, R., McInnes, R., McSweeney, C., Mitchell, J.F.B., Murphy, J., Palmer, M., Roberts, C., Rostron, J., Sexton, D., Thornton, H., Tinker, J., Tucker, S., Yamazaki, K. and Belcher, S. (2019) *UKCP18 Science Overview Report November 2018 (Updated March 2019)*. Exeter: Met Office Hadley Centre. Available at https://www.metoffice.gov.uk/pub/data/weather/uk/ukcp18/science-reports/UKCP18-Overview-report.pdf (Accessed: 22 November 2020).

Lu, D., Mausel, P., Brondízio, E. and Moran, E. (2004) 'Change detection techniques', *International Journal of Remote Sensing*, 25(12), pp. 2365-2401. doi: https://doi.org/10.1080/0143116031000139863

Luo, L., Wang, X., Guo, H., Lasaponara, R., Zong, X., Masini, N., Wang, G., Shi, P., Khatteli, H., Chen, F., Tariq, S., Shao, J., Bachagha, N., Yang, R. and Yao, Y. (2019) 'Airborne and spaceborne remote sensing for archaeological and cultural heritage applications: A review of the century (1907–2017)', *Remote Sensing of Environment*, 232, 111280. dDoi: https://doi.org/10.1016/j.rse.2019.111280

LUC (2019) *Coastal Risk and Priority Places - The development of an interactive map resource.* Historic England Research Report Series no. 37/2019. Available at https://historicengland.org.uk/research/results/reports/37-2019 (Accessed: 27 November 2017).

Marine Scotland (2021). *Maps National Marine Plan Interactive (NMPI): part of Scotland's Environment*. Available at: https://marinescotland.atkinsgeospatial.com/nmpi/default.aspx?layers=423 (Accessed: 15 May 2021).

Markham, A., Osipova, E., Lafrenz Samuels, K. and Caldas, A. (2016) *World Heritage and Tourism in a Changing Climate.* United Nations Environment Programme, Nairobi, Kenya and United Nations Educational, Scientific and Cultural Organization, Paris, France.

Martin, L. (2006) *Beckfoot, Cumbria: Report on Geophysical Surveys. October 2005*. London: English Heritage. London: English Heritage. doi: https://doi.org/10.5284/1095671.

Martin, G. (2011) *Roman Way, Beckfoot Archaeological Evaluation Report*. Carlisle: Gerry Martin Associates Ltd. doi: https://doi.org/10.5284/1017290.

Martin, G (2015) *Roman Way, Beckfoot Archaeological Watching Brief and Excavation*. Carlisle: Gerry Martin Associates Ltd.

Martínez-Fernández, A., Benito-Calvo, A., Campaña, I., Ortega, A.I., Karampaglidis, T., Bermúdez de Castro, J.M. and Carbonell, E. (2020) '3D monitoring of Paleolithic archaeological excavations using terrestrial laser scanner systems (Sierra de Atapuerca, Railway Trench sites, Burgos, N Spain)', *Digital Applications in Archaeology and Cultural Heritage*, 19, e00156. doi: https://doi.org/10.1016/j.daach.2020.e00156

May, F.S.A. and Hope, F.L.S. (1917) 'Catalogue of the Roman Pottery in the Museum, Tullie House, Carlisle', *Transactions of Cumberland & Westmorland Antiquarian & Archaeological Society*, series 2, 17, pp. 114-197.

Met Office (2021) *UK Climate Projections: Headline* Findings, July 2021. Exeter: Met Office Hadley Centre. Available at: https://www.metoffice.gov.uk/binaries/content/assets/metofficegovuk/pdf/research/ukcp/ukcp18_headline_findings_v3.pdf (Accessed: 22 November 2020).

Miller, P., Mills, J., Edwards, S., Bryan, P., Marsh, M., Mitchell, H., and Hobbs, P. (2008). 'A robust surface matching technique for coastal assessment and management', *ISPRS Journal of Photogrammetry and Remote Sensing*, 63, pp 529 – 542. Available at: https://doi.org/10.1016/j.isprsjprs.2008.02.003.

Mounsey, K. (2014) *Beckfoot Farm, Allonby, Cumbria, Geophysical Survey Report.* Wardell Armstrong Archaeology. doi: https://doi.org/10.5284/1030239.

Musumeci, R.E., Foti, E., Li Rosi, D., Sanfilippo, M., Stancanelli, L.M., Iuppa, C., Sapienza, V., Yang, W., Cantarero, M. and Patanè, D. (2021) 'Debris-flow hazard assessment at the archaeological UNESCO world heritage site of Villa Romana del Casale (Sicily, Italy)', *International Journal of Disaster Risk Reduction*, 64, 102509. doi: https://doi.org/10.1016/j.ijdrr.2021.102509

National Collection of Aerial Photography (2019) *Our Work.* Available at: https://ncap.org.uk/about-ncap/our-work (Accessed: 05 May 2019).

Natural England (2015) *National Character Area profile: 6. Solway Basin*. Available at http://publications.naturalengland.org.uk/file/5231898609582080 (Accessed: 21 July 2021).

Natural England (2021a) *Designated Sites View SSSI Condition Summary, Site: Silloth Dunes and Mawbray Bank*. Available at: https://designatedsites.naturalengland.org.uk/ReportConditionSummary.aspx?SiteCode=S1001196&ReportTitle=Upper%20Solway%20Flats%20&%20Marshes%20SSSI (Accessed: 21 July 2021).

Natural England (2021b) *Designated Sites View SSSI glossary* Available at: https://designatedsites.naturalengland.org.uk/SSSIglossary.aspx (Accessed: 21 July 2021).

Natural England (2021c) *Designated Sites View SSSI Condition Summary, Site: Upper Solway Flats*. Available at: https://designatedsites.naturalengland.org.uk/ReportConditionSummary.aspx?SiteCode=S1001196&ReportTitle=Upper%20Solway%20Flats%20&%20Marshes%20SSSI (Accessed: 21 July 2021).

Natural England (2021) *Natural England Open Data Geoportal*. Available at: https://naturalengland-defra.opendata.arcgis.com/ (Accessed: 5 November 2021)

Nesbit, R.C. (1997) *Eyes of the RAF - A History of Photo-Reconnaissance.* Godalming, Surrey: Bramley Books.

Nguyen, H.T., Daniel, S., Guriot, D., Sints, C. and Le Cillec, J.-M. (2020) 'Coarse-to-Fine Registration of Airborne LiDAR Data and Optical Imagery on Urban Scenes', *IEEE Journal of Selected Topics in Applied Earth Observations and Remote Sensing*, 13, pp. 3125-3144. doi: 10.1109/JSTARS.2020.2987305

Nicu, I.C. (2020) 'Natural Hazards Versus Cultural Heritage', in Smith, C. (ed.) Encyclopedia of Global Archaeology. Cham: Springer International Publishing, pp. 7641-7652. doi: https://doi.org/10.1007/978-3-319-51726-1_3185-1

Nicu, I.C. (2021) 'Is digital shoreline analysis system "fit" for gully erosion assessment?', *CATENA*, 203, pp. 1-16. doi: https://doi.org/10.1016/j.catena.2021.105307

Nicu, I.C., Stalsberg, K., Rubensdotter, L., Martens, V.V. and Flyen, A.-C. (2020) 'Coastal Erosion Affecting Cultural Heritage in Svalbard. A Case Study in Hiorthhamn (Adventfjorden)—An Abandoned Mining Settlement', *Sustainability*, 12(6), 2306. doi: https://doi.org/10.3390/su12062306

NNRCMP (2021) *National Network of Regional Coastal Monitoring Programmes of England – Map Viewer and Catalogue*. Available at https://coastalmonitoring.org/cco/ (Accessed: 15 April 2021).

Noon, S. (2010). *LANCUM-413CA5: A ROMAN VESSEL*. Available at: https://finds.org.uk/database/artefacts/record/id/289313 (Accessed: 31 May 2021).

Noon, S. (2012a). *LANCUM-546D25: A ROMAN VESSEL.* Available at: https://finds.org.uk/database/artefacts/record/id/512530 (Accessed: 31 May 2021).

Noon, S. (2012b) *LANCUM-545A51: A BRONZE AGE URN.* Available at: https://finds.org.uk/database/artefacts/record/id/512526 (Accessed: 31 May 2021).

Oakey, M. (2009) *Hadrian's Wall World Heritage Site National Mapping Programme Project*, Research Department Report Series 73-2009, Historic England.

Okyay, U., Telling, J., Glennie, C.L. and Dietrich, W.E. (2019) 'Airborne lidar change detection: An overview of Earth sciences applications', *Earth-Science Reviews*, 198, 102929. doi: https://doi.org/10.1016/j.earscirev.2019.102929

Oliver, R. (1993) *Ordnance Survey maps - a concise guide for historians*. 1st edition London: Charles CLose Society for the study of Ordnance Survey maps.

Oliver, R. (2013) *Ordnance survey maps: a concise guide for historians*. 3rd edition London: Charles Close Society.

Ordnance Survey (2015) *A guide to coordinate systems in Great Britain: An introduction to mapping coordinate systems and the use of GPS datasets with Ordnance Survey mapping*. Southampton.

Ordnance Survey (2019) Beckfoot [Map 1:25000 Scale Colour Raster]. Available at: http://edina.ac.uk/digimap (Accessed: 30 April 2020).

Ordnance Survey (2021) *Ordnance Survey - OS MasterMap Topography Layer support*. Available at: https://www.ordnancesurvey.co.uk/business-government/tools-support/mastermap-topography-support (Accessed: 09 September 2021).

Oyedotun, T.D.T. (2014) 'Shoreline geometry: DSAS as a tool for Historical Trend Analysis', in Clark, L.E., Cook, S.J. and Nield, J.M. (eds.) *Geomorphological Techniques (Online Edition)*. London, UK: British Society for Geomorphology.

Pagliaroli, A., Quadrio, B., Lanzo, G. and Sanò, T. (2014) 'Numerical modelling of site effects in the Palatine Hill, Roman Forum, and Coliseum Archaeological Area', Bulletin of Earthquake Engineering, 12(3), pp. 1383-1403. doi: https://doi.org/10.1007/s10518-013-9436-5

Palma, G., Bourbekeur, T., Ganovelli, F., and Cignoni, P. (2018) 'Scalable non-rigid registration for multi-view stereo data' *ISPRS Journal of Photogrammetry and Remote Sensing,* 142, pp. 328 – 341. doi: https://doi.org/10.1016/j.isprsjprs.2018.06.012

Palma, G., Pingi, P., Siotto E., Bellucci, R., Guidi, G., and Scopigno R. (2019) 'Deformation analysis of Leonardo da Vinci's "Adorazione dei Magi" through temporal unrelated 3D digitization', Journal of Cultural Heritage, 38, pp. 174 – 185. doi: https://doi.org/10.1016/j.culher.2018.11.001

Palmer, M., Howard, T., Tinker, J., Lowe, J., Bricheno, L., Calvert, D., Edwards, T., Gregory, J., Harris, G., Krijnen, J., Pickering, M., Roberts, C. and Wolf, J. (2018) *UKCP18 Marine report, November 2018.* Exeter: Met Office Hadley Centre. Available at: https://www.metoffice.gov.uk/pub/data/weather/uk/ukcp18/science-reports/UKCP18-Marine-report.pdf (Accessed: 22 November 2020).

Parry, S., Baynes, F.J., Culshaw, M.G., Eggers, M., Keaton, J.F., Lentfer, K., Novotny, J. and Paul, D. (2014) 'Engineering geological models: an introduction: IAEG commission 25', Bulletin of Engineering Geology and the Environment, 73(3), pp. 689-706. doi: https://doi.org/10.1007/s10064-014-0576-x

Pelletier, J.D. (2008) Quantitative Modeling of Earth Surface Processes. Cambridge: Cambridge University Press. doi: https://doi.org/10.1017/CBO9780511813849

Peppa, M.V. (2018) *Report on the final 4D results for the four case studies* Cultural Heritage Through Time. Available at: http://cht2-project.eu/wp-content/uploads/2018/05/D_3_3_CHT2-4D-results_GG.pdf (Accessed: 07 August 2019).

Peppa, M.V., Mills, J.P., Moore, P., Miller, P.E. and Chambers, J.E. (2019) 'Automated co-registration and calibration in SfM photogrammetry for landslide change detection', *Earth Surface Processes and Landforms*, 44(1), pp. 287-303. doi: https://doi.org/10.1002/esp.4502

Peppa, M.V., Mills, J.P., Fieber, K.D., Haynes, I., Turner, S., Turner, A., Douglas, M. and Bryan, P.G. (2018) 'Archaeological Feature Detection from Archive Aerial Photography with a SfM-MVS and Image Enhancement Pipeline', *Int. Arch. Photogramm. Remote Sens. Spatial Inf. Sci*., XLII-2, pp. 869-875. doi: https://doi.org/10.5194/isprs-archives-XLII-2-869-2018

Petts, D.A. (2009) 'Burial on Hadrian's Wall', in Symonds, M.F.A. and Mason, D.J.P. (eds) (2009a) *Frontiers of Knowledge: A research framework for Hadrian's Wall, Part of the Frontiers of the Roman Empire World Heritage Site, Volume I: Resource Assessment.* Durham: Durham County Council, pp. 160-163.

Pitts, M. (2009) 'Roman graves rescued: but cemetery doomed?', *Current Archaeology*, September/October 2009, p.7.

Polidori, L. (2020) 'On Laussedat's contribution to the emergence of photogrammetry', *ISPRS The International Archives of the Photogrammetry, Remote Sensing and Spatial Information*

Sciences, XLIII-B2-2020, pp. 893 – 899. doi: https://doi.org/10.5194/isprs-archives-XLIII-B2-2020-893-2020

Pomerleau, F., Colas, F. and Siegwart, R. (2015) 'A Review of Point Cloud Registration Algorithms for Mobil Robotics', *Foundations and Trends in Robotics*, 4(1), pp. 1-104. doi: http://dx.doi.org/10.1561/2300000035

PROTHEGO (2017) *Welcome to PROTHEGO PROTection of European Cultural HEritage from GeO-hazards*. Available at: http://www.prothego.eu/ (Accessed: 26 November 2021).

Qin, R., Tian, J. and Reinartz, P. (2016) '3D change detection – Approaches and applications', *ISPRS Journal of Photogrammetry and Remote Sensing*, 122, pp. 41-56. doi: https://doi.org/10.1016/j.isprsjprs.2016.09.013

Quezada, R., Aguilar, E. and García, H. (2019) 'Macro-modeling of Adobe Piers for Seismic Analysis of Adobe Dwellings in Cuenca, Ecuador', in Aguilar R., Torrealva D., Moreira S., Pando M.A., Ramos L.F. (eds) Structural Analysis of Historical Constructions. RILEM Bookseries, vol 18. Cham. Springer International Publishing. doi: https://doi.org/10.1007/978-3-319-99441-3_142

Radosavljevic, B., Lantuit, H., Pollard, W., Overduin, P., Couture, N., Sachs, T., Helm, V. and Fritz, M. (2016) 'Erosion and Flooding—Threats to Coastal Infrastructure in the Arctic: A Case Study from Herschel Island, Yukon Territory, Canada', *Estuaries and Coasts*, 39(4), pp. 900-915. doi: https://doi.org/10.1007/s12237-015-0046-0

Rayne, C., Gatto, M. C., Abdulaati, L., Al-Haddad, M., Sterry, M., Sheldrick, N., and Mattingly, D. (2020) 'Detecting Change at Archaeological Sites in North Africa Using Open-Source Satellite Imagery', *Remote Sensing,* 12(22), 3694, pp. 1-29. doi: https://doi.org/10.3390/rs12223694

Richardson, C. (1990) 'A Catalogue of Recent Acquisitions to Carlisle Museum and Reported Finds from the Cumbrian Area', *Transactions of Cumberland & Westmorland Antiquarian & Archaeological Society*, series 2, 90, pp. 1 - 98.

Risbøl, O., Briese, C., Doneus, M. and Nesbakken, A. (2015) 'Monitoring cultural heritage by comparing DEMs derived from historical aerial photographs and airborne laser scanning',

Journal of Cultural Heritage, 16(2), pp. 202-209. doi:
https://doi.org/10.1016/j.culher.2014.04.002

Riverscapes Consortium (2020) *Geomorphic change detection software - essential best practices to support change detection* Available at:
https://gcd.riverscapes.xyz/Tutorials/Building_DEMs/bestpractices.html (Accessed: 21 June 2018).

Robinson, J. (1881) 'The Roman Camp near Beckfoot (Mowbray) Cumberland', *Transactions of Cumberland & Westmorland Antiquarian & Archaeological Society 5*, series 1, pp. 136-148. doi: https://doi.org/10.5284/1064607.

Roelvink, D. and Reniers, A. (2012) *A Guide to Modeling Coastal Morphology*. Advances in Coastal and Ocean Engineering vol 12. Singapore: World Scientific Publishing.

Roelvink, D., Reniers, A., van Dongeren, A., van Thiel de Vries, J., McCall, R. and Lescinski, J. (2009) 'Modelling storm impacts on beaches, dunes and barrier islands', *Coastal Engineering*, 56(11), pp. 1133-1152. doi: https://doi.org/10.1016/j.coastaleng.2009.08.006

Rusinkiewicz, S. and Levoy, M. (2001) 'Efficient variants of the ICP algorithm', *Proceedings Third International Conference on 3-D Digital Imaging and Modeling, 2001,* pp. 145-152. doi: https://doi.org/10.1109/IM.2001.924423

Saloustros, S., Pelà, L., Roca, P. and Portal, J. (2015) 'Numerical analysis of structural damage in the church of the Poblet Monastery', *Engineering Failure Analysis*, 48, pp. 41-61. doi: https://doi.org/10.1016/j.engfailanal.2014.10.015

Schaffrath, K.R., Belmont, P. and Wheaton, J.M. (2015) 'Landscape-scale geomorphic change detection: Quantifying spatially variable uncertainty and circumventing legacy data issues', *Geomorphology*, 250, pp. 334-348. doi: https://doi.org/10.1016/j.geomorph.2015.09.020

Sevara, C., Verhoeven, G., Doneus, M. and Draganits, E. (2017) 'Surfaces from the Visual Past: Recovering High-Resolution Terrain Data from Historic Aerial Imagery for Multitemporal Landscape Analysis', *Journal of Archaeological Method and Theory*, 25, pp. 1-32. doi: https://doi.org/10.1007/s10816-017-9348-9

Shan, J. and Toth, C.K. (2018) *Topographic laser ranging and scanning: principles and processing.* Second edition. Boca Raton: Taylor & Francis, CRC Press.

Singh, A. (1989) 'Review Article Digital change detection techniques using remotely-sensed data', *International Journal of Remote Sensing*, 10(6), pp. 989-1003. doi: https://doi.org/10.1080/01431168908903939

Slatyer, R.O. (1983) 'The Origin and Evolution of the World Heritage Convention', *Ambio*, 12(3/4), pp. 138-140.

Smith, W.M., Carrivick, J.L., and Quincey, D.J., (2015) 'Structure from motion photogrammetry in physical geography', *Progress in Physical Geography*, 40(2), pp. 247 – 275. doi: https://doi.org/10.1177/0309133315615805

Smith, M.W., Carrivick, J.L. and Quincey, D.J. (2016) 'Structure from motion photogrammetry in physical geography', *Progress in Physical Geography: Earth and Environment*, 40(2), pp. 247-275. doi: https://doi.org/10.1177%2F0309133315615805

Solway Firth Partnership (1996). *Solway Firth Review*. Unpublished report: Solway Firth Partnership.

Speed, J., (1610) *Cumberland and the Ancient Citie Carlile Described,* George Humble, Popes Head Alley, London, 1611-12. Available at: https://www.lakesguides.co.uk/html/speed/sp14fram.htm (accessed 5th of November 2017).

Stanley, C.R.M. (1981) *World War II Photo Intelligence*. London: Sidgwick & Jackson.

Statutes 2019. International Society for Photogrammetry and Remote Sensing, pp. 1 – 5. Available at: https://www.isprs.org/documents/statutes19.aspx (Accessed: 27 June 2022).

Stillwell, H.D. (1992) 'Natural hazards and disasters in Latin America', *Natural Hazards*, 6(2), pp. 131-159. doi: https://doi.org/10.1007/BF00124620

St Joseph, J.K. (1951). 'Air Reconnaissance of North Britain', *Journal of Roman Studies* 41, pp.52-56.

Sutherland, J. (2012) 'Error analysis of Ordnance Survey map tidelines, UK', *Maritime Engineering*, 165(MA4), pp. 189 – 197. doi: https://doi.org/10.1680/maen.2011.10

Symonds, M.F.A. and Mason, D.J.P. (eds) (2009a) *Frontiers of Knowledge: A research framework for Hadrian's Wall, Part of the Frontiers of the Roman Empire World Heritage Site, Volume I: Resource Assessment.* Durham: Durham County Council.

Symonds, M.F.A. and Mason, D.J.P. (eds) (2009b) *Frontiers of Knowledge: A research framework for Hadrian's Wall, Part of the Frontiers of the Roman Empire World Heritage Site, Volume II: Agenda and Strategy*. Durham: Durham County Council.

Tapete, D., Cigna, F. and Donoghue, D.N.M. (2016) ''Looting marks' in space-borne SAR imagery: Measuring rates of archaeological looting in Apamea (Syria) with TerraSAR-X Staring Spotlight', *Remote Sensing of Environment*, 178, pp. 42-58. doi: https://doi.org/10.1016/j.rse.2016.02.055

The Vienna University of Technology - Department of Geodesy and Geoinformation (2019) *OPALS - Orientation and Processing of Airborne Laser Scanning data.* Available at: https://opals.geo.tuwien.ac.at/html/stable/index.html (Accessed: 09 September 2021).

UNESCO (2007) *Climate Change and World Heritage Report on predicting and managing the impacts of climate change on World Heritage and Strategy to assist State Parties to implement appropriate responses.* World Heritage Reports 22. World Heritage Centre: UNESCO.

UNESCO, ICCROM, ICOMOS and IUCN. (2010). *Managing disaster risks for World Heritage.* World Heritage Resource Manual. UNESCO: Paris, 1–6. Available at: http://whc.unesco.org/en/ news/630/ (Accessed: 26 November 2021).

UN Climate Change Conference UK 2021 (2021) *COP26 explained*. Available at https://2nsbq1gn1rl23zol93eyrccj-wpengine.netdna-ssl.com/wp-content/uploads/2021/07/COP26-Explained.pdf (Accessed: 09 November 2021).

UNESCO (1972) *Convention concerning the protection of the World Cultural and Natural Heritage.* [Online]. Available at: https://whc.unesco.org/en/conventiontext/ (Accessed: 09 November 2021).

UNESCO (1988) *UNESCO Convention Concerning the Protection of the World Cultural and Natural Heritage: Report of the World Heritage Committee Eleventh Session.* Paris, France:

UNESCO Headquarters. Available at https://whc.unesco.org/archive/repcom87.htm (Accessed: 09 November 2021).

UNESCO (2005) *UNESCO Decisions of the 29th session of the World Heritage Committee (Durban 2005)*. Paris, France: UNESCO World Heritage Centre. Available at https://whc.unesco.org/en/sessions/29COM/decisions/ (Accessed: 09 November 2021).

UNESCO (2006) *Policy Document on the Impacts of Climate Change on World Heritage Properties. Paris*, France: UNESCO World Heritage Centre. Available at https://whc.unesco.org/uploads/activities/documents/activity-397-2.pdf (Accessed: 09 November 2021).

UNESCO (2007a) *UNESCO Decisions of the 31st session of the World Heritage Committee (Christchurch 2007)*. Paris, France: UNESCO World Heritage Centre. Available at https://whc.unesco.org/archive/2007/31com-en.htm (Accessed: 09 November 2021).

UNESCO (2007b) *Climate Change and World Heritage Report on predicting and managing the impacts of climate change on World Heritage and Strategy to assist State Parties to implement appropriate responses.* World Heritage Reports 22. World Heritage Centre: UNESCO.

UNESCO (2009a) *UNESCO Decisions of the 32nd session of the World Heritage Committee (Quebec City, 2008).* Paris, France: UNESCO World Heritage Centre. Available at https://whc.unesco.org/archive/2008/whc08-32com-24reve.pdf (Accessed: 09 November 2021).

UNESCO (2009b) *Convention Concerning the Protection of the World Cultural and Natural Heritage World Heritage Committee: Thirty-third session Seville, Spain 22-30 June 2009: Report of Decisions.* Paris, France: UNESCO World Heritage Centre. Available at https://whc.unesco.org/archive/2009/whc09-33com-20e.pdf (Accessed: 09 November 2021).

UNESCO (2012) *Decisions Adopted by the World Heritage Committee at its 36th Session (Saint-Petersburg, 2012).* Available at https://whc.unesco.org/archive/2012/whc12-36com-19e.pdf (Accessed: 09 November 2021).

UNESCO (2015) 'Policy Document for the Integration of a Sustainable Development Perspective into the Processes of the World Heritage Convention'. Available at https://whc.unesco.org/document/139747 (Accessed: 09 November 2021).

UNESCO (2020) *States Parties Ratification Status*. Available at: https://whc.unesco.org/en/statesparties/ (Accessed: 12 November 2021).

UNESCO (2021a) *Liverpool - Maritime Mercantile City*. Available at: https://whc.unesco.org/en/list/1150 (Accessed: 12/11/2021).

UNESCO (2021b) *WHC/21/44.COM/7C Draft updated policy documentation on the impacts of climate change on World Heritage properties*. Available at https://whc.unesco.org/archive/2021/whc21-44com-7C-en.pdf (Accessed: 27 November 2017).

UNESCO (2021c) *World Heritage 44 COM - WHC/21/44.COM/7A.Add: Item 7A of the Provisional Agenda: State of conservation of the properties inscribed on the List of World Heritage in Danger.* Available at https://whc.unesco.org/document/188003 (Accessed: 27 November 2017).

UNESCO (2021d) *Decisions adopted during the extended 44th session of the World Heritage Committee (Fuzhou (China) / Online meeting, 2021)*. Available at https://whc.unesco.org/document/188949 (Accessed: 27 November 2017).

UNESCO, ICCROM, ICOMOS and IUCN (2010) *Managing disaster risks for World Heritage: World Heritage Resource Manual.* Available at https://whc.unesco.org/document/104522 (Accessed: 27 November 2017).

UNESCO World Heritage Centre (2019) *Operational Guidelines for the Implementation of the World Heritage Convention.* Paris, France: UNESCO World Heritage Centre. Available at: Available at https://whc.unesco.org/document/178167 (Accessed: 27 November 2019).

UNESCO World Heritage Centre (2021a) *Draft updated Policy Document on the impacts of climate change on World Heritage properties.* Available at: https://whc.unesco.org/archive/2021/whc21-44com-7C-en.pdf (Accessed: 12 November 2021).

UNESCO World Heritage Centre (2021b) *World Heritage List - Delisted*. Available at:
https://whc.unesco.org/en/list/?&delisted=1 (Accessed: 12 November 2021).

UNESCO World Heritage Centre (2021c) *Operational Guidelines for the Implementation of the World Heritage Convention.* UNESCO World Heritage Centre. Available at: Available at
https://whc.unesco.org/document/190976 (Accessed: 27 November 2021).

UNESCO World Heritage Centre (2021d) *World Heritage List: Frontiers of the Roman Empire*,
Available at: https://whc.unesco.org/en/list/430/ (Accessed: 23rd July 2019).

UNESCO World Heritage Centre (2021e) *Frontiers of the Roman Empire – The Lower German Limes*, Available at: https://whc.unesco.org/en/list/1631 (Accessed: 28th November 2021).

United Nations (2015) Conference of the Parties: Twenty-first session - Paris, 30 November to 11 December 2015. FCCC/CP/2015/L.9/Rev/1. Paris: United Nations. Available at:
https://unfccc.int/resource/docs/2015/cop21/eng/l09r01.pdf (Accessed: 15 September 2018).

United Nations (2018) Tracking Progress Towards Inclusive, Save, Resilient and Sustainable Cities and Human Settlements SDG 11 Synthesis Report High Level Political Forum 2018.

United Nations (2021) *Conference of the Parties serving as the meeting of the Parties to the Paris Agreement: Third session - Glasgow, 31 October to 12 November 2021.*
FCCC/PA/CMA/2021/L.16. New York: United Nations. Available at
https://unfccc.int/sites/default/files/resource/cma2021_L16E.pdf (Accessed 26 November 2021).

United Nations Climate Change and UK Government (2021) *COP26 The Glasgow Climate Change Pact UN Climate Change Conference UK 2021 in partnership with Italy*. Available at:
https://ukcop26.org/ (Accessed: 26 November 2021).

United Nations General Assembly (1994) United Nations framework convention on climate change. Resolution A/RES/48/189. Available at:
https://digitallibrary.un.org/record/180257/files/A_RES_48_189-EN.pdf (Accessed: 15 September 2018).

Weisstein, E.W. (2022) 'Affine Transformation' MathWorld – A Wolfram Web Resource. Available at: (https://mathworld.wolfram.com/AffineTransformation.html (Accessed: 29 September 2022).

Wheaton, J., Brasington, J., Darby, S., and Sear, D. (2010) 'Accounting for uncertainty in DEMs from repeat topographic surveys: improved sediment budgets', Earth Surface Processes and Landforms, 35, pp. 136 – 156. doi: https://doi.org/10.1002/esp.1886

Williams, N. (2011) *Bibra Field Survey Report*. University of Central Lancashire dissertation.

Wilmott, T. (1997) *Birdoswald - Excavations of a Roman fort on Hadrian's Wall and its successor settlements: 1987 - 92*. English Heritage Archaeological Report no 14. London: English Heritage.

Vojinovic, Z., Golub, D., Keerakamolchai, W., Meesuk, V., Sanchez Torres, A., Weesakul, S., Alves, A. and Babel, M. (2021a) 'Adaptation to Flood Risk in Areas with Cultural Heritage', in Babel, M., Haarstrick, A., Ribbe, L., Shinde, V.R. and Dichtl, N. (eds.) *Water Security in Asia: Opportunities and Challenges in the Context of Climate Change*. Springer Water: Springe Cham., pp. 391-399. doi: https://doi.org/10.1007/978-3-319-54612-4_29

Vojinovic, Z., Keerakamolchai, W., Torres, A.S., Weesakul, S., Meesuk, V., Alves, A. and Babel, M.S. (2021b) 'Towards Holistic and Multifunctional Design of Green and Blue Infrastructure for Climate Change Adaptation in Cultural Heritage Areas', in Babel, M., Haarstrick, A., Ribbe, L., Shinde, V.R. and Dichtl, N. (eds.) *Water Security in Asia: Opportunities and Challenges in the Context of Climate Change*. Cham: Springer International Publishing, pp. 381-390. doi: https://doi.org/10.1007/978-3-319-54612-4_28

Westley, K. (2019) 'Refining Broad-Scale Vulnerability Assessment of Coastal Archaeological Resources, Lough Foyle, Northern Ireland', *The Journal of Island and Coastal Archaeology*, 14(2), pp. 226-246. doi: https://doi.org/10.1080/15564894.2018.1435592

Wheaton, J.M., Brasington, J., Darby, S.E. and Sear, D.A. (2010) 'Accounting for uncertainty in DEMs from repeat topographic surveys: improved sediment budgets', *Earth Surface Processes and Landforms*, 35(2), pp. 136-156. doi: https://doi.org/10.1002/esp.1886

Wilcock, P.R. and Iverson, R.M. (2003a) 'Prediction in Geomorphology', in Wilcock, P.R. and Iverson, R.M. (eds) *Prediction in Geomorphology*, Geophysical Monograph series 135, pp. 3-11. doi: https://doi.org/10.1029/135GM01

Wilcock, P.R. and Iverson, R.M. (2003b) 'Preface', in Wilcock, P.R. and Iverson, R.M. (eds) *Prediction in Geomorphology*, Geophysical Monograph series 135, pp. i-vii. doi: https://doi.org/10.1002/9781118668559.fmatter

Williams, R.D. (2012) 'DEMs of Difference', in Clark, L.E., Cook, S.J. and Nield, J.M. (eds.) *Geomorphological Techniques (Online Edition)*. London, UK: British Society for Geomorphology.

Winter, S. (2017a) *Environment Agency Uncovers Landscape with Laser Mapping*. Available at: https://www.gov.uk/government/news/environment-agency-uncovers-landscape-with-laser-mapping (Accessed: 05 May 2019).

Winter, S. (2017b) *Uncovering England's Landscape by 2020*. Available at: https://environmentagency.blog.gov.uk/2017/12/30/uncovering-englands-landscape-by-2020/ (Accessed: 05 May 2019).

Winter, S. (2018) *Blog Creating a better place – Reaching new heights*. Available at: Reaching new heights - Creating a better place (blog.gov.uk) (Accessed: 23rd December 2018).

Xaio, W., Mills, J., Guidi, G., Rodríguez-Gonzálvez, P., Gonizzi Barsanti, S., and González-Aguilera, D. (2018) 'Geoinformatics for the conservation and promotion of cultural heritage in support of the UN Sustainable Development Goals', *ISPRS Journal of Photogrammetry and Remote Sensing*, 142, pp. 389 – 406. doi: https://doi.org/10.1016/j.isprsjprs.2018.01.001

Zimmer, B., Liutkus-Pierce, C., Marshall, S.T., Hatala, K.G., Metallo, A. and Rossi, V. (2018) 'Using differential structure-from-motion photogrammetry to quantify erosion at the Engare Sero footprint site, Tanzania', *Quaternary Science Reviews*, 198, pp. 226-241. doi: https://doi.org/10.1016/j.quascirev.2018.07.006